



APPENDIX II

Modeling and Attainment Demonstration



CHAPTER 1 – MODELING OVERVIEW

Introduction..... II-1-1

Modeling Methodology..... II-1-1

 Design Values..... II-1-1

 Model Selection II-1-1

 Regional Modeling..... II-1-2

 Relative Response Factors and Future Year Design Values II-1-3

Modeling Results II-1-4

Uncertainties Associated with the Technical Analysis..... II-1-4

Document Organization II-1-5

CHAPTER 2 – MODELING PROTOCOL

Background..... II-2-1

Attainment Demonstration II-2-1

Numerical Models..... II-2-1

Emissions Processing..... II-2-4

Biogenic Emissions..... II-2-6

Computational Resources II-2-6

CHAPTER 3 – METEOROLOGICAL MODELING

Overview II-3-1

Comparison of 2018 Observed Meteorology to 10-Year Average II-3-1

Modeling Configuration II-3-5

Model Performance Evaluation: Surface Level II-3-9

Model Performance Evaluation: Diurnal Variations II-3-20

Model Performance Evaluation: Wind Rose II-3-22

Model Performance Evaluation: Planetary Boundary Layer Height II-3-25

Sensitivity Test of Planetary Boundary Layer Scheme II-3-27

Summary II-3-3536



CHAPTER 4 - MODELING EMISSIONS, BOUNDARY CONDITIONS, AND INITIAL CONDITIONS

| | |
|---|-----------------------|
| Modeling Emissions Inventory | II-4-1 |
| Inventory Profile | II-4-1 |
| Temporal and Spatial Allocations of Emissions | II-4-2 |
| On-road Mobile Emissions | II-4-2 |
| Emissions Profiles | II-4- 56 |
| Spatial Distribution | II-4- 67 |
| Biogenic Emissions..... | II-4- 1011 |
| Boundary and Initial Conditions. | II-4- 1112 |
| Total PM2.5 Mass in Boundary Conditions | II-4- 1112 |
| PM2.5 Species in Boundary Conditions | II-4- 1920 |

CHAPTER 5 - ANNUAL PM2.5 ATTAINMENT DEMONSTRATION

| | |
|---|-----------------------|
| Introduction | II-5-1 |
| PM2.5 FRM Sampling | II-5-1 |
| Speciated PM2.5 Sampling | II-5-2 |
| Annual PM2.5 Modeling Approach..... | II-5-4 |
| Performance Evaluation | II-5- 67 |
| Statistical Evaluation of Total PM2.5 mass..... | II-5- 1415 |
| Model Performance of Speciated PM2.5 Predictions..... | II-5- 1617 |
| CMAQ SOA Mass Simulation | II-5- 2122 |
| Base Year Annual PM2.5 | II-5- 2425 |
| Speciated Quarterly Average Data | II-5- 2425 |
| Future Year Annual PM2.5 Air Quality | II-5- 3435 |
| Unmonitored Area Analysis..... | II-5- 3739 |
| Summary and Conclusions | II-5- 4244 |

CHAPTER 6 – ATTAINMENT DEMONSTRATION FOR THE CA-60 NEAR-ROAD MONITORING STATION

Introduction.....II-6-21

Approach to Model the Effect of Near-Road Sources.....II-6-32

 Alternatives for the determination of NRI.....II-6-54

AERMOD Dispersion Modeling Set-Up.....II-6-20

 PM2.5 simulation with AERMODII-6-2426

 Model Evaluation of Hybrid ModelII-6-2630

 Annual PM2.5 Design Values using the Hybrid ApproachII-6-3034

SummaryII-6-3236

CHAPTER 7 – ~~EXCEPTIONAL~~TYPICAL EVENTS DEMONSTRATION ANALYSIS

Introduction.....II-7-1

Fireworks Emissions.....II-7-3

 Professional Fireworks.....II-7-5

Historical AnalysisII-7-7

 Fireworks Summary for 2016-07-05.....II-7-20

 Fireworks Summary for 2017-07-04 and 2017-07-05II-7-23

 Fireworks Summary for 2018-07-05.....II-7-30

 Fireworks Summary for 2019-07-05.....II-7-39

ConclusionII-7-50

Attachment 1: WRF Model Performance Time Series

Attachment 2: CMAQ Model Performance Figures

Attachment 3: Emissions Reductions Summary for Future Control Scenarios

Attachment 4: List of Wildfires that Affected the South Coast Air Basin in 2020

Chapter 1

MODELING OVERVIEW

Introduction

Modeling Methodology

Design Values

Model Selection

Regional Modeling

Relative Response Factors and Future Year Design Values

Modeling Results

Uncertainties Associated with the Technical Analysis

Document Organization

Introduction

Air quality modeling to demonstrate future attainment of air quality standards is an integral part of the planning process to achieve clean air. Modeling provides the means to relate emission reductions from pollution sources to the resulting air quality improvements. The attainment demonstrations provided in this ~~Draft~~ PM2.5 Plan reflect updated emissions estimates, new technical information, enhanced air quality modeling techniques, updated attainment demonstration methodology, and the control strategies provided in Chapter 4.

This ~~Draft~~ PM2.5 Plan aims to develop a control strategy and corresponding attainment demonstration that: 1) ensures that the 2012 annual PM2.5 National Ambient Air Quality Standard (NAAQS) is met by the established deadline in the federal Clean Air Act (CAA) and 2) achieves an expeditious rate of progress towards attaining the air quality standard.

The South Coast Air Basin is classified as an “serious” nonattainment area for the 2012 annual PM2.5 NAAQS with an attainment year of 2025. This plan seeks an extension of the attainment to 2030 and included control strategy and modeling demonstration to attain in 2030. The modeling base year is 2018 and was used to derive meteorological inputs; it also served as an anchor year to project future emissions and was used in the attainment demonstration.

Modeling Methodology

Design Values

U.S. EPA guidance recommends the use of multiple year averages of design values, where appropriate, to dampen the effects of single year anomalies to the air quality trend due to factors such as adverse or favorable meteorology or radical changes in the local emissions profile. The Basin PM2.5 design value trend is presented in Chapter 5 of the ~~Draft~~ PM2.5 Plan, Figure 5-1. The trend in the Basin Annual PM2.5 design values from 2001 through 2022 reveals substantial reductions in concentrations over this timeframe. The year 2020 was particularly anomalous for a variety of reasons such as recorded-setting wildfires and pandemic-era emissions. The five-year period, 2016-2020 was used in the current modeling attainment demonstration. However, due to the anomaly of year 2020 related with COVID-19 pandemic and record-setting wildfires, a five-year weighted design value recommended by U.S. EPA was modified to exclude the impact 2020 measurements. Chapter 5 of the ~~Draft~~ PM2.5 Plan discusses the detail of the 5-year weighted design value calculations.

Model Selection

The attainment demonstration was developed using the U.S. EPA Community Multiscale Air Quality (CMAQ) (version 5.3.3) modeling platform with Statewide Air Pollution Research Center (SAPRC) 07 chemistry and aerosol mechanism of aero6, and the Weather Research and Forecasting Model (WRF)

(version 4.4.2) meteorological fields. Comprehensive descriptions of the CMAQ modeling system are provided by U.S. EPA.¹ Additional descriptions of the SAPRC07 chemistry module and aerosol mechanism of aero6 are provided are available online.² Documentation of the National Center for Atmospheric Research (NCAR) WRF model is available from the University Corporation for Atmospheric Research (UCAR).³

Regional Modeling

The CMAQ air quality modeling platform with SAPRC07 chemistry and WRF meteorology were employed as the primary tool used to demonstrate future year attainment of the PM_{2.5} standard. Simulations are conducted from January 1st to December 31th. Daily average values of PM_{2.5} concentrations were Predicted.

As in the 2022 AQMP, simulations were conducted using a Lambert Conformal grid projection where the western boundary of the domain is at 084 UTM, over 100 miles west of the ports of Los Angeles and Long Beach. The eastern boundary extends beyond the Colorado River, while the northern and southern boundaries of the domain extend to the southern edge of the San Joaquin Valley and the Northern portions of Mexico (3543 UTM). The grid size is 4 x 4 kilometers with 30 vertical layers. Figure II-1-1 depicts the CMAQ modeling domain which includes a grid of 156 cells from west to east and 102 cells from south to north.

¹ <http://www.epa.gov/scram001/>

² <https://intra.engr.ucr.edu/~carter/SAPRC/>

³ <https://www.mmm.ucar.edu/models/wrf>

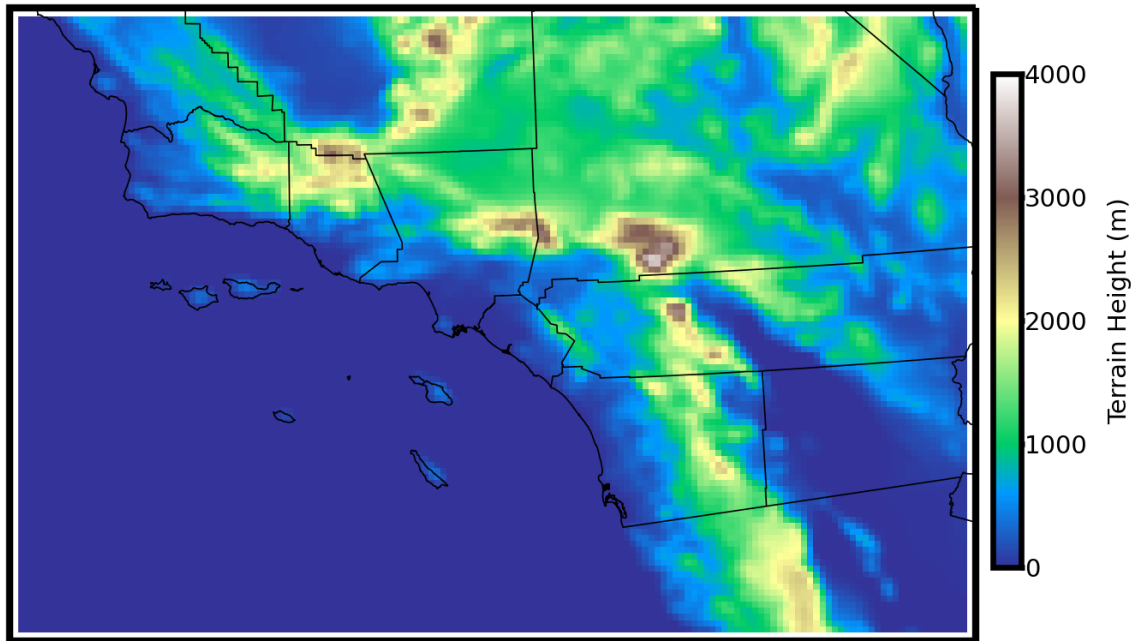


FIGURE II-1-1

CMAQ Regional Modeling Domain for the Draft-PM2.5 Plan

WRF was updated to the most recent version (version 4.4.2) available at the time of this protocol preparation and was evaluated with a set of observation data. The WRF simulations were initialized from National Centers for Environmental Prediction (NCEP) North American Regional reanalysis (NARR) Re-analysis data and run for 4-day increments with the option for four-dimensional data assimilation (FDDA). The atmospheric chemistry package used in the CMAQ simulations relied on SAPRC07 gas phase chemistry with version “c” toluene updates with the AERO6 aerosol mechanism, the Euler Backward Iterative solver, the Yamo horizontal advection scheme, the WRF vertical advection scheme, the multiscale CMAQ horizontal diffusion scheme, the ACM2 vertical diffusion scheme, in-line photolysis calculations, and clean homogeneous initial values.

Relative Response Factors and Future Year Design Values

To bridge the gap between air quality model output evaluation and applicability to the health-based air quality standards, EPA guidance⁴ has proposed the use of relative response factors (RRF). South Coast AQMD developed a tool to calculate the RRF and did not rely on EPA’s MATS/SMAT software. The RRF is simply a ratio of future year predicted air quality with the control strategy fully implemented to the simulated air quality in the base year (U.S. EPA, 2018). For PM2.5 simulations, PM2.5 component-specific

⁴ U.S. EPA (2018) Modeling Guidance for Demonstrating Air Quality Goals for Ozone, PM2.5, and Regional Haze.

relative response factors (RRF) should be calculated for each quarter. The guidance requires that quarterly mean concentrations for each component to be determined among 9 grid cells around a monitoring station if model grid resolution is equal or less than 12km and that the specific grid location be preserved in the future year modeling scenario when calculating. The ratio of base to future year quarterly mean concentrations for each component is the RRF for that component.

The future year design value is estimated by multiplying the non-dimensional RRF to the measured base year design value. Thus, the simulated improvement in air quality, based on multiple meteorological episodes, is translated to a simple metric that directly determines compliance of the standard. Equations II-1-1 and II-1-2 summarize the calculation.

Equation II-1-1:

$$\text{RRF} = \frac{\text{Future Year Model Prediction}}{\text{Base Year Model Prediction}}$$

Equation II-1-2:

$$\text{Future Design Value} = \text{RRF} \times \text{Base Design Value}$$

The modeling analyses described above use the RRF method to project future design values. A future design value less than or equal to the standard constitutes attainment. The RRF approach aims to minimize the effects of biases in the model simulations, thus providing more accurate projections of future air quality.

Modeling Results

Air quality modeling simulations are conducted to quantify the air quality improvements resulting from the measures proposed in the ~~Draft~~ PM2.5 Plan, and to demonstrate that future PM2.5 concentrations will meet the air quality standards. Modeling results show that the measures proposed in this ~~Draft~~ PM2.5 Plan will be able to bring PM2.5 concentrations down and that all areas in the Basin will be in attainment of the 2012 annual PM2.5 standard by 2030.

Uncertainties Associated with the Technical Analysis

As with any attainment plan, there are uncertainties associated with the technical analysis. Uncertainties are inherent to many of the inputs used in the emissions, meteorological and air quality models. Uncertainty in emission projections stem from the uncertainties associated with the demographic and socioeconomic factors, the emission factors and the spatial distribution surrogates used in the development of emissions inventories. Modeling tools also contribute to the uncertainty as all models can only be a limited representation of the real world. Also, uncertainty in the measurements add to the

uncertainty when model performance is assessed. And finally, uncertainty in future climate may also impact our understanding and ability to determine the necessary emission controls to attain the standards. While completely eliminating uncertainties is an impossible task, there are a number of features and practices built into the air quality planning process that manage and control such uncertainties and preserve the integrity of an air quality management plan. These measures include the constant revision of modeling tools and the design of contingency measures that could be enacted in the event that the measures in the Draft PM2.5 Plan do not result in the projected air quality improvements.

Document Organization

This document provides the federal attainment demonstration for PM2.5. Chapter 2 provides the modeling protocol which summarizes the key elements that have been revised relative to the 2022 AQMP modeling protocol. Chapter 3 provides a discussion of the meteorological modeling including a comprehensive model performance evaluation. Chapter 4 provides a brief summary of the modeling emissions, boundary conditions and initial conditions. Chapter 5 discusses the annual PM2.5 attainment demonstration for the 2030 attainment year. The PM2.5 analysis includes discussions of base-year modeling performance, and projections of future year PM2.5 concentrations for baseline emissions. Table II-1-2 lists the Attachments to this document.

TABLE II-1-2
ATTACHMENTS

| Number | Description |
|---------------|---|
| Attachment-1 | WRF Model Performance Time Series |
| Attachment-2 | CMAQ Model Performance Figures |
| Attachment-3 | Emissions Reductions Summary for Future Control Scenarios |

Chapter 2

MODELING PROTOCOL

Background

Attainment Demonstration

Numerical Models

Emissions Processing

Biogenic Emissions

Computational Resources

Background

One of the basic requirements of a modeling attainment demonstration is the development of a comprehensive modeling protocol that defines the scope of the regional modeling analyses. This includes the attainment demonstration methodology, meteorological and chemical transport platforms, gridded and speciated emission inventories, and geographical characteristics of the modeling domains. The protocol also defines the methodology to assess model performance and the selection of the simulation periods. The 2016 AQMP provided a comprehensive discussion of the modeling protocol used for the development of the PM_{2.5} and ozone attainment demonstrations. The 2016 AQMP Modeling Protocol served as the prototype of the Draft 2024 PM_{2.5} Plan modeling protocol. This Draft 2024 PM_{2.5} Plan demonstrates attainment of the 2012 annual PM_{2.5} standard with 2018 as the base year and 2030 as the attainment year. Future attainment years (See Table II-2-1) are identified based on nonattainment designation, pollutant standards, and geographical area.

TABLE II-2-1
UPCOMING ATTAINMENT YEARS FOR THE 2012 ANNUAL PM_{2.5} NAAQS FOR THE SOUTH COAST AIR BASIN

| Attainment Year | Remarks |
|-----------------|--|
| 2018 | Base Year for Modeling and Emissions Projection |
| 2025 | 2012 PM _{2.5} Serious Area Attainment Due |
| 2030 | 2012 PM _{2.5} Serious Area with 5 -year Extension |

Attainment Demonstration

The annual PM_{2.5} attainment demonstration was performed based on the U.S. EPA guidance document, “Modeling Guidance for Demonstrating Air Quality Goals for Ozone, PM_{2.5}, and Regional Haze”, issued on November 29, 2018 (U.S. EPA, 2018). To predict the future annual PM_{2.5} design values, PM_{2.5} component-specific relative response factors (RRF) should be calculated for each quarter. The guidance requires that quarterly mean concentrations for each component to be determined among 9 grid cells around a monitoring station if model grid resolution is equal or less than 12km and that the specific grid location be preserved in the future year modeling scenario when calculating. The ratio of base to future year quarterly mean concentrations for each component is the RRF for that component.

Numerical Models

Table II-2-2 provides a side-by-side comparison of the 2016, 2022 AQMP and the current Draft 2024 PM_{2.5} Plan modeling protocols. In general, changes have occurred in the following categories: emissions inventories, future-year simulations, the level of the non-attainment designation and the attainment demonstration methodology. As such, these changes are expected to occur with each subsequent modeling update. Table II-2-3 highlights the main differences in CMAQ setup since the 2022 AQMP.

TABLE II-2-2

NUMERICAL MODELING PLATFORMS AND DOMAINS FOR 2024 PM2.5 PLAN AND PREVIOUS AQMPS

| | 2016 AQMP | 2022 AQMP | Draft 2024 PM2.5 Plan |
|--------------------------|---|---|---|
| Modeling Base Year | 2012 Ozone: May – Sep PM: Annual | 2018 Ozone: May - Sep | 2018 Entire Year |
| Chemical Transport Model | CMAQ version 5.0.2 | CMAQ version 5.2.1 | CMAQ version 5.3.3 |
| Meteorological Model | WRF version 3.6 with Updated Land Use | WRF version 4.0.3 Unified Noah | WRF version 4.4.2 Pleim-Xiu |
| Emission: On-Road | EMFAC 2014 | EMFAC 2017 | EMFAC 2021 |
| Off-Road | Category Specific Calculation | Category Specific Calculation | Category Specific Calculation |
| Modeling Domain | 624 km by 408 km | 624 km by 408 km | 624 km by 408 km |
| Grid Resolution | 4km by 4km grid | 4km by 4km grid | 4km by 4km grid |
| Vertical Layer | 18 layers with 14 layer below 2000 m AGL and 50 hPa as top boundary | 30 layers with 14 layer below 2000 m AGL and 50 hPa as top boundary | 30 layers with 14 layer below 2000 m AGL and 50 hPa as top boundary |

TABLE II-2-3
CHEMICAL TRANSPORT MODELING PLATFORM FOR THE ~~DRAFT 2024~~ PM2.5 PLAN

| Options | Draft 2024 PM2.5 Plan |
|------------------------------|--|
| Numerical Model | CMAQ version 5.3.3 |
| Modeling Grid | 156 by 102 grids with 4 km grid distance |
| Vertical Layers | 30 layers |
| Gas Phase Chemical Mechanism | SAPRC07 with version “c” toluene updates |
| Aerosol Mechanism | AERO6 |
| Chemical Solver | Euler Backward Iterative solver (EBI) |
| Horizontal Advection | Yamo |
| Vertical Advection | WRF |
| Horizontal Diffusion | Multiscale CMAQ scheme |
| Vertical Diffusion | ACM2 |
| Photolysis | In-line Calculation |
| Initial Values | Clean Homogeneous Condition |
| Boundary Values | Nested modeling with 12km statewide CMAQ The 12km CMAQ domain used boundaries from the global model of Community Atmosphere Model with Chemistry (CAM-chem) |

The Weather Research and Forecast (WRF) model remains the primary tool for meteorological modeling. WRF was updated with the most recent version (version 4.4.2) available and was evaluated with a set of observation data to ensure the accuracy and reliability of meteorological predictions. WRF simulations were conducted with three nested domains with grid resolutions of 36 km, 12 km and 4 km. The innermost domain spans 652 km by 460 km in the east–west and north–south directions, respectively, which includes the greater Los Angeles area, its surrounding mountains, and ocean waters off the coast of the South Coast Air Basin (Figure II-2-1). A Lambert conformal map projection was used with reference latitudes of 30° and 60° N and the center of the modeling domain positioned at 37° N and 120° 30’ W. Details on the WRF model configuration are provided in Chapter 3 of Appendix II.

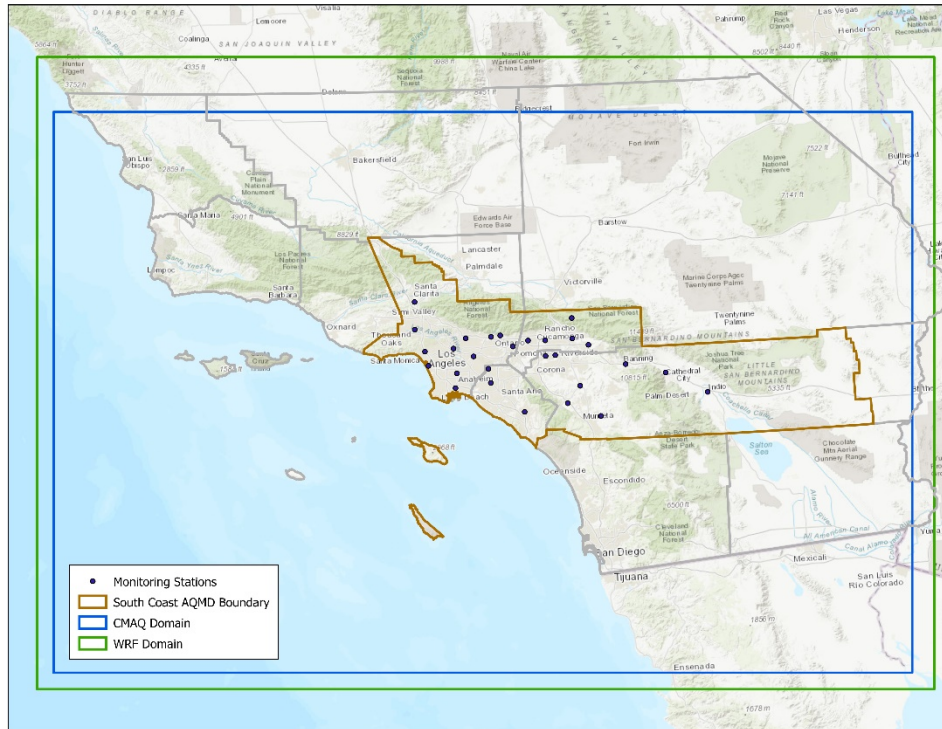


FIGURE II-2-1

THE RELATIVE LOCATIONS OF THE INNER MOST WRF DOMAIN COMPARED TO THE CMAQ DOMAIN. THE BOUNDARY OF SOUTH COAST AQMD JURISDICTION BOUNDARY AND AIR MONITORING LOCATIONS ARE OVERLAID BY A THICK SOLID LINE AND BLACK DOTS, RESPECTIVELY.

Emissions Processing

Emissions inventories are often developed on an annual basis for large geographic areas and a process must be developed to allocate the emissions to a time-dependent grid for use in chemical transport modeling. Traditionally, emissions were allocated to the modeling grid using generic or average activity patterns and profiles. These approaches did not sufficiently reflect the real-world characteristics of emissions sources. Shortcomings of previous emissions allocation methods included an inability to account for traffic flows responding to changes in weather, vessels transiting outside of well-known shipping lanes, or aircraft following airport-specific landing and takeoff trajectories. For these reasons, new approaches were developed to spatially and temporally allocate emissions from on-road mobile sources, Ocean-Going Vessels (OGV), and aircraft. Each method used information from sensor or transponder-based datasets, which accurately reflected where and when emissions were occurring. Further details on the updated allocation methods are presented in Chapter 4 of Appendix II.

TABLE II-2-4

SUMMARY OF EMISSION PROCESSING FOR THE DRAFT 2024-PM2.5 PLAN

| Options | Draft 2024-PM2.5 Plan |
|------------------------|--|
| On-Road Emissions | EMFAC 2021 |
| | Temporal allocation using Caltrans real-time PeMS single loop detector-based traffic data for light & medium-duty vehicles. Heavy-duty vehicle temporal allocation based on PeMS data and an algorithm to detect heavy-duty vehicle classes ¹ |
| Aircraft Emissions | ACARS/GATE ¹ spatial allocation |
| OGV Emissions | AIS-based ² spatial allocation |
| Vehicle Miles Traveled | 2020 Regional Transportation Plan/Sustainable Communities Strategy (RTP/SCS) |
| Off-Road Emissions | Category Specific Calculation |
| Mexico Emissions | CARB's Mexican emissions profile |

¹ Aircraft Communication Addressing and Reporting System (ACARS)/Gridded Aircraft Trajectory Emissions (GATE)

² Automated Identification System

¹ Kwon J, Varaiya P, Skabardonis A. Estimation of Truck Traffic Volume from Single Loop Detectors with Lane-to-Lane Speed Correlation. Transportation Research Record. 2003;1856(1):106-117, <https://doi.org/10.3141%2F1856-11>

TABLE II-2-5

LIST OF EMISSIONS CATEGORIES WITH TEMPORAL PROFILE USED

| Day-Specific Profile | Generic Profile |
|---|---|
| <ul style="list-style-type: none"> • Wildfires¹ • Prescribed burns¹ • Biogenic and On-Road motor vehicle emissions are adjusted using day/hour-specific meteorological data. | <ul style="list-style-type: none"> • Agricultural burning • Residential wood combustion • Facilities • Paved road dust • Unpaved road dust • Windblown dust • Livestock dust |

¹ Wildfires and prescribed burns were modeled using day-specific profiles for the model performance evaluation only. For the attainment demonstration, wildfire emissions were excluded, and prescribed burns were modeled using a generic profile.

Biogenic Emissions

Daily biogenic VOC emissions were calculated using the Model of Emissions of Gases and Aerosols from Nature version 3.0 (MEGAN3.0) using 2018 meteorology as input. MEGAN was executed in its default configuration, except for the normalized Leaf Area Index (LAIv) input. LAIv was developed by the California Air Resources Board using 2018 data from the Moderate Resolution Imaging Spectroradiometer (MODIS) on the National Aeronautical Space Administration’s Terra and Aqua satellites. Because MODIS does not provide data in urban areas, LAIv in these areas was based on tree survey data from the US Forest Service. A detailed description of the biogenic inventory is provided in Chapter 4 of Appendix II.

Computational Resources

The main computation platform employs high performance nodes. New servers, compiled to enhance computational capability, were configured with Red-Hat Enterprise Linux 7 and 64-bit operating systems. Details of the computing resources are summarized in Table II-2-6.

TABLE II-2-6
DETAILS OF COMPUTATIONAL RESOURCES USED IN THE 2016, 2022 AQMPS AND THE DRAFT 2024
PM2.5 PLAN

| 2016 AQMP | 2022 AQMP | Draft 2024 PM2.5 Plan |
|---|--|---|
| <ul style="list-style-type: none"> • HP DL560 G8, 64 bit 4x8 cores • HP DL560 G8, Total 320 processors • HP DL560 G8 Total 64 processors | <ul style="list-style-type: none"> • HP DL380 G10, 64 bit 2x16 cores • HPE DL380 G10 Total 320 processors • HP DL560 G8, Total 256 processors | <ul style="list-style-type: none"> • Same as 2022 AQMP |

Chapter 3

METEOROLOGICAL MODELING

Overview

Comparison of 2018 Observed Meteorology to 10-Year Average

Modeling Configuration

Model Performance Evaluation: Surface Level

Model Performance Evaluation: Diurnal Variations

Model Performance Evaluation: Wind Rose

Model Performance Evaluation: Planetary Boundary Layer Height

Sensitivity Test of Planetary Boundary Layer Scheme

Summary

Overview

This chapter provides a description of the meteorological modeling that serves as the foundation of the ~~Draft 2024~~ PM2.5 plan modeling analysis. The Weather Research and Forecasting (WRF) model was used to generate meteorological fields for further modeling analysis. The model offers a variety of user options to cover atmospheric boundary layer parameterizations, turbulent diffusion, cumulus parameterizations, land surface-atmosphere interactions, which can be customized to specific geographical and climatological situations. South Coast AQMD staff performed extensive sensitivity tests and developments to improve WRF performance for the South Coast Air Basin, where prediction of complex meteorological structures associated with air quality episodes is particularly challenging due to the region's unique geography and climate. This chapter describes the numerical configuration, sensitivity test on key parameterizations, input database, and initial and boundary values used in the ~~Draft 2024~~ PM2.5 Plan modeling analysis.

Comparison of 2018 Observed Meteorology to 10-Year Average

Meteorological data from airport weather stations across the Basin and the Coachella Valley were used to assess differences between regional weather patterns observed in 2018 and average conditions from 10 years (2013-2022). The 15 weather stations used for this analysis were Los Angeles International Airport (LAX), Santa Monica Municipal Airport (SMO), Hawthorne Municipal Airport (HHR), Long Beach Airport (LGB), John Wayne Airport (SNA), Fullerton Municipal Airport (FUL), Chino Airport (CNO), Ontario International Airport (ONT), Riverside Municipal Airport (RAL), March Air Reserve Base (RIV), Palm Springs International Airport (PSP), Burbank Bob Hope Airport (BUR) and Van Nuys Airport (VNY). The location of the stations is shown in Figure II-3-1. Comparisons of 2018 and 2013-2022 daily total rain, daily average wind speed, relative humidity and temperature at the station of LAX are shown as examples in Figures II-3-2 through II-3-5. Comparisons for all other stations are included in Attachment 1 of Appendix II.

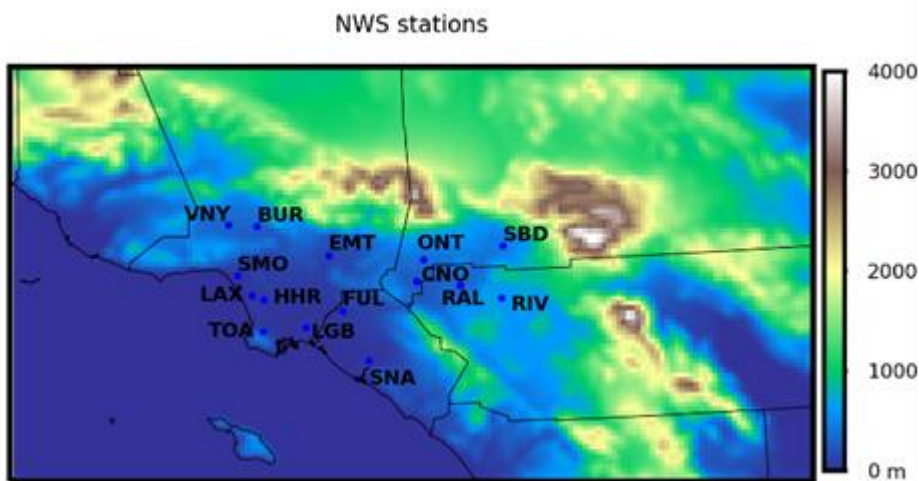


FIGURE II-3-1

15 NATIONAL WEATHER SERVICE (NWS) STATIONS AND TOPOGRAPHY IN THE BASIN

As shown in Figure II-3-2, the daily total rain at the station of LAX recorded higher precipitation for some years such as 2017, 2019 and 2021. Lower precipitation is observed during years such as 2013 and 2022. Typically, the first quarter and the 4th quarter of the year are the rain seasons. For example, the first quarter of 2017 and the last quarter of 2021 observed more than 2 inches daily total rain. There are more rain days with > 1 inch daily total rain in the year of 2019 from both first quarter and 4th quarter. On the other side, the year of 2013 is dry and observed the lowest rain amount comparing with other years. Regarding both precipitation days and rain amount, the year of 2018 observed values between the lower and the higher values among the 10 years precipitation record. Figure II-3-3, II-3-4, and II-3-5 are normalized histogram of daily average at station of LAX in 2018 and the 10-year (2013-2022) for wind speed, relative humidity, and temperature respectively. The higher value range for the above three variables in 2018 are in line with the counterparts from the 10 years observations. The histogram of 2018 didn't show much shifting to the higher or the lower values comparing with the 10 years normalized histogram. For example, the higher wind speed is in the 2.5 m/s - 4 m/s range for both 2018 and the 10 years observations. The higher relative humidity is in the 65% - 85% range for both 2018 and the 10 years observations.

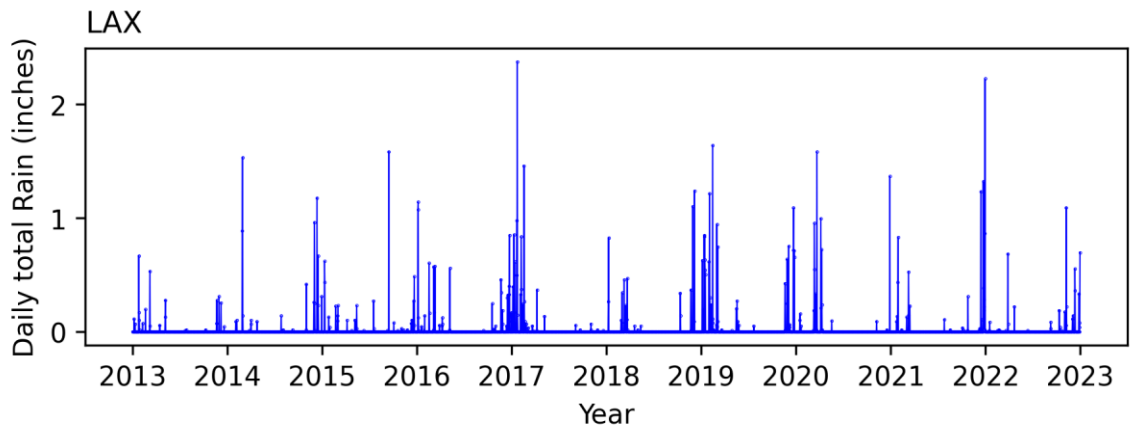


FIGURE II-3-2
DAILY TOTAL RAIN AT STATION OF LAX DURING 2013 - 2022

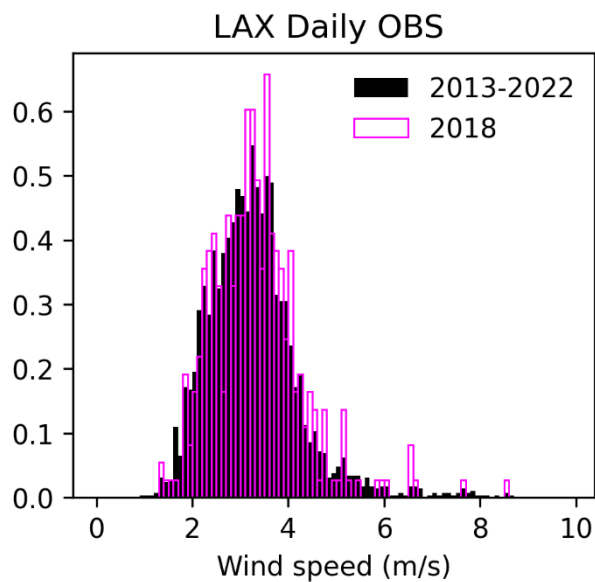


FIGURE II-3-3
NORMALIZED HISTOGRAM OF DAILY AVERAGE WIND SPEED AT STATION OF LAX IN 2018 AND THE 10-YEAR (2013-2022)

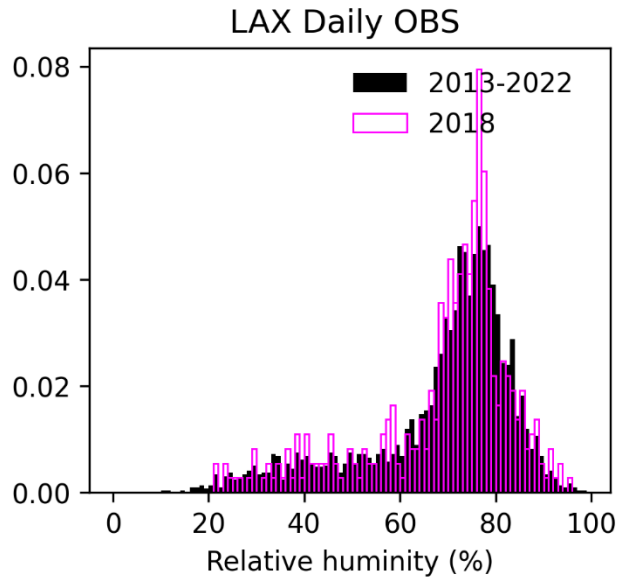


FIGURE II-3-4

NORMALIZED HISTOGRAM OF DAILY AVERAGE RELATIVE HUMIDITY AT STATION OF LAX IN 2018 AND THE 10-YEAR (2013-2022)

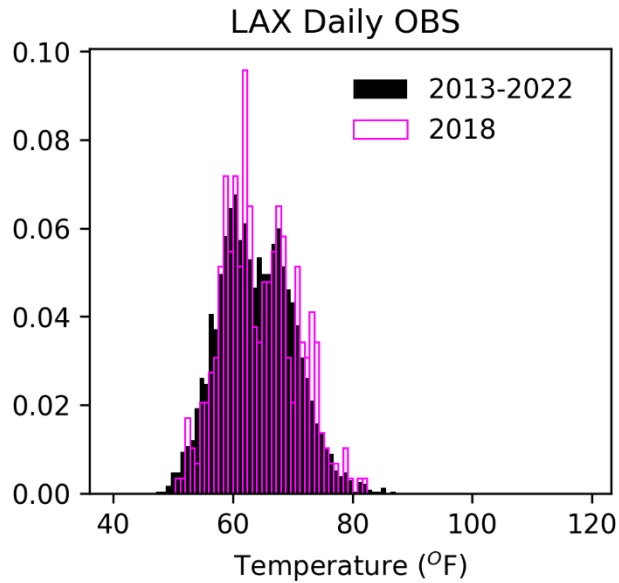


FIGURE II-3-5

NORMALIZED HISTOGRAM OF DAILY AVERAGE TEMPERATURE AT STATION OF LAX IN 2018 AND THE 10-YEAR (2013-2022)

Modeling Configuration

The WRF model is one of the most widely used meteorological models for both operational forecasting and research applications. WRF has been applied to a wide range of phenomena across geographic scales from tens of meters to thousands of kilometers, such as regional climate, monsoons, baroclinic waves, mesoscale fronts, hurricanes, deep convection, land-sea breezes, mountain-valley circulations, large eddy simulations, and fire events. The model is supported by the National Center for Atmospheric Research (NCAR) and actively developed by a worldwide user community. The WRF system contains two dynamical solvers, referred to as the ARW (Advanced Research WRF) core and the NMM (Nonhydrostatic Mesoscale Model) core. The ARW configuration was used for the Draft 2024 PM2.5 Plan modeling analysis. The ARW is primarily developed and maintained by the NCAR Mesoscale and Microscale Meteorology Laboratory.

The WRF model is a fully compressible and nonhydrostatic model (with a run-time hydrostatic option). For vertical coordinate, the model uses either a terrain-following (TF) or hybrid vertical coordinate (HVC). The grid staggering is the Arakawa C-grid¹ (Skamarock, W. C., 2019). It uses a time-split small step for acoustic and gravity-wave modes. The dynamics conserve scalar variables. The WRF is designed to be a flexible, state-of-the-art atmospheric simulation system that is portable and efficient on parallel computing platforms.

The WRF simulation domain designed for the Draft 2024 PM2.5 Plan encompasses the greater Los Angeles and suburban areas, its surrounding mountains, and ocean off the coast of the Basin, as shown in Figure II-3-6. WRF simulations were conducted with three nested domains at grid resolutions of 36 km, 12 km, and 4 km. The innermost domain has 163 by 115 grid points, which span 652km by 460km in east-west and north-south directions, respectively. Figure II-3-6 also shows the relative locations and sizes of the three nested grids. The innermost domain presented in Figure II-3-6, excluding three boundary columns and rows, served as the CMAQ (Community Multiscale Air Quality Model) chemical transport modeling domain.

The WRF simulation employed 30 layers vertically with the lowest computational layer at approximately 20 m above ground level (agl) and the top layer at 50 hPa. Four-Dimensional Data Assimilation (FDDA) was conducted using grid analysis data enhanced with available surface and vertical sounding data. Sea surface temperatures (SST) are a critical control on the land-sea breeze and up-slope/down-slope flow. SST data from the Global Data Assimilation Experiment (GODAE) were used to update the WRF modeling every 6 hours to better represent the sea surface temperature. The Yon-Sei University (YSU) scheme² (Hong and

¹ Skamarock, W. C., J. B. Klemp, J. Dudhia, D. O. Gill, Z. Liu, J. Berner, W. Wang, J. G. Powers, M. G. Duda, D. M. Barker, and X.-Y. Huang (2019). A Description of the Advanced Research WRF Version 4. NCAR Tech. Note NCAR/TN-556+STR, 145 pp.
doi:10.5065/1dfh-6p97

² Hong, S.-Y., and H.-L. Pan (1996). Nonlocal boundary layer vertical diffusion in a medium-range forecast model. *Mon. Wea. Rev.*, 124, 2322–2339, doi:10.1175/1520-0493

Pan, 1996) was used to model the planetary boundary layer (PBL). The flowchart (Figure II-3-7) of WRF simulation shows the meteorology input data, processing steps, observation nudging, and one-way nesting for high resolution inner domain.

After careful testing of different WRF physics options, the longwave radiation scheme of Rapid Radiative Transfer Model (RRTM)³, the shortwave radiation scheme of Dudhia⁴ and WRF Single-Moment 3-class scheme of micro physics were chosen for simulations. Kain-Fritsch cumulus schemes⁵ were used in all three domains. The Pleim-Xiu land surface model (LSM) is used.

³ Mlawer, E. J., S. J. Taubman, P. D. Brown, M. J. Iacono, and S. A. Clough (1997). Radiative transfer for inhomogeneous atmosphere: RRTM, a validated correlated-k model for the longwave. *J. Geophys. Res.*, 102 (D14), 16 663 - 16 682.

⁴ Dudhia, J. (1989), Numerical study of convection observed during the winter monsoon experiment using a mesoscale two-dimensional model, *J. Atmos. Sci.*, 46(20), 3077–3107, doi:10.1175/1520-046919890463C3077:NSOCOD3E2.0.CO;2. 16 682.

⁵ Kain, J.S. (2004). The Kain–Fritsch Convective Parameterization: An Update. *J. Appl. Meteor.*, 43, 170–181.

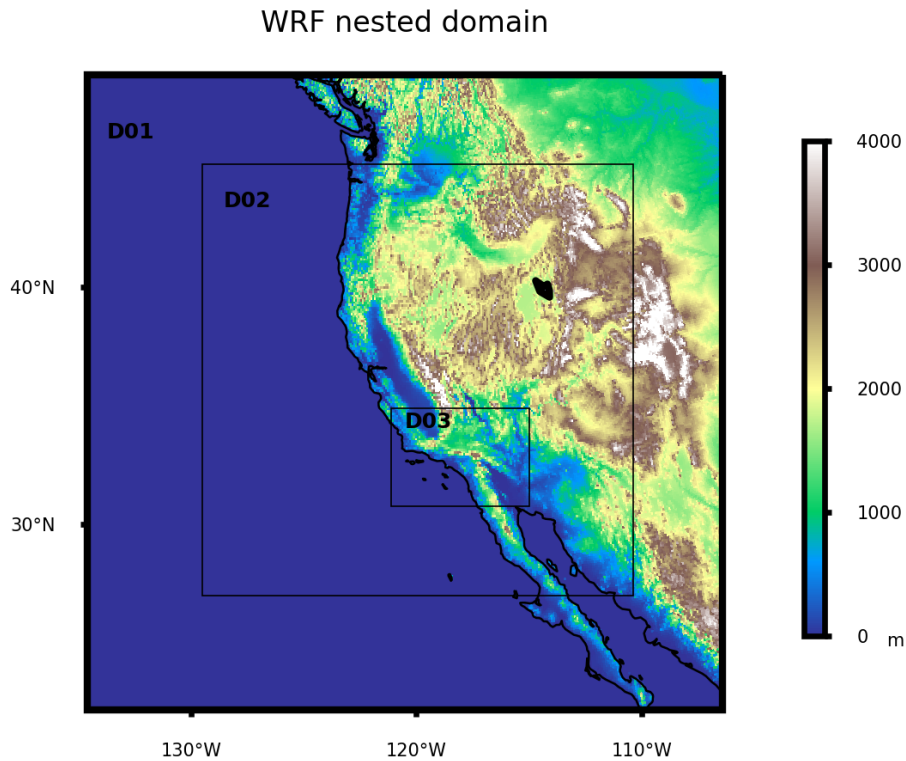


FIGURE II-3-6

THREE NESTED MODELING DOMAINS EMPLOYED IN THE WRF SIMULATIONS. COLOR SCALE INDICATES ELEVATION.

Table II-3-1 below provides a summary of the WRF configuration of the major options relevant for air quality modeling used for the Draft 2024 PM2.5 Plan in comparison with the 2022 AQMP. Major parameters used for the Draft 2024 PM2.5 Plan are similar to those used for the 2022 AQMP.

TABLE II-3-1
OVERVIEW OF WRF CONFIGURATION FOR DRAFT 2024-PM2.5 PLAN IN COMPARISON WITH 2022 AQMP

| Component | 2022 AQMP | Draft 2024-PM2.5 Plan |
|--------------------------------|--|-----------------------|
| Numerical Platform | WRF v4.0.3 | WRF v4.4.2 |
| Number of domains | 3 nested domains | |
| Nested Domain setting | D01: 36 km (83 X 83) | |
| | D02: 12 km (169 X 169) | |
| | D03: 4 km (163 X 115) | |
| Number of vertical layers | 30 layers, the lowest layer is at ~ 20 m agl. | |
| Simulation Length | 4 days with 24-hour spin-up | |
| Initial and boundary values | NCEP NARR ¹ Re-analysis (32 km X 32 km) | |
| Sea Surface Temperature | GHRSSST ² | |
| Boundary layer scheme | YSU ³ scheme | |
| Land Surface model | Unified Noah | Pleim-Xiu |
| Cumulus parameterization | Kain-Fritsch | |
| Micro physics | WRF Single-Moment 3-class | |
| Radiation | RRTM scheme for longwave, Dudhia scheme for shortwave | |
| Four-dimensional data analysis | Analysis nudging with NWS surface and upper air Measurements | |

¹NARR - North American Regional Reanalysis

²GHRSSST - The Group for High Resolution Sea Surface Temperature (<https://www.ghrsst.org/>)

³YSU - Yon-Sei University

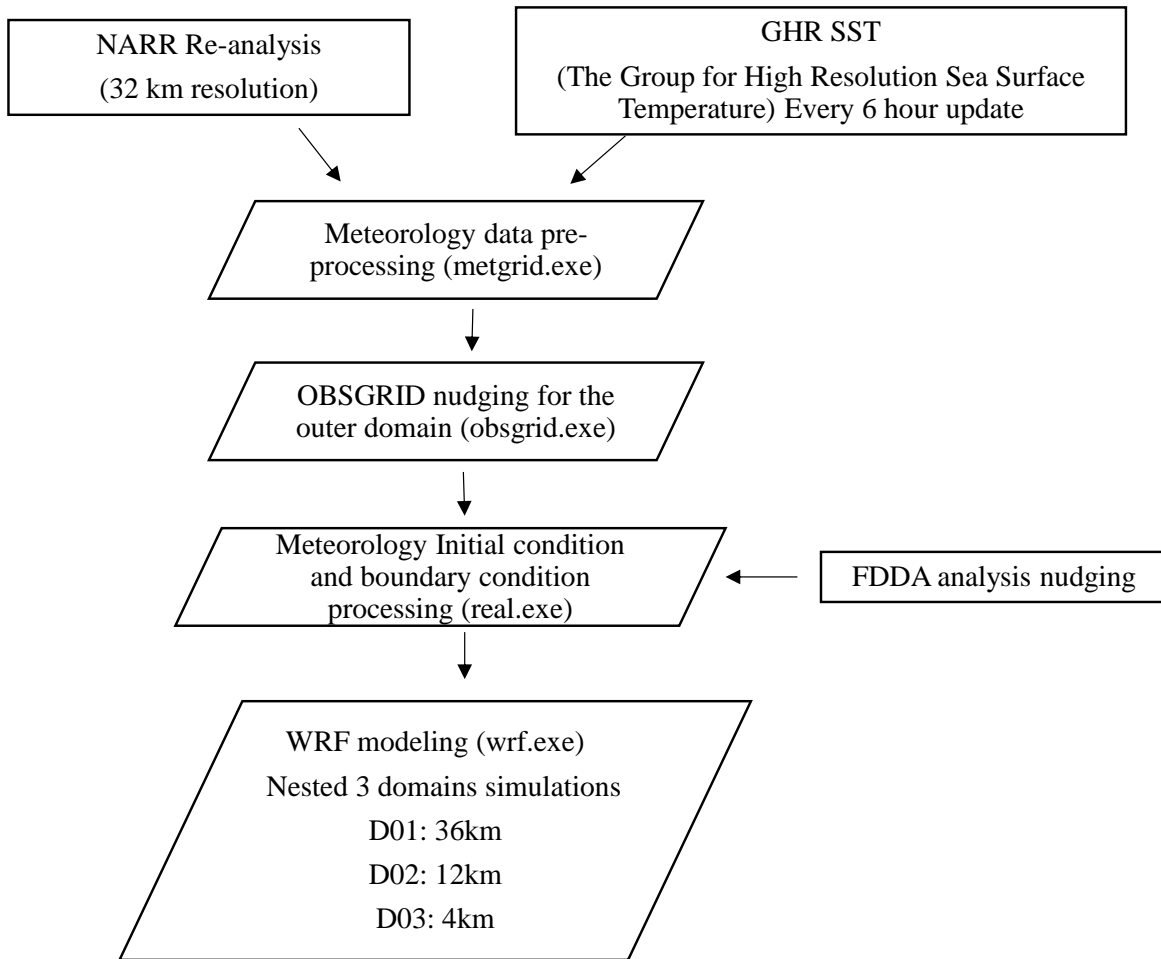


FIGURE II-3-7

FLOWCHART OF WRF SIMULATION FOR 2024 DRAFT PM2.5 PLAN

Model Performance Evaluation: Surface Level

The performance of the WRF simulations is summarized in Table II-3-2 for 4 quarters of 2018. All the results shown in Table II-3-2 are averaged values for the 15 airport weather stations. Overall, WRF simulations for 4 quarters provided representative meteorological fields that well characterized observed conditions in 2018. These fields were used directly in the CMAQ joint particulate simulations.

The performance of WRF simulations used as transport fields for CMAQ modeling is shown in Figure II-3-8 through Figure II-3-16. The model performance was evaluated for each month at airport stations in the model domain for January through December 2018. For simplicity, only one summer month (July) and one winter month (January) are shown in Figure II-3-8 through Figure II-3-16.

Three weather stations are carefully selected from near coastal areas (HHR, Hawthorne municipal Airport) through inland Orange County (FUL, Fullerton Municipal airport) to further east in San Bernardino County (CNO, Chino Airport) for surface level model performance evaluations. Diurnal variations of temperature,

humidity and surface wind were well represented by the WRF simulations. Temperature and wind speed predictions were more accurate in the summer season than the winter months (Figure II-3-8 – Figure II-3-13). The observed temperature gradient from the coastal station of HHR to the inland station of CNO was also well characterized by the WRF model. Median observed summer temperatures in 2018 were 296.6, 298.7, and 300.9 K at HHR, FUL and CNO, respectively. The WRF model showed similar median temperature for these stations. Temperature is one of the key factors for atmospheric photochemical reactions, and high temperature is favorable for ozone formation. For the stations of CNO, the WRF simulations showed slight underestimation of daily high temperatures during July 2018. At the station of FUL and HHR, the WRF simulation showed better performance in predicting daily high temperatures in the summer. During the winter, daily high temperature predictions were closer to observed values during the 2nd half of January 2018 at all three stations. While the model tended to overpredict the daily minimum temperatures during the 2nd half of January 2018 at CNO and FUL.

Both observational data and WRF simulations at all stations showed distinct diurnal variations in wind speed during the summer, with a strong sea breeze in the early afternoon. Mostly, stronger wind speed indicates less accumulation of air pollutants. Daily maximum wind speeds were relatively consistent throughout July 2018, with much more variability observed during January 2018 (e.g., range of daily maximum wind speeds from ~2-13 m/s during January at CNO from both measurements and simulations). The model performance in predicting the wind speed was significantly better for July 2018 compared to January 2018 at all stations; R values for model-observation correlations were 0.81, 0.70, and 0.78 in July 2018 at CNO, FUL, and HHR stations, respectively. It is noticed that the model underestimated daily maximum wind speeds at the HHR station during July 2018.

The WRF model predicted water vapor mixing ratio trends well at all stations. The WRF simulations yield water vapor mixing ratios comparable to observed values in both January and July. The model-observation correlation coefficients are 0.85, 0.87, and 0.89 in January 2018 and 0.72, 0.70, and 0.71 in July 2018 at CNO, FUL, and HHR stations, respectively.

TABLE II-3-2

WRF PERFORMANCE STATISTICS FOR QUARTER AVERAGE OF 2018 AT 15 NWS STATIONS

| | Statistic | Q1 | Q2 | Q3 | Q4 |
|----|-----------------------------|-------|-------|-------|-------|
| T | T Mean Observation (K) | 288.1 | 291.8 | 297.8 | 290.4 |
| | T Mean Simulation (K) | 287.1 | 292 | 297.4 | 289.6 |
| | T Bias (K) | -1 | 0.2 | -0.3 | -0.8 |
| | T Gross Error (K) | 2 | 1.4 | 1.4 | 1.7 |
| | T RMSE (K) | 2.7 | 1.9 | 1.9 | 2.3 |
| | Q Mean Observation (K) | 5.8 | 8.1 | 10.8 | 6.6 |
| Q | Q Mean Simulation (K) | 6 | 8.5 | 12.2 | 7.3 |
| | Q Bias (K) | 0.3 | 0.4 | 1.4 | 0.7 |
| | Q Gross Error (K) | 1 | 0.9 | 1.7 | 1.3 |
| | Q RMSE (K) | 1.5 | 1.3 | 3 | 2 |
| | WS Mean Observation (kg/kg) | 2 | 2.7 | 2.6 | 1.9 |
| WS | WS Mean Simulation (kg/kg) | 2.1 | 2.5 | 2.5 | 1.9 |
| | WS Bias (kg/kg) | 0.1 | -0.2 | -0.1 | 0 |
| | WS Gross Error (kg/kg) | 1.4 | 1.2 | 1.1 | 1.4 |
| | WS RMSE (kg/kg) | 1.8 | 1.6 | 1.4 | 1.9 |

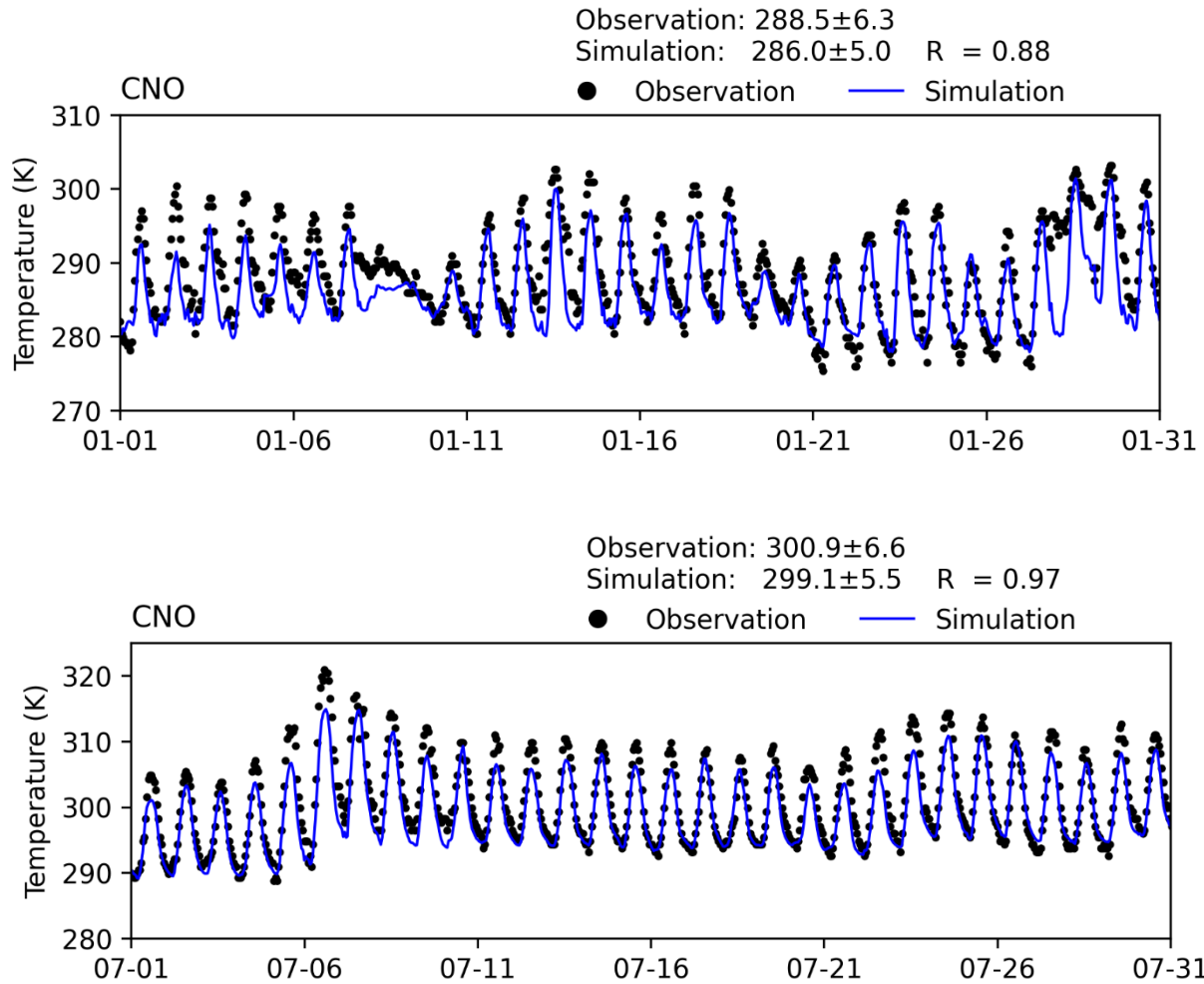


FIGURE II-3-8

TIME SERIES OF HOURLY TEMPERATURE FROM MEASUREMENT AND WRF SIMULATIONS AT CHINO (CNO) STATION FOR JANUARY 2018 AND JULY 2018

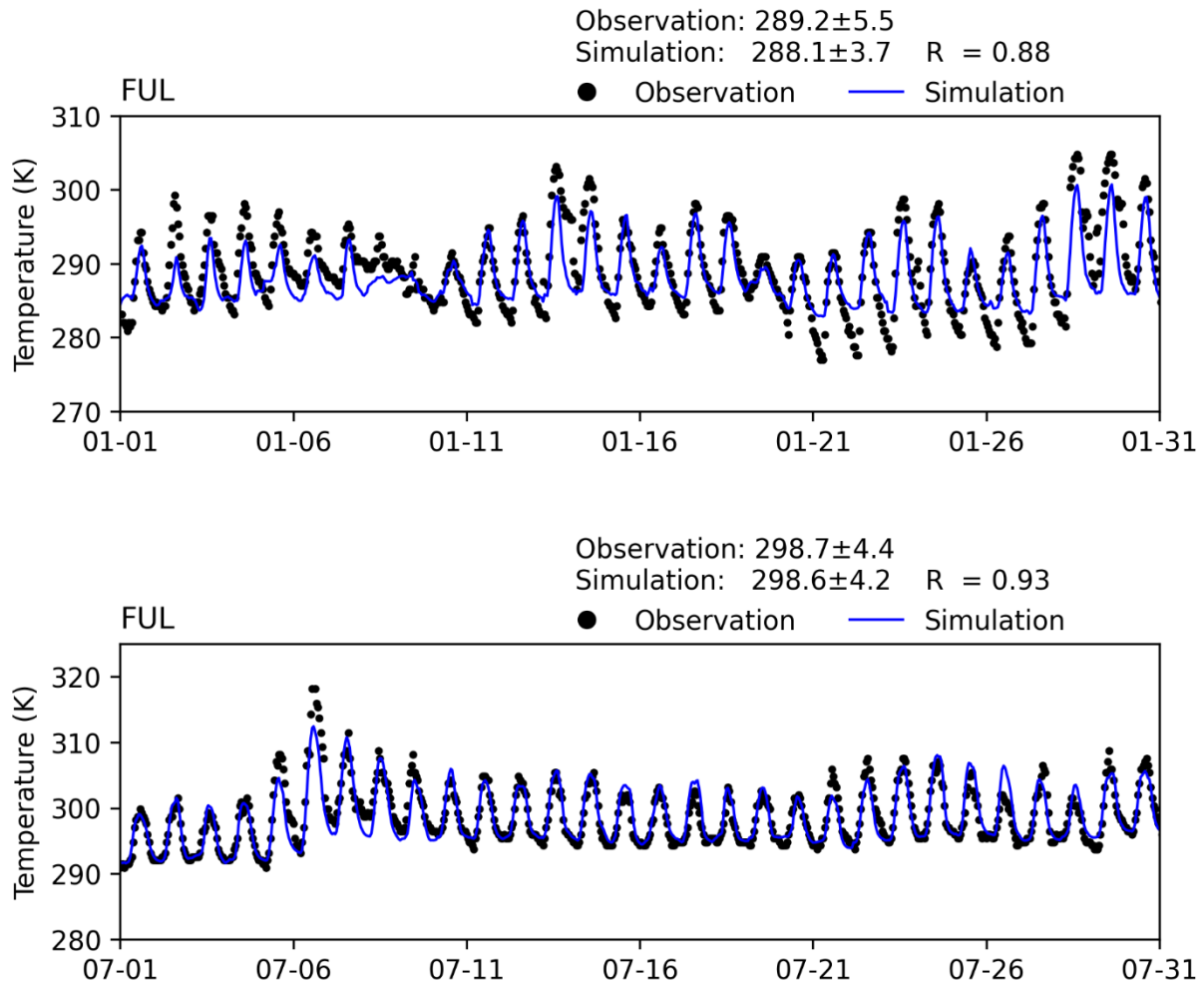


FIGURE II-3-9

TIME SERIES OF HOURLY TEMPERATURE FROM MEASUREMENTS AND WRF SIMULATIONS AT FULLERTON (FUL) STATION FOR JANUARY 2018 AND JULY 2018

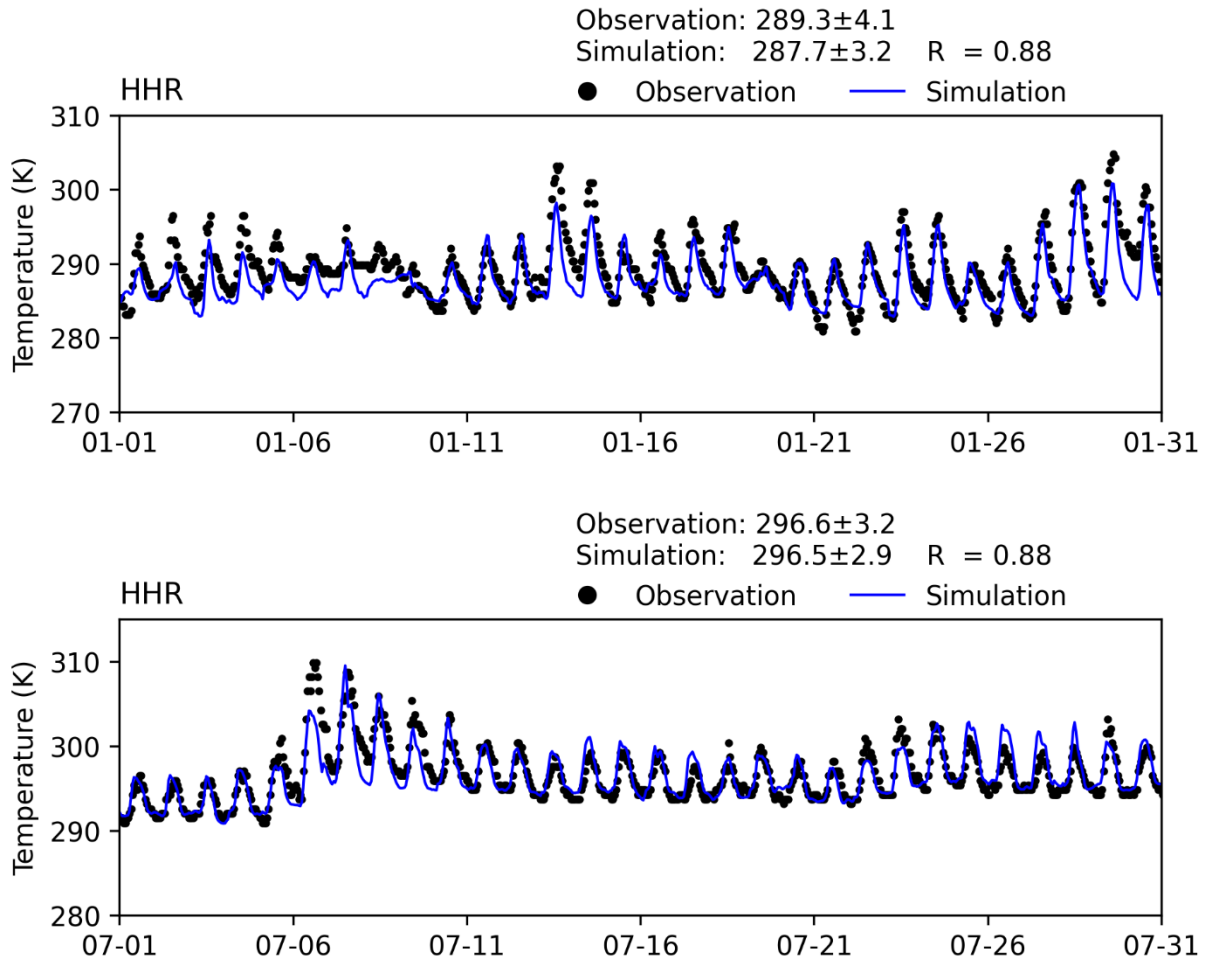


FIGURE II-3-10

TIME SERIES OF HOURLY TEMPERATURE FROM MEASUREMENTS AND WRF SIMULATIONS AT HAWTHORNE (HHR) STATION FOR JANUARY 2018 AND JULY 2018

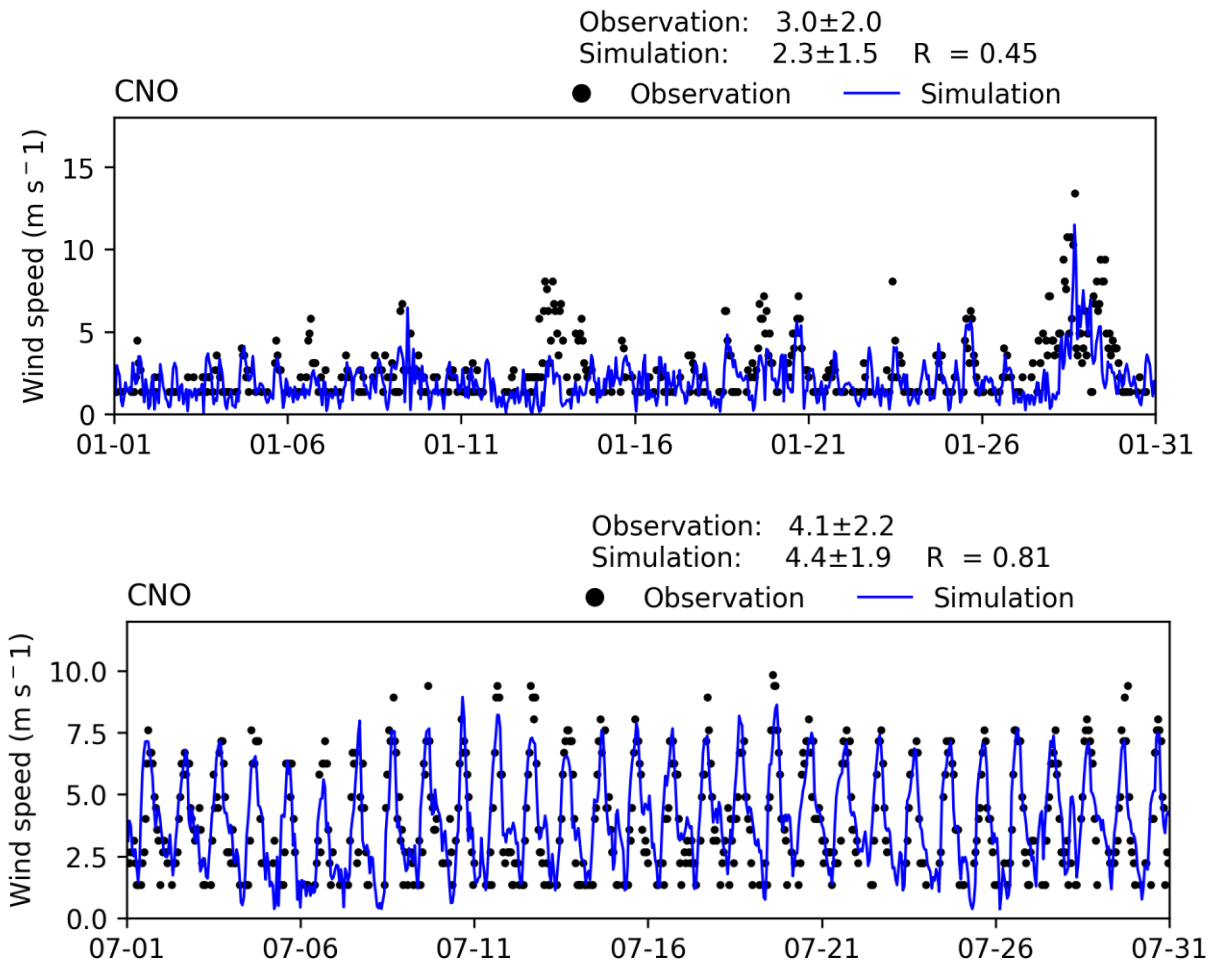


FIGURE II-3-11

TIME SERIES OF HOURLY WIND SPEED FROM MEASUREMENTS AND WRF SIMULATIONS AT CHINO (CNO) STATION FOR JANUARY 2018 AND JULY 2018

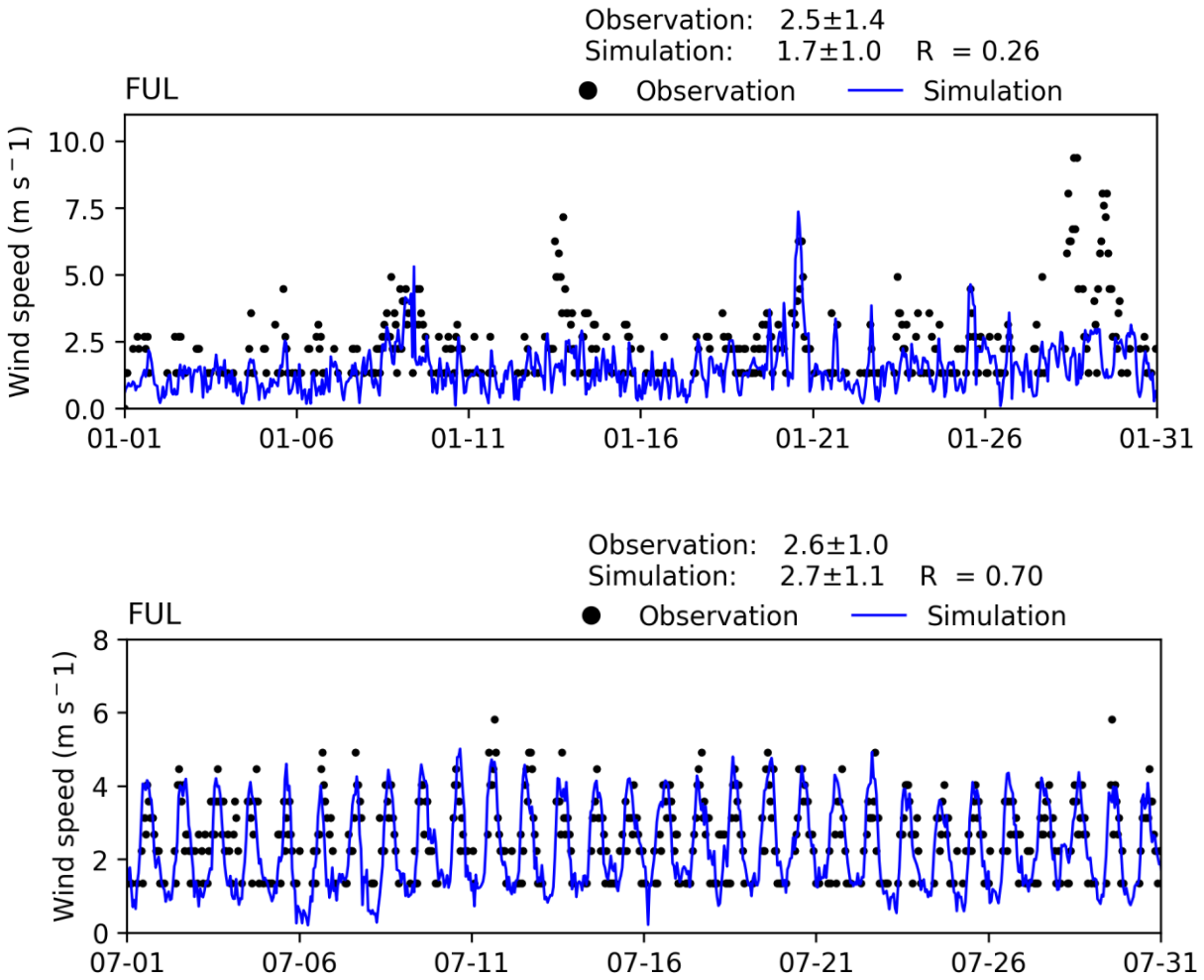


FIGURE II-3-12

TIME SERIES OF HOURLY WIND SPEED FROM MEASUREMENTS AND WRF SIMULATIONS AT FULLERTON (FUL) STATION FOR JANUARY 2018 AND JULY 2018

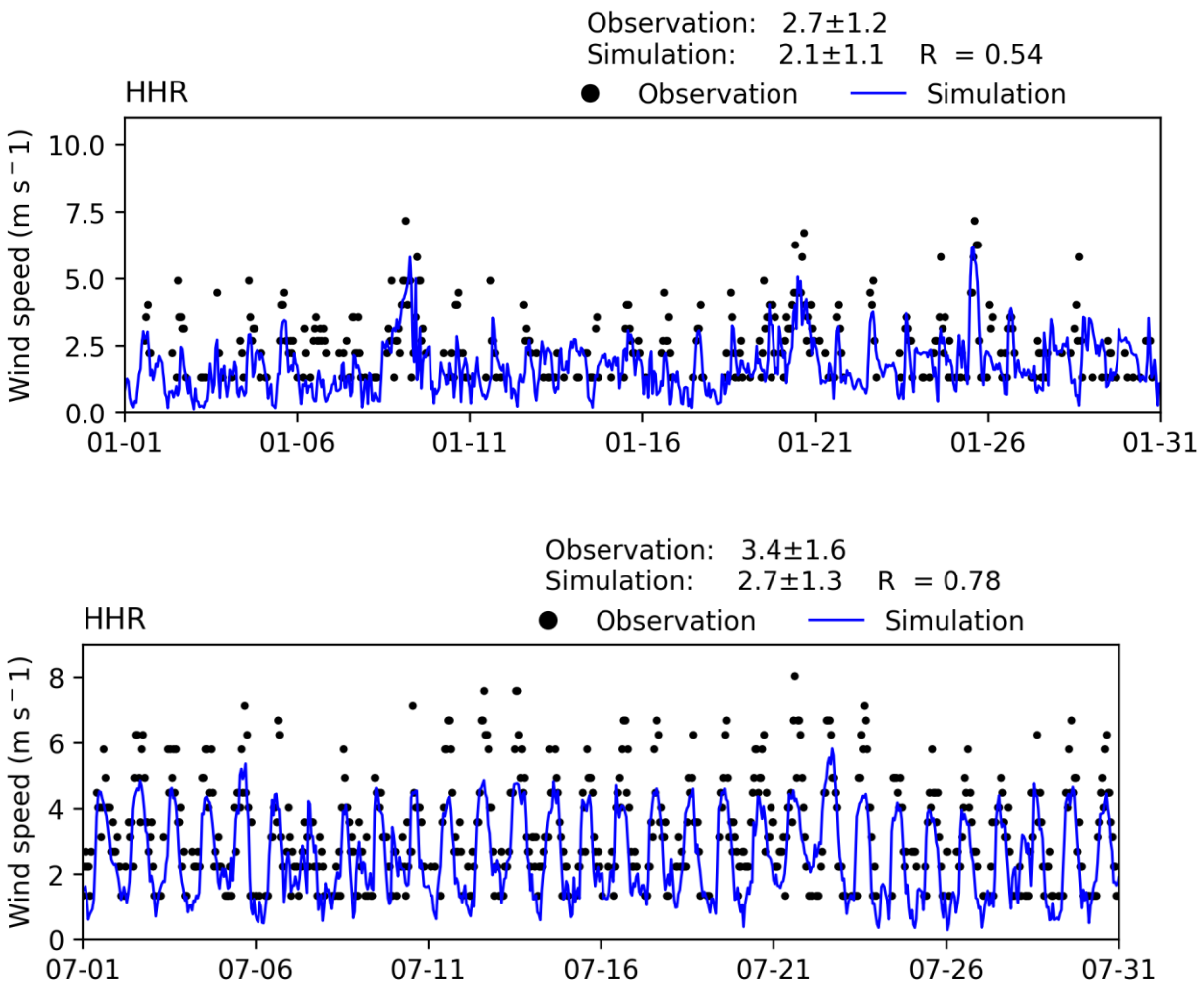


FIGURE II-3-13

TIME SERIES OF HOURLY WIND SPEED FROM MEASUREMENTS AND WRF SIMULATIONS AT HAWTHORNE (HHR) STATION FOR JANUARY 2018 AND JULY 2018

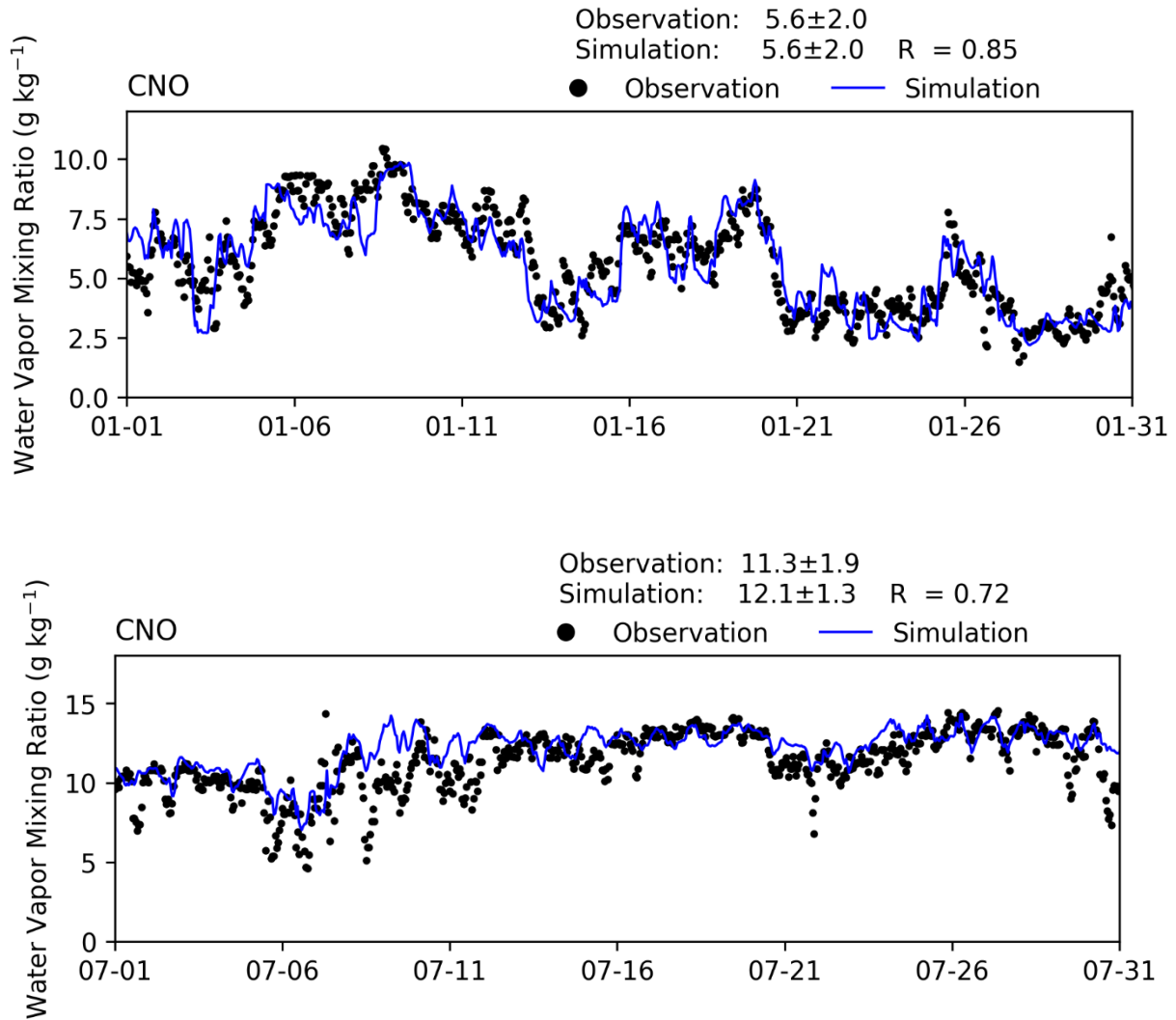


FIGURE II-3-14

TIME SERIES OF HOURLY WATER VAPOR MIXING RATIO FROM MEASUREMENTS AND WRF SIMULATIONS AT CHINO (CNO) STATION FOR JANUARY 2018 AND JULY 2018

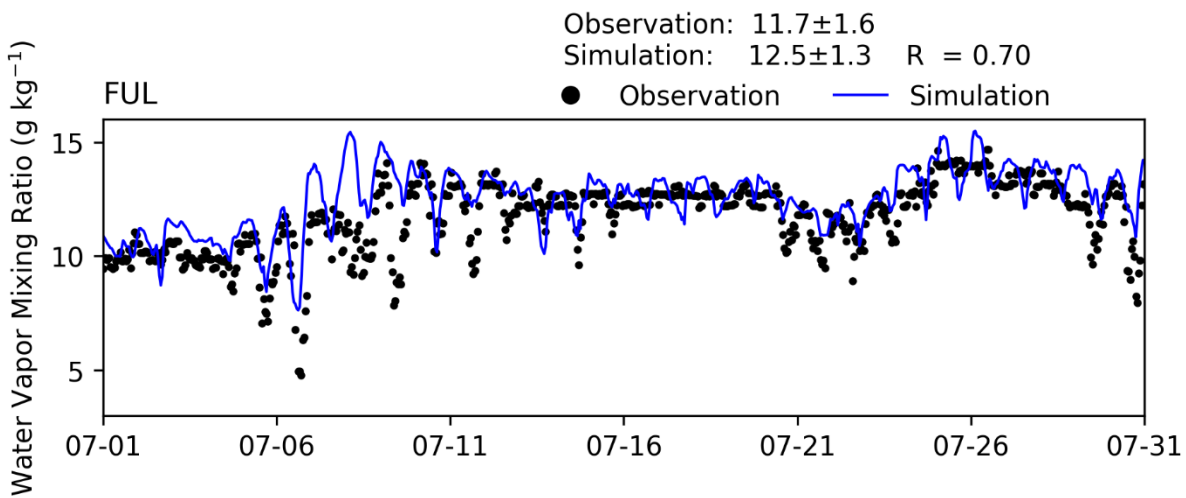
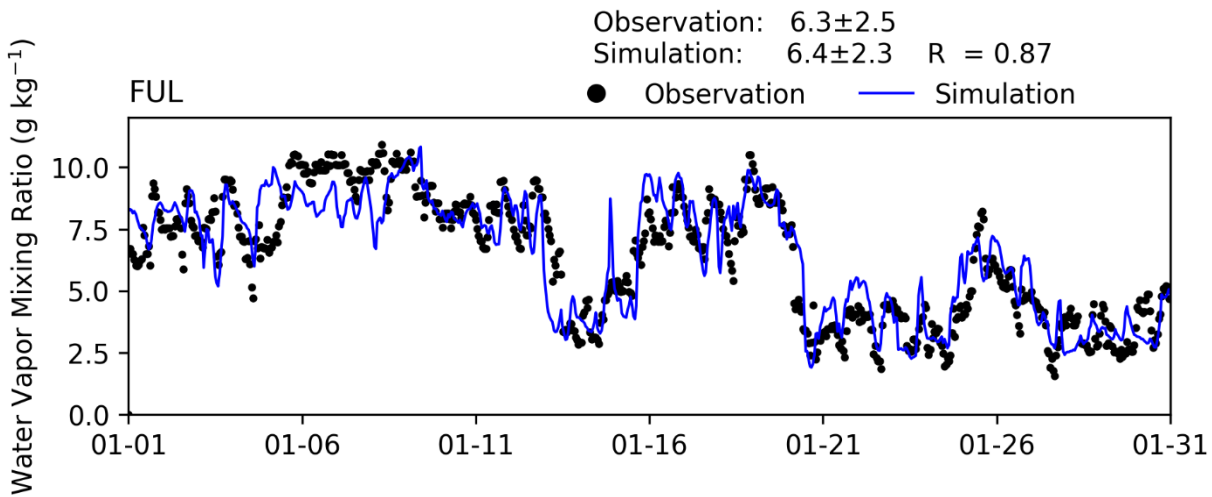


FIGURE II-3-15

TIME SERIES OF HOURLY WATER VAPOR MIXING RATIO FROM MEASUREMENTS AND WRF SIMULATIONS AT FULLERTON (FUL) STATION FOR JANUARY 2018 AND JULY 2018

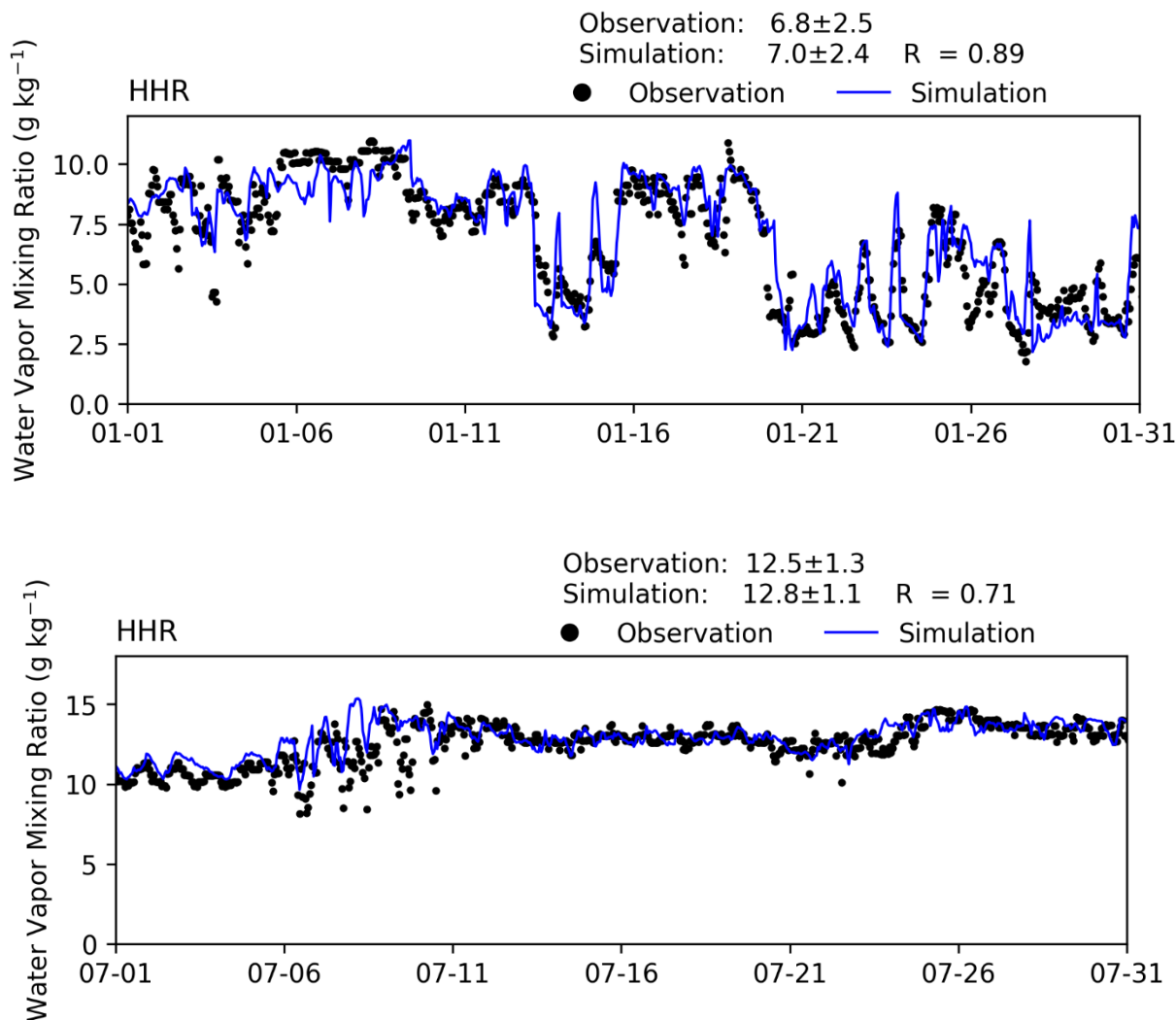


FIGURE II-3-16

TIME SERIES OF HOURLY WATER VAPOR MIXING RATIO FROM MEASUREMENTS AND WRF SIMULATIONS AT HAWTHORNE (HHR) STATION FOR JANUARY 2018 AND JULY 2018

Model Performance Evaluation: Diurnal Variations

Comparisons of simulated and measured monthly average diurnal temperature and water vapor mixing ratio variations at the Fullerton (FUL) station are shown in Figure II-3-17 and Figure II-3-18. Seasonal differences between summer and winter, as represented by July and January, respectively, and diurnal patterns were well reproduced in the WRF simulation. For example, daily temperatures in both observed and simulated diurnal profiles peaked around 14:00 local time during summer (~ 297 K) and winter (~ 290 K). Water vapor mixing ratios did not exhibit distinct diurnal variation in either observed or simulated data.

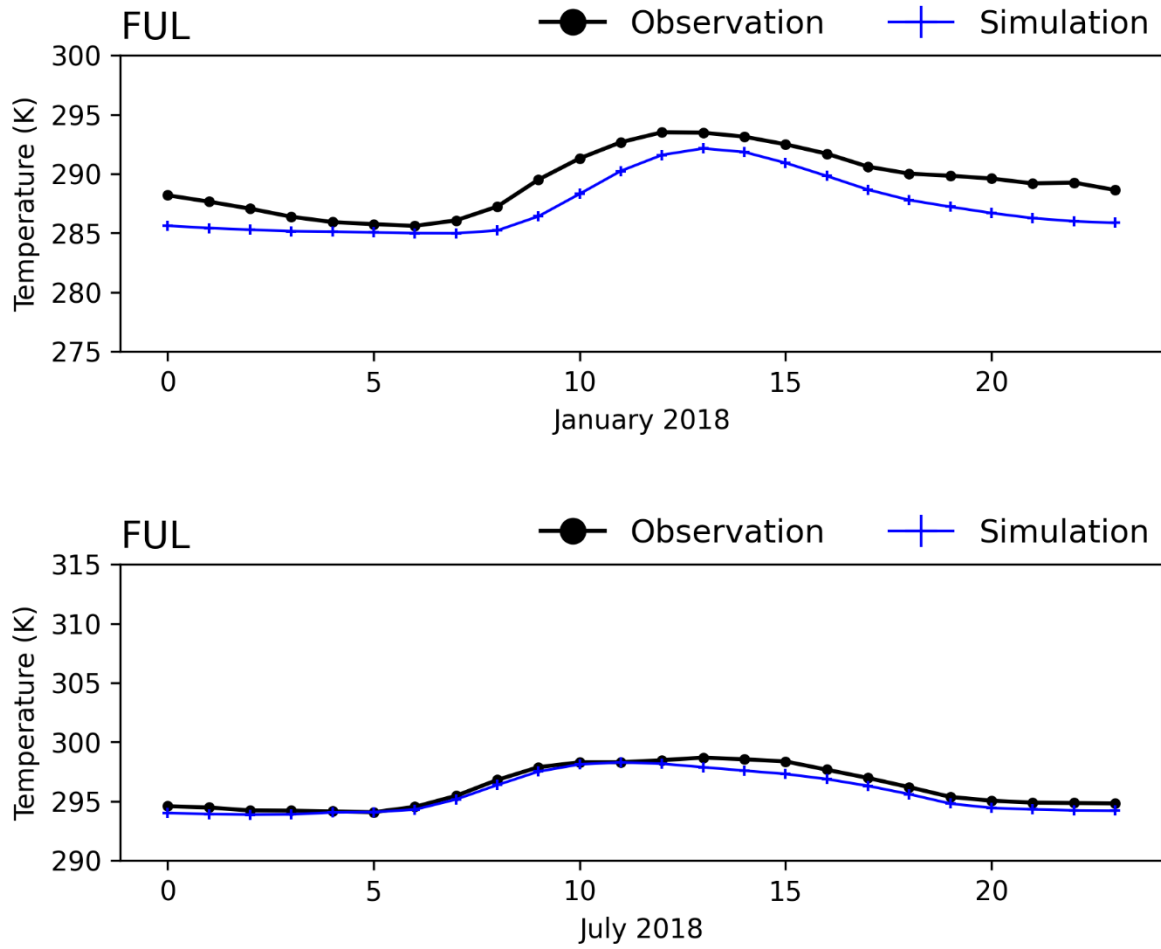


FIGURE II-3-17

MEASURED VS. SIMULATED COMPOSITE DIURNAL TEMPERATURE VARIATION AT FULLERTON (FUL) STATION FOR JANUARY 2018 AND JULY 2018

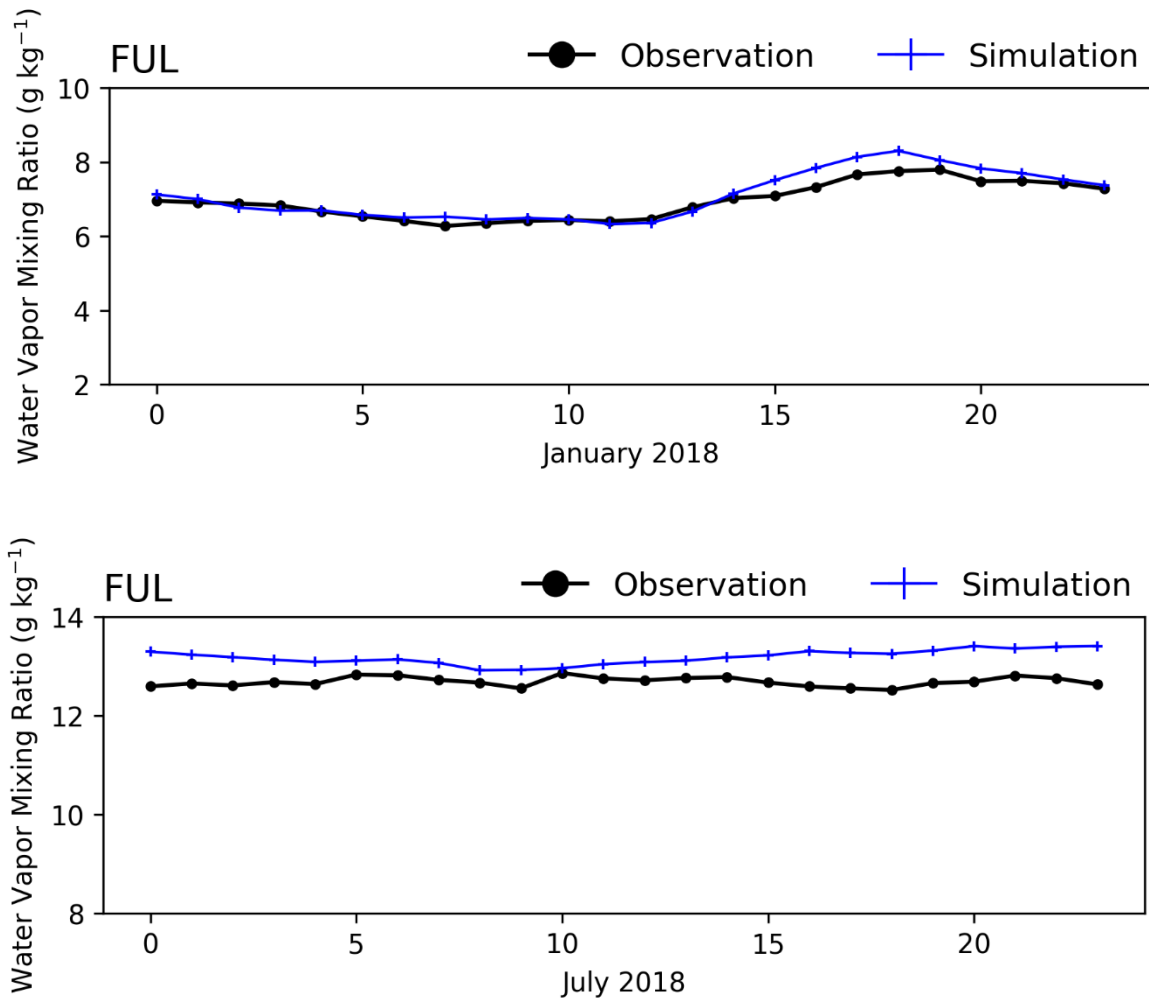


FIGURE II-3-18

WATER VAPOR MIXING RATIO AT FULLERTON (FUL) STATION FROM MEASUREMENTS AND WRF SIMULATIONS FOR JANUARY 2018 AND JULY 2018

Model Performance Evaluation: Wind Rose

The measured and WRF simulated wind rose at each station for 1-year period of January – December 2018 are shown in Figure II-3-19 – Figure II-3-23. Consistent with the sections above, the wind rose at HHR (near coastal areas), FUL (inland Orange County) and CNO (further east in San Bernardino County) are presented. Another two stations: BUR (inland Los Angeles County) and ONT (San Bernardino County) are included as well to evaluate the model performance in further downwind areas. In general, the WRF simulations reproduce the dominant wind direction as the measurements at each station. For example, model and observations both show that westerly and south-westerly directions are the prevailing wind directions for the stations of CNO, FUL, HHR and ONT. The wind direction is mostly from the southeast at the BUR station, as presented in both observations and simulations. For the wind speed, among the five

stations, the FUL and BUR stations have calm winds, mostly under 6 m/s, while other stations showed stronger wind between 6 - 8 m/s. In general, the WRF simulation underestimates the observed wind speed at HHR and ONT stations. Overall, WRF simulates surface wind speed and direction reasonably well as shown in the wind roses.

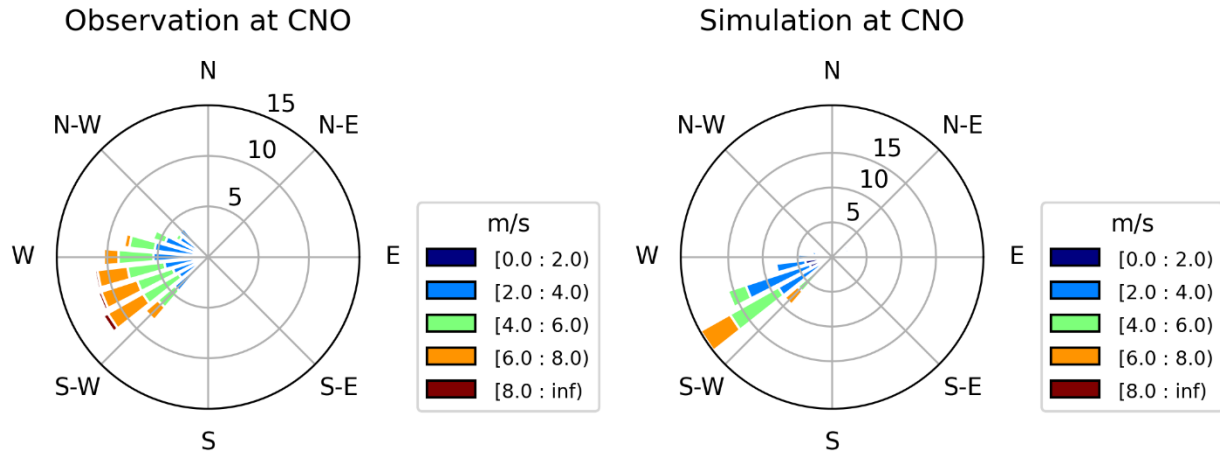


FIGURE II-3-19

WIND ROSE FROM MEASUREMENT AND WRF SIMULATION AT CHINO (CNO) STATION IN 2018

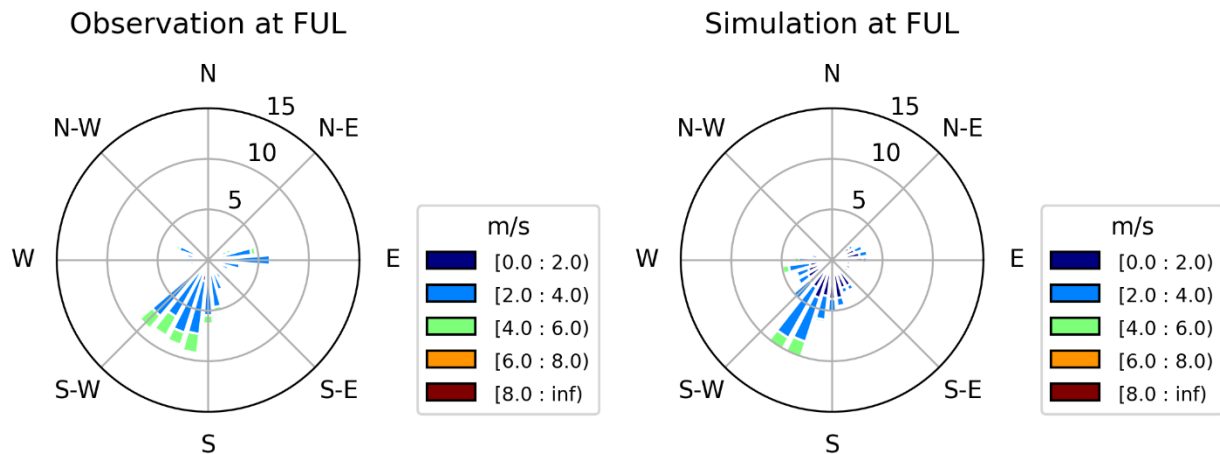


FIGURE II-3-20

WIND ROSE FROM MEASUREMENT AND WRF SIMULATION AT FULLERTON (FUL) STATION IN 2018

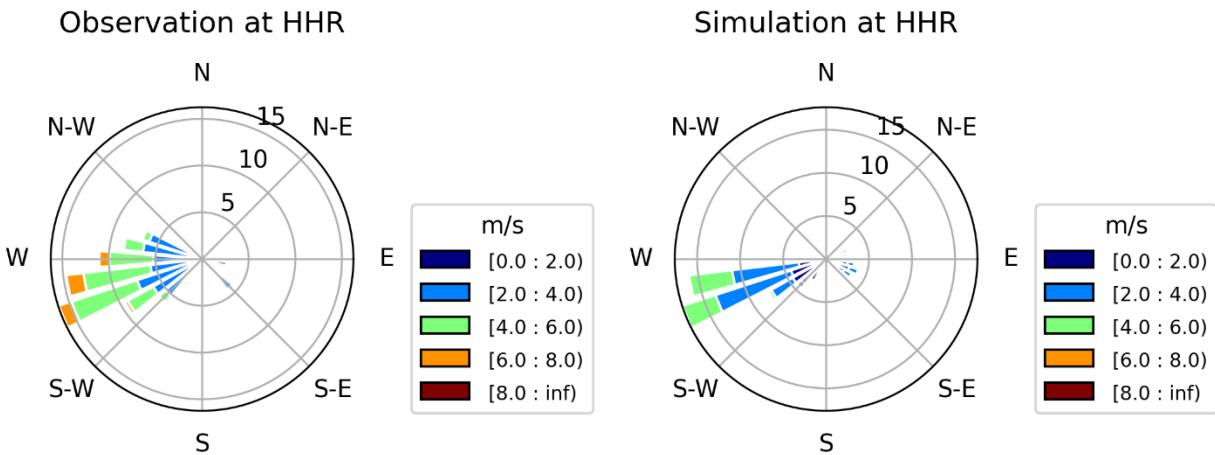


FIGURE II-3-21

WIND ROSE FROM MEASUREMENT AND WRF SIMULATION AT HAWTHORNE (HHR) STATION IN 2018

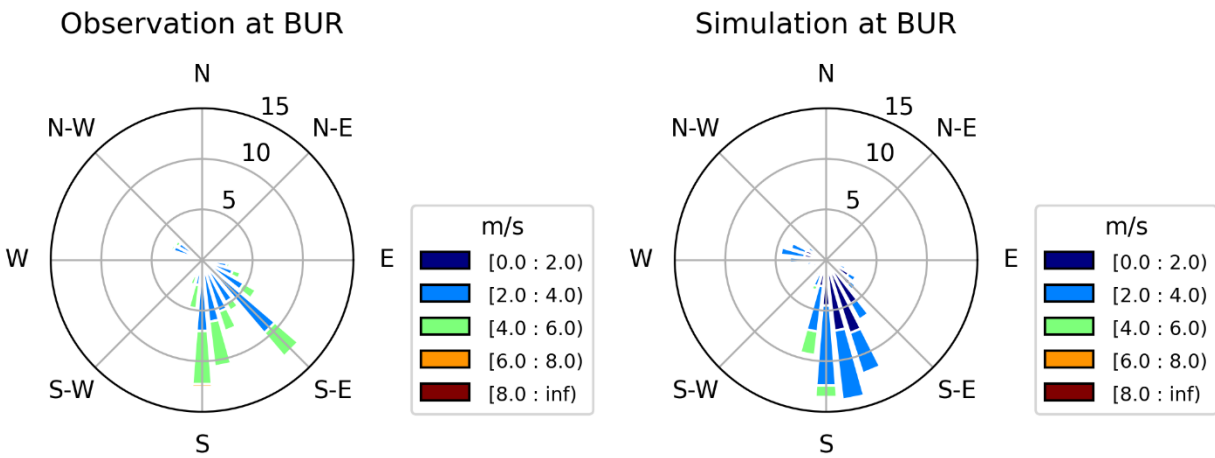


FIGURE II-3-22

WIND ROSE FROM MEASUREMENT AND WRF SIMULATION AT BURBANK (BUR) STATION IN 2018

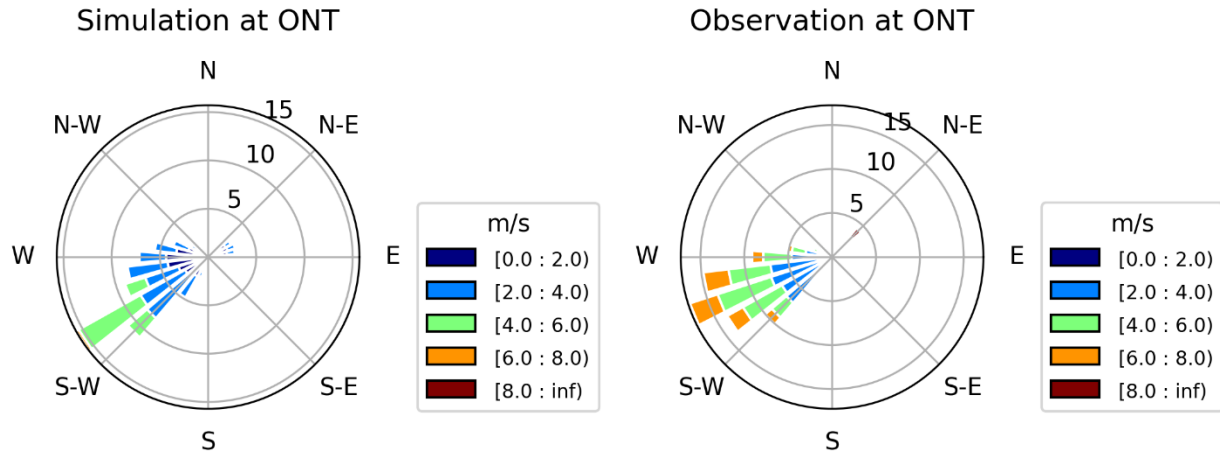


FIGURE II-3-23

WIND ROSE FROM MEASUREMENT AND WRF SIMULATION AT ONTARIO (ONT) STATION IN 2018

Model Performance Evaluation: Planetary Boundary Layer Height

Time series of hourly PBLH from ceilometer measurements and WRF simulations at ONT and IRV during July 2018 are shown in Figure II-3-24. Simulated PBLHs generally showed good agreement with ceilometer derived PBLHs except for very high reported PBLH values (> 2 km). These very high PBLH measurements may have been measurements artifacts caused by cloud interference in ceilometer profiles. Time series of average PBLH diurnal variation from measurements and WRF simulations for the summer season (June-August 2018) at ONT and IRV are shown in Figure II-3-24. The diurnal cycle in PBL height was well captured by the simulations. For example, at ONT, both measured and simulated PBLHs were lowest during early morning, increased to maximum values of ~800m at midday due to stronger convection and vertical mixing, and then slowly decayed to lower heights during the late afternoon and early night. Usually, the days with lower PBL height will lead to lower ventilation of air pollutions, and higher PBL height will help with dispersion of surface pollutions.

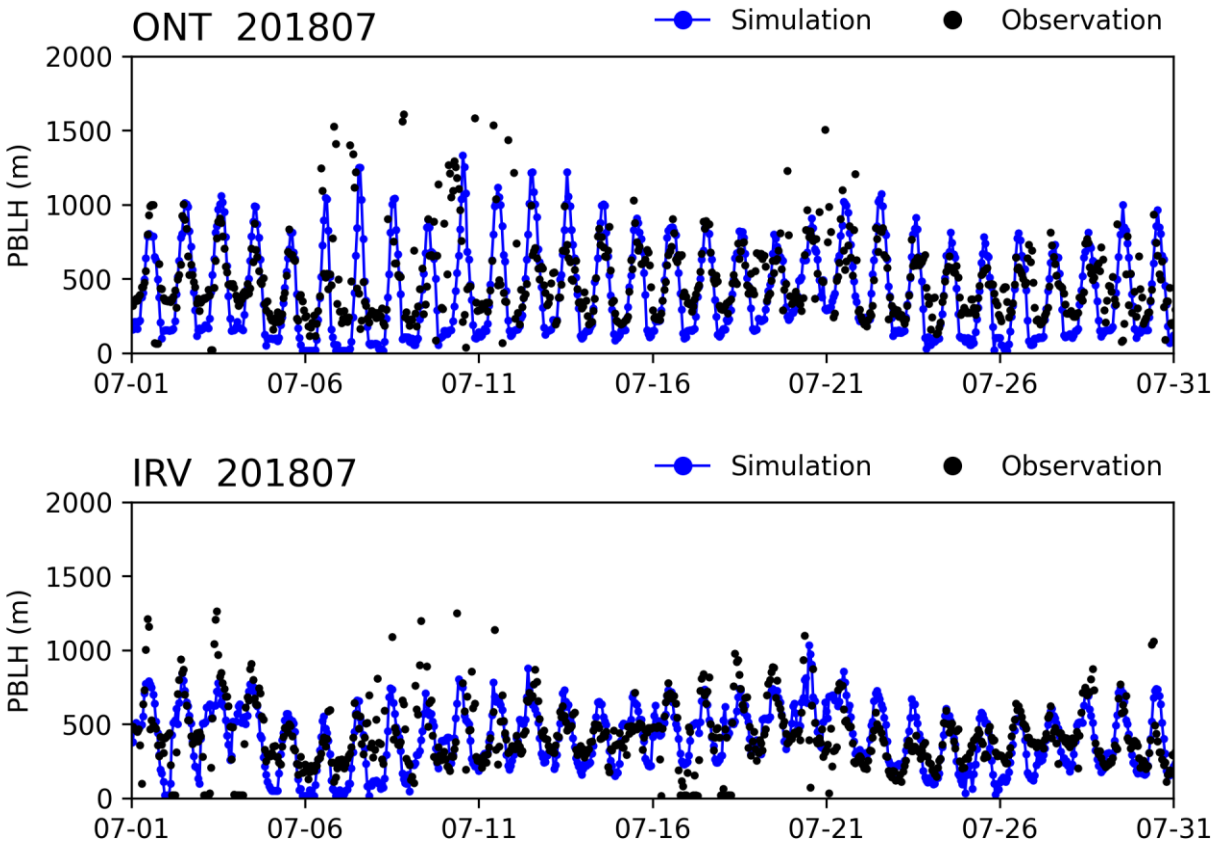


FIGURE II-3-24

TIME SERIES OF HOURLY PBLH FROM CEILOMETER MEASUREMENTS AND WRF SIMULATIONS FOR JULY 2018 AT ONTARIO (ONT) STATION AND AT IRVINE (IRV) STATION

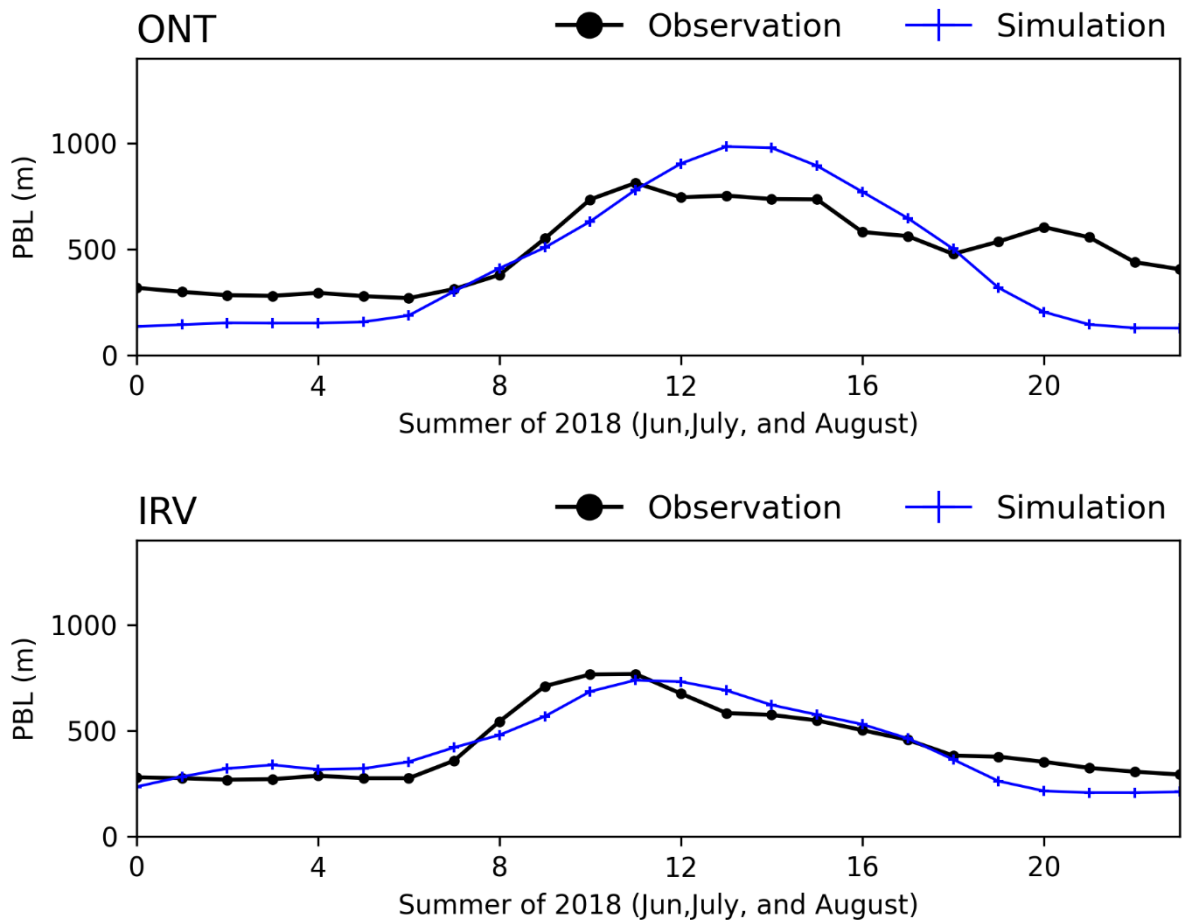


FIGURE II-3-25

TIME SERIES OF SEASONAL COMPOSED PBLH DIURNAL VARIATION FROM CEILOMETER MEASUREMENT AND WRF SIMULATIONS FOR SUMMER SEASON (JUNE-AUGUST 2018) AT ONTARIO (ONT) STATION AND IRVINE (IRV) STATION

Sensitivity Test of Planetary Boundary Layer Scheme

A set of WRF sensitivity simulations regarding the planetary boundary layer scheme was conducted. The planetary boundary layer scheme of Asymmetric Convective Model version 2 (ACM2)⁶ (Pleim, J. E., 2007) was tested in the WRF model. Comparing this set of sensitivity simulations with the simulation with YSU planetary boundary layer scheme, statistical results for temperature, water vapor and wind predictions are similar for both winter and summer seasons. The ACM2 PBL scheme showed slightly better performance for temperature and water vapor mixing ratio comparing with the YSU PBL scheme. The

⁶ Pleim, J. E. (2007). A Combined Local and Nonlocal Closure Model for the Atmospheric Boundary Layer. Part I: Model Description and Testing. *J. Appl. Meteor. Climatol.*, 46, 1383–1395, <https://doi.org/10.1175/JAM2539.1>.

YSU PBL scheme had marginally better performance for wind speed and the ACM2 PBL scheme has small lower bias for wind speed.

TABLE II-3-3

WRF PERFORMANCE STATISTICS FOR QUARTER AVERAGE OF 2018 AT 15 NWS STATIONS

| | Statistic | Q1 | Q2 | Q3 | Q4 |
|----|-----------------------------|-------|-------|-------|-------|
| T | T Mean Observation (K) | 288.1 | 291.8 | 297.8 | 290.4 |
| | T Mean Simulation (K) | 287.3 | 292.4 | 297.8 | 289.7 |
| | T Bias (K) | -0.8 | 0.6 | 0 | -0.7 |
| | T Gross Error (K) | 1.9 | 1.6 | 1.5 | 1.7 |
| | T RMSE (K) | 2.6 | 2.1 | 2 | 2.3 |
| Q | Q Mean Observation (K) | 5.8 | 8.1 | 10.8 | 6.6 |
| | Q Mean Simulation (K) | 5.7 | 8.2 | 11.9 | 7 |
| | Q Bias (K) | -0.1 | 0.1 | 1.1 | 0.4 |
| | Q Gross Error (K) | 0.9 | 0.9 | 1.6 | 1.2 |
| | Q RMSE (K) | 1.4 | 1.3 | 2.9 | 1.9 |
| WS | WS Mean Observation (kg/kg) | 2 | 2.7 | 2.6 | 1.9 |
| | WS Mean Simulation (kg/kg) | 2 | 2.4 | 2.3 | 1.8 |
| | WS Bias (kg/kg) | 0 | -0.3 | -0.3 | -0.1 |
| | WS Gross Error (kg/kg) | 1.4 | 1.3 | 1.2 | 1.4 |
| | WS RMSE (kg/kg) | 1.8 | 1.6 | 1.5 | 1.9 |

The performance of the WRF simulations with ACM2 PBL scheme is summarized in Table II-3-3 for 4 quarters of 2018. All the results shown in Table II-3-3 are averaged values for the 15 airport weather stations. Overall, the results from YSU PBL scheme and YSU PBL scheme are consistent with each other with small discrepancies. Both WRF simulations proved representative meteorological fields that well characterized the observed values in summer and winter of 2018.

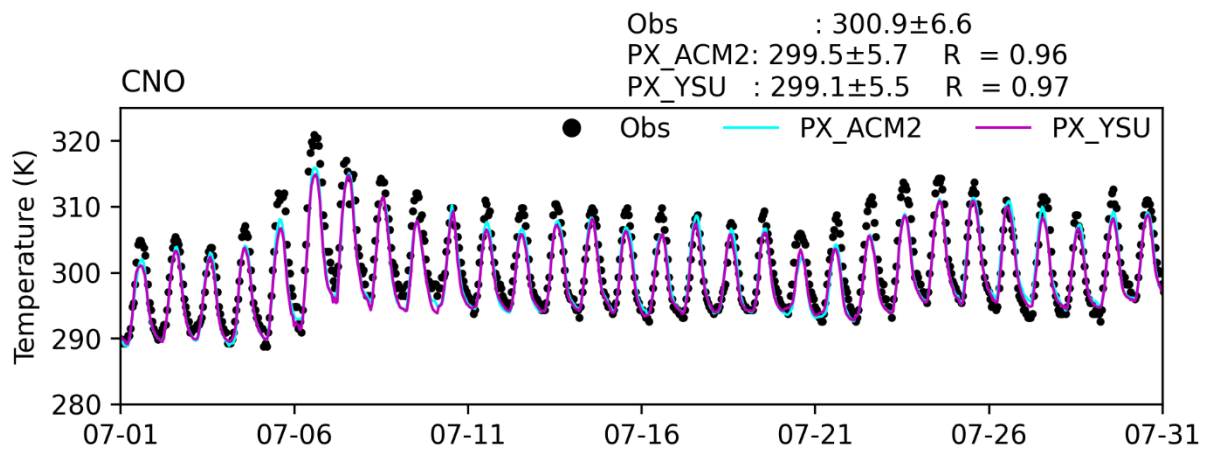
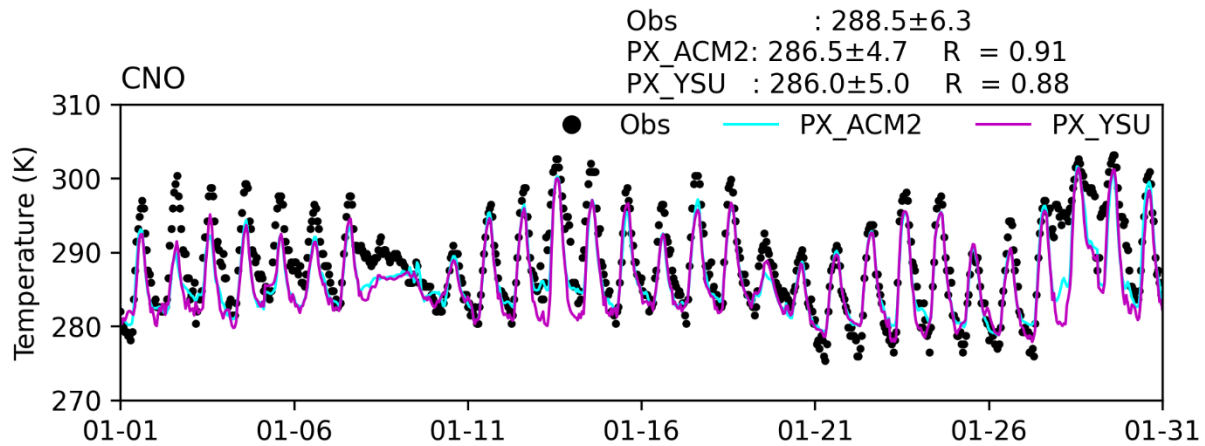
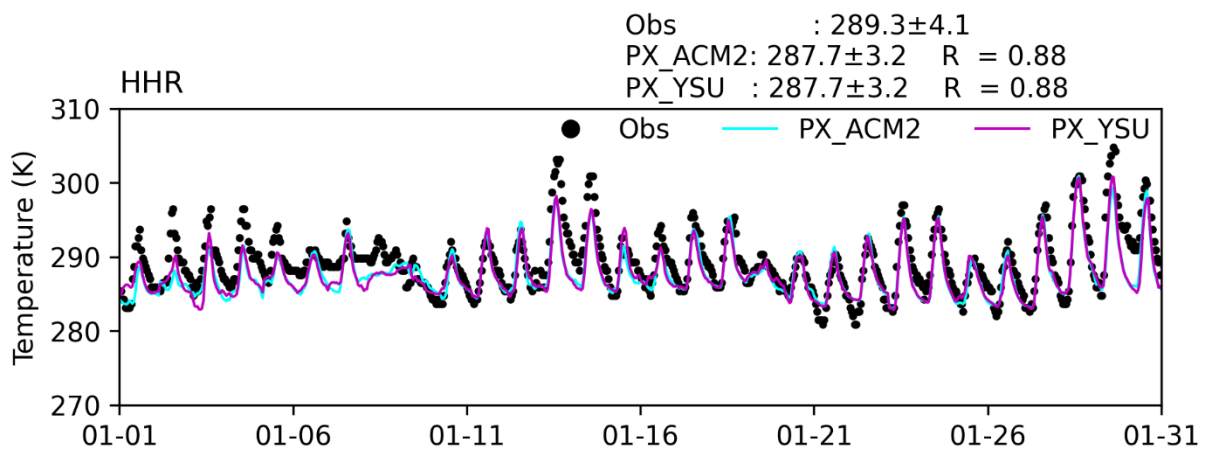


FIGURE II-3-26

TIME SERIES OF HOURLY TEMPERATURE FROM MEASUREMENT AND WRF SIMULATIONS AT CHINO (CNO) STATION FOR JANUARY 2018 AND JULY 2018



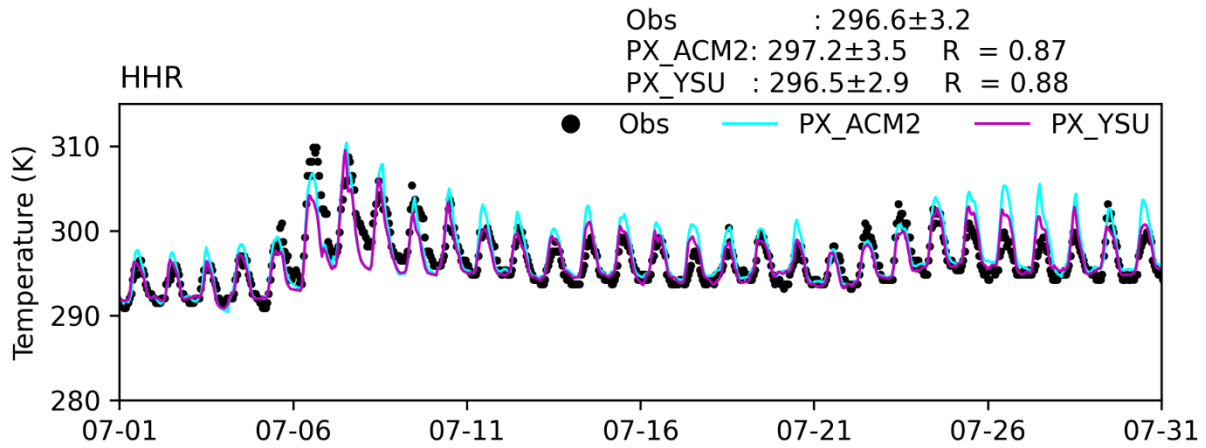
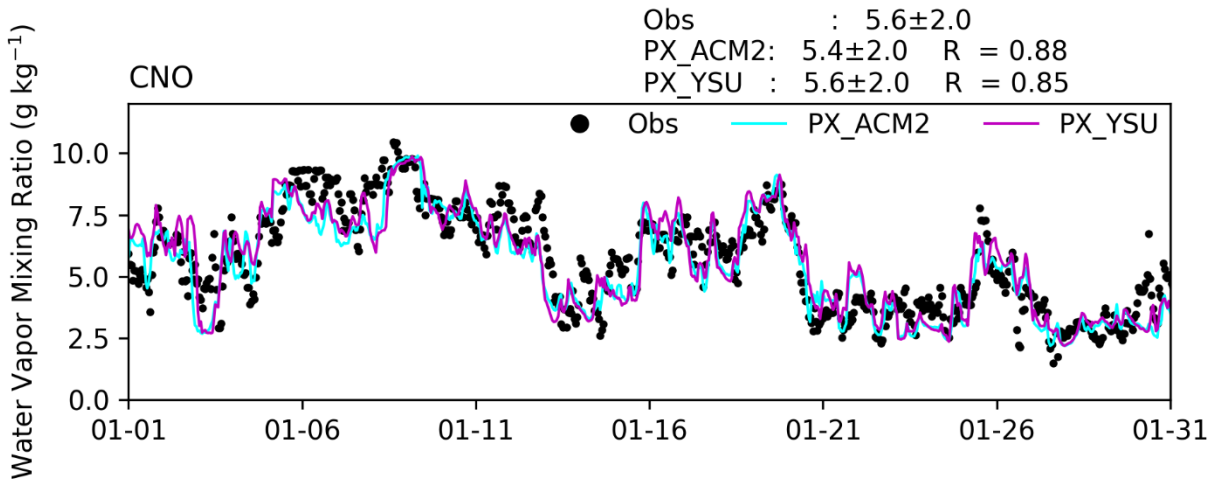


FIGURE II-3-27

TIME SERIES OF HOURLY TEMPERATURE FROM MEASUREMENTS AND WRF SIMULATIONS AT HAWTHORNE (HHR) STATION FOR JANUARY 2018 AND JULY 2018



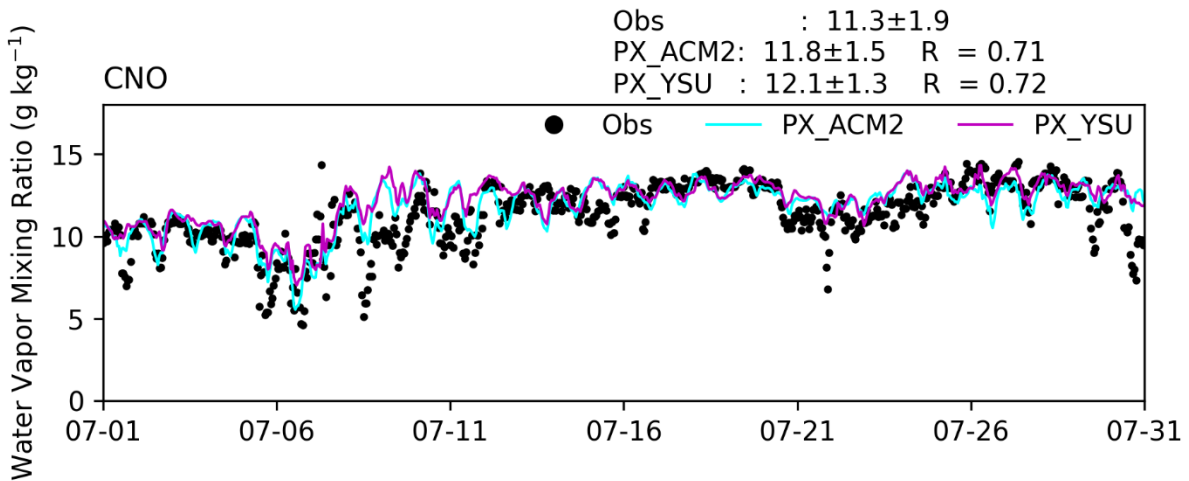


FIGURE II-3-28

TIME SERIES OF HOURLY WATER VAPOR MIXING RATIO FROM MEASUREMENTS AND WRF SIMULATIONS AT CHINO (CNO) STATION FOR JANUARY 2018 AND JULY 2018

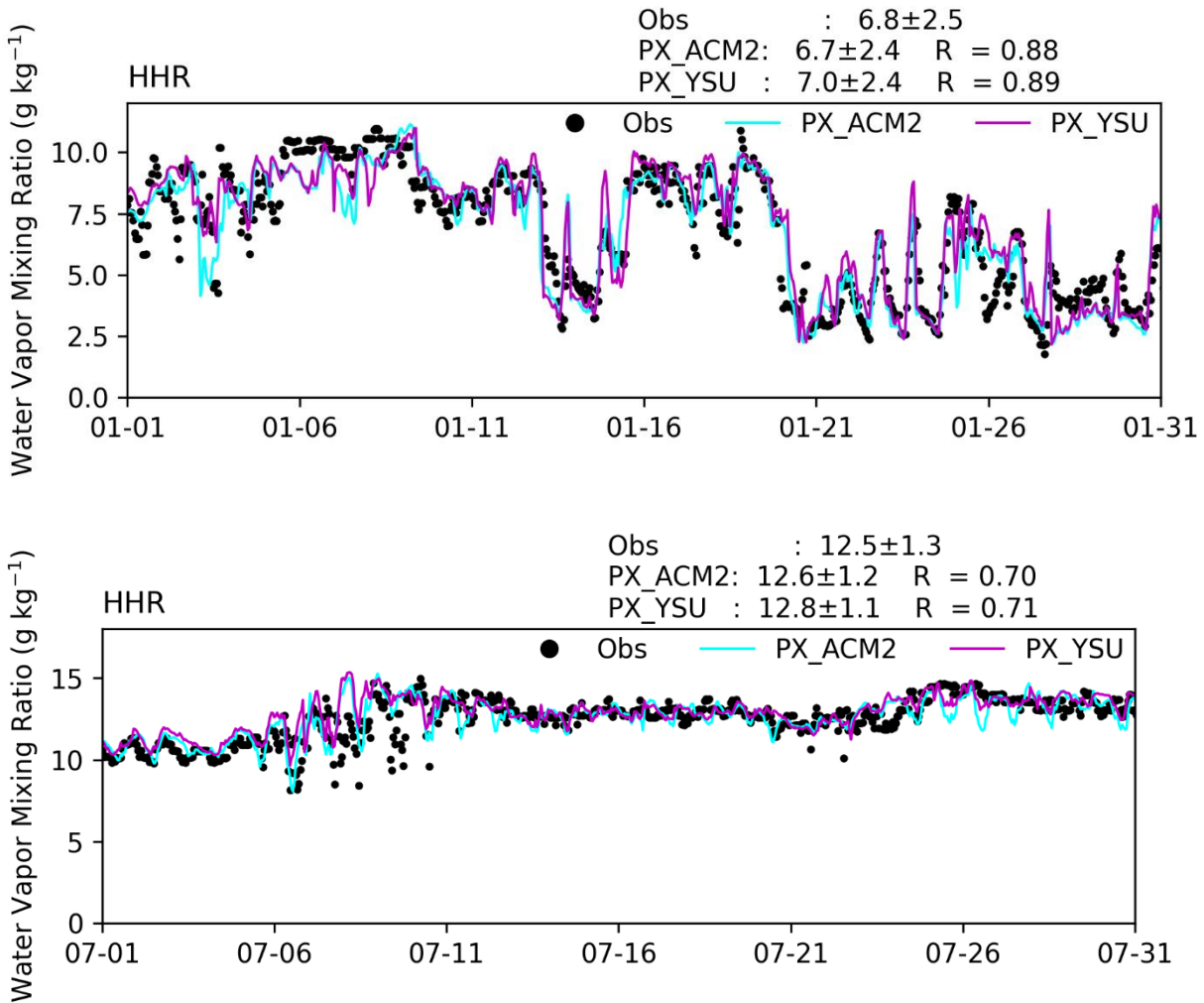


FIGURE II-3-29

TIME SERIES OF HOURLY WATER VAPOR MIXING RATIO FROM MEASUREMENTS AND WRF SIMULATIONS AT HAWTHORNE (HHR) STATION FOR JANUARY 2018 AND JULY 2018

The surface level model performance comparison between the YSU PBL scheme and ACM2 PBL scheme were evaluated for each month at airport stations in the model domain for January through December 2018. For simplicity, only one summer month (July) and one winter month (January) are shown in Figure II-3-26 through Figure II-3-29. Two stations were selected as examples for surface level model performance evaluation: CNO and HHR. The station of CNO represents inland area and the station of HHR represents coastal climate. In general, the two sets of WRF simulations generated similar hourly temperature and water vapor mixing ratio at each station. The WRF simulations with ACM2 PBL scheme have slightly higher daily maximum temperatures during winter, while it shows warm bias during summertime in the coastal station of HHR. For water vapor mixing ratio, the WRF simulations with ACM2 PBL scheme showed lower values comparing with the WRF simulations with YSU PBL scheme. In all, the performance of WRF with ACM2 PBL scheme is very close to WRF with YSU PBL scheme and the

WRF with YSU PBL scheme was used as the primary model platform to generate meteorological fields for the ~~Draft-PM2.5 plan~~ Plan.

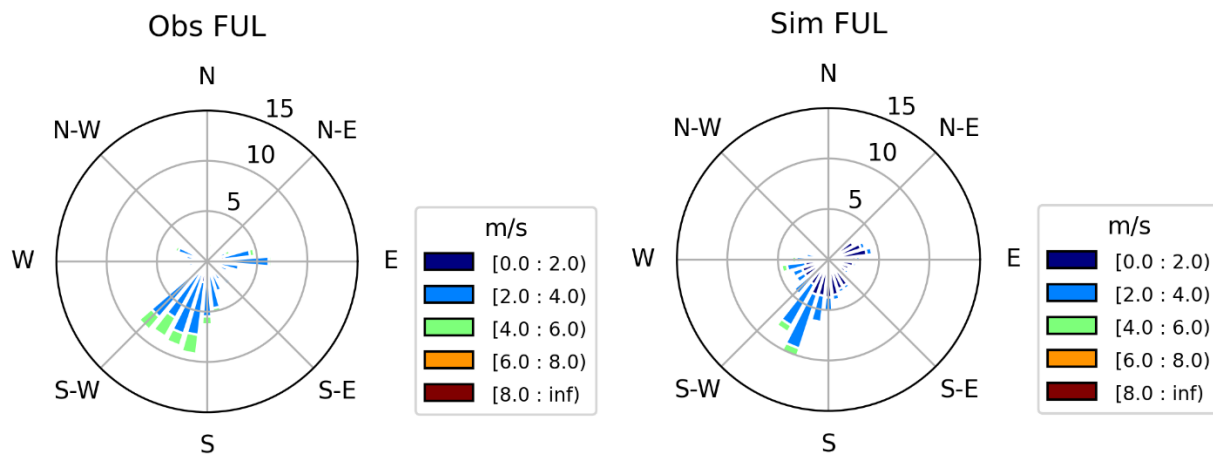


FIGURE II-3-30

WIND ROSE FROM MEASUREMENT AND WRF SIMULATION AT FULLERTON (FUL) STATION FOR THE ENTIRE YEAR OF 2018

The measured and WRF simulated wind rose at the station of FUL for 1-year period of January – December 2018 are shown in Figure II-3-30. In general, the WRF simulations with ACM2 reproduces the dominant wind direction as the measurement. For example, model and observations both show that westerly and south-westerly directions are the prevailing wind directions for the stations of FUL. In general, the WRF with ACM2 PBL scheme simulates surface wind speed and direction reasonably well as shown in the wind roses, although the simulation show slightly more underestimates of the observed wind speed comparing with the WRF simulations with YSU PBL scheme.

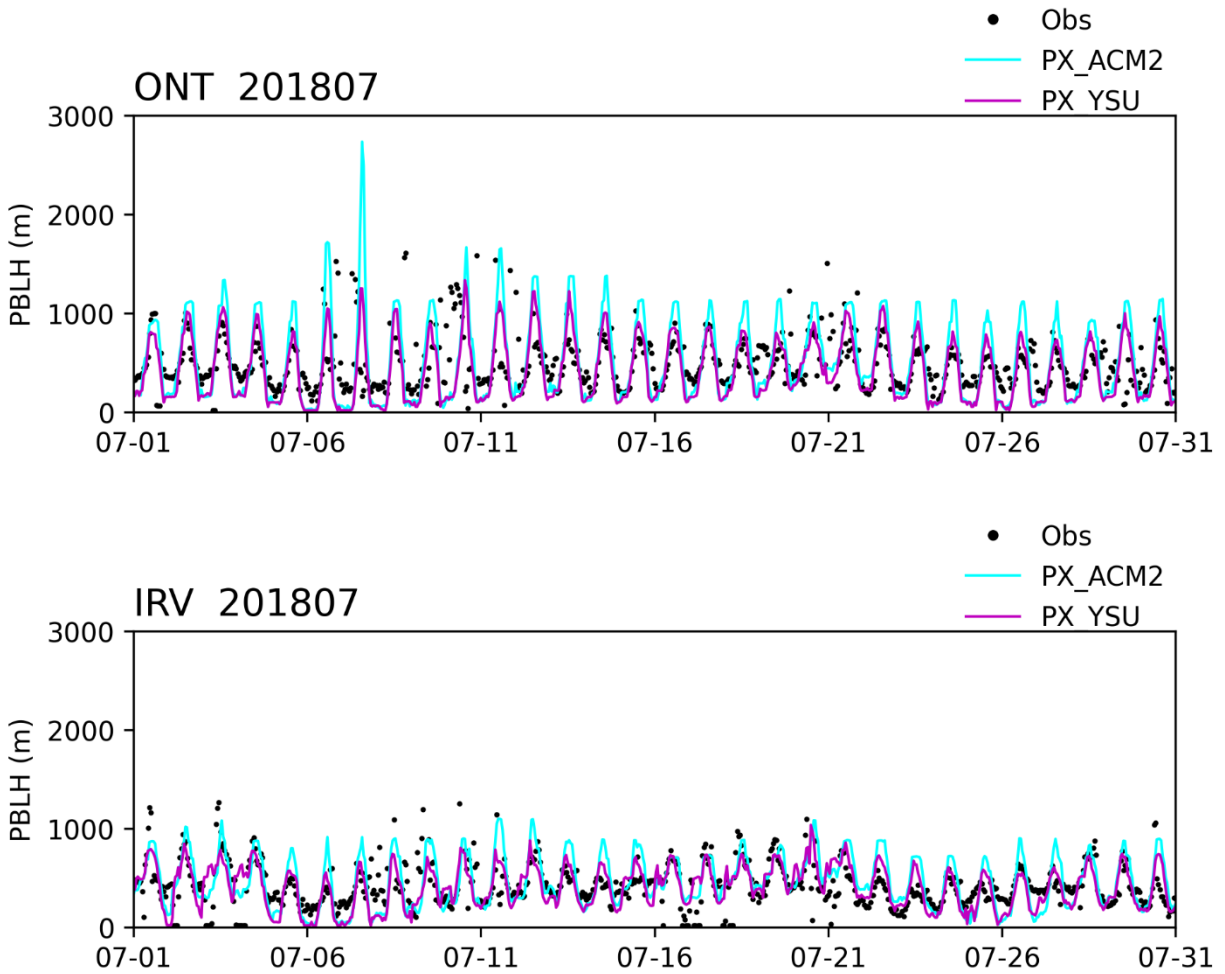


FIGURE II-3-31

TIME SERIES OF HOURLY PBLH FROM CEILOMETER MEASUREMENTS AND WRF SIMULATIONS FOR JULY 2018 AT ONTARIO (ONT) STATION AND AT IRVINE (IRV) STATION

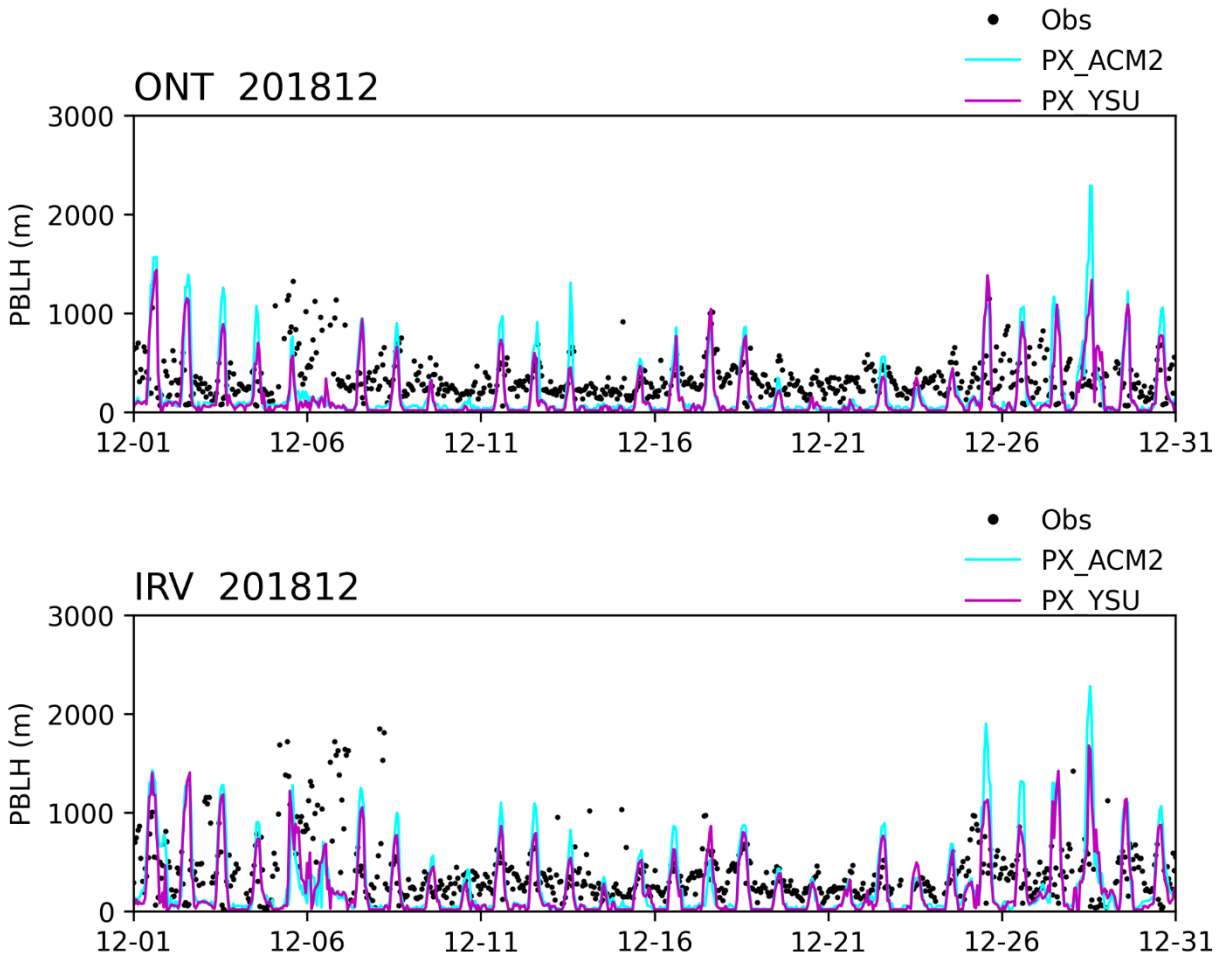


FIGURE II-3-32

TIME SERIES OF HOURLY PBLH FROM CEILOMETER MEASUREMENTS AND WRF SIMULATIONS FOR DECEMBER 2018 AT ONTARIO (ONT) STATION AND AT IRVINE (IRV) STATION

Time series of hourly PBLH from ceilometer measurements and WRF simulations at ONT and IRV during December 2018 are shown in Figure II-3-32. The simulation with ACM2 PBL scheme showed higher daily maximum PBL and this pattern is consistent with the simulated higher daily maximum temperature comparing with the simulations with YSU PBL scheme.

Summary

The performance of the WRF simulations for the year of 2018 is evaluated with observations from airport weather stations and PBL height measurement from ceilometers. Overall, WRF simulations for each season provided representative meteorological fields that well characterized observed conditions in 2018. Regarding different option of planetary boundary layer scheme, set of WRF sensitivity simulations of Asymmetric Convective Model version 2 (ACM2) was conducted. Comparing this set of sensitivity simulations with the simulation with YSU planetary boundary layer scheme, statistical results for temperature, water vapor and wind predictions are similar for both winter and summer seasons. The ACM2 PBL scheme showed slightly better performance for temperature and water vapor mixing ratio comparing with the YSU PBL scheme. The YSU PBL scheme had marginally better performance for wind speed and the ACM2 PBL scheme has small lower bias for wind speed. Since the modeling discrepancies between different PBL height scheme are very small, the meteorological fields obtained with WRF simulations with YSU PBL scheme are used as meteorological inputs for CMAQ modeling of PM_{2.5} in this plan.

Chapter 4

MODELING EMISSIONS, BOUNDARY CONDITIONS, AND INITIAL CONDITIONS

Modeling Emissions Inventory

Inventory Profile

Temporal and Spatial Allocations of Emissions

Boundary and Initial Conditions

Modeling Emissions Inventory

Table II-4-1 provides the baseline and controlled modeling emissions inventories that are consistent with the emissions used in the attainment demonstration and alternative analyses. The CMAQ simulations were based on the annual emissions inventory, with adjustments made for source-specific temporal profiles and daily temperature variations. An extensive discussion of the overall emissions inventory is provided in Appendix I. Approaches used in generating gridded hourly emissions for each modeling day are presented in this Chapter.

TABLE II-4-1
ANNUAL AVERAGE ANTHROPOGENIC EMISSIONS INVENTORY IN SOUTH COAST AIR BASIN
(TONS/DAY)

| Year | Annual Average | | | | |
|-----------------------------|----------------|--------------------|-----|------------------|-----|
| | VOC | NOX | SOX | PM2.5 | NH3 |
| (a) Baseline | | | | | |
| 2018 | 402 | 383 | 14 | 56 | 75 |
| 2025 | 364 | 239 | 15 | 54 | 78 |
| 2030 | 344 | 210 | 15 | 54 | 79 |
| (b) Controlled ¹ | | | | | |
| 2030 | 340 | 178 175 | 15 | 52 53 | 76 |

¹Emission account for reductions due to control strategies described in Chapter 4.

Inventory Profile

This section discusses the baseline modeling inventories for the base year 2018 and the future years 2025 and 2030, as outlined in the Draft PM2.5 Plan. The primary focus of this plan is to demonstrate attainment of the 2012 annual PM2.5 National Ambient Air Quality Standard (NAAQS) set at 12 µg/m³.

The baseline emissions projection assumes no additional emission controls beyond the measures and programs already in place. These projections consider emissions resulting from population growth, increased vehicle miles traveled (VMT), and the implementation of all previously adopted rules and regulations. The cut-off date for South Coast AQMD regulations is October 2020 (except for Rule 1109.1, adopted in November 2021), and for CARB's regulations, the cut-off date is December 2021. Controlled emission projections reflect the anticipated benefits of implementing control measures in relation to future baseline emissions. Comprehensive descriptions of these control measures can be found in Chapter 4 and Appendix IV of the Draft PM2.5 Plan report. For further details on emission sources, readers can refer to Appendix I which contains emission summary reports categorized by source for both the base year and future baseline scenarios used in this modeling analysis. Detailed summaries of emissions

reductions by source category for future (2025 and 2030) controlled scenarios are available in Attachment 3 of Appendix II.

Temporal and Spatial Allocations of Emissions

Point, mobile, and area emissions inventories specific to each day were generated for the base year 2018. On-road mobile source emissions were calculated using data from SCAG transportation modeling, CARB's EMFAC2021 emissions rates, observed daily traffic fluctuations, and modeled daily temperature variations. To create day-specific hourly emissions, annual emissions were distributed using temporal profiles. Each source type was assigned profiles for monthly throughputs, day-of-week variations, and diurnal changes.

Point source emissions were allocated spatially based on the precise locations of emitting facilities. Conversely, countywide emissions stemming from area and off-road sources were distributed using spatial surrogates. For this purpose, a comprehensive set of over 110 spatial surrogates was employed, a compilation refined by CARB during each AQMP development cycle. Each emissions source, identified by its Emission Inventory Code, was associated with an appropriate surrogate profile. These surrogates represented a diverse range of sources, encompassing gas stations, landfills, military bases, single-family homes, and railyards. In alignment with our established AQMP practices, socioeconomic data for both the base and future years, incorporating population, employment, and housing statistics, as provided by SCAG during its RTP/SCS process, were incorporated into these surrogates. Further elaboration on the temporal and spatial allocation of on-road and total emissions are provided in following sections.

On-road Mobile Emissions

On-road mobile sources are responsible for a large fraction of the total VOC, NO_x, CO, NH₃ and PM_{2.5} emissions in our modeling domain. These emission sources are highly dependent on both time and location, with variations up to a factor of 8 between overnight and peak traffic hours at specific locations. On-road mobile emission patterns also exhibit substantial variation throughout the week and year, influenced by factors such as special events, holidays, and weather conditions. Location-specific variations may also arise due to proximity to high-employment areas, sporting events, or/and seasonal activities.

Real-time traffic flow measurements from 2018 were used to apportion traffic volumes on an hourly basis throughout the five counties (Ventura, Los Angeles, Orange, Riverside and San Bernardino). These measurements include data from thousands of sensors scattered throughout the Basin, covering both light- and heavy-duty vehicle flow. Given the limited availability of monitoring data in the five outlying counties (San Luis Obispo, Santa Barbara, Kern, Imperial, and San Diego), grid-based on-road emissions

were generated for those regions using generic traffic profiles that account for variations by day of the week (Kwon et al., 2003)¹.

In Figures II-4-1 to II-4-4, we compare daily on-road emissions of NO_x, Primary Elemental Carbon (PEC), Primary Organic Carbon (POC), and CO between the 2022 AQMP estimated with EMFAC2017 (blue) and the ~~Draft~~ PM2.5 Plan estimated with EMFAC2021 (orange) over the south coast air basin (SCAB) in 2018. On-road emissions estimated with EMFAC2021 exhibit very similar daily/weekly patterns and seasonal variation as those estimated with EMFAC2017. Despite of the similar temporal variation in emissions in the two models, EMFAC2021 estimates higher NO_x (higher by 10% on average) and CO (higher by 24% on average) emissions compared to EMFAC2017 whereas it estimates noticeably lower POC emissions than EMFAC2017 (lower by 38% on average). PEC estimated with the two emission models (EMFAC2017 and EMFAC2021) are comparable (differs by 5% on average). The higher estimates of NO_x and CO in EMFAC2021 compared to EMFAC2017 are mostly because new vehicle emissions test data show that light-duty vehicles have higher exhaust emissions and updated DMV data for 2018 indicate that medium heavy-duty trucks are older than what was assumed in EMFAC2017. The lower primary particulate emissions (PEC and POC) in EMFAC2021 compared to EMFAC2017 can be attributed to the model updates on emissions and speed correction factors for brake wear that are obtained from new emission tests.

¹ Kwon J, Varaiya P, Skabardonis A. Estimation of Truck Traffic Volume from Single Loop Detectors with Lane-to-Lane Speed Correlation. Transportation Research Record. 2003;1856(1):106-117, <https://doi.org/10.3141%2F1856-11>

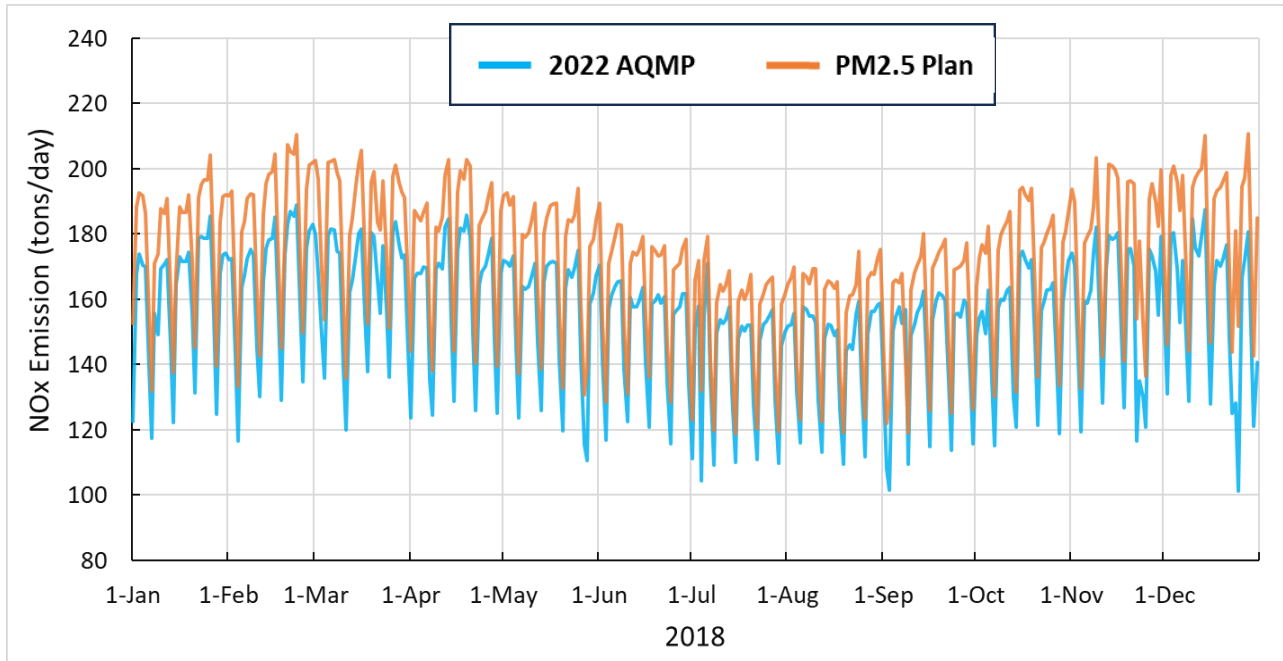


FIGURE II-4-1

A COMPARISON OF TOTAL DAILY ON-RAOD NITROGEN OXIDES (NO_x) EMISSION OVER THE SOUTH COAST AIR BASIN FROM THE 2022 AQMP AND THE DRAFT-PM2.5 PLAN DURING THE BASE YEAR 2018.

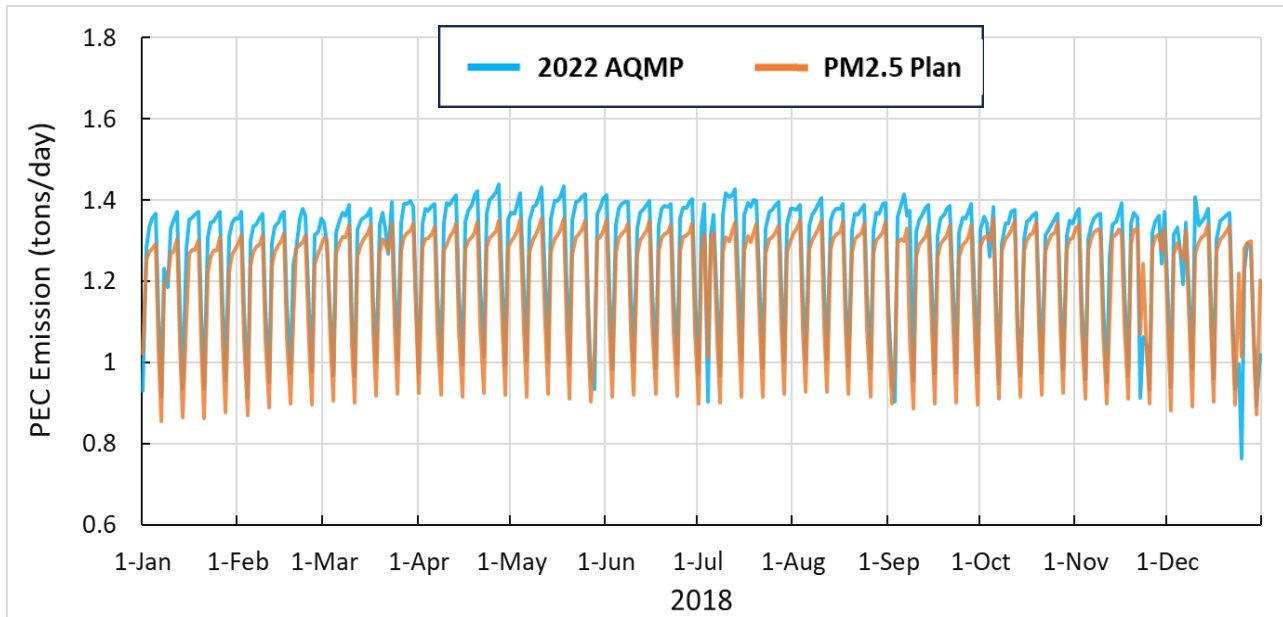


FIGURE II-4-2

A COMPARISON OF TOTAL DAILY ON-RAOD PRIMARY ELEMENTAL CARBON (PEC) EMISSION OVER THE SOUTH COAST AIR BASIN FROM THE 2022 AQMP AND THE DRAFT-PM2.5 PLAN DURING THE BASE YEAR 2018.

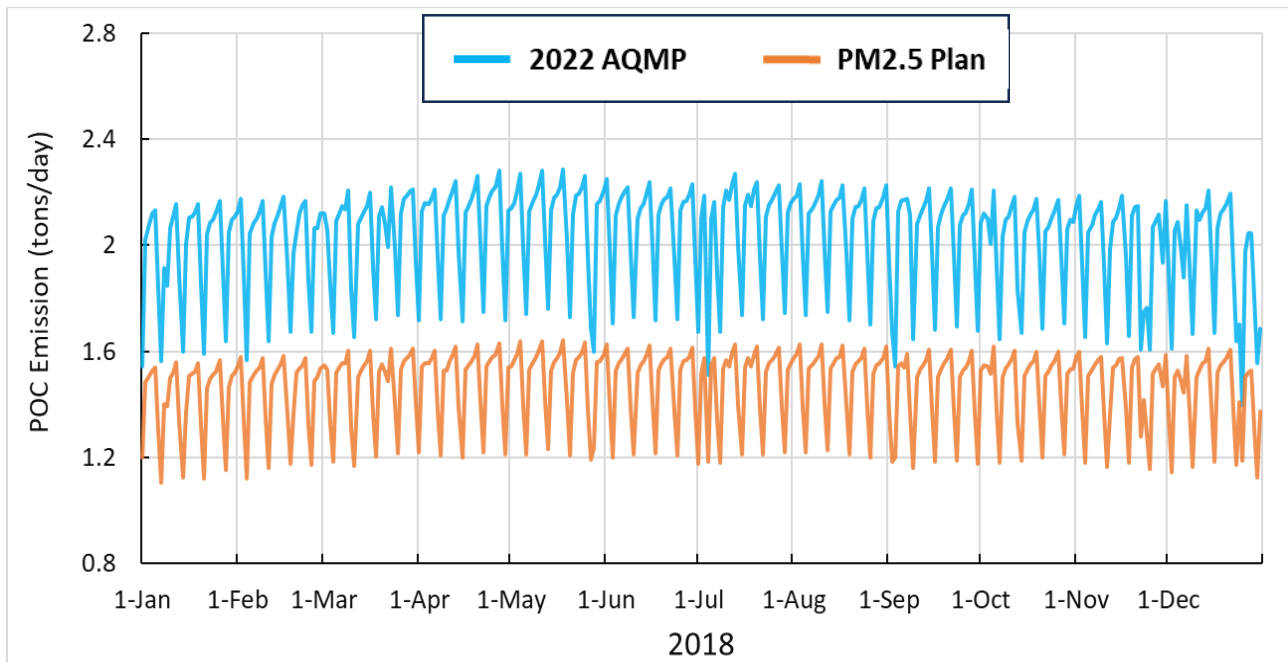


FIGURE II-4-3

A COMPARISON OF TOTAL DAILY ON-ROAD PRIMARY ORGANIC CARBON (POC) EMISSION OVER THE SOUTH COAST AIR BASIN FROM THE 2022 AQMP AND THE DRAFT-PM2.5 PLAN DURING THE BASE YEAR 2018.

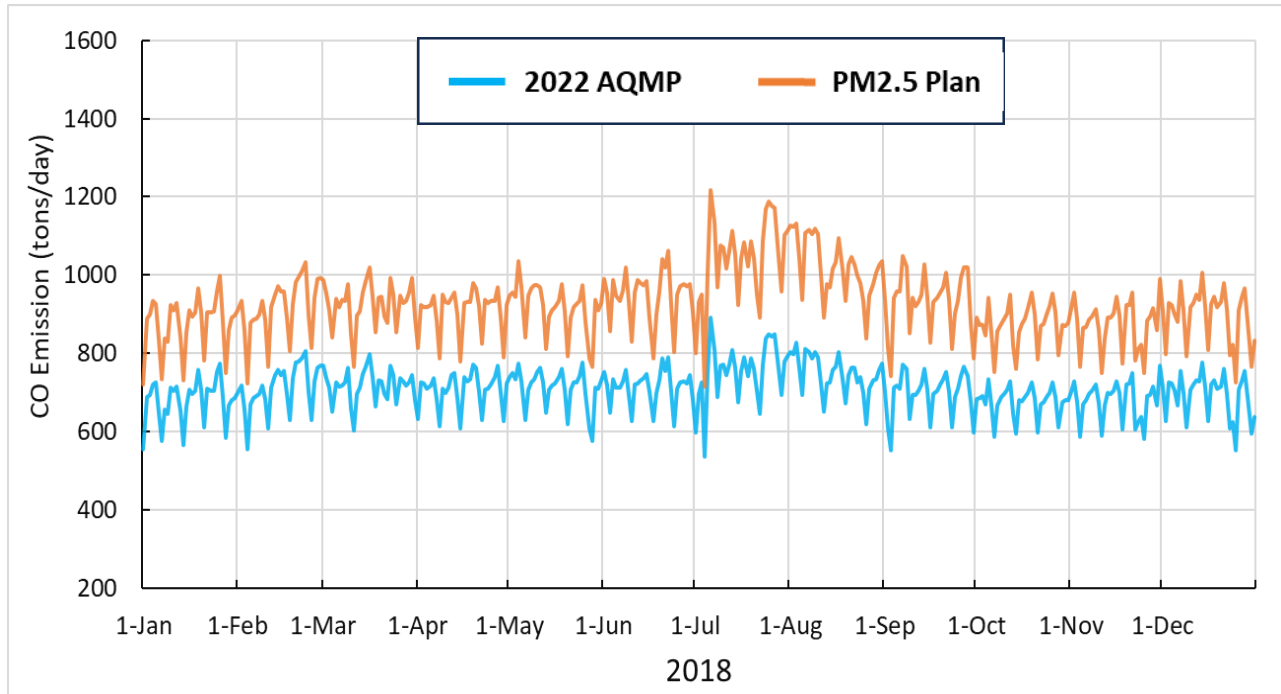


FIGURE II-4-4

A COMPARISON OF TOTAL DAILY ON-ROAD CARBON MONOXIDE (CO) EMISSION OVER THE SOUTH COAST AIR BASIN FROM THE 2022 AQMP AND THE DRAFT-PM2.5 PLAN DURING THE BASE YEAR 2018.

Emissions Profiles

Day specific emissions were generated for 2018. Figure II-4-5 illustrates the total daily emissions of NO_x, NH₃, and Primary PM_{2.5} contained in the CMAQ modeling domain during the base year of 2018. Note that the emissions totals are much higher than those presented in Table II-4-1. This is because the values in Table II-4-1 represent basin-wide total emissions while those in Figure II-4-5 comprise totals from the entire modeling domain. The profile clearly depicts a changing emissions pattern with two distinct cycles represented: a weekly cycle, illustrated by Sunday through Saturday peaks and valleys, and day-to-day variations in emissions within the weekly cycle. Daily variations are primarily driven by daily vehicular activities and ambient temperature and humidity changes. Although not included in Figure II-4-5, spatially and temporally resolved emissions from prescribed fires were also included in the emissions in the modeling domain. The attainment demonstration does not include emissions from wildfires.

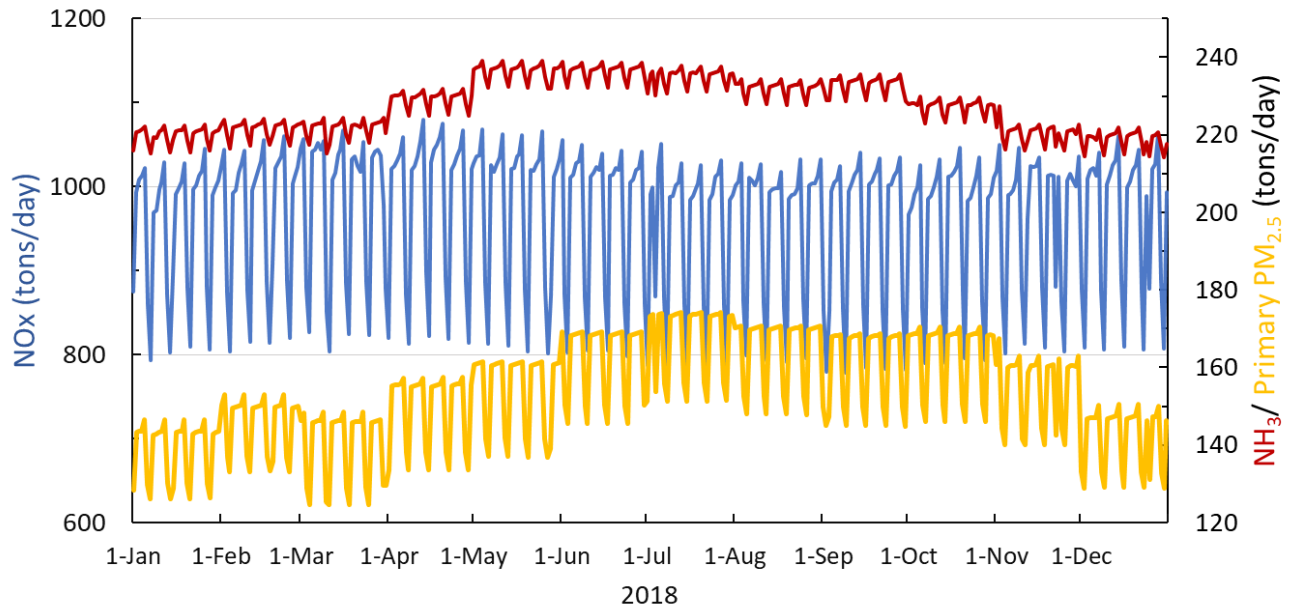


FIGURE II-4-5

2018 DAILY EMISSIONS OF NO_x, NH₃, AND PRIMARY PM_{2.5} IN THE MODELING DOMAIN.

Spatial Distribution

Figures II-4-6 through V-4-8 illustrate the spatial distribution of on-road emissions for primary PM_{2.5}, NO_x, and NH₃ in the modeling domain. Figures II-4-9 through II-4-11 show the spatial distribution of total emissions from all sources for these key primary pollutants across the entire modeling domain. The maps reveal that on-road emissions tend to cluster in urban areas, such as the downtown areas of Los Angeles, San Diego, and Long Beach, as well as along major arterial highways like I-5 and I-15. This concentration results from the high density of vehicles and substantial traffic volumes in these regions. When examining the total emissions of these key pollutants, urban centers emerge as major sources, characterized by their high population density and significant anthropogenic activities, including heavy transportation and various industrial and commercial operations. Notably, the spatial distribution of primary emissions also highlights elevated emissions in Mexican cities near the US-Mexico border. These emissions from across the border can influence background pollutant levels and directly impact Southern California's air quality, particularly under specific meteorological conditions, such as southerly winds during the summer, which facilitate the transport of air pollution across borders.

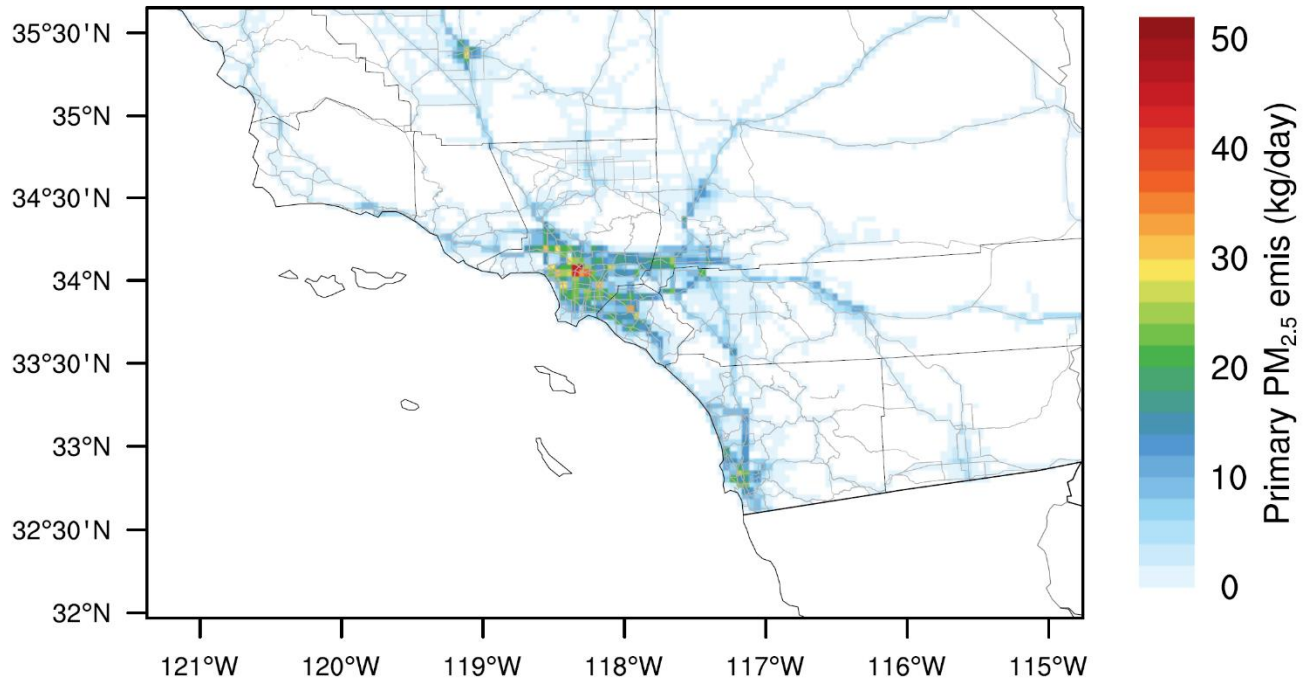


FIGURE II-4-6

ON-ROAD PRIMARY PM_{2.5} EMISSIONS OVER THE MODELING DOMAIN DURING THE BASE YEAR 2018.

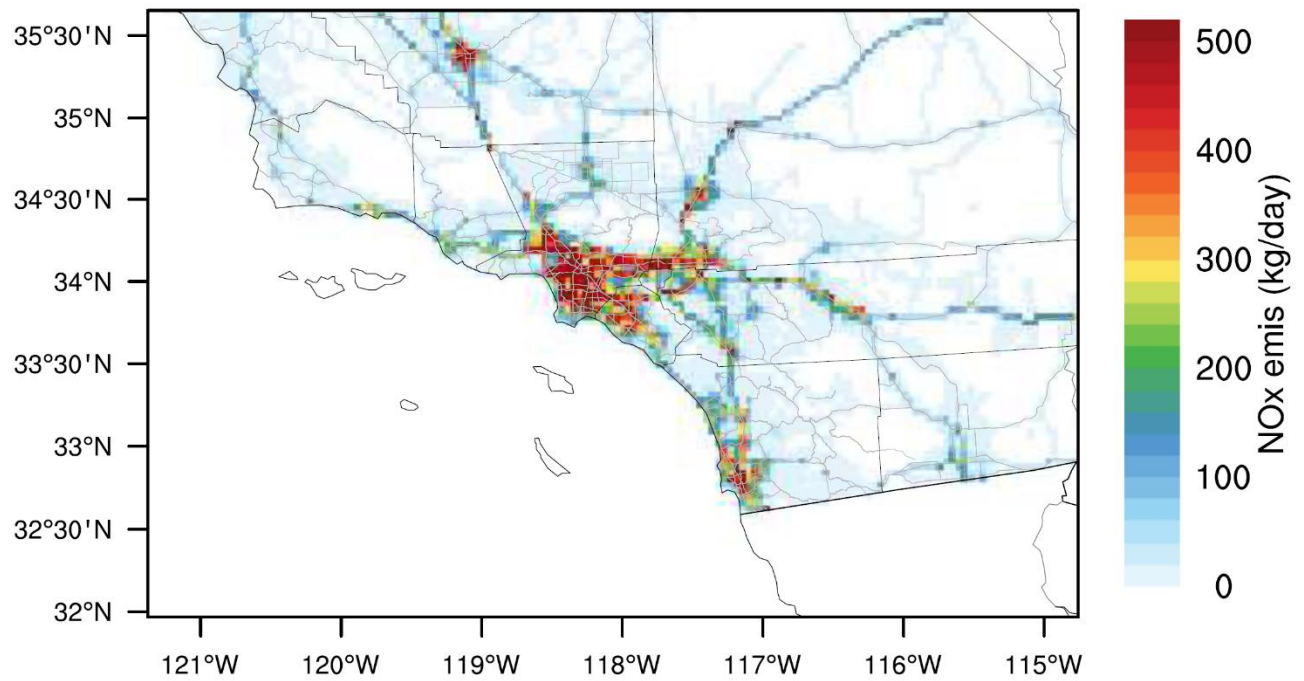


FIGURE II-4-7

ON-ROAD NO_x EMISSIONS OVER THE MODELING DOMAIN DURING THE BASE YEAR 2018.

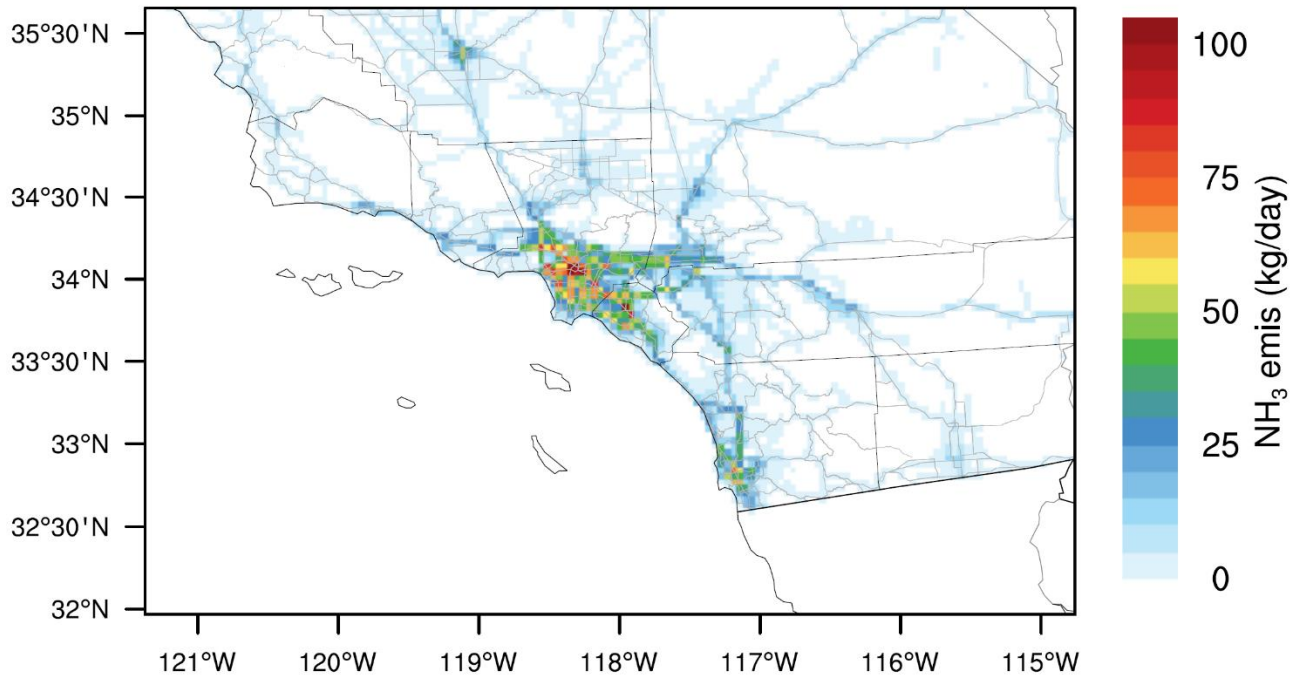


FIGURE II-4-8

ON-ROAD NH₃ EMISSIONS OVER THE MODELING DOMAIN DURING THE BASE YEAR 2018.

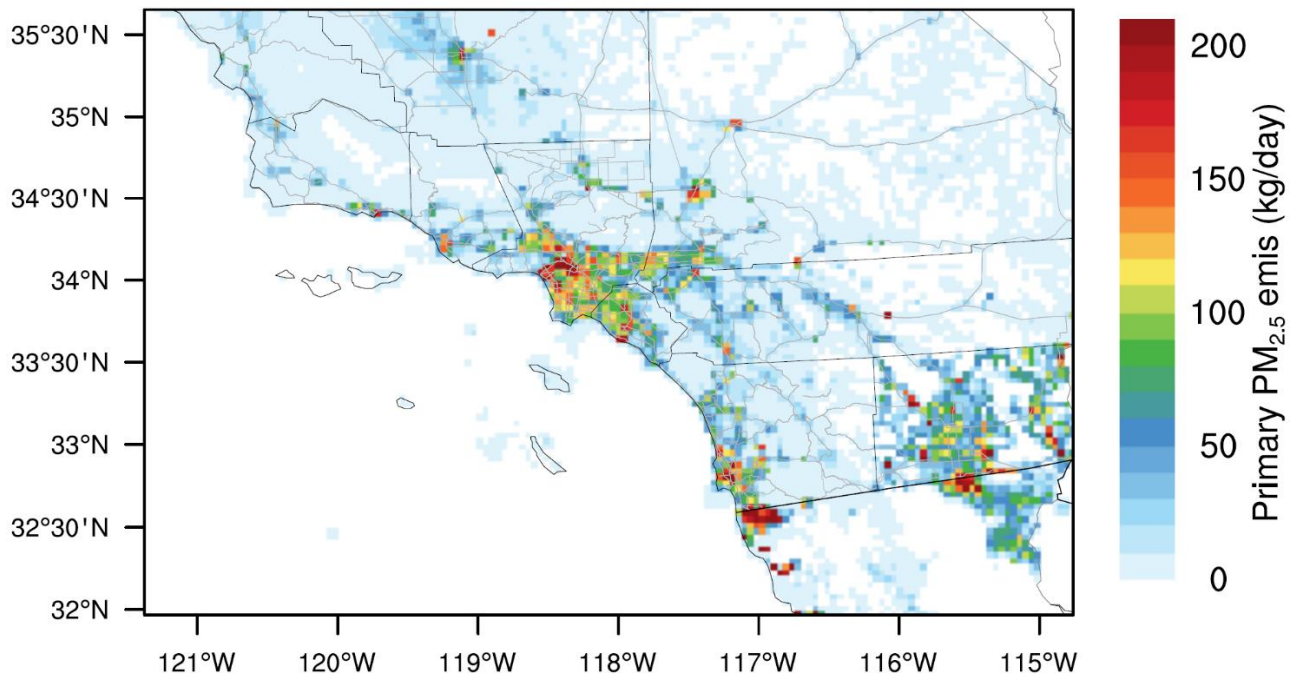


FIGURE II-4-9

TOTAL PRIMARY PM_{2.5} EMISSIONS FROM ALL SOURCES OVER THE MODELING DOMAIN DURING THE BASE YEAR 2018.

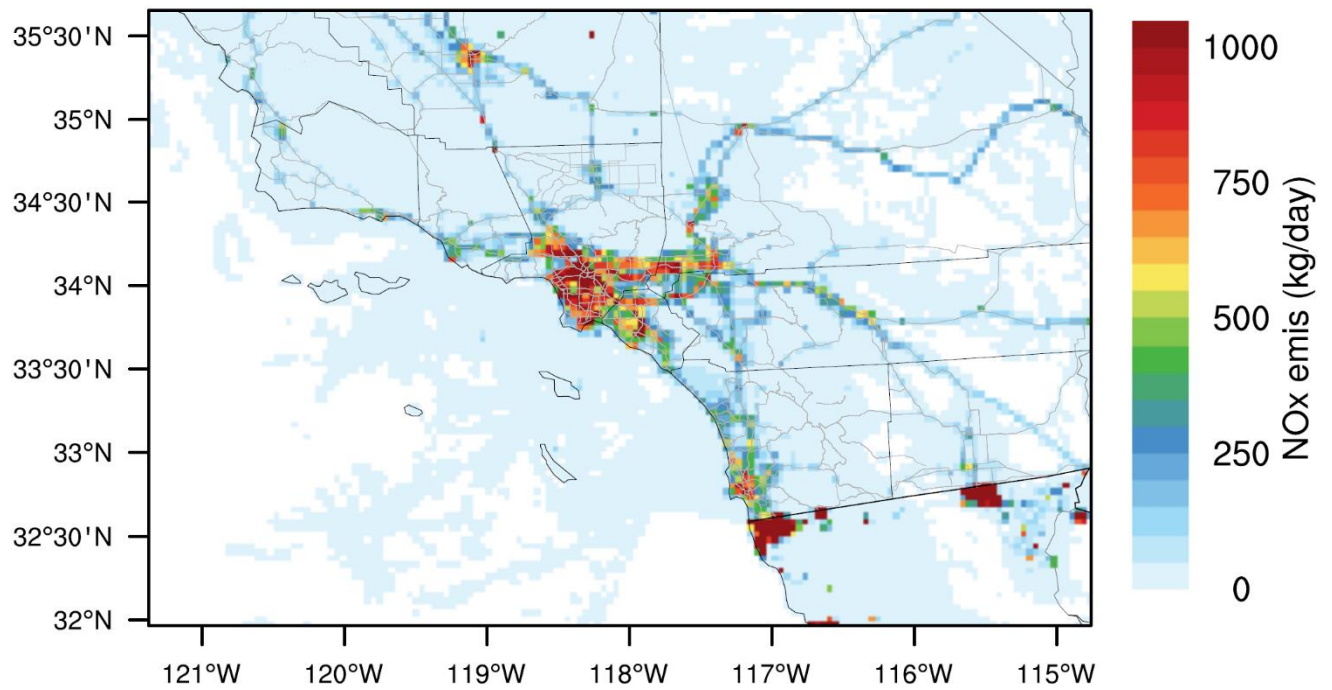


FIGURE II-4-10

TOTAL NO_x EMISSIONS FROM ALL SOURCES OVER THE MODELING DOMAIN DURING THE BASE YEAR 2018.

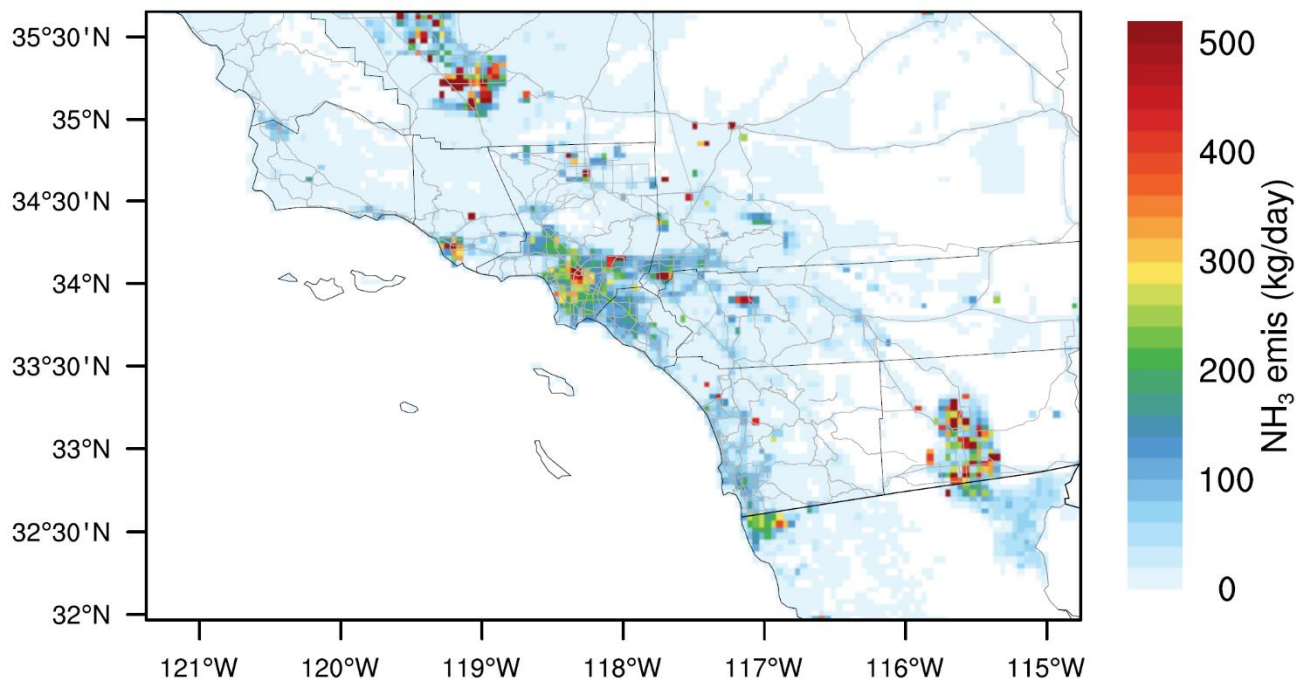


FIGURE II-4-11

TOTAL NH₃ EMISSIONS FROM ALL SOURCES OVER THE MODELING DOMAIN DURING THE BASE YEAR 2018.

Biogenic Emissions

Biogenic VOC emissions were calculated at an hourly frequency using the Model of Emissions of Gases and Aerosols from Nature version 3.0 (MEGAN3.0) with 2018 meteorological data as input (simulated with WRFv4.4.2). MEGAN was employed in its default configuration, with the exception of the normalized Leaf Area Index (LAIv) input. The LAIv input we used here was developed by the California Air Resources Board and was derived from 2018 data obtained from the Moderate Resolution Imaging Spectroradiometer (MODIS) on NASA’s Terra and Aqua satellites. In urban areas where MODIS data were unavailable, LAIv was based on tree survey data from the US Forest Service. Figure II-4-12 illustrates the daily total emissions of biogenic VOC, in tons per day, within the Basin. The trend shows higher emissions during spring and summer months, with multiple peaks occurring from June to August, coinciding with periods of high temperatures. Table II-4-1 shows the total emissions from biogenic sources within the Basin.

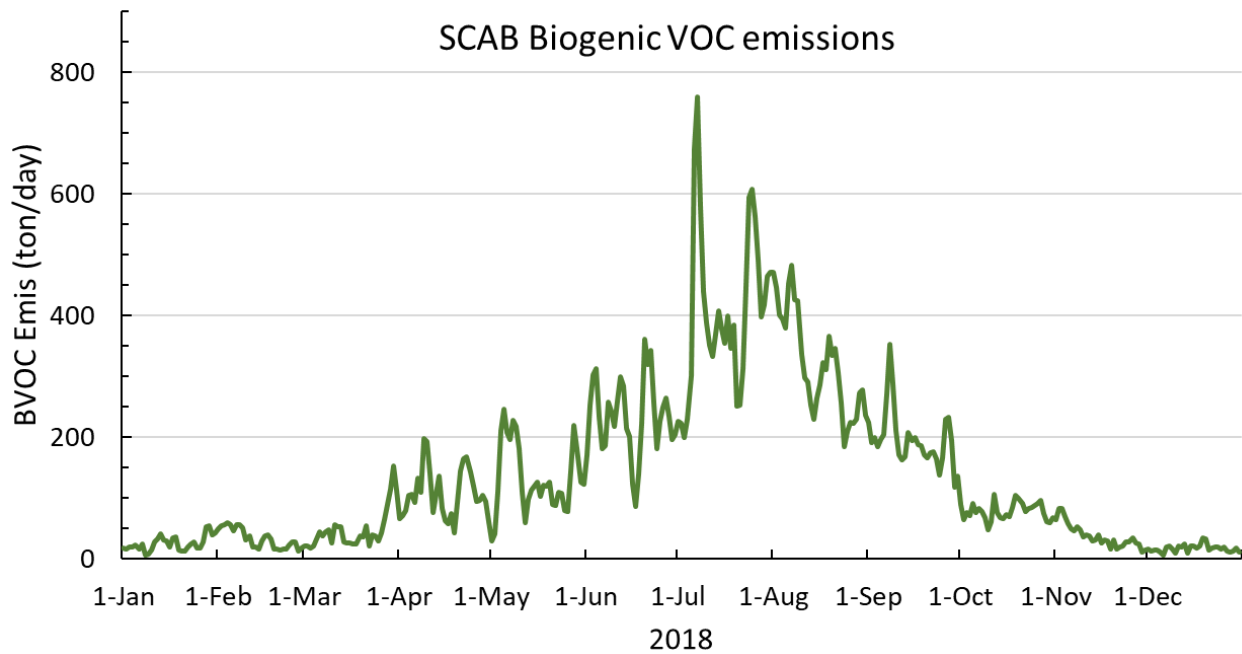


FIGURE II-4-12

2018 DAILY BIOGENIC VOC EMISSIONS IN THE SOUTH COAST AIR BASIN

TABLE II-4-1

ANNUAL AVERAGES EMISSIONS FROM BIOGENIC SOURCES IN THE BASIN (TONS/DAY)

| | TOG | VOC | NO _x |
|---------------------------------|-------|-------|-----------------|
| Basin-wide Emissions (tons/day) | 135.1 | 132.1 | 5.3 |

Boundary and Initial Conditions

We utilized the Community Atmosphere Model with Chemistry (CAM-chem; Emmons et al., 2020)², a component of the National Center for Atmospheric Research (NCAR) Community Earth System Model (CESM), to generate boundary conditions (BCONs) for our modeling domains. Specifically, CAM-chem provided BCONs for the 12 km statewide Community Multi-scale Air Quality (CMAQ) domain, while the boundary conditions for the 4 km inner South Coast domain were derived from the 12 km CMAQ output.

CAM-chem is a well-established global atmospheric model known for simulating tropospheric and stratospheric compositions. We extracted boundary conditions encompassing inorganic gases, volatile organic compounds (VOCs), and aerosol species such as elemental carbon, organic matter, sulfate, and nitrate from CAM-chem simulations conducted in 2018³. These CAM-chem simulation results are publicly accessible at <https://www.acom.ucar.edu/cam-chem/cam-chem.shtml>. To prepare this data for integration into the CMAQ model, we used the 'mozart2camx' computer program, originally designed for processing outputs from the MOZART global model. Some modifications were made to adapt it for CAM-chem output processing.

Vertical layering in the BCON data adheres to the meteorological files, utilizing pressure levels at each layer interface for vertical interpolation. For horizontal alignment, bilinear interpolation was applied to interpolate data from the global model grids to the regional CMAQ grids. Speciation profiles were employed to map CAM-chem species into CMAQ species for trace gases (SAPRC07TC) and aerosols. The final CAM-chem derived BCONs for the CMAQ domain represent day-specific mixing ratios, varying in spatial (horizontal and vertical) and temporal (every 6 hours) dimensions.

Total PM_{2.5} Mass in Boundary Conditions

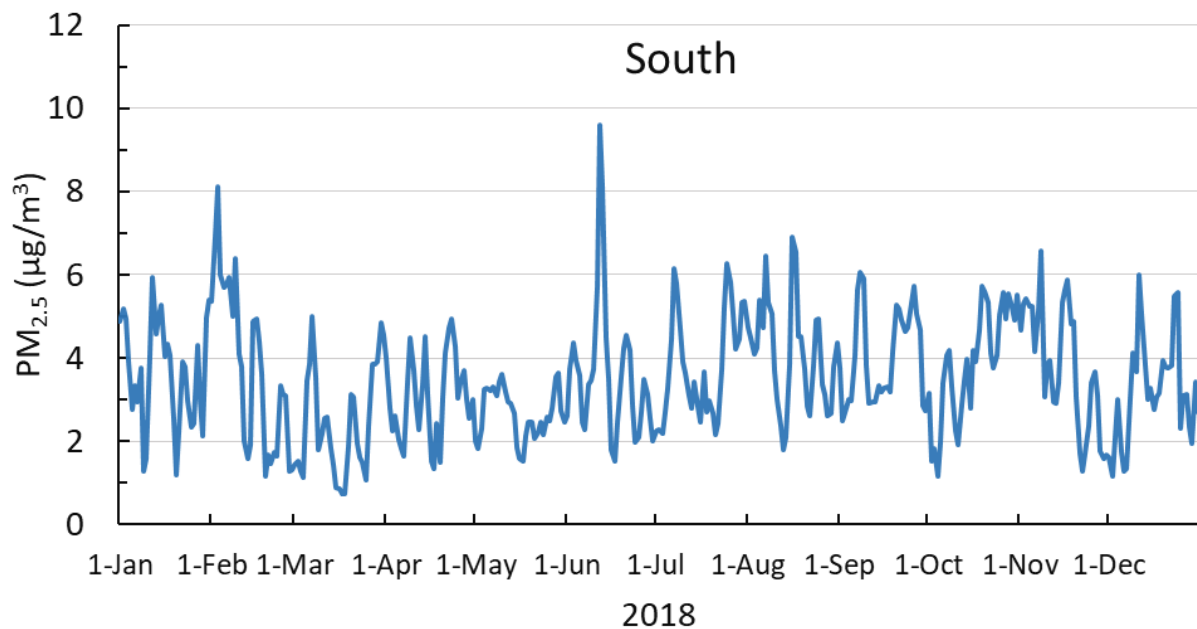
Figures II-4-13 and II-4-14 illustrate daily averages of surface total PM_{2.5} along the four boundaries of our modeling domain. The mean surface PM_{2.5} levels along the southern and northern boundaries exhibit similarities, typically ranging from 1 to 6 µg/m³. Notably, there are periodic peaks in PM_{2.5} concentrations (ranging from 6 to 10 µg/m³) along the southern boundary during the summer season, possibly attributed

² Emmons, L. K., Schwantes, R. H., Orlando, J. J., Tyndall, G., Kinnison, D., Lamarque, J.-F., et al., (2020). The Chemistry Mechanism in the Community Earth System Model version 2 (CESM2). *Journal of Advances in Modeling Earth Systems*, 12, e2019MS001882, <https://doi.org/10.1029/2019MS001882>

³ Buchholz, R. R., Emmons, L. K., Tilmes, S., & The CESM2 Development Team, (2019). CESM2.1/CAM-chem Instantaneous Output for Boundary Conditions. UCAR/NCAR - Atmospheric Chemistry Observations and Modeling Laboratory. <https://doi.org/10.5065/NMP7-EP60>.

to regional transport from Mexico when southerly winds prevail. In contrast, the northern boundary is influenced by emissions from central California, resulting in a seasonal average surface PM2.5 concentration of approximately 3-4 $\mu\text{g}/\text{m}^3$. The western boundary, situated over the Pacific Ocean west of the Basin, consistently shows the lowest concentrations, with an average PM2.5 concentration peaking in summer and fall seasons ($\sim 3 \mu\text{g}/\text{m}^3$) and dropping in spring ($\sim 2 \mu\text{g}/\text{m}^3$).

The eastern boundary, on the other hand, exhibits a broader range, with average PM2.5 concentrations ranging from 2 to 12 $\mu\text{g}/\text{m}^3$. These concentrations tend to be higher than those observed along other boundaries, particularly during the summer months. This difference may be attributed to elevated background particulate levels resulting from wildfires and biogenic sources originating from the eastern region. Additionally, the prevailing general circulation in Southern California moves from west to east, causing the eastern boundary to experience a higher background level of PM2.5 due to the influence of upwind emissions compared to other boundaries. The peak of PM2.5 ($>12 \mu\text{g}/\text{m}^3$) occurred in June at the eastern boundary is likely attributed to a wildfire event.



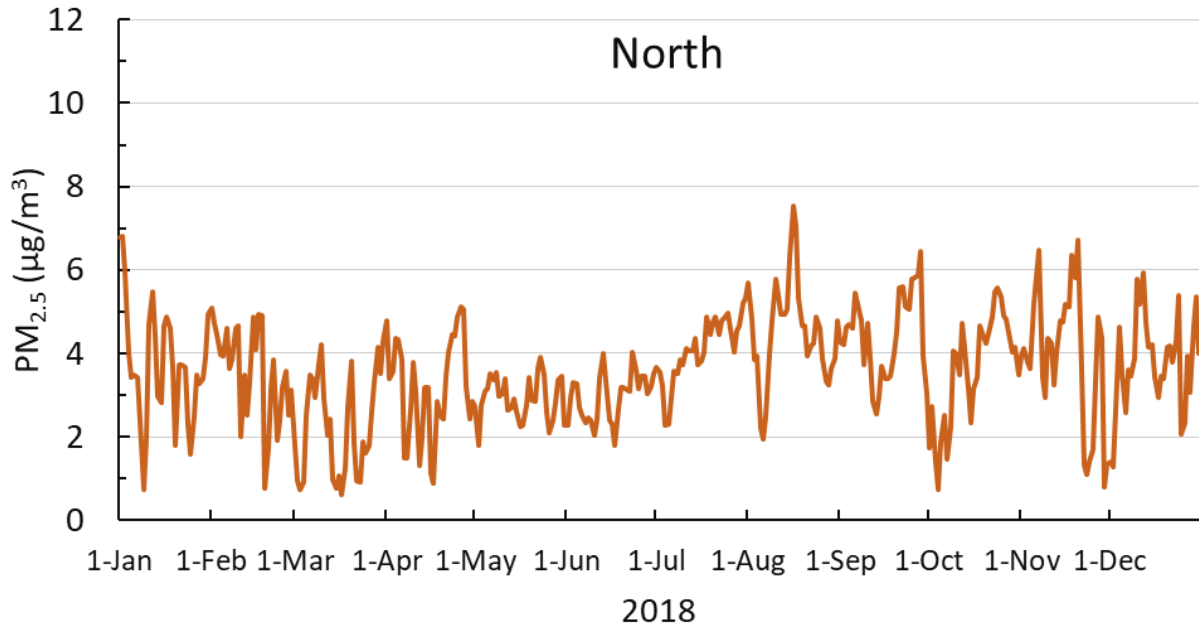
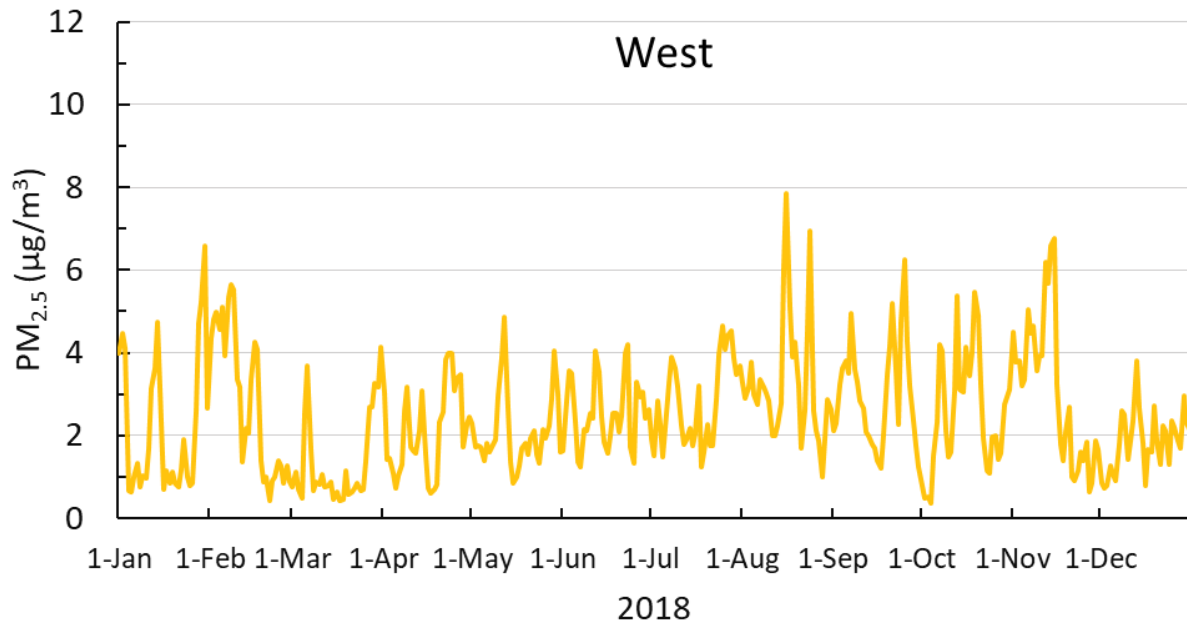


FIGURE II-4-13

DAILY AVERAGES OF SURFACE PM_{2.5} CONCENTRATION ALONG THE SOUTH AND NORTH BOUNDARIES



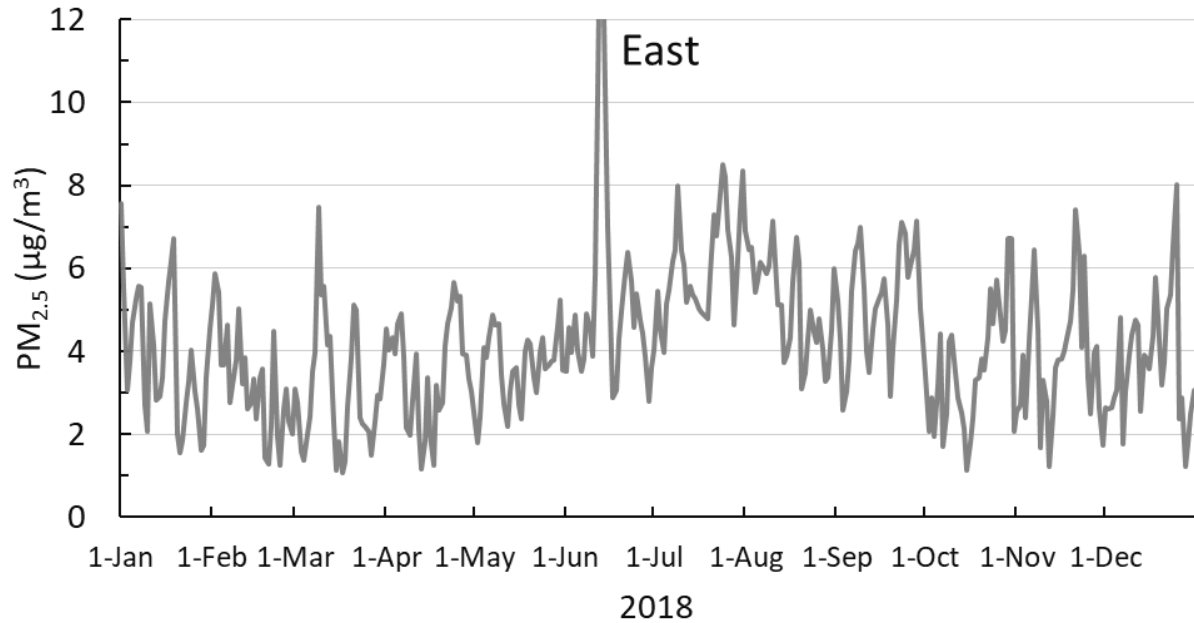


FIGURE II-4-14

DAILY AVERAGES OF SURFACE PM_{2.5} CONCENTRATION ALONG THE WEST AND EAST BOUNDARIES

Figures II-4-15 through II-4-18 depict vertical profiles of seasonal PM_{2.5} concentrations, extending from the ground surface to the mid-troposphere, along the four boundaries of our modeling domain. In all seasons, PM_{2.5} is predominantly concentrated within the atmospheric boundary layer, with background PM_{2.5} levels above the boundary layer typically below 2 µg/m³. Both near-surface PM_{2.5} and background PM_{2.5} in the free troposphere peaks in the summer months along all four boundaries. This phenomenon is likely attributable to increased secondary production under warm and humid summer conditions. The most notable disparity between near-surface (or boundary layer) and free-tropospheric PM_{2.5} concentrations occurs during winter due to reduced vertical mixing and ventilation compared to warmer seasons.

Both near-surface and free-tropospheric PM_{2.5} concentrations are higher along the eastern boundary compared to the other boundaries. This disparity arises from downwind transport and greater influences from wildfires and biogenic matter compared to the other boundaries. Conversely, the western boundary consistently has the lowest PM_{2.5} levels within both the boundary layer and free troposphere due to the relatively cleaner airflow originating from the ocean.

South

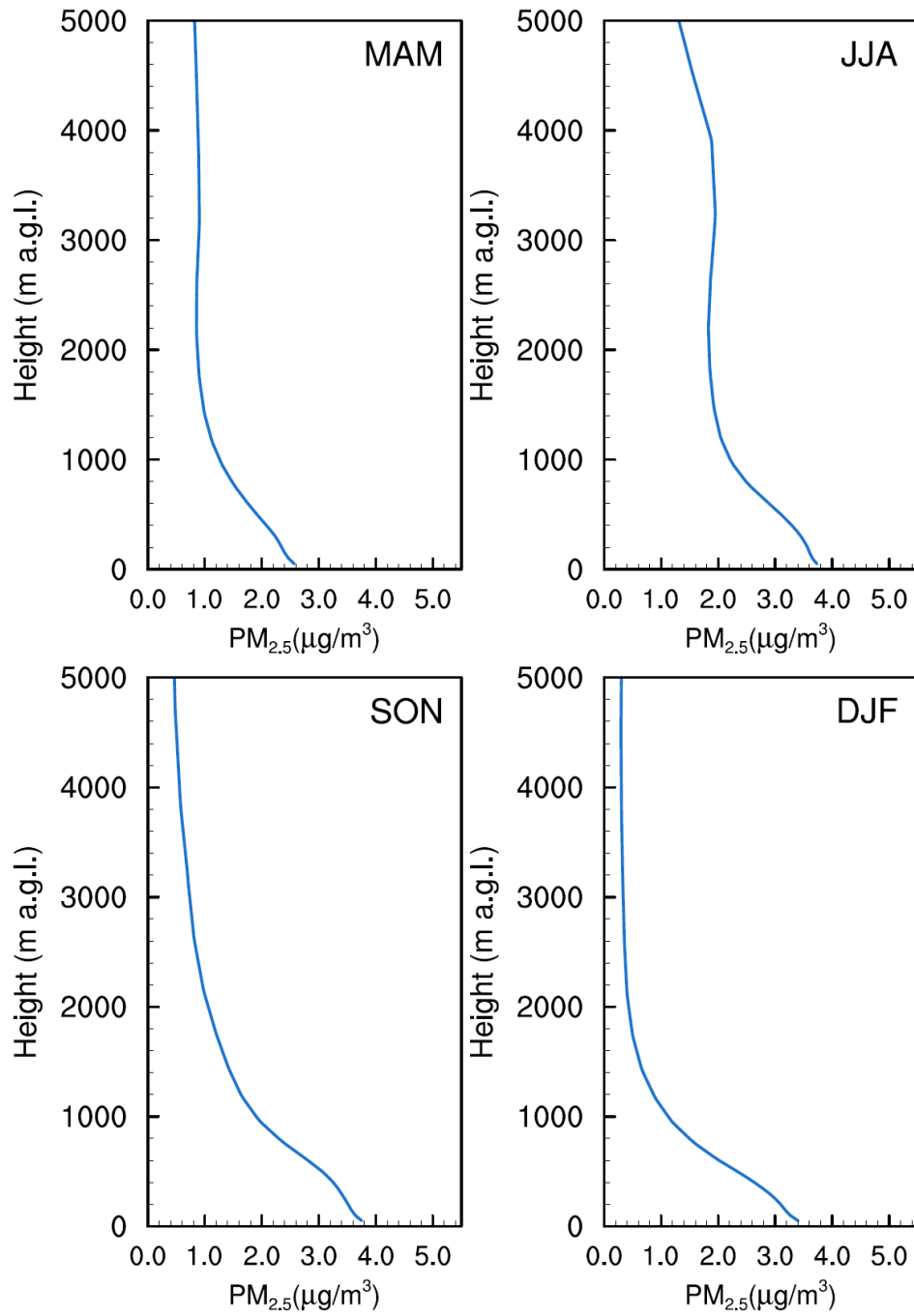


FIGURE II-4-15

PM_{2.5} VERTICAL PROFILE ALONG THE SOUTHERN BOUNDARY IN FOUR SEASONS

North

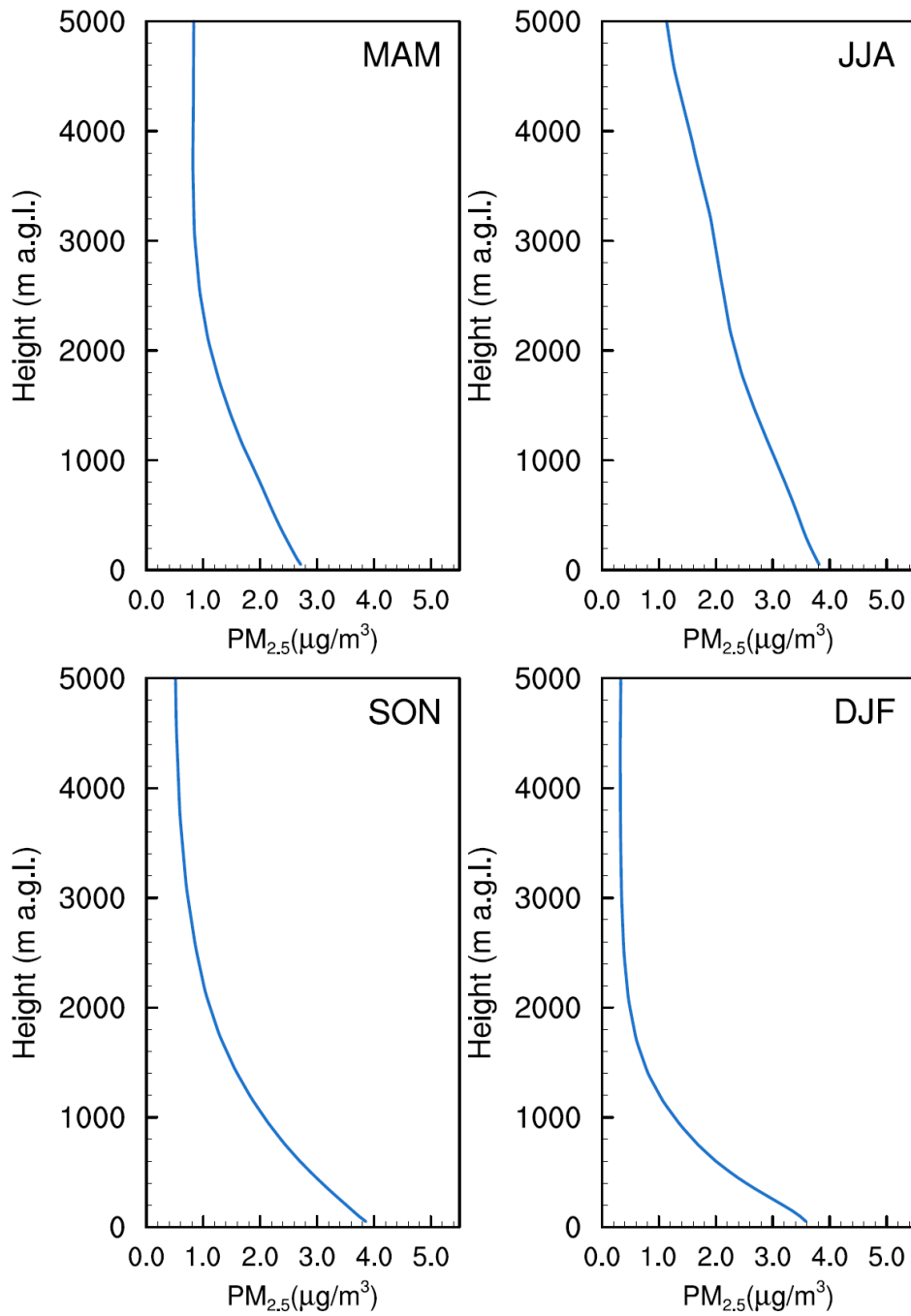


FIGURE II-4-16

PM_{2.5} VERTICAL PROFILE ALONG THE NORTHERN BOUNDARY IN FOUR SEASONS

West

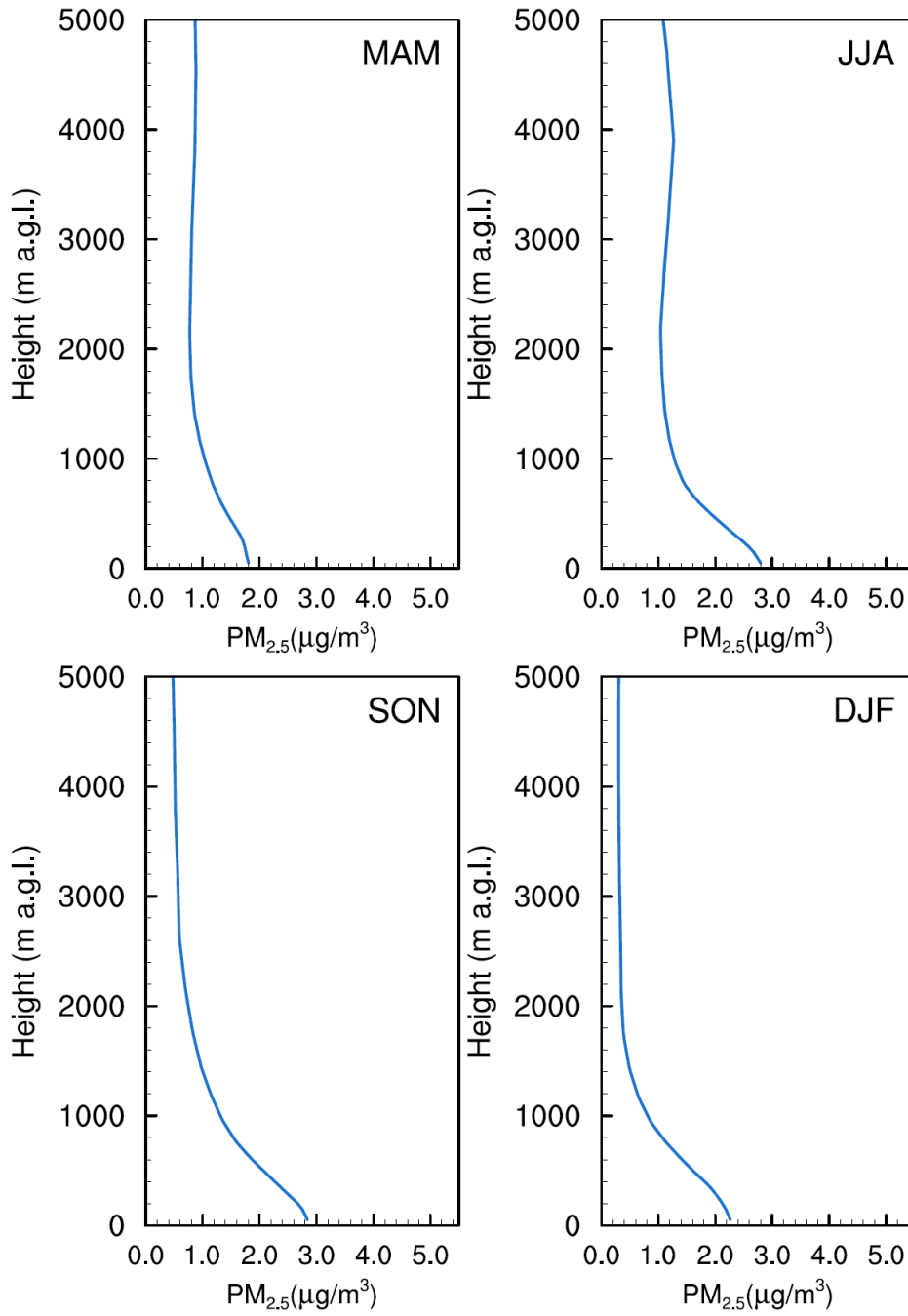


FIGURE II-4-17

PM_{2.5} VERTICAL PROFILE ALONG THE WESTERN BOUNDARY IN FOUR SEASONS

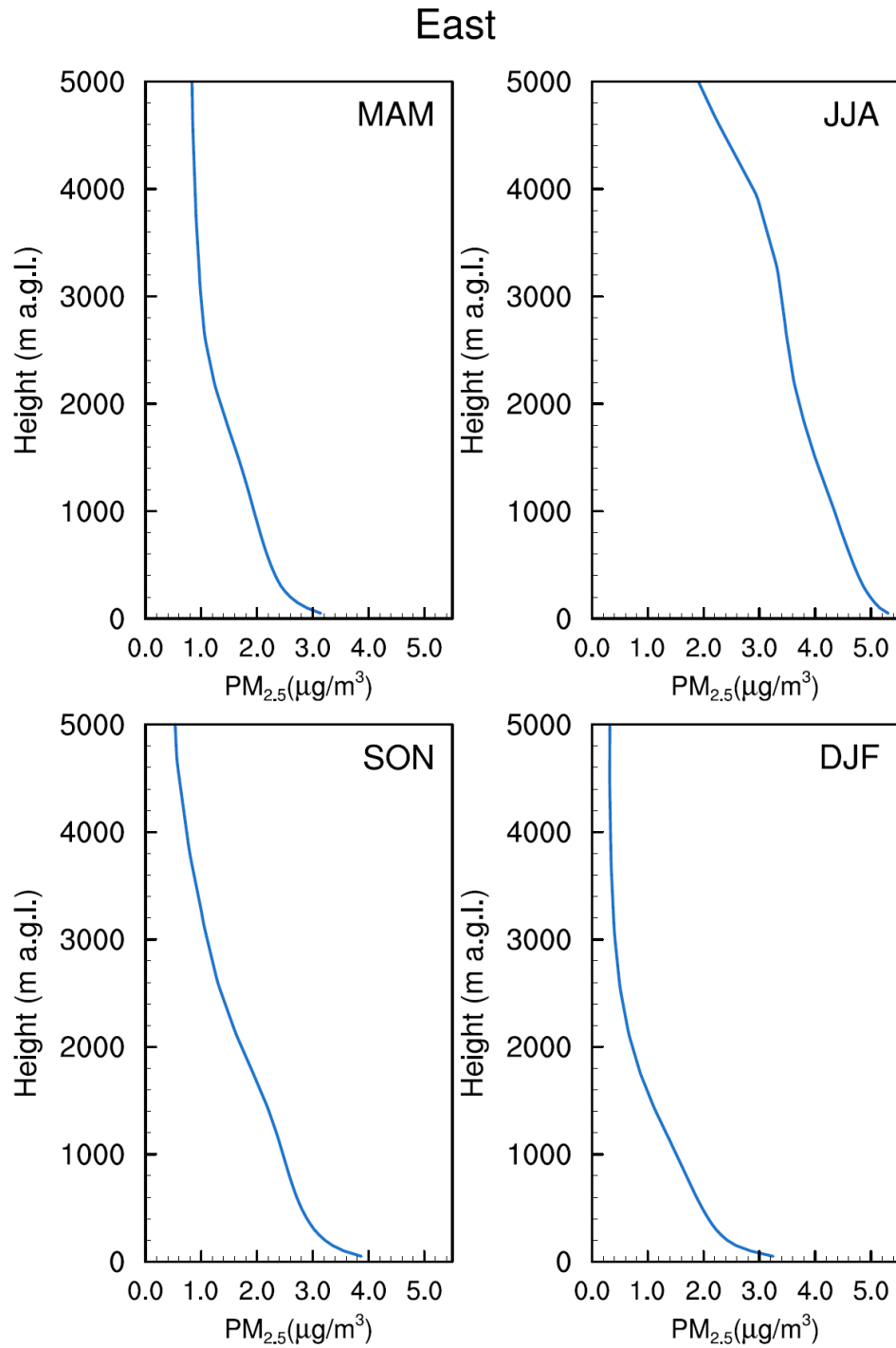


FIGURE II-4-18

PM_{2.5} VERTICAL PROFILE ALONG THE EASTERN BOUNDARY IN FOUR SEASONS

The boundary values used in future year simulations were retrieved using the same approach as in the base year (2018), except for anthropogenic emissions, which were adjusted based on the projected future

emission levels in the State. In this approach, out of state emissions were not adjusted due to the lack of accurate information, but the impact of statewide emission reductions was considered.

PM2.5 Species in Boundary Conditions

We further examine the boundary and initial conditions of several major PM2.5 species, including nitrate, sulfate, elemental carbon (EC), and organic carbon (OC). Figures II-4-19 and II-4-22 illustrate daily averages of these PM2.5 species along the four boundaries of our modeling domain. The boundary conditions exhibit significant variations across four different directions and among various PM2.5 species. OC emerges as the predominant PM2.5 species along all four boundaries, with annual average concentrations ranging from 0.72 to 1.88 $\mu\text{g}/\text{m}^3$. This is followed by sulfate (0.43-0.73 $\mu\text{g}/\text{m}^3$), nitrate (0.30-0.38 $\mu\text{g}/\text{m}^3$), and EC (0.05-0.19 $\mu\text{g}/\text{m}^3$). Table II-4-2 provides an overview of the annual averages of PM2.5 species along these four boundaries.

Nitrate and sulfate levels are at their highest along the southern boundary due to anthropogenic emissions originating from cities in Southern California and Mexico (Figures II-4-19 and II-4-20). However, at the western boundary, nitrate and sulfate concentrations are comparable to the levels in other boundary directions. This is possibly attributed to various factors, including transport by land-sea oscillations, long-range transport from Asia, and marine/ship emissions. EC concentrations peak at the southern and eastern boundaries due to anthropogenic emissions from Mexico and wildfires occurring in the western U.S. states (Figure II-4-21). OC exhibits higher levels at the northern and eastern boundaries, possibly due to the influence of wildfires and biogenic sources. Compared to nitrate, sulfate, and EC, OC generally has a shorter atmospheric lifetime and thus is closer to its sources than other species (e.g., Cheung et al., 2011)⁴. Therefore, unlike other species, OC concentrations are at their lowest along the western boundaries (Figure II-4-22), owing to the relatively clean airflow originating from the ocean.

When comparing PM2.5 species to gaseous pollutants such as NO_x, it's worth noting that particulate matter has a longer atmospheric lifetime. This extended lifetime allows PM2.5 species to disperse more evenly across different boundaries than most gaseous pollutants. In contrast, gaseous pollutants like NO_x show substantial concentration variations across boundaries, with notably low levels at the western boundary (close to zero) and comparatively higher levels at other boundaries (Figure not shown).

⁴ Cheung, K., Daher, N., Kam, W., Shafer, M. M., Ning, Z., Schauer, J. J., & Sioutas, C. (2011). Spatial and temporal variation of chemical composition and mass closure of ambient coarse particulate matter (PM_{10-2.5}) in the Los Angeles area. *Atmospheric environment*, 45(16), 2651-2662, <https://doi.org/10.1016/j.atmosenv.2011.02.066>

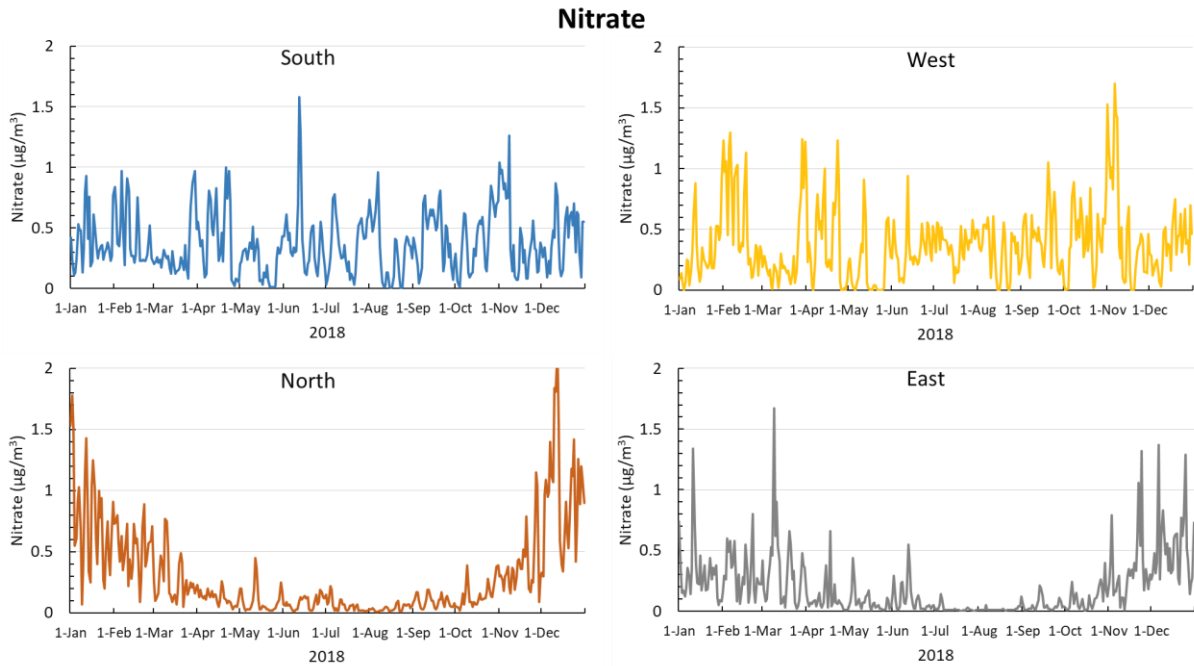


FIGURE II-4-19

DAILY AVERAGES OF SURFACE NITRATE CONCENTRATION ALONG THE FOUR BOUNDARIES OF MODELING DOMAIN

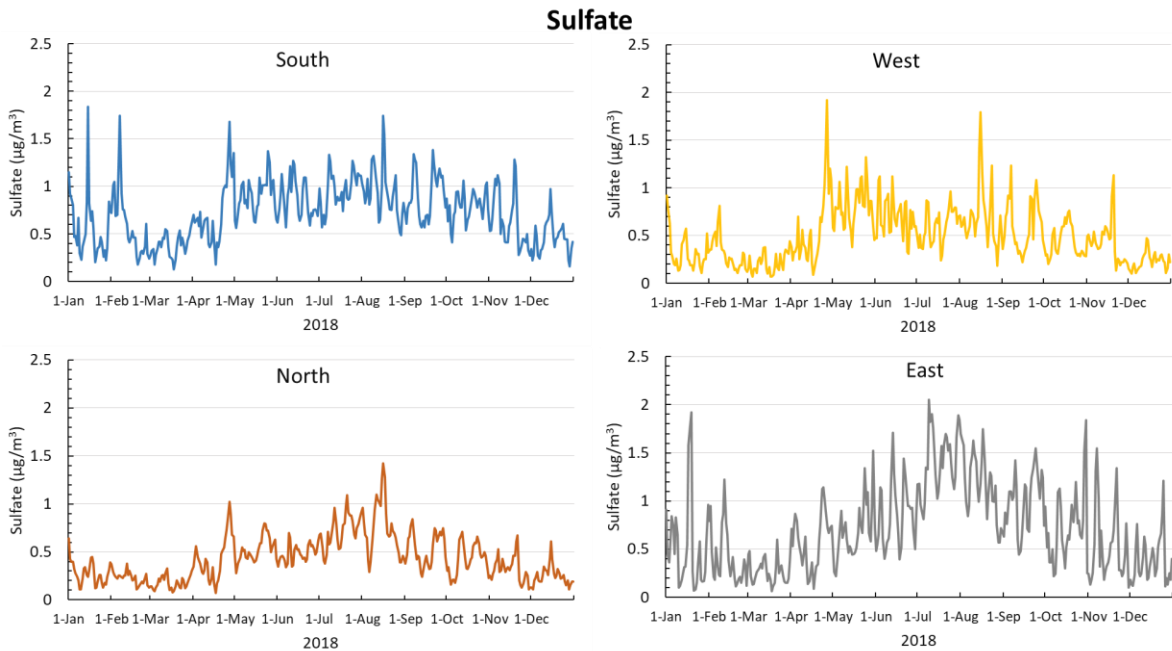


FIGURE II-4-20

DAILY AVERAGES OF SURFACE SULFATE CONCENTRATION ALONG THE FOUR BOUNDARIES OF MODELING DOMAIN

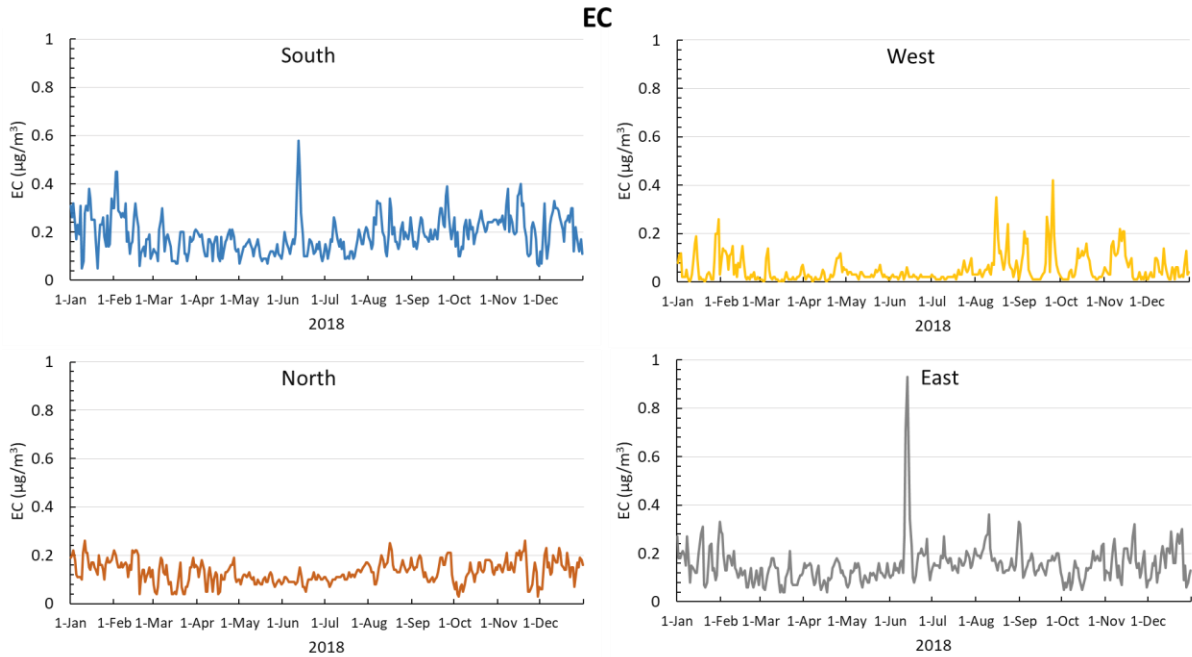


FIGURE II-4-21

DAILY AVERAGES OF SURFACE ELEMENTAL CARBON CONCENTRATION ALONG THE FOUR BOUNDARIES OF MODELING DOMAIN

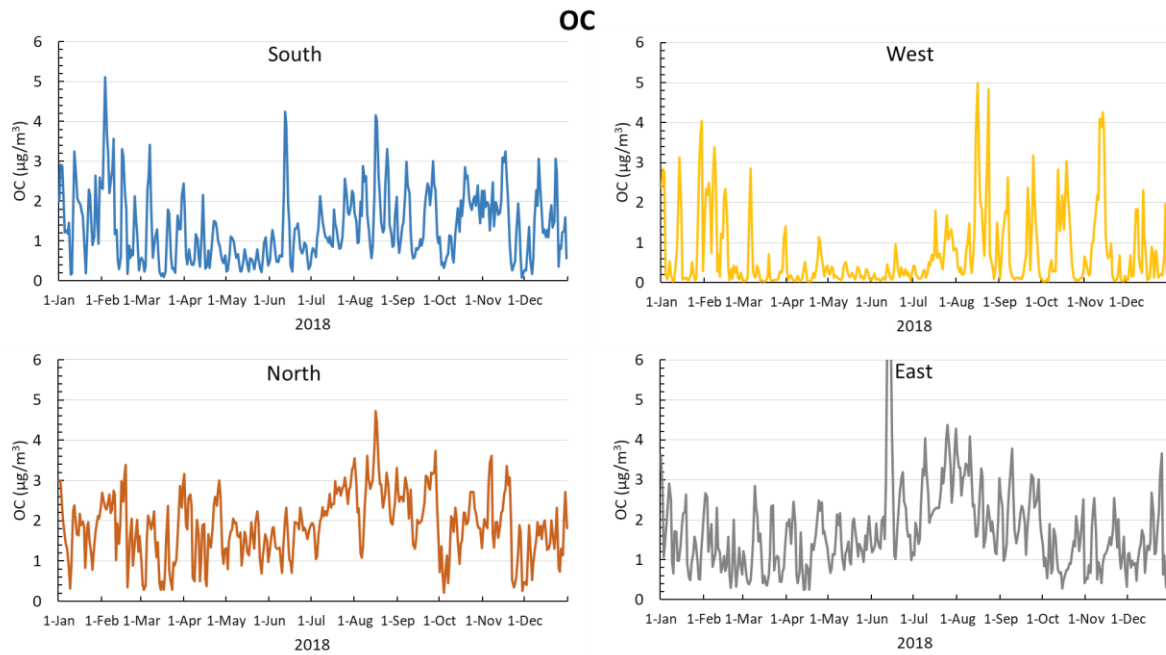


FIGURE II-4-22

DAILY AVERAGES OF SURFACE ORGANIC CARBON CONCENTRATION ALONG THE FOUR BOUNDARIES OF MODELING DOMAIN

TABLE II-4-2

ANNUAL AVERAGES OF MAJOR PM2.5 SPECIES AND TOTAL PM2.5 ALONG THE FOUR BOUNDARIES OF MODELING DOMAIN ($\mu\text{g}/\text{m}^3$)

| | South | West | North | East |
|-------------|-------|------|-------|------|
| Nitrate | 0.38 | 0.37 | 0.30 | 0.19 |
| Sulfate | 0.73 | 0.49 | 0.43 | 0.71 |
| EC | 0.19 | 0.05 | 0.13 | 0.15 |
| OC | 1.36 | 0.72 | 1.88 | 1.70 |
| Total PM2.5 | 3.48 | 2.47 | 3.59 | 4.19 |

Chapter 5

ANNUAL PM2.5 ATTAINMENT DEMONSTRATION

Introduction

Annual PM2.5 Modeling Approach

Performance Evaluation

Base Year Annual PM2.5

Future Year Annual PM2.5 Air Quality

Unmonitored Area Analysis

Summary and Conclusions

Introduction

On April 15, 2015, the South Coast Air Basin was designated a ‘moderate’ non-attainment area for the 2012 annual PM2.5 standard of 12 µg/m³. This designation set an attainment deadline of December 31, 2021, based on CAA subpart 4, which establishes that attainment must be reached by the end of the 6th calendar year after the effective date of “moderate” designation. Acknowledging the challenges in meeting the standard, including the feasibility of proposed measures, uncertainties in drought conditions, and the potential inability to credit all ozone strategy reductions towards PM2.5 attainment if approved under CAA Section 182(e)(5), South Coast AQMD requested a voluntary bump-up to the “serious” classification, with a new attainment date of 2025. On December 9, 2020, U.S. EPA reclassified the Basin from “moderate” to “serious” nonattainment for the 2012 annual PM2.5 NAAQS with an attainment deadline by December 31, 2025.¹ “Serious” nonattainment areas are required to attain the standard as expeditiously as practicable, but no later than the end of the tenth calendar year after the designation, i.e., December 31, 2025. Under CAA Section 188(e), “serious” nonattainment areas may request an attainment date extension to no later than the end of the fifteenth calendar year after the designation, i.e., December 31, 2030. This plan requests an extension of attainment in 2030 due to unforeseen challenges associated with near-road monitored PM2.5 levels, lack of progress from the sources subject to federal and international sources and adverse meteorology.

PM2.5 FRM Sampling

The South Coast AQMD maintains a sampling network of Federal Reference Method (FRM) PM2.5 monitors at 20 sites throughout the Basin and Coachella Valley. This network is supplemented by Federal Equivalent Method (FEM) continuous PM2.5 monitors at a subset of these locations to report real-time data to the public and to feed for forecasting algorithms. FRM samplers pull ambient air through a filter over a 24-hour period. The filter is then removed and weighed to determine ambient PM2.5 concentrations during the sampling period. The FEM samplers used by South Coast AQMD are Beta Attenuation monitors that report hourly PM2.5 concentrations continuously, which are averaged over a 24-hour period to determine daily averages. While measurements from FRM and FEM produce similar concentrations, there still is some variation, with FEM samplers typically reading higher than collocated FRM samplers. FRM measurements are used in the determination of attainment status, whereas FEM measurements are used to supplement FRM measurements for days with missing data, if the FEM monitor is determined to be eligible for NAAQS comparison by U.S. EPA. The calculation of 5-year-weighted base year design values used FRM samples with missing FRM samples replaced by NAAQS-comparable FEM samples.

Speciated PM_{2.5} Sampling

South Coast AQMD adopted a Multi-Channel Fine Particulate (MCFP) sampling system for the PM₁₀ Technical Enhancement Program (PTEP) monitoring program in 1995.¹ New PM samplers, speciated air sampling system (SASS) samplers, were deployed at the four Chemical Speciation Network (CSN) sites in the Basin. The SASS sampler collects PM_{2.5} particles on 47mm quartz and Teflon filters simultaneously within the same sampler continuously for 24-hours for subsequent laboratory chemical analysis. Samples were originally collected one out of every six days.

PM_{2.5} speciation data, measured as individual species at the four CSN sites in the Basin during the period 2017-2019, provided the PM_{2.5} chemical characterization for evaluation and validation of the CMAQ annual modeling. The four CSN sites include Riverside-Rubidoux, Fontana, Anaheim and Central Los Angeles (Figure II-5-1). These four sites represent each county that the monitor is located in. PM_{2.5} mass, ions, organic and elemental carbon, and metals, for a total of 43 chemical species, were analyzed from a one-in-six-day sampling schedule at the 4 sites. The speciation profiles in these four sites are used to estimate the speciation profiles at the other monitoring stations using interpolation with inverse distance weighting per U.S. EPA's guidance.

¹ Bong Mann Kim, Solomon Teffera & Melvin D. Zeldin (2000). Characterization of PM_{2.5} and PM₁₀ in the South Coast Air Basin of Southern California: Part 1—Spatial Variations, *Journal of the Air & Waste Management Association*, 50:12, 2034-2044, Available at: <https://doi.org/10.1080/10473289.2000.10464242>

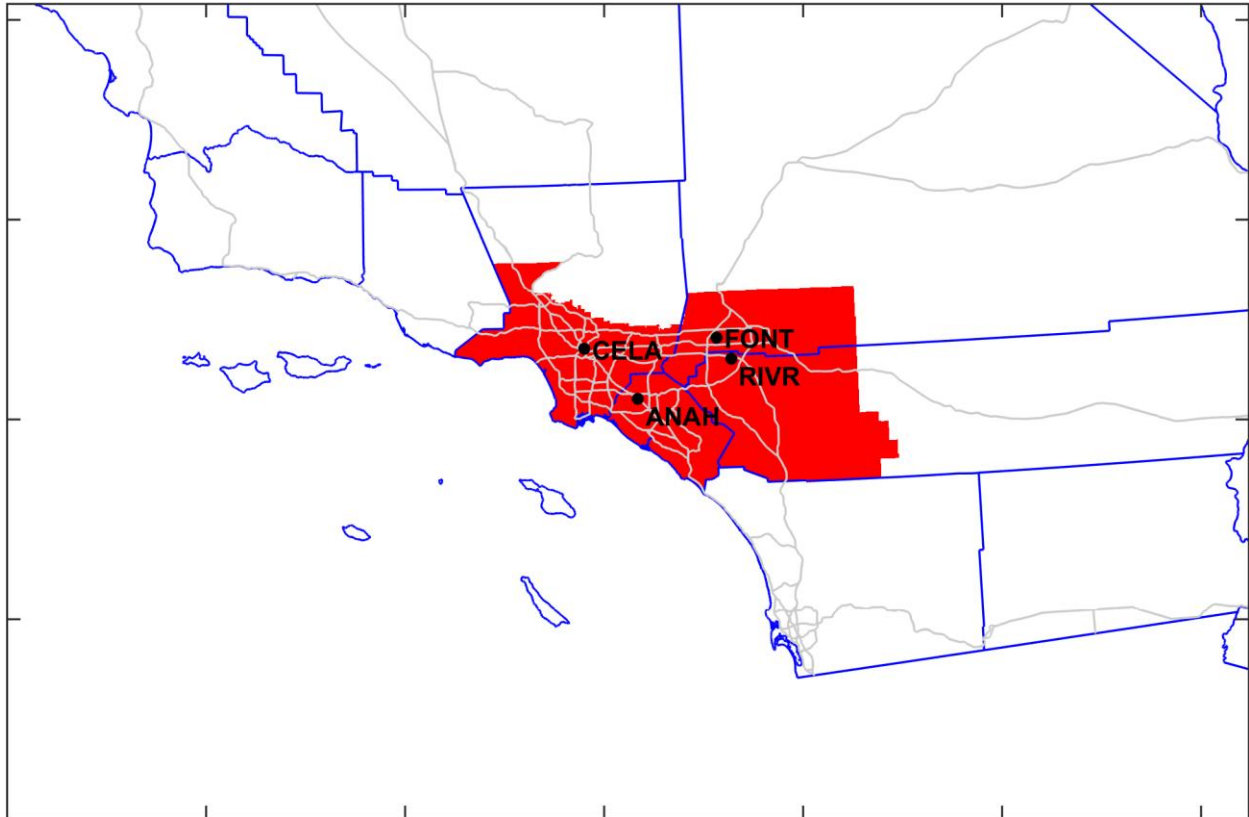


FIGURE II-5-1

SAMPLING SITES IN THE BASIN

PM2.5 speciation data measured by the SASS samplers are used to derive the species fractions required for the PM2.5 attainment demonstration methodology. U.S. EPA's PM2.5 modeling guidance recommends calculating future year PM2.5 design values by multiplying quarterly, species-specific Relative Response Factors (RRFs) with the base year speciated design values for each quarter for each monitoring site. Base year design values are determined from the FRM mass data, however the FRM filters are not chemically speciated. Therefore, the guidance document recommends multiplying the species fractions that are measured in a speciation sampler such as the SASS to the FRM mass data to derive chemically speciated design values for the FRM data. Discussion in the measured design values and the calculation of speciation profiles is presented later in this chapter.

Annual PM_{2.5} Modeling Approach

This PM_{2.5} Plan’s annual PM_{2.5} modeling follows the U.S. EPA modeling guidance² to estimate the future year annual PM_{2.5} levels, which is based on the site and species-specific RRF approach. A five-year weighted quarterly average from the 2016 to 2020 period was established as the base year 2018 design value. The year 2020, however, was excluded in calculation of 2018 base year design values due to exceptionality of 2020. Refer to Chapter 5 for more details.—on the formulation of the modified 5-year weighted design value.

The year 2020 was characterized by a large disruption in air pollutant emissions due to the response to the COVID-19 pandemic and by the exceptionally widespread wildfire activity in the state. The COVID-19 Pandemic started to influence economic activity in March of 2020 in the South Coast AQMD region. During the initial months of “safer at home” orders in late March to June 2020, light-duty and heavy-duty vehicle traffic decreased by 43 percent and 26 percent, respectively, with respect to the month before the COVID stay-at-home measures began. In addition, cargo movement at the ports of Los Angeles and Long Beach decreased by 12 percent, and flights in major airports in the Basin decreased by over 50% during April to June, compared to the same period in 2019. Activity at the ports and airports remained significantly below the business-as-usual level in 2020. Wildfires are a significant source of both fine particulate matter and VOCs. Additional VOC emissions from wildfire activity may lead to increases in secondary PM_{2.5} throughout the Basin. The 2020 fire season was extremely active, with a record amount of acreage burned. Over 4 million acres burned in California in 2020, more than double the previous modern record set in 2018. Both fires within the South Coast Air Basin such as the Bobcat, El Dorado, Silverado, Blue Ridge, Ranch2, Apple and Snow fires and fires in Northern and Central California affected air quality in 2020. In total, we identified 13 events that potentially affected PM_{2.5} concentrations in the Basin and that triggered smoke advisories for the Basin.³ These 13 events, listed in Attachment 4 of this appendix, spanned for long periods from mid-June through mid-December. Accordingly, it is unreasonable to use such extraordinary circumstances impacting human activities and associated emissions in a SIP planning which is based on business-as-usual normal situation. More discussions on the COVID-19 impacts, meteorology and wildfire impacts in relation with ozone can be found in Chapter 2 of the 2022 AQMP.

The modeling platform is developed to model an entire year to calculate quarterly PM_{2.5} averages. A day-specific emissions inventory was developed to reflect the temperature and relative humidity dependency of mobile sources and biogenic emissions. Also, seasonal fuel switching, and the resulting emission rates were incorporated in the modeling inventory.

In addition to the base year (2018), future milestone years simulated under this plan were 2025 and 2030, with the former being the target attainment year for a ‘serious’ non-attainment area and the latter for an extended attainment deadline for a ‘serious’ non-attainment area. Both baseline and control scenarios were simulated for each of the future years. CMAQ output was averaged over the 3X3 grid around each monitoring station following U.S. EPA’s modeling guidance.

² Modeling Guidance for Demonstrating Attainment of Air Quality Goals for Ozone, PM_{2.5}, and Regional Haze, U.S. EPA, November 2018. Available at: https://www.epa.gov/sites/default/files/2020-10/documents/o3-pm-rh-modeling_guidance-2018.pdf

³ Smoke advisories released in 2020 available here: <https://www.aqmd.gov/home/news-events/news-and-media/2020-news-archives#>

The base year design values are listed in Table II-5-1. The future year design values are calculated using the base year quarterly averages and the RRF calculated using modeled concentrations for the base year and future scenario. Site- and species-specific RRFs are calculated from CMAQ simulations and then, they are applied to the quarterly average design values which are averaged for the period of 2016 to 2019 using the 5-year weighted average approach. The average of the quarterly species-specific projections is the future design value.

**TABLE II-5-1
FIVE-YEAR WEIGHTED ANNUAL PM2.5 DESIGN VALUES FOR 2018 ($\mu\text{g}/\text{m}^3$)**

| Monitoring Site | Annual 2018 DVB |
|--------------------------------|-----------------|
| Anaheim-Pampas Lane | 10.55 |
| Azusa | 10.13 |
| Big Bear | 6.35 |
| Los Angeles-North Main Street | 11.97 |
| Compton-700 North Bullis Road | 12.25 |
| Fontana-Arrow Highway | 11.35 |
| Long Beach-Route 710 Near Road | 12.28 |
| North Long Beach | 10.53 |
| Mira Loma Van Buren | 13.53 |
| Mission Viejo-26081 Via Pera | 7.94 |
| Ontario- Route 60 Near Road | 13.98 |
| Pasadena-S Wilson Avenue | 9.68 |
| Pechanga | 6.36 |
| Pico Rivera-4144 San Gabriel | 11.87 |
| Reseda | 9.74 |
| Riverside-Rubidoux | 12.13 |
| South Long Beach | 10.58 |
| San Bernardino-4th Street | 10.87 |

Performance Evaluation

The EPA guidance assesses model performance on the ability to predict both PM2.5 component species concentrations and the total mass. No specific performance criteria thresholds are recommended in EPA’s modeling guidance document. This is because the model uses relative response factors rather than direct predictions to forecast future concentrations. Performance is evaluated by examining key statistics and graphical representations of differences between model-predicted concentrations and observations. The statistics examine model bias and error, while graphical representations of model prediction as a function of time and concentration scatter plots supplement the model performance evaluation. The CMAQ modeling results presented for each station are based on the same “1-cell” basis, as recommended by the guidance.

For the CMAQ performance evaluation, the modeling domain is separated into several sub-regions or zones. Figure II-5-2 depicts the sub-regional zones used for base-year simulation performance. The different zones present unique air quality profiles. The Basin is represented by five zones: “Coastal”, “San Fernando”, “Foothills”, “Urban Source”, and “Urban Receptor”. The “Urban Receptor” region typically has the highest PM2.5 concentrations in the Basin. Table II-5-2 lists the stations, their abbreviations, and their assigned performance evaluation zone.

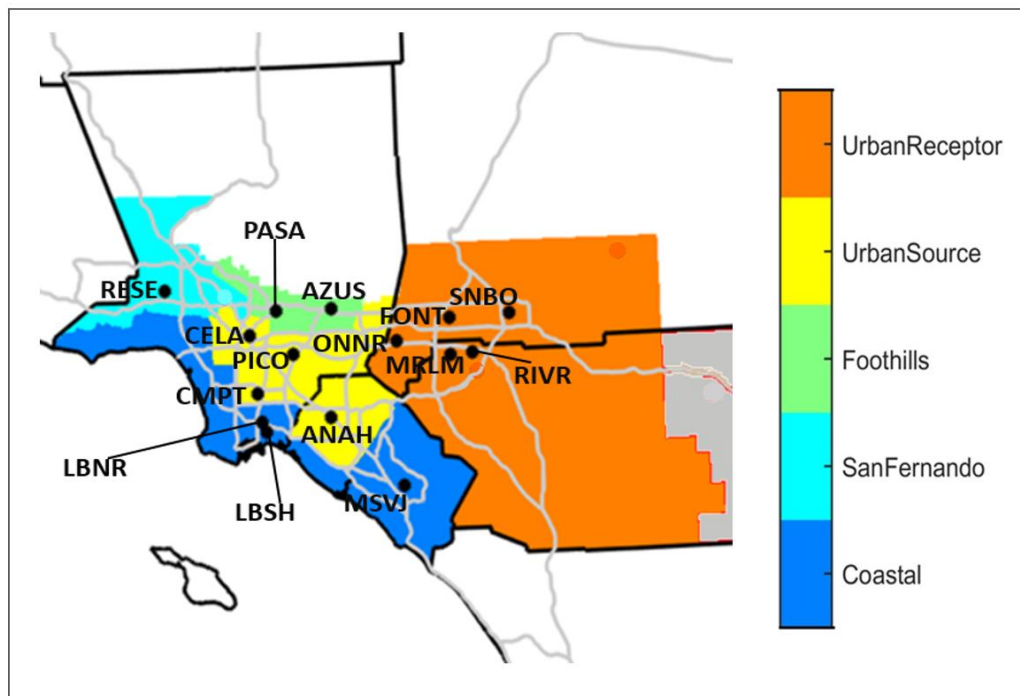


FIGURE II-5-2

PERFORMANCE EVALUATION ZONES. BLACK DOTS INDICATE THE LOCATION OF FRM STATIONS.

TABLE II-5-2
FRM STATIONS IN THE SOUTH COAST AIR BASIN

| | Station Location | Station Abbreviation | Performance Evaluation Zone |
|--------|------------------|----------------------|-----------------------------|
| Blue | Long Beach | LGBH | Coastal |
| | Mission Viejo | MSVJ | Coastal |
| | South Long Beach | SLBH | Coastal |
| Green | Azusa | AZUS | Foothills |
| | Pasadena | PASA | Foothills |
| | Reseda | RESE | San Fernando |
| Orange | Fontana | FONT | Urban Receptor |
| | Mira Loma | MRLM | Urban Receptor |
| | Ontario | ONFS | Urban Receptor |
| | Riverside | RIVR | Urban Receptor |
| | San Bernardino | SNBO | Urban Receptor |
| Yellow | Anaheim | ANAH | Urban Source |
| | Compton | CMPT | Urban Source |
| | Los Angeles | CELA | Urban Source |
| | Pico Rivera | PICO | Urban Source |

Daily predicted and observed PM_{2.5} concentrations at CELA, ANAH, FONT, MRLM, and RIVR are presented in Figures II-5-3 through II-5-7. While absolute concentrations may differ, the model simulates trends in PM_{2.5} reasonably well. Both modelled and observed PM_{2.5} concentrations have high variability and display the highest peaks in the 1st and 4th quarter. Concentrations have less day-to-day variation in the 2nd and 3rd quarters at all the 5 sites. This behavior is likely due to differences in meteorology throughout the year. Weather patterns during the first quarter and the second half of the 4th quarter are typically highly variable; precipitation days, cold, high-winds and unstable conditions associated with synoptic scale storms are all commonly experienced during the winter months. On the contrary, spring and summer weather patterns are dominated by high pressure systems, leading to less day-to-day variation in boundary layer heights and wind speeds.

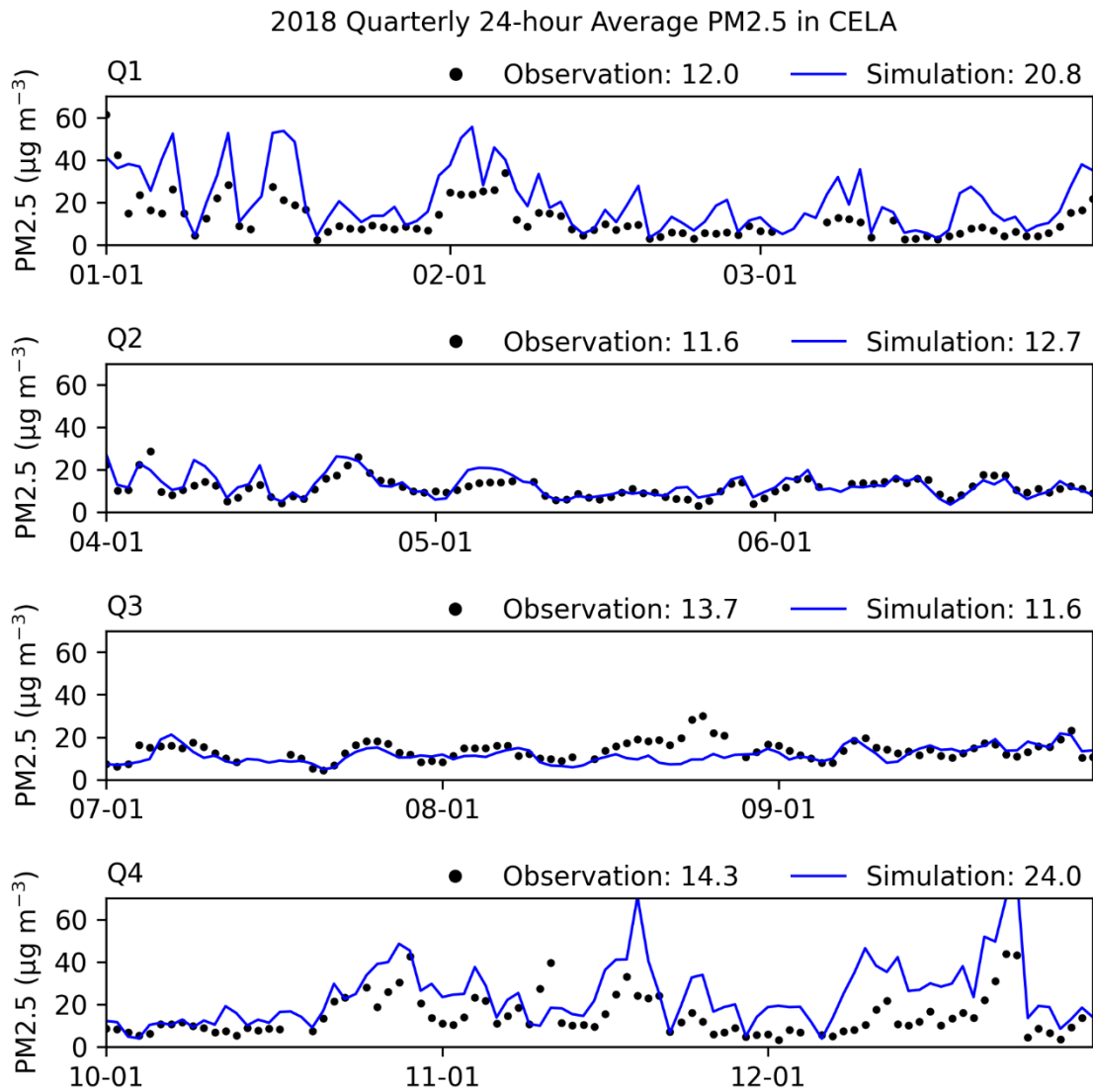


FIGURE II-5-3

2018 MODELLED AND MEASURED 24-HOUR AVERAGE PM2.5 CONCENTRATIONS IN LOS ANGELES

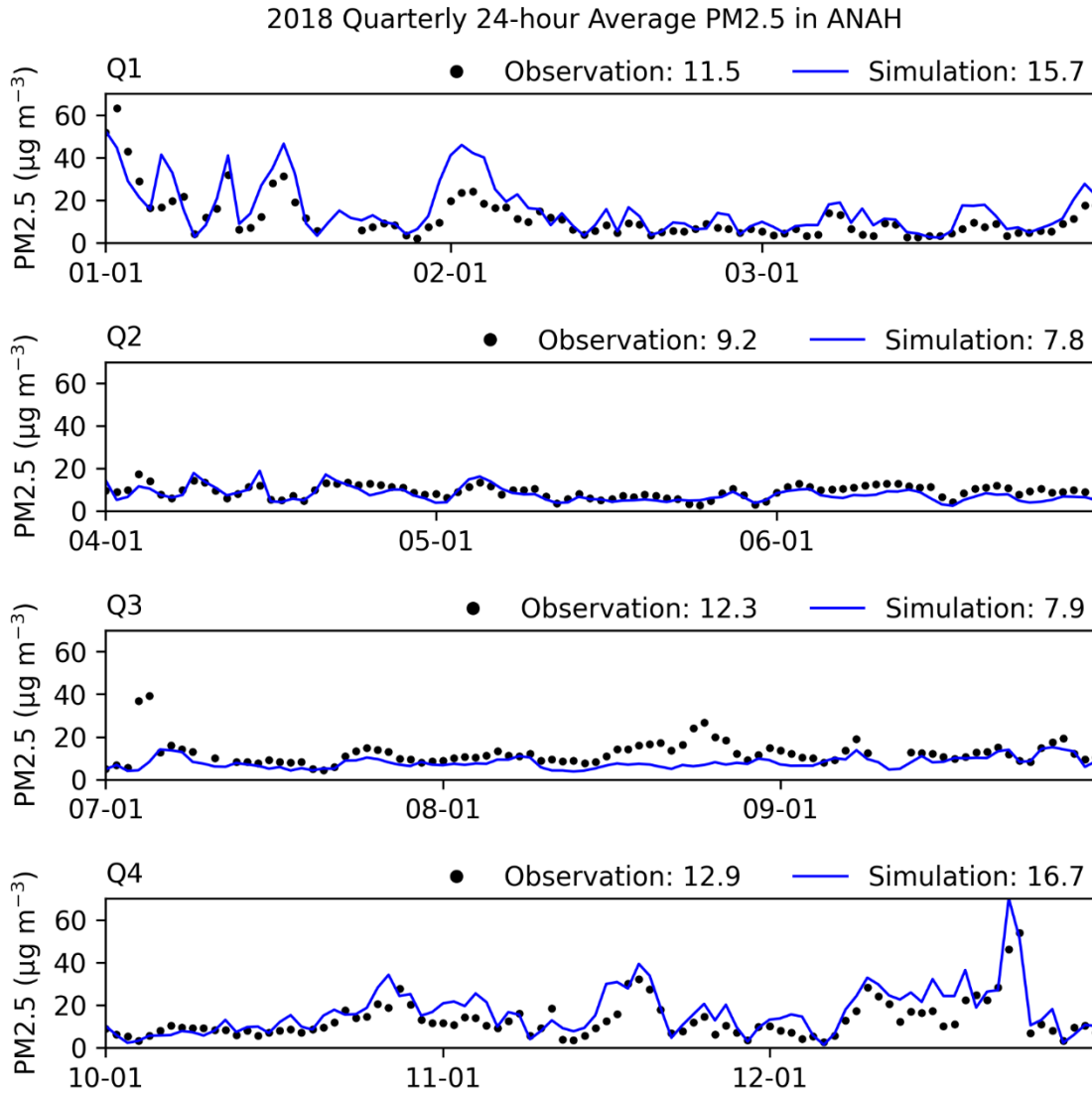


FIGURE II-5-4

2018 MODELLED AND MEASURED 24-HOUR AVERAGE PM_{2.5} CONCENTRATIONS IN ANAHEIM

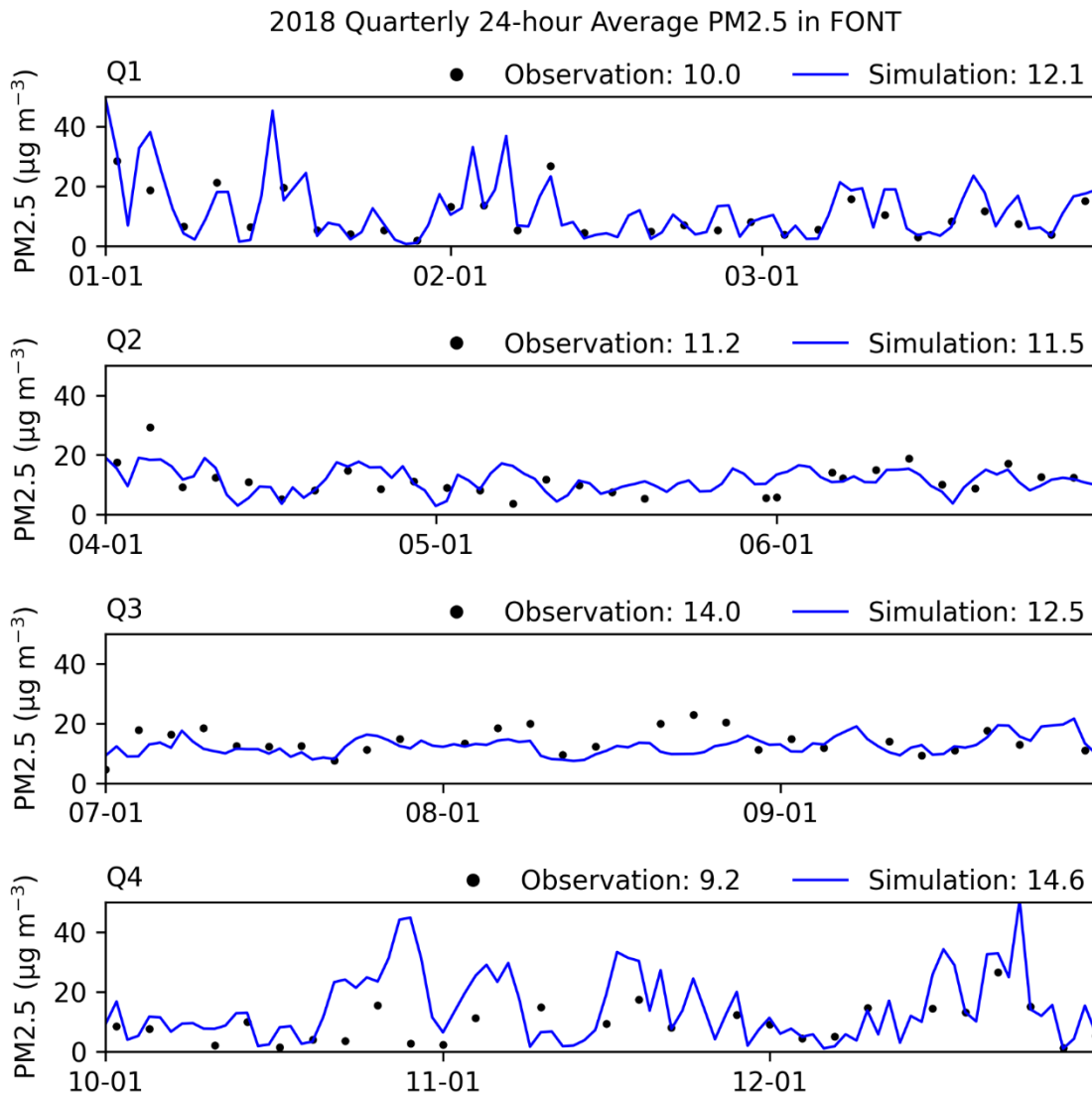


FIGURE II-5-5

2018 MODELLED AND MEASURED 24-HOUR AVERAGE PM_{2.5} CONCENTRATIONS IN FONTANA

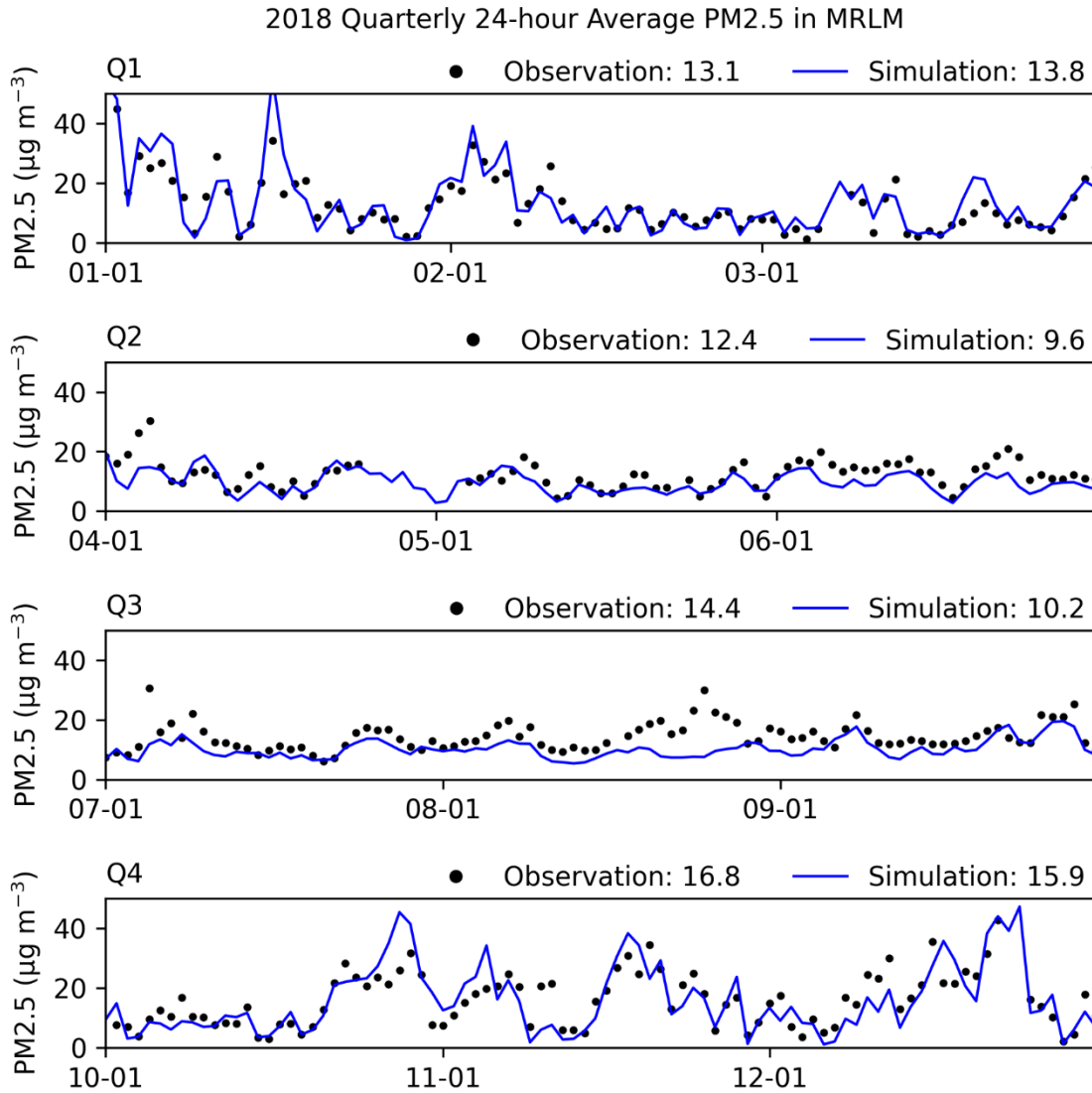


FIGURE II-5-6

2018 MODELLED AND MEASURED 24-HOUR AVERAGE PM_{2.5} CONCENTRATIONS IN MIRA LOMA

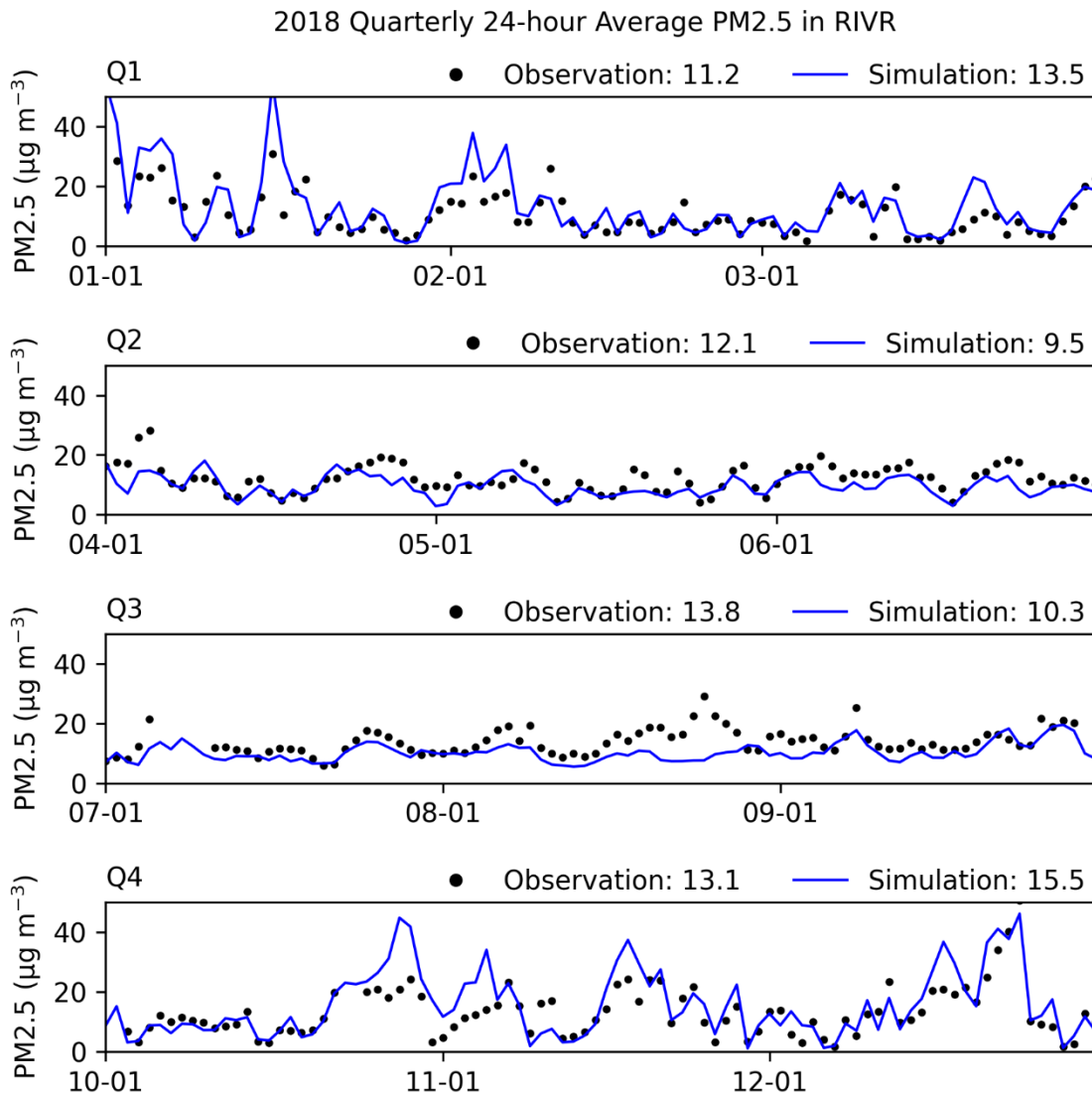


FIGURE II-5-7

2018 MODELLED AND MEASURED 24-HOUR AVERAGE PM2.5 CONCENTRATIONS IN RIVERSIDE

Scatter plots comparing daily FRM observations and corresponding model predictions for each region are presented in Figure II-5-8.

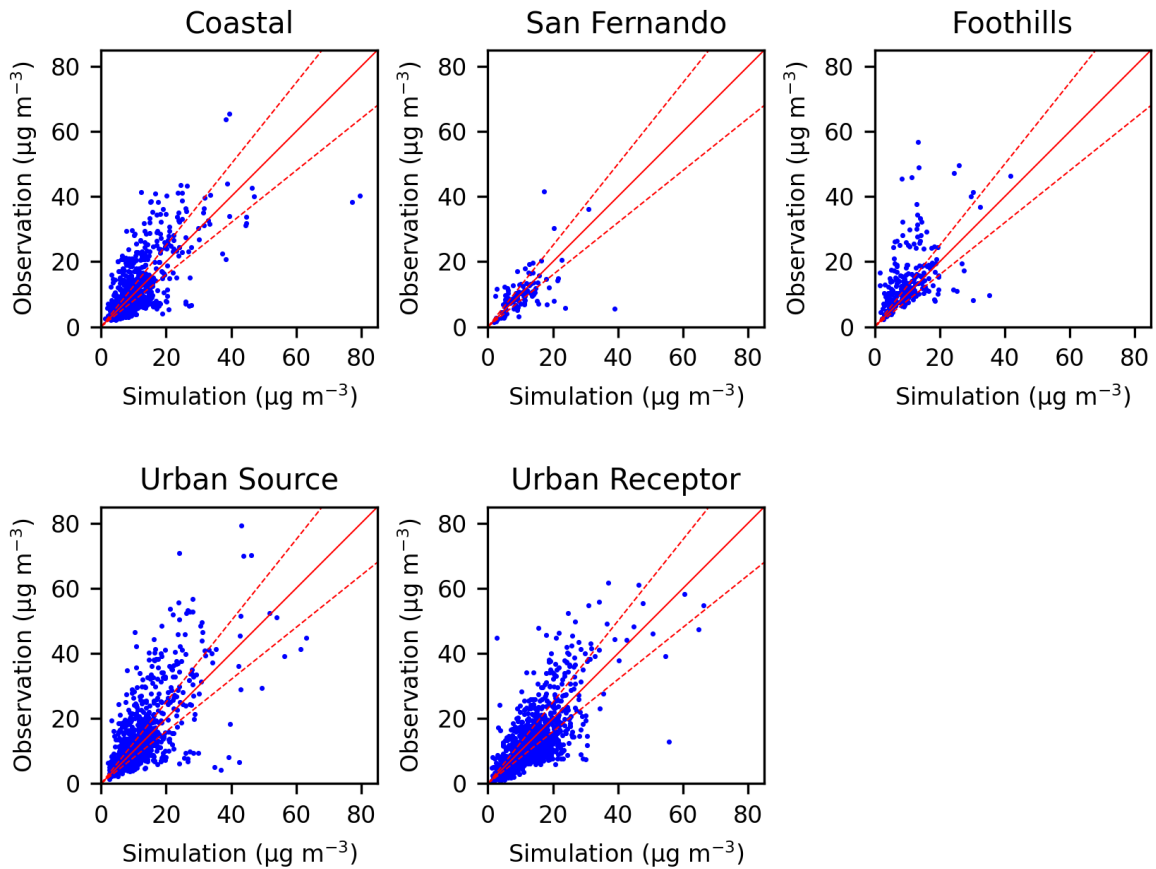


FIGURE II-5-8

2018 MODELLED AND FRM MEASURED PM_{2.5} COMPARISON FOR EACH REGION. DASHED LINES INDICATE AGREEMENT WITHIN 20 PERCENT.

Statistical Evaluation of Total PM2.5 mass

CMAQ over-predicts total PM2.5 mass in the “Coastal”, “Foothills” and “Urban Source” regions. The “San Fernando”, “Urban Receptor” regions, are well represented by CMAQ in the base year. The “Urban Receptor” region typically contains the highest PM2.5 concentrations in the South Coast Basin. Statistical measures to evaluate the modeling performance in each geographical zone are provided in Table II-5-3.

The statistics used to evaluate the daily CMAQ PM2.5 performance include the following:

| <u>Statistic</u> | <u>Equation</u> | <u>Definition</u> |
|------------------------|---|--|
| Bias Error | $BiasError = \frac{1}{N} \sum (Obs - Pred)$ <p>where “N” is the number of values.</p> | Average of the differences in observed and predicted daily values. Negative values indicate under-prediction. |
| Normalized Bias Error | $NormBiasError = \frac{1}{N} \sum \left(\frac{Obs - Pred}{Obs} \right) \cdot 100$ | Average of the quantity: absolute difference in observed and predicted daily values normalized by the observed daily concentration |
| Gross Error | $GrossError = \frac{1}{N} \sum Obs - Pred $ | Average of the absolute differences in observed and predicted daily values |
| Normalized Gross Error | $NormGrossError = \frac{1}{N} \sum \left \frac{Obs - Pred}{Obs} \right \cdot 100$ | Average of the quantity: absolute difference in observed and predicted daily values normalized by the observed daily concentration |

TABLE II-5-3

QUARTERLY STATISTICAL ANALYSIS OF TOTAL PM_{2.5} MASS FOR EACH OF THE SIX ANALYSIS ZONES

| Region | Quarter | Mean Sim. (µg/m ³) | Mean Obs. (µg/m ³) | Bias Error (µg/m ³) | Norm Bias (%) | Gross Error (µg/m ³) | Norm Gross (%) |
|-----------------------|---------------|--------------------------------|--------------------------------|---------------------------------|---------------|----------------------------------|----------------|
| Coastal | Q1 | 15.4 | 11.1 | -4.3 | -60.9 | 5.9 | 67.5 |
| Coastal | Q2 | 7.6 | 8.9 | 1.3 | 11.1 | 2.3 | 27.5 |
| Coastal | Q3 | 7.8 | 11.4 | 3.6 | 26.4 | 4.0 | 31.8 |
| Coastal | Q4 | 17.6 | 13.1 | -4.5 | -45.8 | 6.5 | 58.6 |
| Coastal | Annual | 12.0 | 11.1 | -0.9 | -16.3 | 4.6 | 45.9 |
| Foothills | Q1 | 14.6 | 8.0 | -6.7 | -97.9 | 6.8 | 100.5 |
| Foothills | Q2 | 12.0 | 11.1 | -0.8 | -10.8 | 2.3 | 22.0 |
| Foothills | Q3 | 12.1 | 13.2 | 1.2 | -22.6 | 3.8 | 50.1 |
| Foothills | Q4 | 19.8 | 9.9 | -9.9 | -119.0 | 11.0 | 123.7 |
| Foothills | Annual | 14.6 | 10.6 | -4.1 | -62.6 | 6.0 | 74.2 |
| San Fernando | Q1 | 9.4 | 8.5 | -1.0 | -12.2 | 2.5 | 34.0 |
| San Fernando | Q2 | 9.2 | 10.4 | 1.2 | -1.0 | 2.4 | 31.3 |
| San Fernando | Q3 | 9.4 | 12.1 | 2.7 | 11.3 | 4.1 | 31.0 |
| San Fernando | Q4 | 12.2 | 11.2 | -1.0 | -22.7 | 4.8 | 42.2 |
| San Fernando | Annual | 10.1 | 10.5 | 0.4 | -7.5 | 3.5 | 35.1 |
| Urban Receptor | Q1 | 14.0 | 12.1 | -1.9 | -17.6 | 4.3 | 39.0 |
| Urban Receptor | Q2 | 10.1 | 12.2 | 2.1 | 13.0 | 3.1 | 25.6 |
| Urban Receptor | Q3 | 10.9 | 14.5 | 3.7 | 20.9 | 4.2 | 26.4 |
| Urban Receptor | Q4 | 16.7 | 14.3 | -2.4 | -25.7 | 5.5 | 49.1 |
| Urban Receptor | Annual | 13.0 | 13.3 | 0.3 | -2.4 | 4.3 | 35.1 |
| Urban Source | Q1 | 17.8 | 12.2 | -5.7 | -59.3 | 7.1 | 65.6 |
| Urban Source | Q2 | 10.0 | 10.5 | 0.5 | 3.5 | 2.5 | 25.0 |
| Urban Source | Q3 | 9.7 | 13.1 | 3.4 | 20.4 | 4.1 | 27.1 |
| Urban Source | Q4 | 20.4 | 13.8 | -6.6 | -56.8 | 7.9 | 65.9 |
| Urban Source | Annual | 14.5 | 12.4 | -2.1 | -23.1 | 5.4 | 45.9 |

Model performance in the “Urban Receptor” region consistently outperforms the four other regions exhibiting the smaller normalized bias and normalized gross error for the annual analysis. Model performance in the “Urban Receptor” region is also strong when evaluating statistics on a quarterly basis. It is important to model this region accurately, as it contains the stations with the highest PM_{2.5} concentrations in the Basin.

Model Performance of Speciated PM2.5 Predictions

Figures II-5-9 through II-5-12 compare predicted and observed particulate sulfate, nitrate, elemental carbon, and organic carbon concentrations for the four stations where speciation data are available (ANAH, CELA, FONT, and RIVR). Note that organic carbon concentrations in the figures are based on direct measurements and are not adjusted with the SANDWICH method.

The model predicts ammonium ion, sulfate, nitrate, EC, and OM reasonably well in general. However, the model tends to overpredict concentrations at Central Los Angeles, which is near major sources of emissions. Conversely, the model tends to underestimate PM2.5 species concentrations at inland stations in Fontana and Riverside. Overall, the model captures the relative contributions of PM2.5 species reasonably well, showing that OM is the largest contributors to total PM2.5; OM fraction of total PM2.5 mass is 44% which agrees with measurements showing 41% of total mass being OM. OM predictions have significantly improved compared to 2016 AQMP values possibly due to the addition of a pseudo-SOA precursor thus increasing the estimates of SOA by CMAQ.

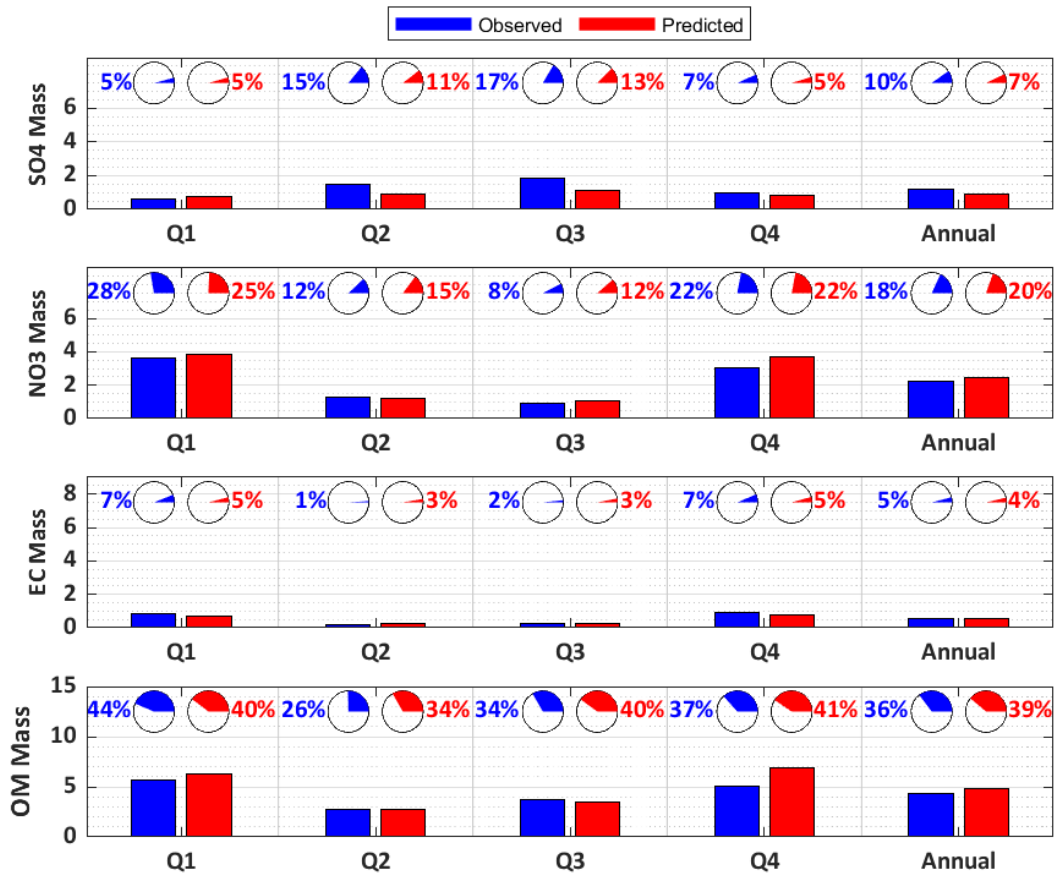


FIGURE II-5-9

2018 MODELLED AND MEASURED PM2.5 SPECIATION IN ANAHEIM. BARS INDICATE THE ABSOLUTE PM2.5 CONCENTRATION OF EACH SPECIES IN µg/m³. PIE CHARTS REPRESENT THE SPECIES FRACTION. OM IS CALCULATED FROM OC AS OM = 1.4 × OC.

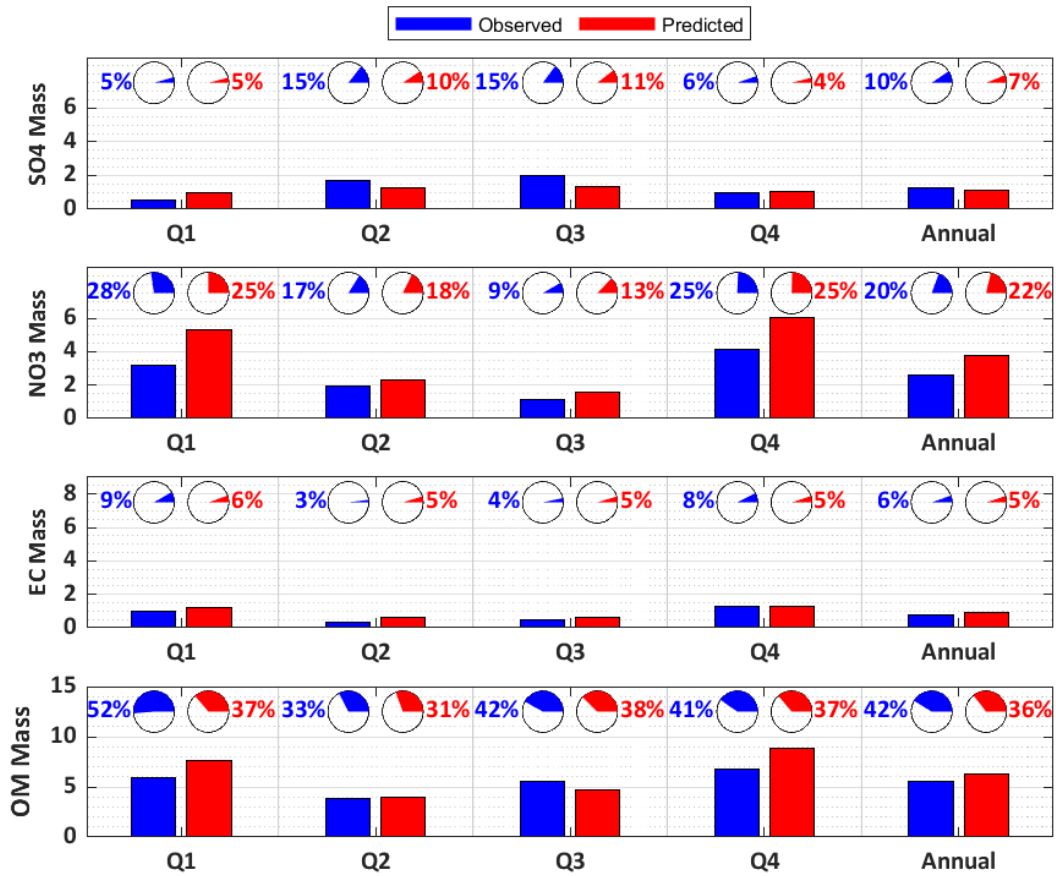


FIGURE II-5-10

2018 MODELLED AND MEASURED PM2.5 SPECIATION IN LOS ANGELES. BARS INDICATE THE ABSOLUTE PM2.5 CONCENTRATION OF EACH SPECIES IN $\mu\text{g}/\text{m}^3$. PIE CHARTS REPRESENT THE SPECIES FRACTION. OM IS CALCULATED FROM OC AS $\text{OM} = 1.4 \times \text{OC}$.



FIGURE II-5-11

2018 MODELLED AND MEASURED PM2.5 SPECIATION IN FONTANA. BARS INDICATE THE ABSOLUTE PM2.5 CONCENTRATION OF EACH SPECIES IN µg/m³. PIE CHARTS REPRESENT THE SPECIES FRACTION. OM IS CALCULATED FROM OC AS OM = 1.4 × OC.

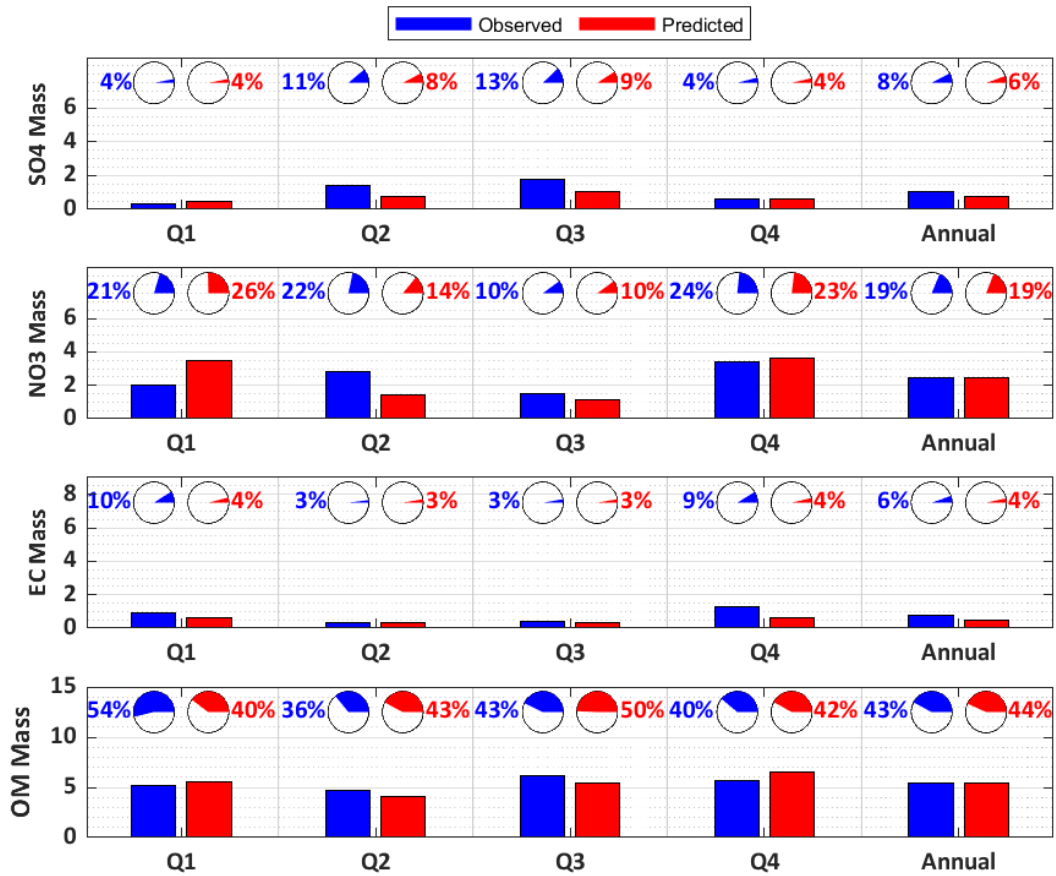


FIGURE II-5-12

2018 MODELLED AND MEASURED PM2.5 SPECIATION IN RIVERSIDE. BARS INDICATE THE ABSOLUTE PM2.5 CONCENTRATION OF EACH SPECIES IN $\mu\text{g}/\text{m}^3$. PIE CHARTS REPRESENT THE SPECIES FRACTION. OM IS CALCULATED FROM OC AS $\text{OM} = 1.4 \times \text{OC}$.

CMAQ SOA Mass Simulation

Traditionally, air quality models tend to underpredict secondary organic aerosols (SOA) concentrations. Mounting evidence from field and laboratory observations coupled with atmospheric model analysis shows that primary combustion emissions of organic compounds exhibit a broad spectrum of volatility, leading to dynamic partitioning of these compounds, especially in the early stages of their atmospheric lifetime (Murphy et al., 2017).⁴ Starting from CMAQ version 5.2, the model accounts for the semi-volatile partitioning and gas-phase aging of these primary organic aerosol (POA) compounds consistent with experimentally derived parameterizations. A new surrogate species termed potential secondary organic aerosol from combustion (pcSOA) was added to the model. It provides a cumulative representation of the SOA from combustion sources that could be missing from current chemical transport model predictions. The reasons for this missing mass likely include:⁵

- Missing intermediate volatility organic compound (IVOC) emissions in current inventories.
- Multigenerational aging of organic vapor products from known SOA precursors (e.g., toluene, alkanes).
- Underestimation of SOA yields due to vapor losses at the walls in smog chamber experiments.
- Organic-water interactions and aqueous-phase processing of known organic vapor emissions.

The result of this new parameterization is a good model performance with respect to measured organic aerosol by CMAQ, as shown in Figures II-5-9 through II-5-12. The quarterly averages of primary organic aerosol (POA) and secondary organic aerosol (SOA) mass concentrations are depicted in Figures II-5-13 to II-5-16 for each station. Generally, POA concentrations are elevated in the first and fourth quarters. This trend is attributed to increased residential fuel combustion during colder months, which contribute to higher POA levels. SOA concentrations are also high in fall and winter due to the formation of SOA from the oxidation of combustion related pollutant emissions, as well as due lower temperatures and higher humidity in winter, that contribute to the accumulation of air pollutants. Some inland stations, such as RESE, FONT, MRLM, ONFS, and SNBO exhibit also high SOA concentrations in the third quarter. These high concentrations can be attributed to increased biogenic volatile organic compound (VOC) emissions in the summer, resulting in higher SOA levels due to the elevated temperatures during this season.

⁴ Murphy, B. N., Woody, M. C., Jimenez, J. L., Carlton, A. M. G., Hayes, P. L., Liu, S., Ng, N. L., Russell, L. M., Setyan, A., Xu, L., Young, J., Zaveri, R. A., Zhang, Q., and Pye, H. O. T.: Semivolatile POA and parameterized total combustion SOA in CMAQv5.2: impacts on source strength and partitioning, *Atmos. Chem. Phys. Discuss.*, <https://doi.org/10.5194/acp-2017-193>

⁵ Implemented Semivolatile POA and Potential Combustion SOA (pcSOA). Information available here: [CMAQ/CCTM/docs/Release_Notes/SemiVolPOA_pcSOA.md at 5.2 · USEPA/CMAQ · GitHub](https://github.com/USEPA/CMAQ-CCTM/docs/Release_Notes/SemiVolPOA_pcSOA.md)

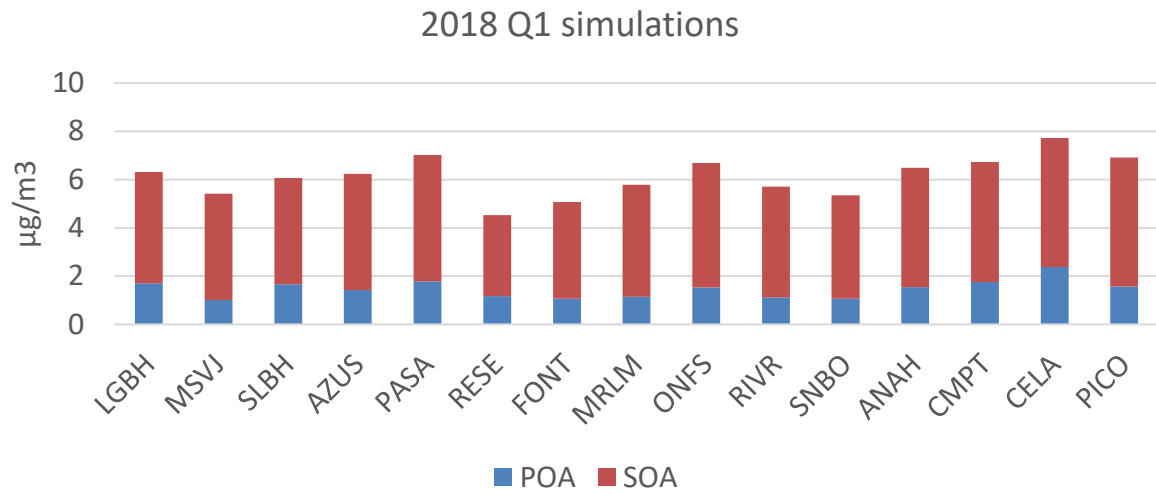


FIGURE II-5-13

QUARTERLY AVERAGE OF POA AND SOA MASS CONCENTRATIONS OF FIRST QUARTER IN 2018.

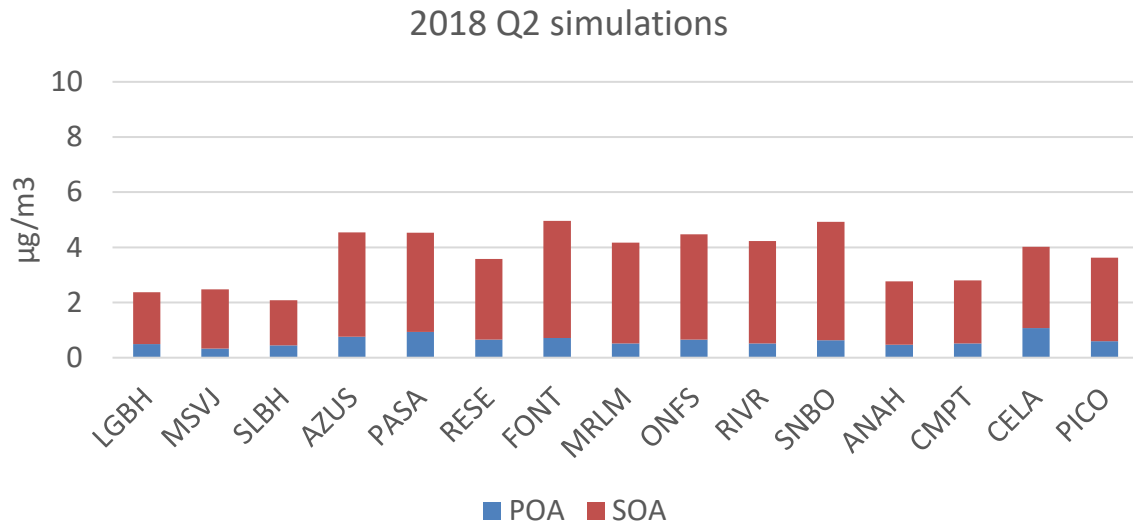


FIGURE II-5-14

QUARTERLY AVERAGE OF POA AND SOA MASS CONCENTRATIONS OF SECOND QUARTER IN 2018.

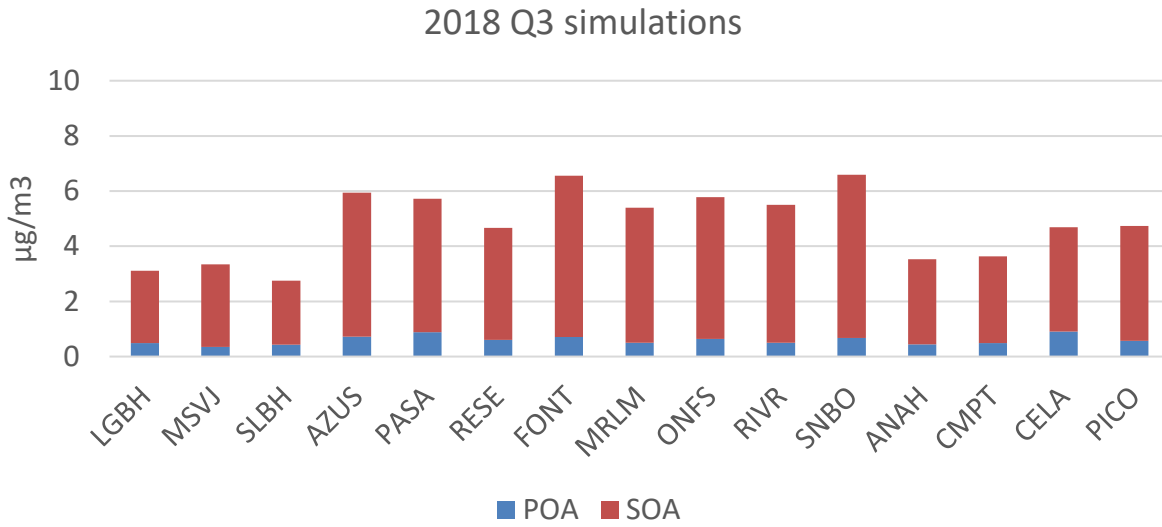


FIGURE II-5-15

QUARTERLY AVERAGE OF POA AND SOA MASS CONCENTRATIONS OF THIRD QUARTER IN 2018.

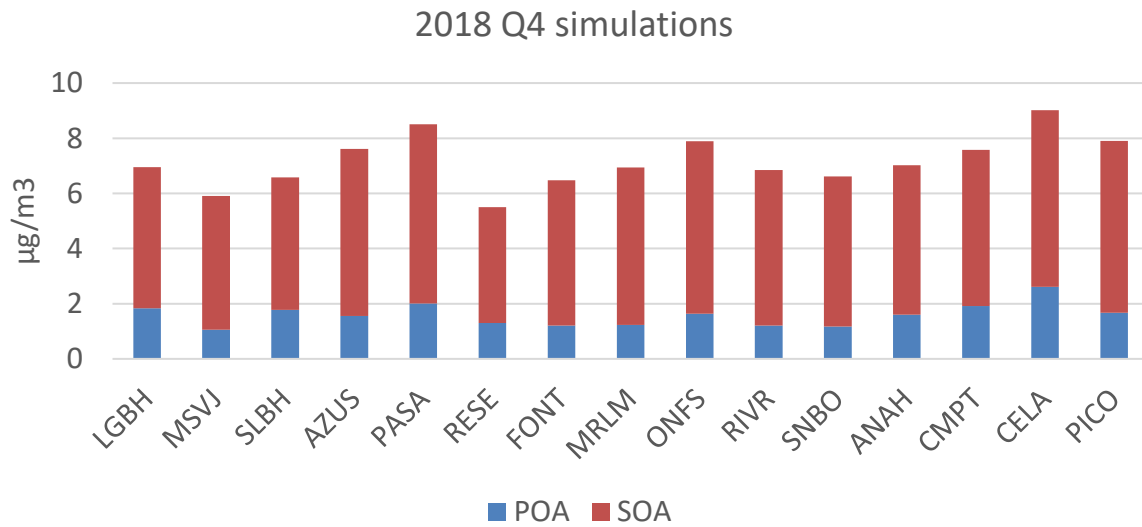


FIGURE II-5-16

QUARTERLY AVERAGE OF POA AND SOA MASS CONCENTRATIONS OF FOURTH QUARTER IN 2018.

Base Year Annual PM2.5

Quarterly average of PM2.5 FRM mass concentrations, using the modified 5-year weighted average of measurements during 2016-2020 is shown in Figure II-5-17. As shown, among the four stations, Anaheim has the lowest level of PM2.5 concentrations in all quarters, and the highest values occur at Rubidoux (13.50 $\mu\text{g}/\text{m}^3$) and CELA (13.49 $\mu\text{g}/\text{m}^3$) in quarter 4. In general, the sites in the western half of the Basin: Los Angeles and Anaheim, tend to have the highest average levels in the fourth quarter. Rubidoux also presents the highest concentration in the fourth quarter, whereas Fontana experiences the highest concentration in the third quarter. All stations tend to have the lowest concentrations in the first or second quarter. Typically, spring storms and favorable atmospheric dispersion drive PM2.5 concentrations down in the second quarter. Fontana, Rubidoux, and Los Angeles presented the lowest concentrations during the first quarter, whereas Anaheim had the lowest value in the second quarter.

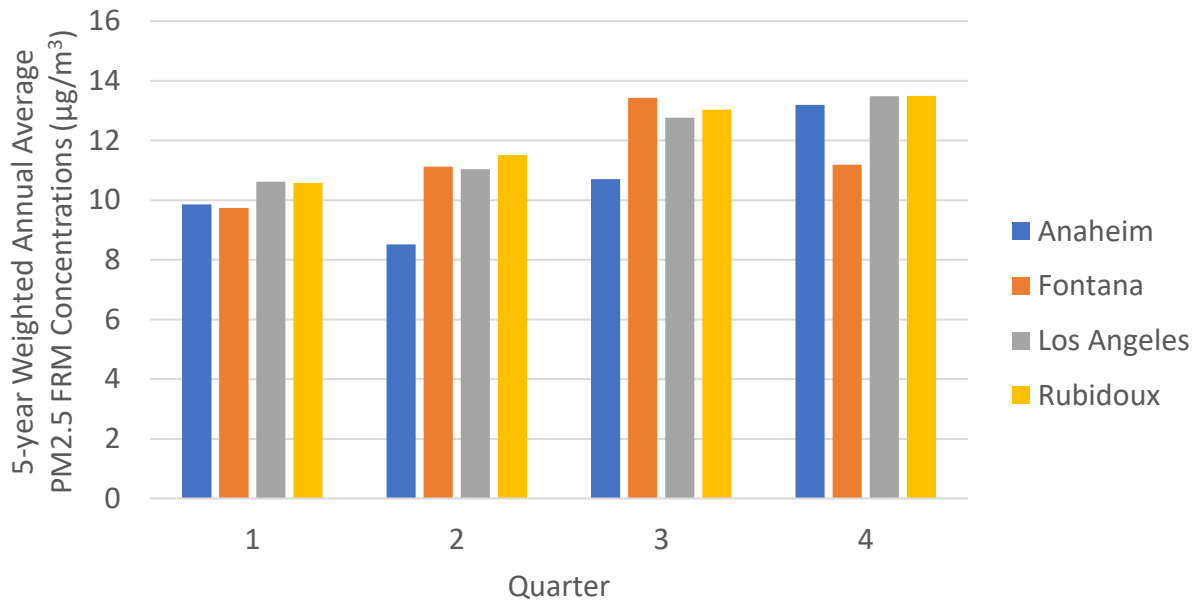


FIGURE II-5-17

QUARTERLY AVERAGE OF PM2.5 FRM MASS CONCENTRATIONS, USING THE MODIFIED 5-YEAR WEIGHTED AVERAGE OF MEASUREMENTS DURING 2016-2020 AT CSN MONITORS.

Speciated Quarterly Average Data

The measurements of individual species obtained from the CSN sites may differ from the retained mass of a specific species in the FRM filter, due to the inherent differences in the measurement techniques. To reconcile the expected differences between speciated and FRM measurements, species are adjusted following the SANDWICH method,⁶ which is described in the U.S. EPA modeling guidance.⁷ This adjustment results in reduced nitrates (relative to the amount measured by routine speciation networks), higher mass associated with sulfates and nitrates (reflecting water included in gravimetric FRM measurements), and an estimate of organic carbonaceous mass, which is derived from the difference between FRM-measured PM_{2.5} and the sum of all components except measured organic carbon. EPA's mass balance method sets a ceiling for OC mass (OCM) to be 80 percent of the total PM_{2.5} mass. However, based on scientific literature on PM_{2.5} speciation data taken in the greater Los Angeles area,^{8,9} this ceiling was set as the 50 percent of PM_{2.5} FRM mass. EPA's guidance also sets a floor value for OCM to be the measured OC value. However, the sum of individual species measured from CSN is sometimes larger than the FRM mass. Under this condition, the measured OC as floor would erroneously exaggerate the OC fraction while reducing the other species, therefore, the OC floor was scaled by the ratio of FRM mass divided by the total CSN mass.

Directly measured ammonium (associated with nitrate and sulfate) at CSN stations, which is equivalent to particulate ammonium retained on FRM filters, was used for the speciation profiles. These measurements, however, were capped with fully neutralized ammonium, which is calculated as follows:

$$\text{Ammonium ceiling} = 0.375 \times \text{sulfate} + 0.29 \times \text{retained nitrate}$$

Additionally, particle water bound (PBW) should be estimated as sulfate and nitrate retained on FRM filters include water because ammonium sulfate and ammonium nitrate are hygroscopic. PBW was estimated using a polynomial regression equation fitted to the equilibrium model Aerosol Inorganic Matter (AIM) as a function of sulfate, nitrate, and ammonium concentrations (described above). Most of FRM monitors in the basin do not have a co-located CSN monitor. Thus, as recommended by EPA guidance, we interpolated the individual speciation components

⁶ Frank, Neil. (2006). Retained Nitrate, Hydrated Sulfates, and Carbonaceous Mass in Federal Reference Method Fine Particulate Matter for Six Eastern U.S. Cities. *Journal of the Air & Waste Management Association* (1995). 56. 500-11. 10.1080/10473289.2006.10464517.

⁷ Modeling Guidance for Demonstrating Attainment of Air Quality Goals for Ozone, PM_{2.5}, and Regional Haze, U.S. EPA, November 2018. Available at: https://www.epa.gov/sites/default/files/2020-10/documents/o3-pm-rh-modeling_guidance-2018.pdf

⁸ Hayes et al., 2013. Organic aerosol composition and sources in Pasadena, California, during the 2010 CalNex campaign. *Journal of Geophysical Research*, 118, 9233-9257

⁹ Shirmohammadi et al., 2016. Fine and Ultrafine Particulate Organic Carbon in the Los Angeles Basin: Trends in Sources and Composition. *Science of Total Environment*, 541, 1083-1096

from co-located CSN monitors to latitude and longitude of FRM monitors that do not have a co-located CSN monitor. Inverse Distance Squared Weights interpolation method was used. This method gives a particular monitor a weight inversely proportional with squared distance from a given point.

Figures II-5-18 through II-5-21 provide SANDWICH-applied species fractions for each CSN site and each quarter. OC and nitrate are the two most common species with OC comprising between 30% to 43% of total PM2.5 mass, and nitrate comprising between 13% to 22% of the total PM2.5 mass, depending on quarter and location. OC in general tends to be higher in Urban Receptor and San Fernando regions both during the 3rd quarter while nitrate is the lowest during the same quarter. Higher temperatures and abundant sunlight increase evaporative emissions of SOA precursors and increase photochemical processing of those precursors.

On average, secondary ammonium, nitrate and sulfate comprise between 30% to 48% of the total PM2.5 concentration and show strong seasonal variability (Figure II-5-22); the highest contribution levels occur in quarter 2, among the four CSN stations. High nitrate concentrations in the fall or winter are caused by the favorable formation of ammonium nitrate under cool temperatures, high humidity, and frequent nocturnal inversions; the CSN stations on the east side – Fontana and Riverside – have the highest nitrate levels. On the contrary, high summertime temperatures reduce concentrations of nitrate, which is relatively volatile. The higher values of sulfate typically occur under conditions of strong inversions and strong sea breeze transport toward inland areas, which is the characteristic of late spring and summer. In addition, heterogeneous formation of sulfate is favored by higher temperatures occurring in the summer. Higher temperatures with abundant afternoon sunlight and the persistence of morning fog and low clouds trigger – the marine boundary layer, both homogeneous and heterogeneous sulfate formation reactions to produce secondary sulfate. Higher temperatures and abundant sunlight increase evaporative emissions of SOA precursors and increase photochemical processing of those precursors.

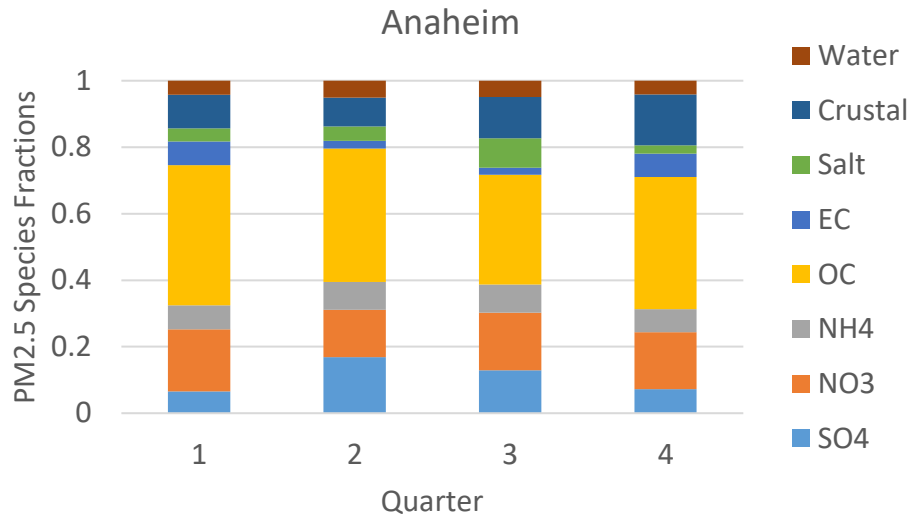


FIGURE II-5-18

SANDWICH-APPLIED QUARTERLY AVERAGES OF PM2.5 SPECIES FRACTIONS DURING 2017 TO 2019 IN ANAHEIM

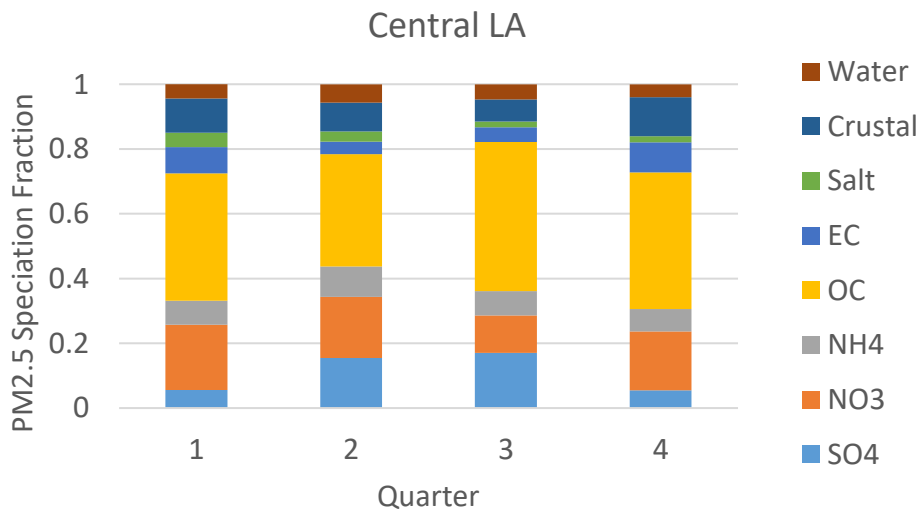


FIGURE II-5-19

SANDWICH-APPLIED QUARTERLY AVERAGES OF PM2.5 SPECIES FRACTIONS DURING 2017 TO 2019 IN CENTRAL LOS ANGELES (CELA)

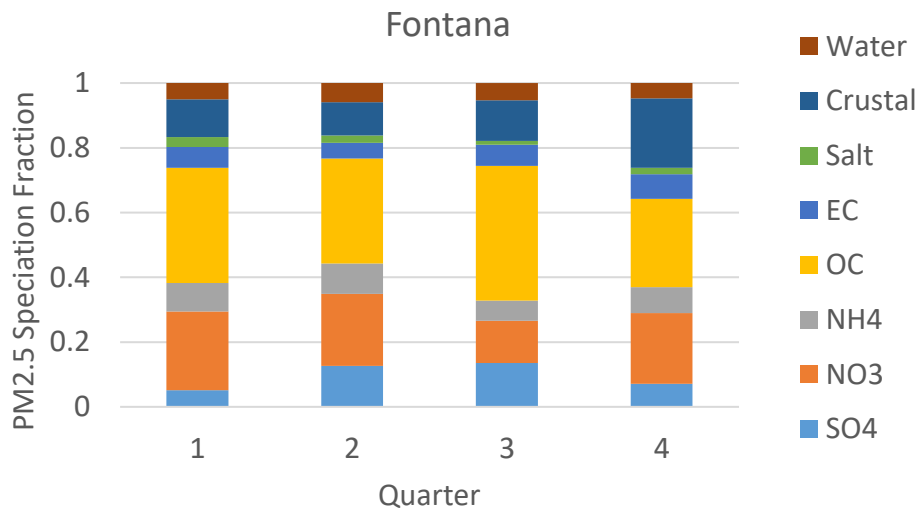


FIGURE II-5-20

SANDWICH-APPLIED QUARTERLY AVERAGES OF PM2.5 SPECIES FRACTIONS DURING 2017 TO 2019 IN FONTANA

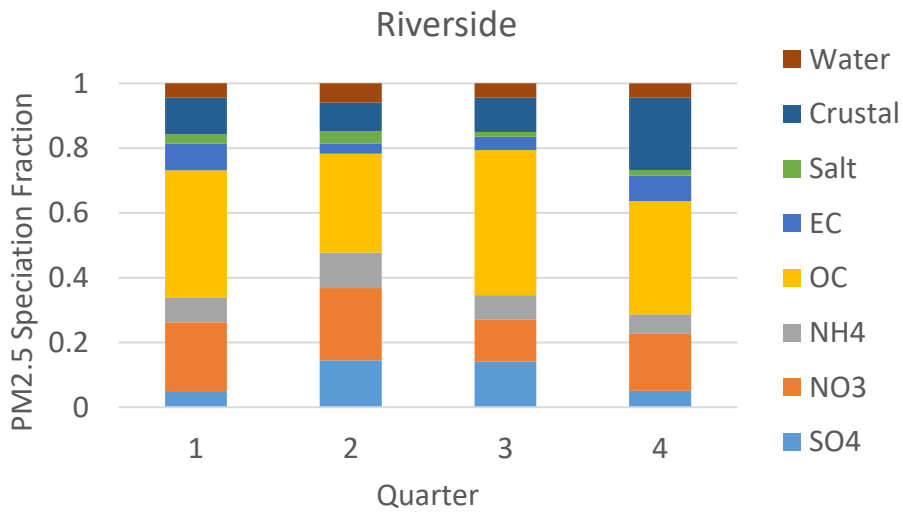


FIGURE II-5-21

SANDWICH-APPLIED QUARTERLY AVERAGES OF PM2.5 SPECIES FRACTIONS DURING 2017 TO 2019 IN RIVERSIDE

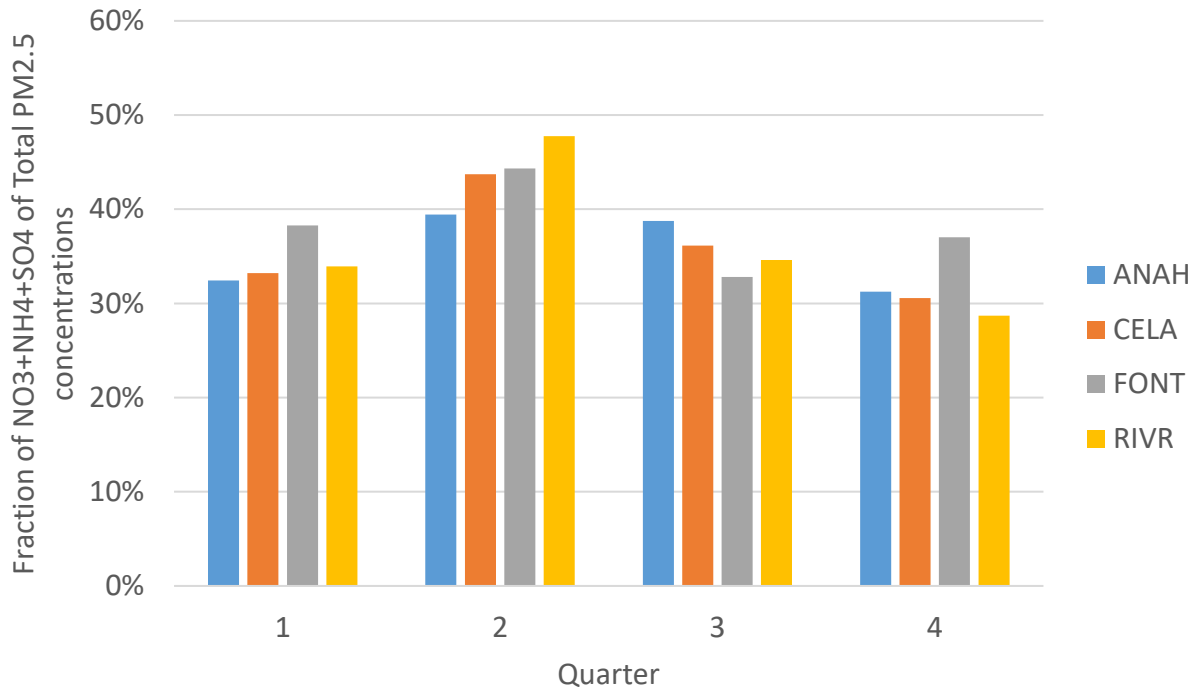


FIGURE II-5-22

5-YEAR WEIGHTED QUARTERLY AVERAGE FRACTIONS OF NO₃, NH₄, AND SO₄ COMBINED MASS TO THE TOTAL PM_{2.5} MASS

Speciated base year annual design values at different stations are shown in Figure II-5-23. Figure II-5-24 through Figure II-5-30 show the base year quarterly DV for the four CSN sites along with the stations with the top three highest annual design value in the basin which includes Ontario Near-road (ONNR), Mira Loma (MRLM), and Compton (CMPT). Among all the stations in the basin, the highest base year annual design value is observed at ONNR with an annual DV of 13.98 $\mu\text{g}/\text{m}^3$, followed by MRLM with a DV of 13.52 $\mu\text{g}/\text{m}^3$. MRLM is the station with the highest quarterly DV in the basin, with quarter 4 quarterly average exceeding 16 $\mu\text{g}/\text{m}^3$. Among the four CSN stations, the highest sulfate concentration was observed in central Los Angeles (4.81 $\mu\text{g}/\text{m}^3$), while the highest concentration of nitrate occurred in Fontana (2.22 $\mu\text{g}/\text{m}^3$) followed by Rubidoux (2.19 $\mu\text{g}/\text{m}^3$); Rubidoux also has the highest ammonium concentrations (0.95 $\mu\text{g}/\text{m}^3$).

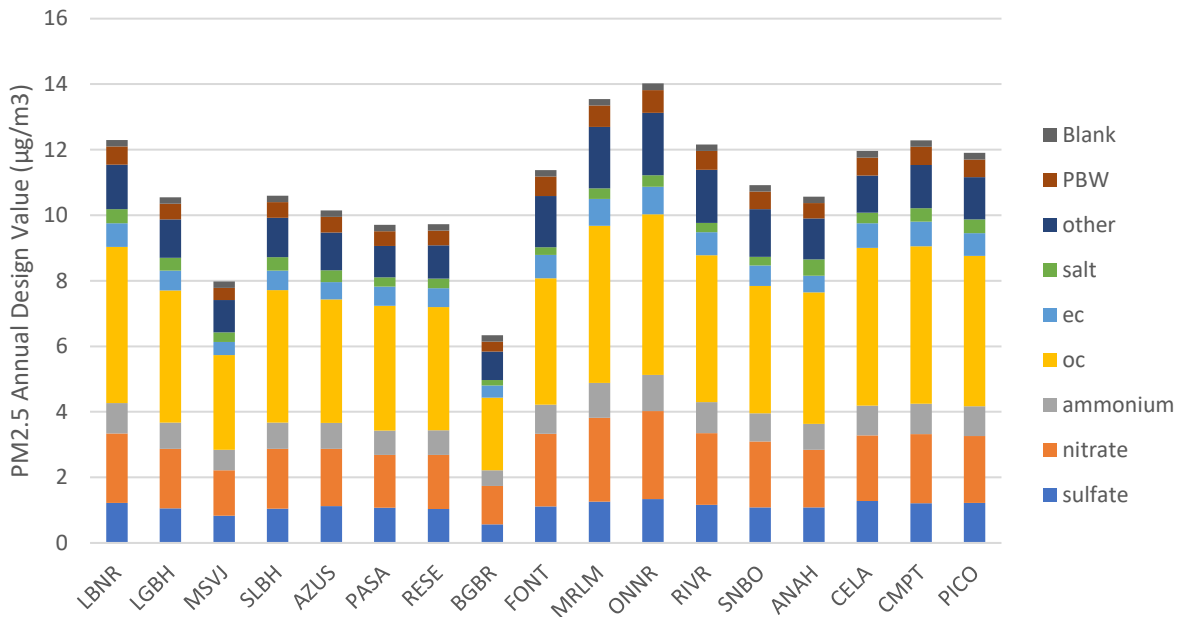


FIGURE II-5-23

BASE YEAR SPECIATED ANNUAL PM2.5 DESIGN VALUES FOR ALL STATIONS IN THE BASIN. TABLE II-5-2 SHOWS THE STATION NAMES AND ABBREVIATIONS FOR REFERENCE.

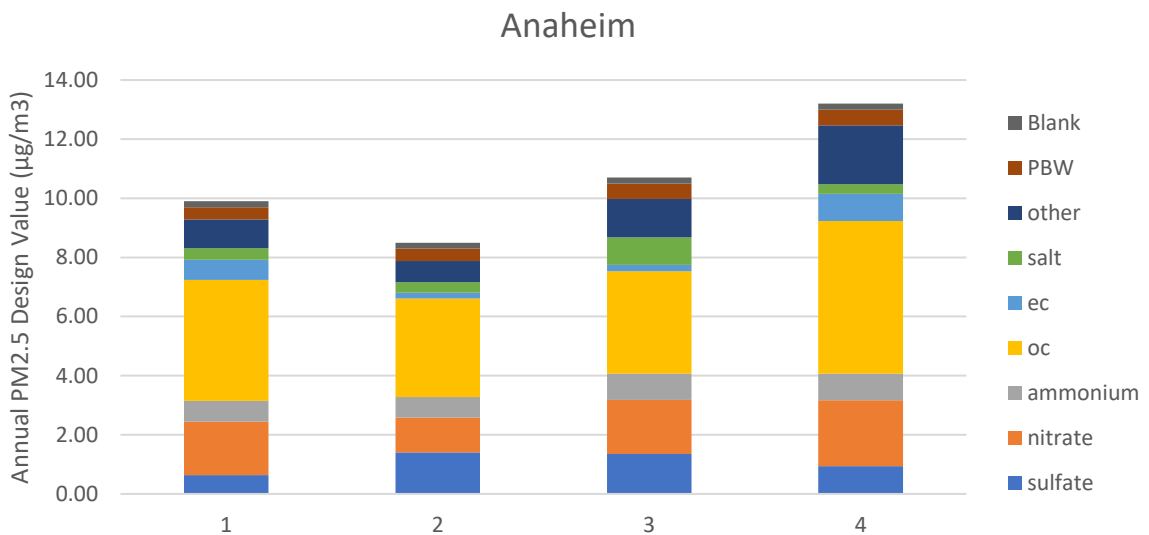


FIGURE II-5-24

BASE YEAR QUARTERLY PM2.5 DESIGN VALUES FOR ANAHEIM.

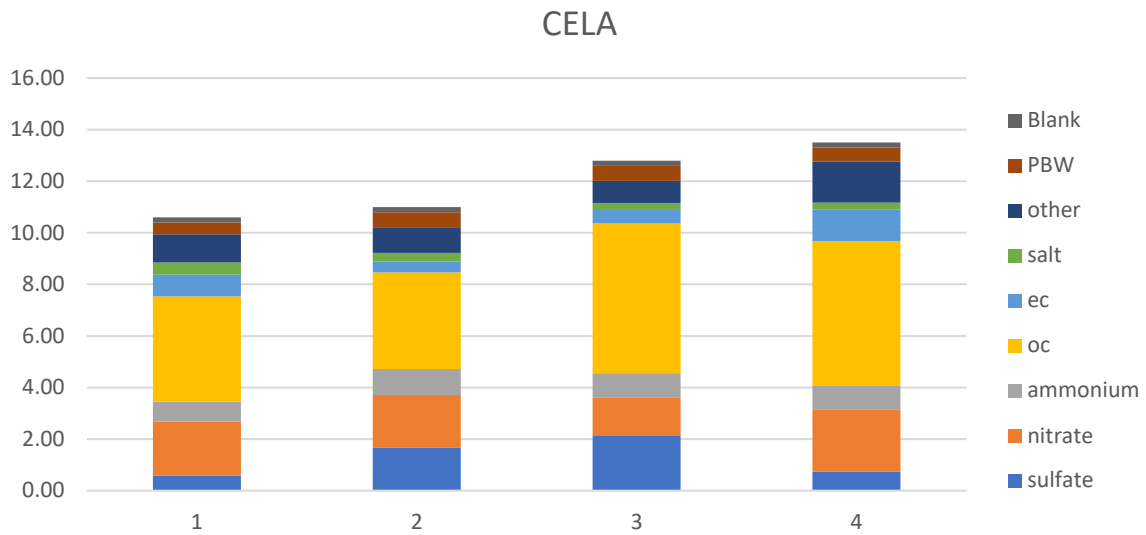


FIGURE II-5-25

BASE YEAR QUARTERLY PM2.5 DESIGN VALUES FOR CENTRAL LOS ANGELES (CELA).

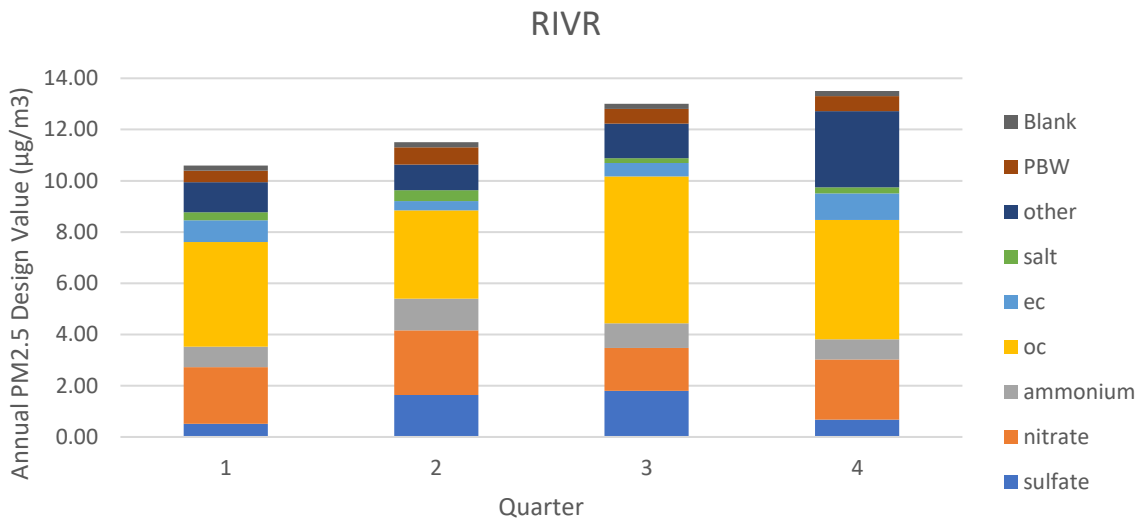


FIGURE II-5-26

BASE YEAR QUARTERLY PM2.5 DESIGN VALUES FOR RUBIDOUX (RIVR).

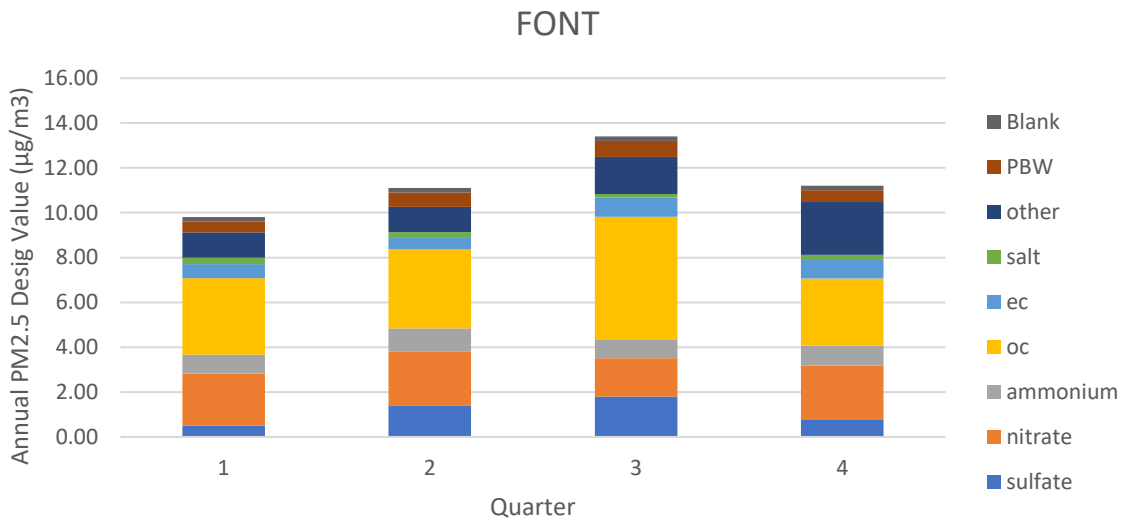


FIGURE II-5-27

BASE YEAR QUARTERLY PM2.5 DESIGN VALUES FOR FONTANA (FONT).

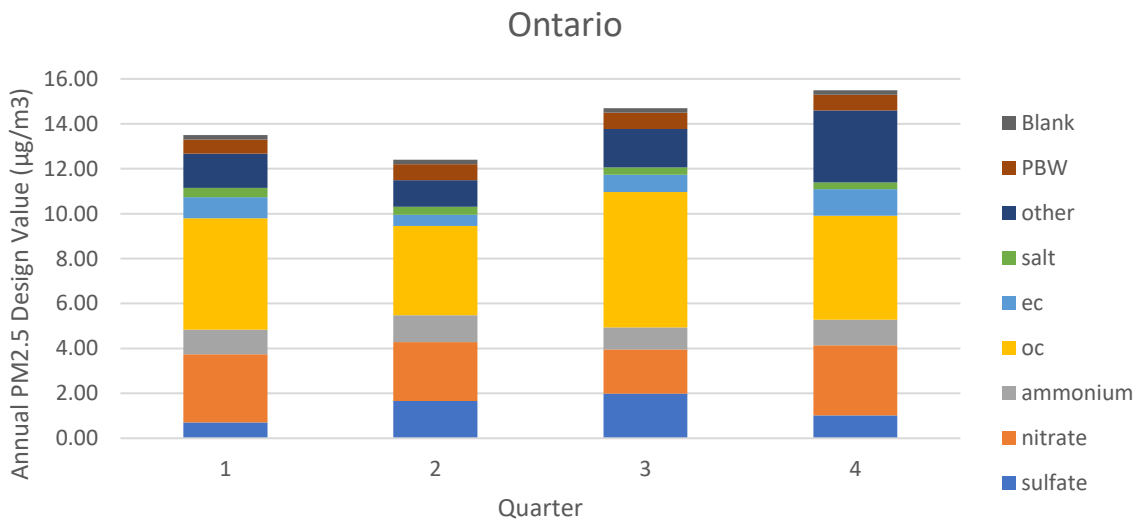


FIGURE II-5-28

BASE YEAR QUARTERLY PM2.5 DESIGN VALUES FOR ONTARIO NEAR-ROAD (ONNR).

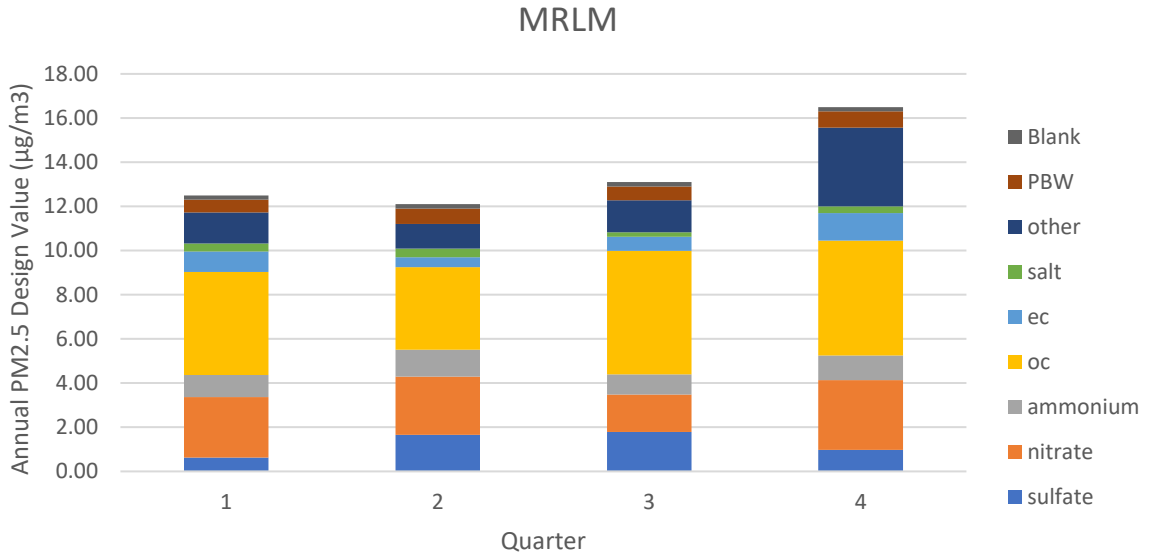


FIGURE II-5-29

BASE YEAR QUARTERLY PM2.5 DESIGN VALUES FOR MIRA LOMA (MRLM).

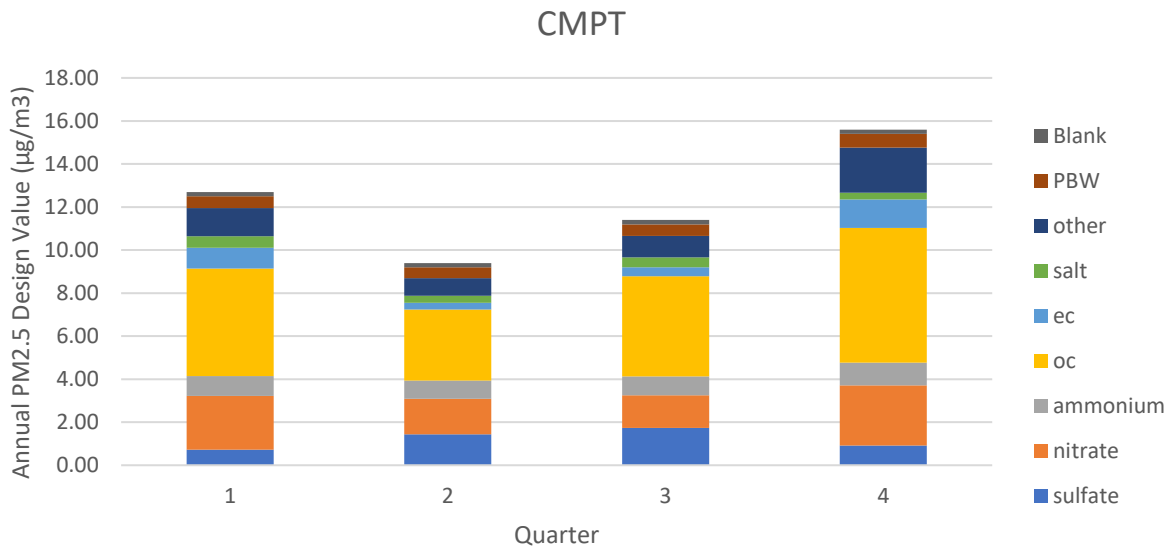
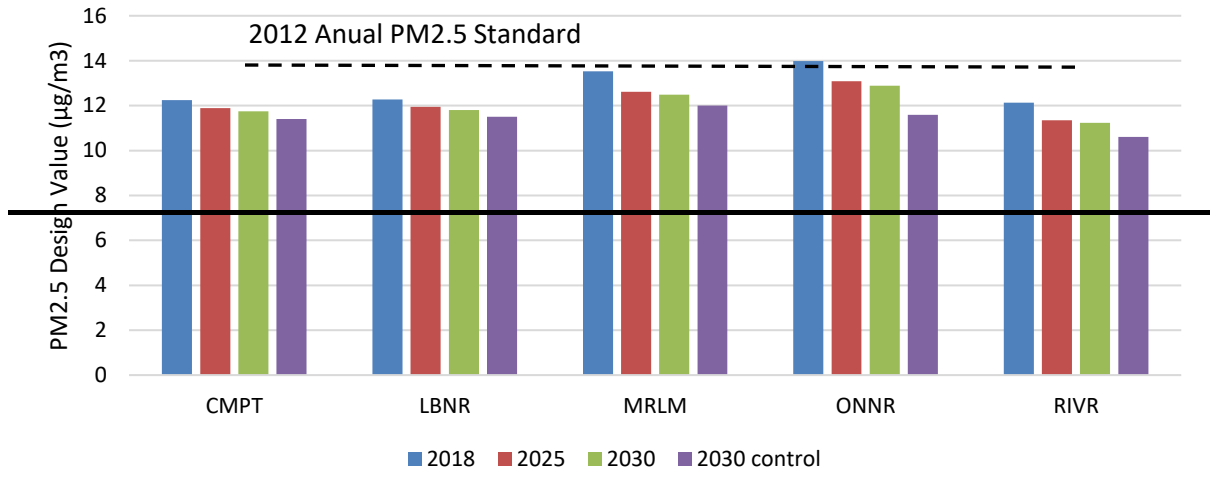


FIGURE II-5-30

BASE YEAR QUARTERLY PM2.5 DESIGN VALUES FOR COMPTON (CMPT).

Future Annual PM2.5 air quality

PM2.5 annual concentrations projected for milestone years are shown in Figure II-5-31. Ontario Near Road is projected to remain as the design value site in 2025 and 2030. The annual design value for Ontario Near Road in the 2030 attainment scenario is projected to be 12.35 $\mu\text{g}/\text{m}^3$. All other areas will be in attainment of the federal annual standard (12 $\mu\text{g}/\text{m}^3$) by 2030 with the proposed PM strategy presented in Chapter 4 of this Plan. A demonstration of Ontario Near Road projection using a hybrid modeling approach is provided in Chapter 5 and in chapter 6 of this Appendix II. Applying the hybrid approach, Ontario Near Road is expected to have 11.59 $\mu\text{g}/\text{m}^3$ in 2030 with the controls proposed in this Plan. Tables II-5-4 through II-5-6 provide the projected future year PM2.5 annual design values speciated by PM2.5 components for 2025, 2030 baseline and 2030 attainment.



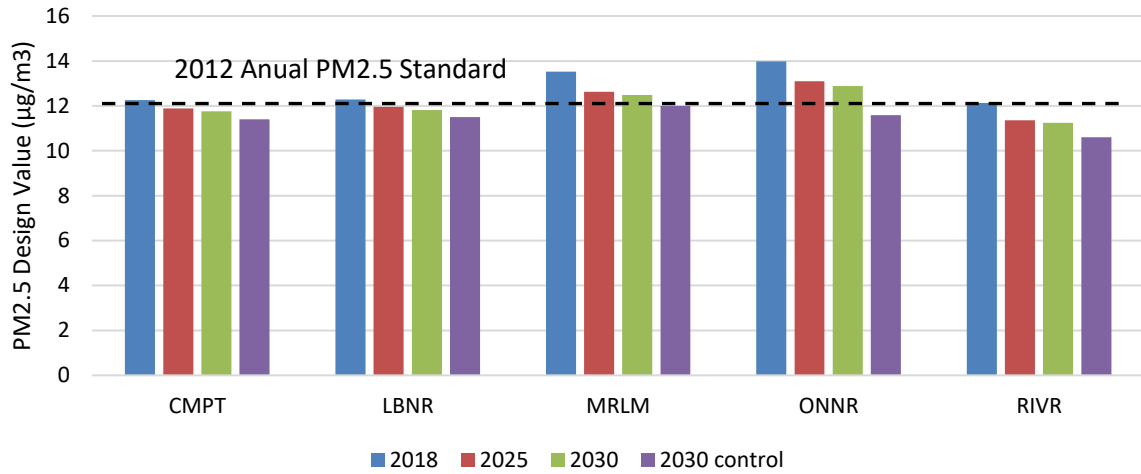


FIGURE II-5-31

ANNUAL PM2.5 DESIGN VALUES AT THE TOP 5 STATIONS. FEDERAL STANDARD IS DENOTED WITH HORIZONTAL BLACK DASHED LINE. THE DV FOR THE 2030 CONTROL CASES AT ONTARIO NEAR-ROAD (ONNR) IS BASED ON THE HYBRID MODELING APPROACH

TABLE II-5-4

RRF-BASED PREDICTED 2025 BASELINE ANNUAL DESIGN VALUES ($\mu\text{g}/\text{m}^3$)

| Sites | SO4 | NO3 | NH4 | OC | EC | Salt | Others | Water | Blank | Total |
|-------|-----|-----|-----|-----|-----|------|--------|-------|-------|-------|
| ANAH | 1.1 | 1.4 | 0.7 | 4.2 | 0.4 | 0.5 | 1.3 | 0.5 | 0.2 | 10.2 |
| AZUS | 1.2 | 1.3 | 0.6 | 4.0 | 0.4 | 0.4 | 1.2 | 0.5 | 0.2 | 9.7 |
| BGBR | 0.6 | 0.8 | 0.4 | 2.2 | 0.4 | 0.2 | 0.9 | 0.2 | 0.2 | 5.9 |
| CELA | 1.3 | 1.6 | 0.8 | 5.0 | 0.6 | 0.3 | 1.2 | 0.5 | 0.2 | 11.5 |
| CMPT | 1.3 | 1.7 | 0.8 | 5.0 | 0.6 | 0.4 | 1.4 | 0.5 | 0.2 | 11.9 |
| FONT | 1.2 | 1.6 | 0.7 | 4.0 | 0.6 | 0.2 | 1.7 | 0.6 | 0.2 | 10.7 |
| LBNR | 1.3 | 1.8 | 0.8 | 5.0 | 0.6 | 0.4 | 1.4 | 0.5 | 0.2 | 12.0 |
| LGBH | 1.1 | 1.5 | 0.7 | 4.2 | 0.5 | 0.4 | 1.2 | 0.4 | 0.2 | 10.3 |
| MRLM | 1.3 | 1.9 | 0.8 | 4.9 | 0.6 | 0.3 | 2.0 | 0.6 | 0.2 | 12.6 |
| MSVJ | 0.8 | 1.2 | 0.5 | 2.9 | 0.3 | 0.3 | 1.0 | 0.4 | 0.2 | 7.6 |
| ONNR | 1.4 | 2.0 | 0.8 | 5.0 | 0.6 | 0.4 | 2.0 | 0.7 | 0.2 | 13.1 |
| PASA | 1.1 | 1.3 | 0.6 | 4.0 | 0.4 | 0.3 | 1.0 | 0.4 | 0.2 | 9.3 |
| PICO | 1.3 | 1.6 | 0.8 | 4.8 | 0.5 | 0.4 | 1.3 | 0.5 | 0.2 | 11.5 |
| RESE | 1.1 | 1.2 | 0.6 | 3.8 | 0.4 | 0.3 | 1.0 | 0.4 | 0.2 | 9.1 |
| RIVR | 1.2 | 1.6 | 0.7 | 4.6 | 0.5 | 0.3 | 1.7 | 0.5 | 0.2 | 11.4 |
| SLBH | 1.1 | 1.6 | 0.7 | 4.2 | 0.5 | 0.4 | 1.2 | 0.4 | 0.2 | 10.3 |
| SNBO | 1.1 | 1.5 | 0.6 | 4.0 | 0.5 | 0.3 | 1.5 | 0.5 | 0.2 | 10.1 |

TABLE II-5-5

RRF-BASED PREDICTED 2030 BASELINE ANNUAL DESIGN VALUES ($\mu\text{g}/\text{m}^3$)

| Sites | SO4 | NO3 | NH4 | OC | EC | Salt | Others | Water | Blank | Total |
|-------|-----|-----|-----|-----|-----|------|--------|-------|-------|-------|
| ANAH | 1.1 | 1.4 | 0.6 | 4.2 | 0.4 | 0.5 | 1.3 | 0.5 | 0.2 | 10.2 |
| AZUS | 1.2 | 1.2 | 0.6 | 4.0 | 0.4 | 0.4 | 1.2 | 0.5 | 0.2 | 9.5 |
| BGBR | 0.6 | 0.8 | 0.4 | 2.2 | 0.4 | 0.2 | 1.0 | 0.2 | 0.2 | 5.9 |
| CELA | 1.3 | 1.5 | 0.7 | 5.0 | 0.6 | 0.3 | 1.2 | 0.5 | 0.2 | 11.4 |
| CMPT | 1.3 | 1.6 | 0.8 | 5.0 | 0.6 | 0.4 | 1.4 | 0.5 | 0.2 | 11.8 |
| FONT | 1.2 | 1.5 | 0.6 | 4.0 | 0.5 | 0.2 | 1.7 | 0.6 | 0.2 | 10.5 |
| LBNR | 1.3 | 1.7 | 0.8 | 5.0 | 0.6 | 0.4 | 1.4 | 0.5 | 0.2 | 11.8 |
| LGBH | 1.1 | 1.5 | 0.7 | 4.2 | 0.5 | 0.4 | 1.2 | 0.4 | 0.2 | 10.1 |
| MRLM | 1.3 | 1.7 | 0.7 | 4.9 | 0.6 | 0.3 | 2.1 | 0.6 | 0.2 | 12.5 |
| MSVJ | 0.8 | 1.1 | 0.5 | 2.9 | 0.3 | 0.3 | 1.0 | 0.4 | 0.2 | 7.5 |
| ONNR* | 1.4 | 1.8 | 0.7 | 5.0 | 0.6 | 0.4 | 2.1 | 0.7 | 0.2 | 12.9 |
| PASA | 1.1 | 1.2 | 0.6 | 4.0 | 0.4 | 0.3 | 1.0 | 0.4 | 0.2 | 9.2 |
| PICO | 1.3 | 1.5 | 0.7 | 4.9 | 0.5 | 0.4 | 1.4 | 0.5 | 0.2 | 11.3 |
| RESE | 1.1 | 1.2 | 0.6 | 3.8 | 0.4 | 0.3 | 1.1 | 0.4 | 0.2 | 9.0 |
| RIVR | 1.2 | 1.5 | 0.6 | 4.6 | 0.5 | 0.3 | 1.8 | 0.5 | 0.2 | 11.2 |
| SLBH | 1.1 | 1.5 | 0.7 | 4.2 | 0.5 | 0.4 | 1.3 | 0.4 | 0.2 | 10.2 |
| SNBO | 1.1 | 1.4 | 0.6 | 3.9 | 0.5 | 0.3 | 1.6 | 0.5 | 0.2 | 10.0 |

* indicates results using the traditional CMAQ based RRF approach

TABLE II-5-6

RRF-BASED PREDICTED 2030 ATTAINMENT ANNUAL DESIGN VALUES ($\mu\text{g}/\text{m}^3$)

| Sites | SO4 | NO3 | NH4 | OC | EC | Salt | Others | Water | Blank | Total |
|-------|-----|-----|-----|-----|-----|------|--------|-------|-------|-------|
| ANAH | 1.1 | 1.2 | 0.6 | 4.2 | 0.4 | 0.5 | 1.3 | 0.5 | 0.2 | 9.9 |
| AZUS | 1.2 | 1.0 | 0.5 | 4.0 | 0.4 | 0.4 | 1.2 | 0.5 | 0.2 | 9.2 |
| BGBR | 0.6 | 0.7 | 0.4 | 2.2 | 0.4 | 0.2 | 1.0 | 0.2 | 0.2 | 5.7 |
| CELA | 1.3 | 1.3 | 0.6 | 5.0 | 0.5 | 0.3 | 1.2 | 0.5 | 0.2 | 11.0 |
| CMPT | 1.3 | 1.4 | 0.7 | 5.1 | 0.6 | 0.4 | 1.4 | 0.5 | 0.2 | 11.4 |
| FONT | 1.2 | 1.2 | 0.5 | 3.9 | 0.5 | 0.3 | 1.7 | 0.6 | 0.2 | 10.0 |
| LBNR | 1.3 | 1.5 | 0.7 | 5.0 | 0.5 | 0.4 | 1.4 | 0.5 | 0.2 | 11.5 |
| LGBH | 1.1 | 1.3 | 0.6 | 4.2 | 0.5 | 0.4 | 1.2 | 0.4 | 0.2 | 9.9 |
| MRLM | 1.3 | 1.4 | 0.6 | 4.9 | 0.6 | 0.3 | 2.1 | 0.7 | 0.2 | 12.0 |
| MSVJ | 0.8 | 1.0 | 0.5 | 2.8 | 0.3 | 0.3 | 1.0 | 0.4 | 0.2 | 7.3 |
| ONNR* | 1.4 | 1.5 | 0.6 | 5.0 | 0.6 | 0.4 | 2.1 | 0.7 | 0.2 | 12.4 |
| PASA | 1.1 | 1.0 | 0.5 | 4.1 | 0.4 | 0.3 | 1.0 | 0.4 | 0.2 | 9.0 |
| PICO | 1.3 | 1.3 | 0.6 | 4.9 | 0.5 | 0.4 | 1.4 | 0.5 | 0.2 | 11.0 |
| RESE | 1.1 | 1.0 | 0.5 | 3.8 | 0.4 | 0.3 | 1.1 | 0.4 | 0.2 | 8.7 |
| RIVR | 1.2 | 1.2 | 0.5 | 4.5 | 0.5 | 0.3 | 1.8 | 0.6 | 0.2 | 10.8 |
| SLBH | 1.1 | 1.4 | 0.7 | 4.2 | 0.4 | 0.4 | 1.2 | 0.4 | 0.2 | 10.0 |
| SNBO | 1.1 | 1.1 | 0.5 | 3.9 | 0.4 | 0.3 | 1.6 | 0.6 | 0.2 | 9.6 |

* indicates results using the traditional CMAQ based RRF approach

Unmonitored Area Analysis

U.S. EPA modeling guidance requires that the attainment demonstration include an analysis that confirms that all grid cells in the modeling domain meet the federal standard. This “unmonitored area analysis” is essential since speciation monitoring is conducted at a limited number of sites in the modeling domain. Variability in the species profiles at selected locations coupled with the differing responses to emissions control scenarios are expected to result in spatially variable impacts to PM2.5 air quality in any grid cell. As described earlier in this chapter, speciation profiles from CSN sites are interpolated using inverse distance squared weighting. With interpolation of the CSN speciation profiles, attainment demonstrations can be directly conducted for the remaining grid cells where FRM mass data has been collected over the modified 5-year weighted period of 2016-2019.

The methodology used to assess the unmonitored grid cell impact is as follows. The speciation fractions throughout the Basin for each relevant species except particle bound water were estimated with inverse distance squared interpolation for each quarter of 2018. In the unmonitored area analysis, the modified five-year weighted annual PM2.5 design values were calculated for all Federal Reference Method (FRM) monitoring stations within the modelling domain for the 2016 to 2019 period for each quarter. Quarterly design values were interpolated using inverse distance squared weighting interpolation. The product of the interpolated total PM2.5 mass from the FRM monitors and the interpolated speciation fractions from the CSN monitors yields spatial distributions of speciated mass in each quarter. In order to maintain consistency with the attainment demonstration at individual stations, base and future year species concentrations at each grid cell were replaced with the average value of the 3x3 grid encompassing the selected grid cell. Model derived base and future-year quarterly averaged species concentrations were used to calculate RRFs for each species except water. RRFs were multiplied by quarterly averaged species concentrations to project future species concentrations. Particle-bound water was then calculated using a polynomial regression of the Aerosol Inorganic Model (AIM) and summed along with a “blank” concentration to calculate the quarterly-averaged PM2.5 future-year design values. Quarterly PM2.5 concentrations were averaged to produce future-year design values throughout the Basin. This approach is consistent with the U.S. EPA’s guidance.¹⁰

Figure II-5-32 shows the annual PM2.5 design values in the base year 2018 for the entire basin. Figures II-5-33 through II-5-35 provide the Basin-wide spatial extent of annual PM2.5 projected for 2025 baseline, 2030 baseline and 2030 attainment scenario. Without additional controls in the baseline 2025 and 2030, the number of grid cells with concentrations exceeding the federal standard is restricted to a small region around the Ontario CA-60 near-road and the Mira Loma monitoring stations, across the border between northwestern Riverside County and southwestern San Bernardino County. Figure II-5-35 shows the projected PM2.5 concentrations in 2030 with the full implementation of the PM2.5 control strategy, and

¹⁰ Modeling Guidance for Demonstrating Attainment of Air Quality Goals for Ozone, PM2.5, and Regional Haze, U.S. EPA, November 2018. Available at: https://www.epa.gov/sites/default/files/2020-10/documents/o3-pm-rh-modeling_guidance-2018.pdf

demonstrate that all areas in the basin are projected to be below the federal standard of $12 \mu\text{g}/\text{m}^3$. Table II-5-7 summarizes the design values projected for the entire basin including unmonitored areas.

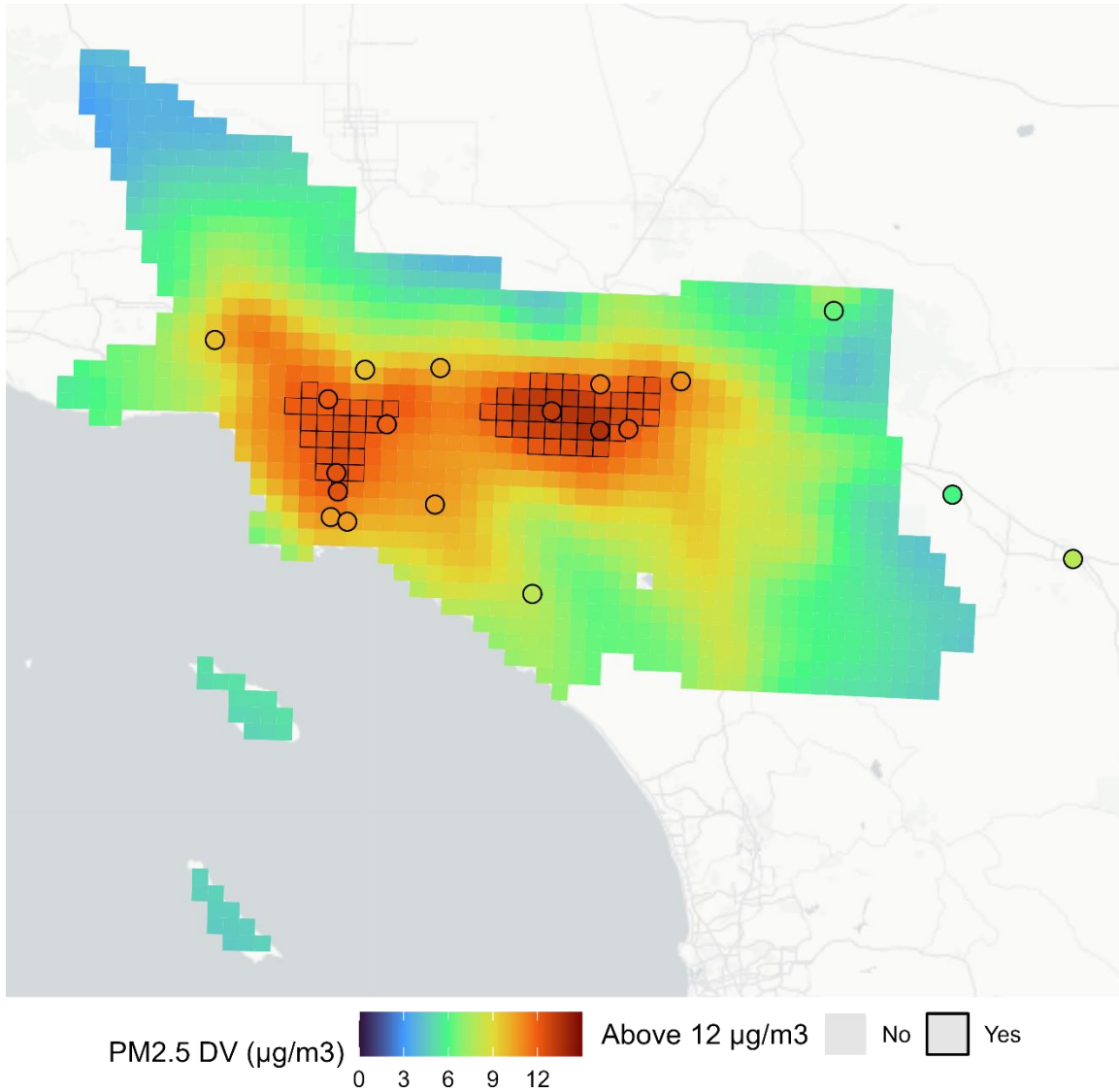


FIGURE II-5-32

PM2.5 DESIGN VALUES ($\mu\text{g}/\text{m}^3$) FROM THE 2018 BASE YEAR SCENARIO. CELLS EXCEEDING $12 \mu\text{g}/\text{m}^3$ ARE OUTLINED IN BLACK.

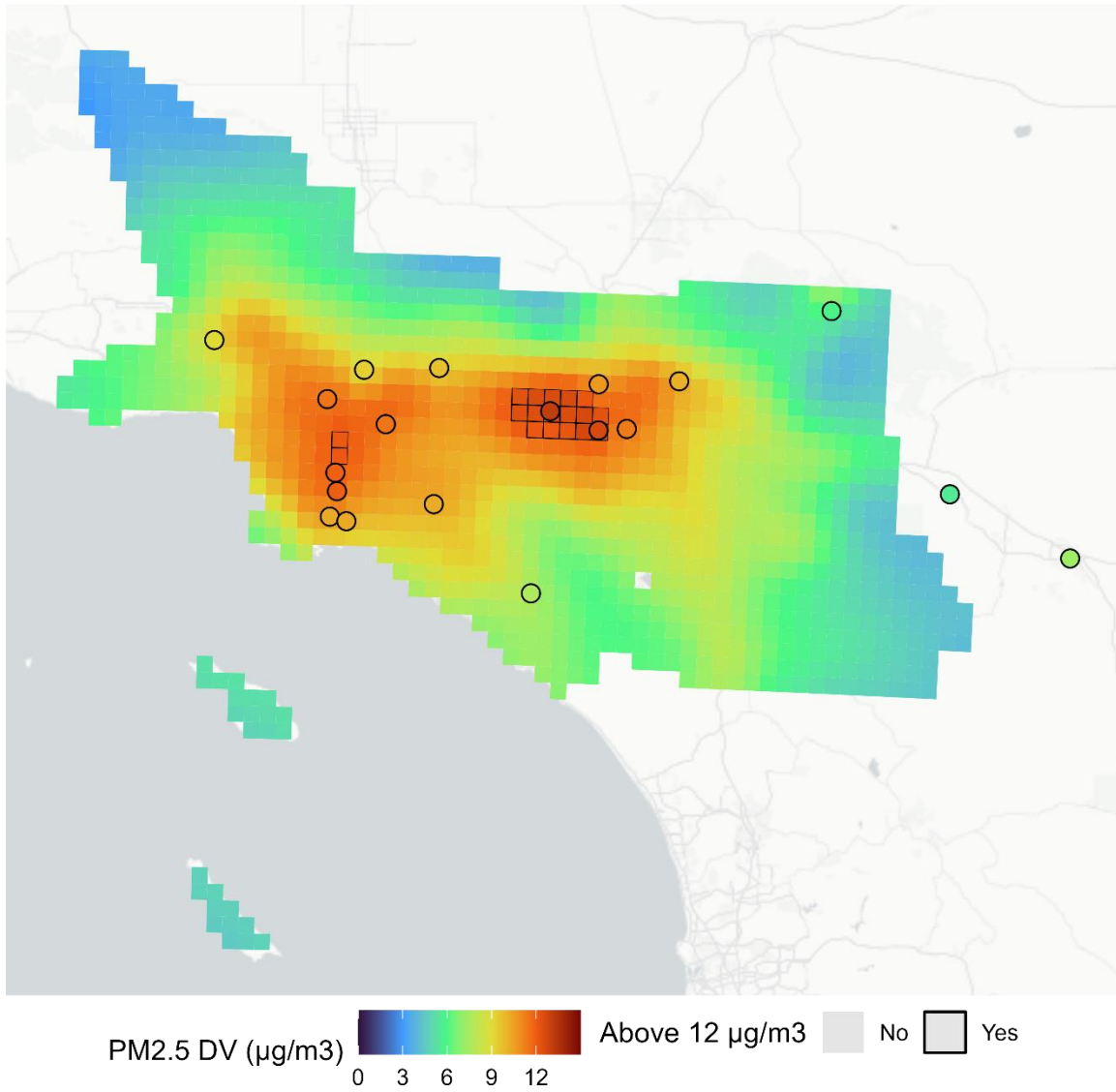


FIGURE II-5-33

ANNUAL PM2.5 DESIGN VALUES ($\mu\text{g}/\text{m}^3$) FROM THE 2025 BASELINE SCENARIO. CELLS EXCEEDING 12 $\mu\text{g}/\text{m}^3$ ARE OUTLINED IN BLACK.

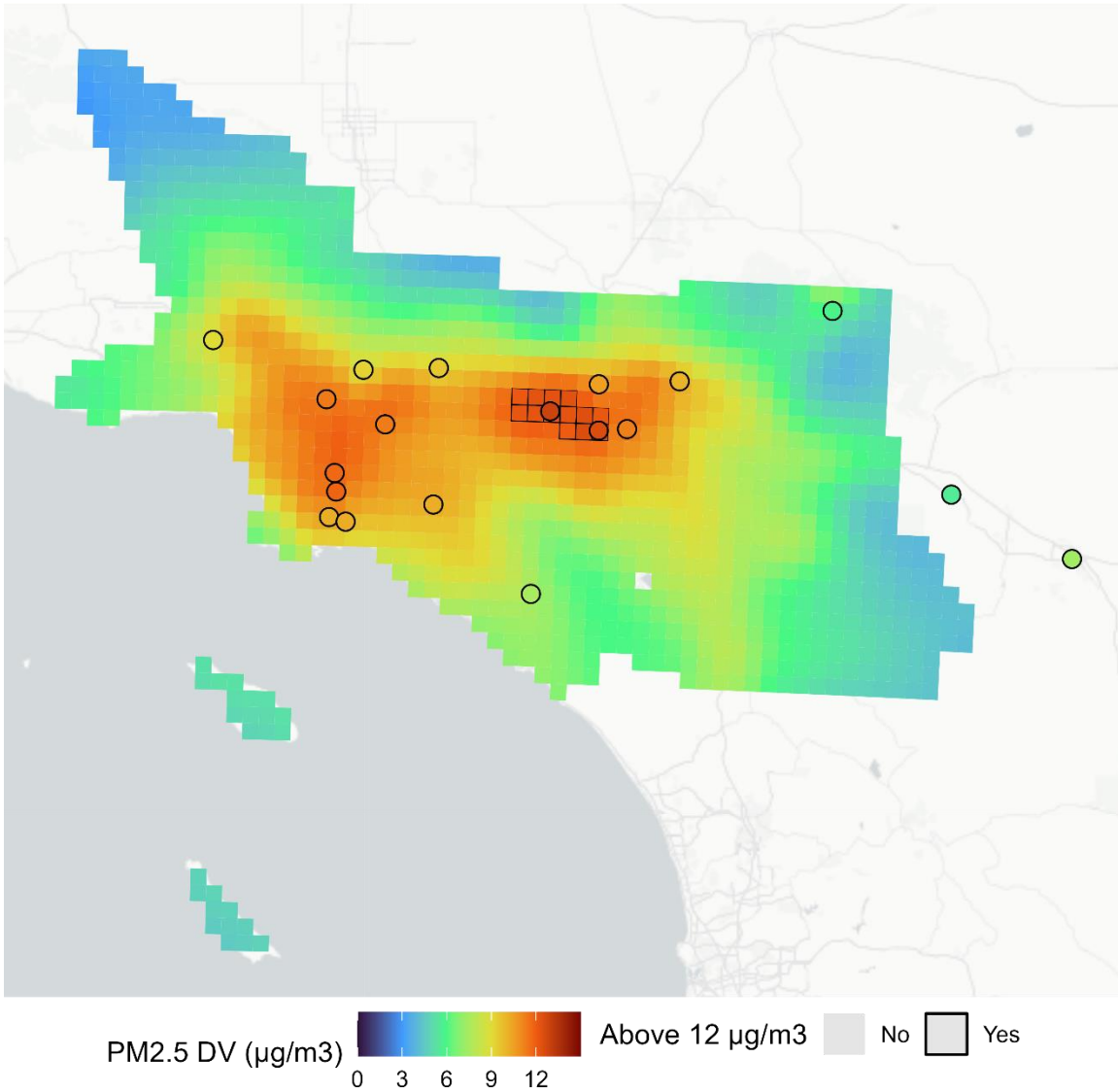


FIGURE II-5-34

ANNUAL PM2.5 DESIGN VALUES ($\mu\text{g}/\text{m}^3$) FROM THE 2030 BASELINE SCENARIO. CELLS EXCEEDING 12 $\mu\text{g}/\text{m}^3$ ARE OUTLINED IN BLACK.

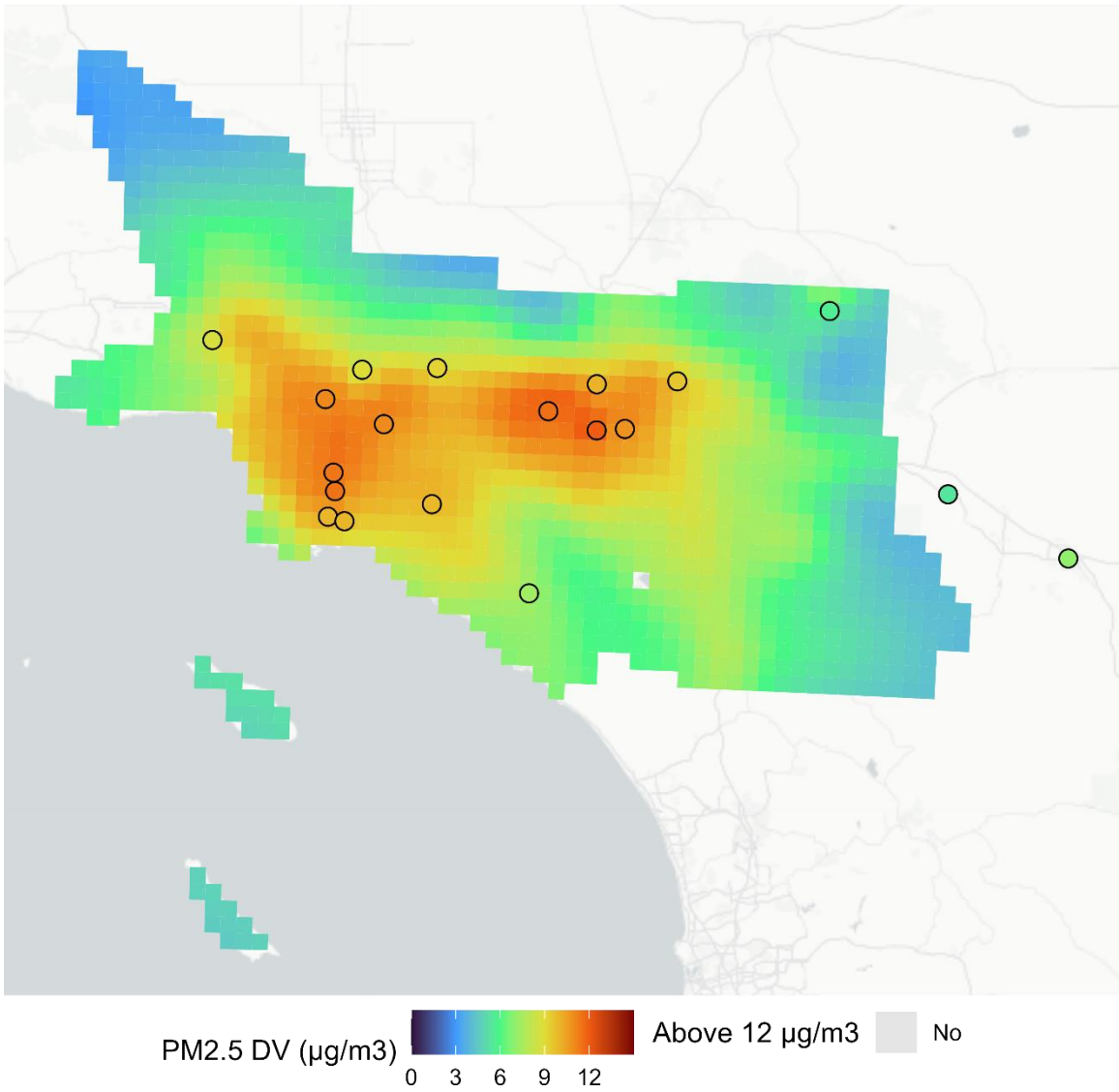


FIGURE II-5-35

ANNUAL PM2.5 DESIGN VALUES ($\mu\text{g}/\text{m}^3$) FROM THE 2030 ATTAINMENT SCENARIO.

TABLE II-5-7

UNMONITORED AREA ANALYSIS PROJECTED BASIN-MAXIMUM ANNUAL PM2.5 DESIGN VALUES

| Simulation | Maximum Annual PM2.5 Concentration in the Basin |
|-----------------|---|
| 2025 Baseline | 13.1 |
| 2030 Baseline | 12.9 |
| 2030 Attainment | 12.0 |

Summary and Conclusions

This section presents the performance of the modeling platform developed for this Draft-PM2.5 plan and demonstrates the attainment of the annual PM2.5 standard in 2030 in the South Coast Air Basin. The modeling platform reproduces the PM2.5 temporal trends throughout the year 2018 and shows good agreement with PM2.5 speciation. The control strategy presented in this Draft-PM2.5 plan is expected to lead the South Coast Air Basin to attainment of the 2012 annual PM2.5 standard in 2030. This was demonstrated using a traditional photochemical-modeling-based approach recommended by U.S. EPA and an alternative hybrid approach for Ontario CA-60 near-road site, which was developed in consultation with U.S. EPA and CARB. The latter approach is presented in detail in the next chapter of this appendix.

Chapter 6

ATTAINMENT DEMONSTRATION FOR THE CA-60 NEAR-ROAD MONITORING STATION

Introduction

Approach to Model the Effect of Near-Road Sources

AERMOD Dispersion Modeling Set-Up

PM2.5 simulation with AERMOD

Model Evaluation of Hybrid Model

Annual PM2.5 Design Values using the Hybrid Approach

Summary

Introduction

The current design site in the basin is the near-road monitor located by CA-60 freeway in Ontario. The monitor is sited just 16 meters away from the freeway, as shown in Figure II-6-1, and is heavily influenced by the emissions released from vehicles as well as resuspended particles caused by moving traffic. The Ontario CA-60 near-road monitor (referred to as CA60NR hereinafter) has been operational since 2015, and since the monitor started collecting data, it has been the station with the highest annual average PM2.5 concentration in the basin. This monitor surpassed the concentrations at the previous design site in Mira Loma, which is located approximately 12 km eastward. However, the differences in annual PM2.5 concentrations between Mira Loma and CA60NR have narrowed since 2015 (see Figure 5-11 in Chapter 5). This trend can be attributed to the fact that emissions from on-road sources have decreased substantially more than all other sources in the basin, and as a result, PM2.5 concentrations at near-road monitors are decreasing faster than concentrations at regional monitors that represent air quality of wider areas.

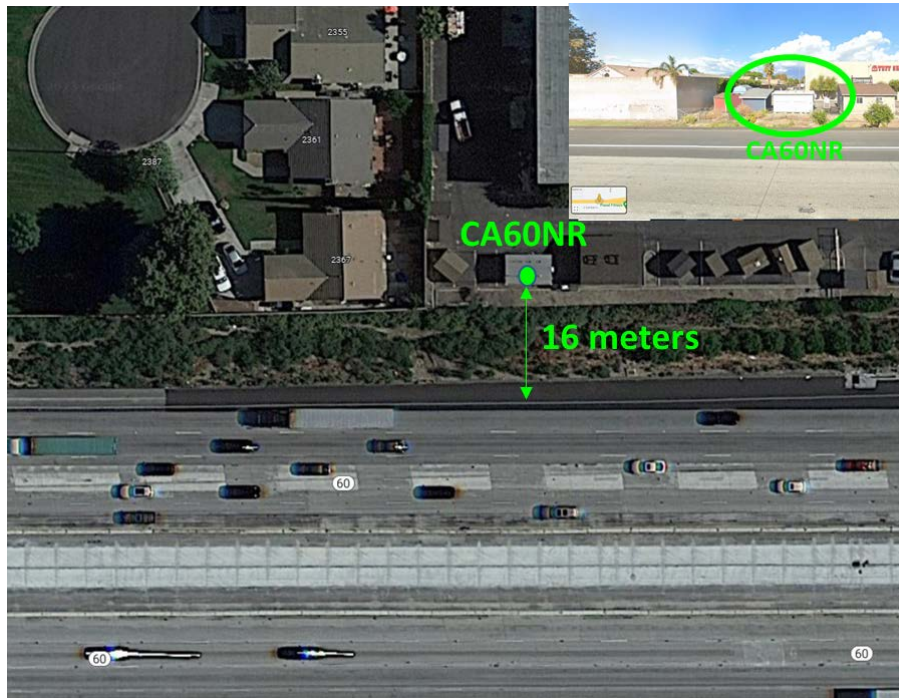


FIGURE II-6-1

LOCATION OF THE ONTARIO CA-60 NEAR-ROAD MONITOR

Regional photochemical transport modeling is designed to calculate air quality that is representative at the grid resolution of the model. This attainment demonstration uses a model resolution of 4 km by 4 km grid, and thus, should model concentration at monitors that are representative of a similar area. Near-road sites are heavily impacted by near-road sources and thus are not representative of the overall grid. U.S. EPA's modeling guidance acknowledges that attainment demonstration at near-road sites may

require a different treatment compared to other monitors as is indicated in modeling guidance, Section 4.6:

“PM2.5 measurement data from monitors that are not representative of “area-wide” air quality, but rather of relatively unique micro-scale, or localized hot spot, or unique middle-scale impact sites, are not eligible for comparison to the annual PM2.5 NAAQS.”

“... numerous cases where local source contributions may not be dominant, but are a sizable contributor to total PM2.5 (~10- 30% of total annual average PM2.5). In these cases, a more refined analysis of the contribution of local primary PM2.5 sources to PM2.5 at the monitor(s) will help explain the causes of nonattainment at and near the monitor.”

And in section 6.0:

“There may be some areas for which the supplemental evidence is persuasive enough to support a conclusion that the area can expect to achieve timely attainment despite failing the modeled attainment test...”

For monitors affected by localized sources like the CA60NR site, the U.S. EPA modeling guidance suggests additional modeling techniques that would support the attainment demonstration. These techniques include increasing model resolution to a finer grid and using dispersion modeling to assess the impact of primary PM2.5 emissions from near sources on the monitor:

“A grid model can be run at very high horizontal resolution (1 or 2 km or finer) or a Gaussian dispersion model can be used. Grid based models simulate chemical transformation and complex meteorological conditions, while dispersion models are generally more simplistic; being limited to a local scale, using Gaussian approximations with little or no chemistry. Therefore, while dispersion models may not be an appropriate tool for determining secondary PM2.5 or ozone concentrations, they work well for use in determining local primary PM2.5 impacts.”

This chapter describes the application of hybrid approach using a combination of regional photochemical grid modeling (CMAQ) and dispersion modeling (AERMOD) to show that the annual PM2.5 concentrations at the CA60NR monitor are projected to decline more steeply than what the regional model suggests. The overall approach is to use CMAQ to model the impact of all sources at the grid resolution used in the attainment demonstrations, and to use AERMOD to quantify the elevated PM2.5 concentrations resulting from the proximity of the monitor to the emissions from vehicle and road dust resuspension along the freeway.

Approach to Model the Effect of Near-Road Sources

As the modeling guidance suggests, regional modeling may not be sufficient to represent the air pollution dynamics at near-road monitors and dispersion models can be used to determine primary PM2.5 impacts from on-road sources. Figure II-6-2 depicts how near-road sources contribute to PM2.5 concentrations around the monitor compared to how a regional model would quantify the grid cell-average impacts from

near-road sources. While the measurements at the near-road monitor observe a large contribution from near-road sources, a regional model only observes those near-road impacts averaged over the entire area of the modeling grid cell, resulting in an overall smaller impact. Regional modeling using CMAQ represents the air quality resulting from the regional sources plus the grid cell-average impacts of the near-road sources, whereas dispersion modeling using AERMOD can resolve the steep gradients in PM2.5 impacts from near-road sources. Thus, the use of AERMOD is used to quantify the near-road increment portion of the impacts from near-road sources that are beyond the grid cell-average near-road impacts. Because of the proximity of the monitor to the freeway, it is reasonable to assume that the impacts on PM2.5 primarily result from direct PM2.5 emissions and that the near-road impacts on secondary PM2.5 are negligible.

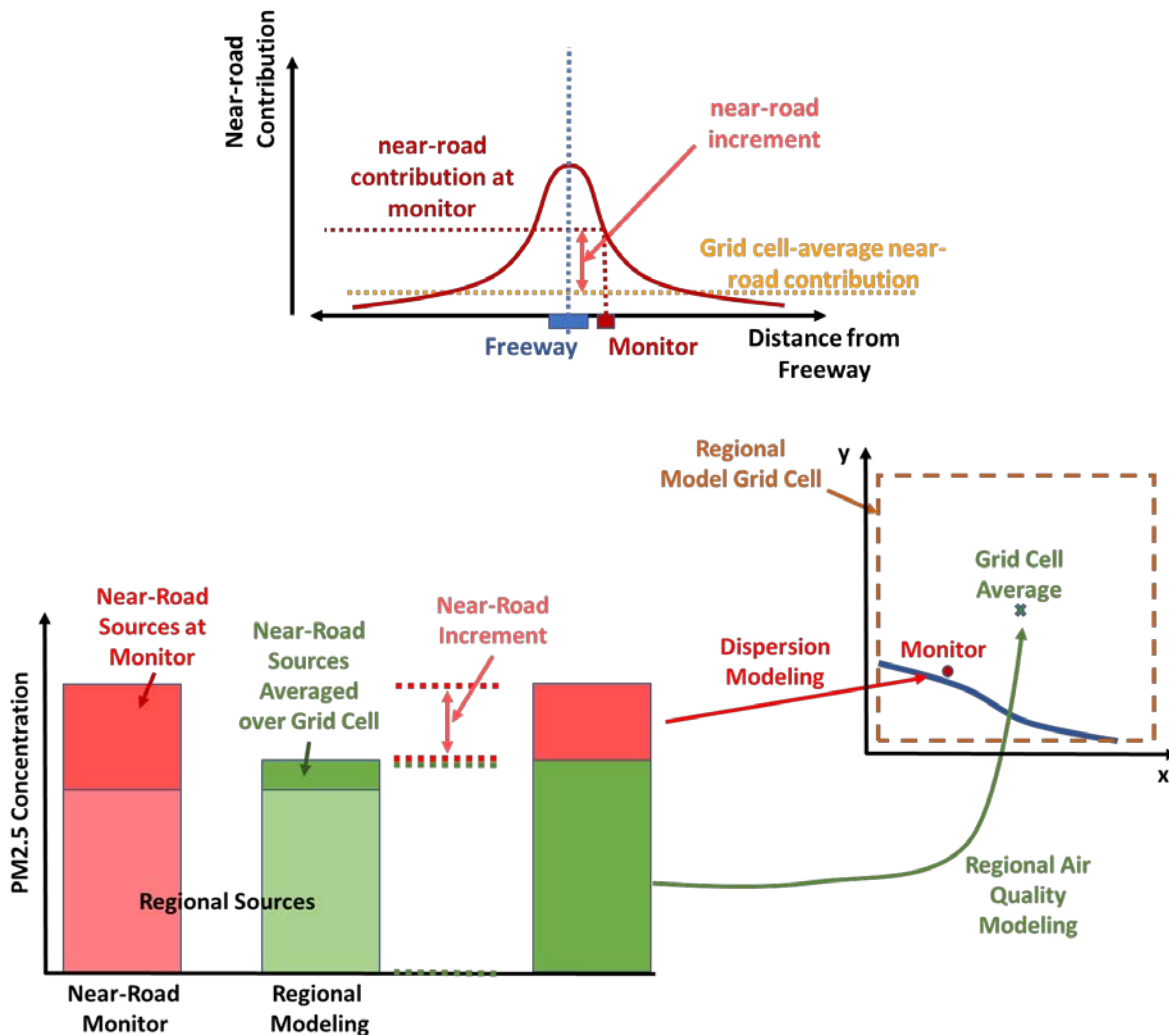


FIGURE II-6-2

SCHMATIC OF THE HYBRID APPROACH TO INTEGRATE REGIONAL MODELING WITH DISPERSION MODELING OF NEAR-ROAD SOURCES

The receptor grid in the dispersion modeling setup spans the same area as the 4 km-by-4km regional modeling grid cell where the CA60NR monitor is located. The spacing of the receptors is 100 meters, with an additional receptor at the location of the monitor. The average of the concentrations at all receptors represents the receptor grid-average impact from near-road sources. The difference between the concentration at the CA60NR receptor monitor and the average across all dispersion modeling receptors is the AERMOD near-road increment (NRI_{AERMOD}):

$$C_{AERMOD,grid} = \frac{1}{N} \sum_{i=1}^N C_{AERMOD,i} \quad (II.6.1)$$

$$NRI_{AERMOD} = C_{AERMOD,CA60NR} - C_{AERMOD,grid} \quad (II.6.2)$$

where $C_{AERMOD,grid}$ is the near-road source contribution averaged over the AERMOD receptor grid, $C_{AERMOD,i}$ is the PM2.5 contribution at a given receptor i and N is the total number of receptors in the AERMOD modeling setup, and $C_{AERMOD,CA60NR}$ is the modeled near-road source contribution to PM2.5 concentration at the CA60NR monitor.

Alternatives for the determination of NRI

The magnitude of the NRI is a critical factor in the attainment demonstration for this near-road site. Because there are no speciated measurements at the CA60NR site, it is not possible to directly quantify the contribution of near-road sources to the overall PM2.5 measurements. Four potential approaches are considered to determine the NRI:

- 1) NRI based on AERMOD modeling, NRI_{AERMOD} , already described above.
- 2) NRI based on AERMOD for the monitor contribution, and CMAQ for the modeling grid cell average ($NRI_{AERMOD-CMAQ}$):

This approach is to calculate the NRI based on the concentrations calculated by AERMOD at the monitor and the near-road source contribution calculated using CMAQ at the CA60NR monitor cell. The calculation of the near-road source contribution to the CA60NR monitor cell ($C_{CMAQ,CA60NR}$) is calculated as follows:

$$C_{CMAQ,CA60NR} = C_{CMAQ,Base} - C_{CMAQ,NoCA60NR} \quad (II.6.3)$$

Where $C_{CMAQ,Base}$ is the PM2.5 concentration at the CA60NR monitor CMAQ grid cell in the base year simulation, and $C_{CMAQ,NoCA60NR}$ is the PM2.5 concentration in the simulation with all the base year emission sources included except for the near-road sources that are included in the AERMOD modeling setup. Then, this second alternative NRI, $NRI_{AERMOD-CMAQ}$, is calculated using the following expression:

$$NRI_{AERMOD-CMAQ} = C_{AERMOD,CA60NR} - C_{CMAQ,CA60NR} \quad (II.6.4)$$

This $NRI_{AERMOD-CMAQ}$ is used as the benchmark NRI, because the regional model (CMAQ) is the best tool available to determine the regional impacts from regional sources and which includes

secondary formation of PM2.5, and dispersion modeling (AERMOD) is the best tool suited for short scale transport modeling typically used for source permitting.

3) NRI based on measured concentrations in nearby monitors:

As a third alternative, the NRI can be assessed by comparing PM2.5 levels at CA60NR with those at nearby monitoring stations. This approach was used in the attainment demonstration for annual PM2.5 in the Allegheny County, where there is a monitor that is in the vicinity of a large facility.¹ However, the case of CA60NR is different as there is not a single large facility affecting the monitor, but a collection of moving sources running along the CA-60 freeway. Three neighboring monitors, which are located within a 20-kilometer radius, are used in this approach: Mira Loma, Fontana and Rubidoux. It is important to note that the annual PM2.5 design value is calculated using speciated components of PM2.5. However, neither the CA60NR monitor nor the closest monitors at Mira Loma and Fontana have speciated measurements available. Consequently, the speciation profile of the NRI is estimated based on dispersion modeling results. The NRI based on measured PM2.5 at neighboring sites, $NRI_{Monitors}$, is calculated as follows:

$$NRI_{Monitors} = DV_{CA60NR} - \frac{1}{N} \sum_{i=1}^N DV_i \quad (II.6.5)$$

Where DV_{CA60NR} is the design value observed at the CA60NR monitor, and DV_i is the design value observed at monitor i .

4) NRI based on the relative proportion of AERMOD and CMAQ modeled values ($NRI_{RelativeModel}$):

The fourth approach is to assume that the modeled $NRI_{AERMOD-CMAQ}$ and plus the regional sources modeled by CMAQ are in the same proportion as ($C_{CMAQ,Base}$) correspond to the monitored regional and local portions design value at the near-road monitor, DV_{CA60NR} . Then, the portion of the design value that corresponds to the near-road increment is defined by the ratio of the modeled $NRI_{AERMOD-CMAQ}$ to the total modeled concentration. This approach implies that the performance of CMAQ modeling regional sources and the performance of AERMOD modeling near-road sources are comparable.

The expression to calculate the $NRI_{RelativeModel}$ is as follows:

$$NRI_{RelativeModel} = DV_{CA60NR} \cdot \frac{NRI_{AERMOD-CMAQ}}{(NRI_{AERMOD-CMAQ} + C_{CMAQ,Base})} \quad (II.6.6)$$

Each equation represents slightly different definitions of NRI. The four NRI approaches are later evaluated to establish uncertainty bounds for calculating future design values using hybrid modeling results.

¹ Revision to the Allegheny County Portion of the Pennsylvania State Implementation Plan. Attainment Demonstration for the Allegheny County, PA PM2.5 Nonattainment Area, 2012 NAAQS.

<https://www.regulations.gov/search?filter=EPA-R03-OAR-2020-0157>

The estimated NRI is then subtracted from the base year design value, and the remaining portion corresponds to the contribution of all regional sources plus the grid cell average contribution of the near-road sources. This second portion of the DV is referred as the regional component of the DV (RDV):

$$RDV = (\text{Base Year DV}) - \text{NRI} \quad (\text{II.6.7})$$

Once the NRI and RDV components are disaggregated from the measured design value, future design value can be estimated by applying two differentiated Relative Reduction Factors (RRF) to these two components. The RDV component is projected using the RRF calculated from regional air quality modeling (RRF_{CMAQ}), and the NRI is projected using the RRF calculated using the dispersion modeling results (RRF_{AERMOD}). Figure II-6-3 illustrates this procedure. The resulting future year design value is calculated as follows:

$$\text{Future DV} = RDV * RRF_{CMAQ} + \text{NRI} * RRF_{AERMOD} \quad (\text{II.6.8})$$

It is important to note that dispersion modeling is used to estimate the NRI, which is an increment from what the regional modeling simulates. Thus, the regional modeling set-up includes all near-road sources, to account for the grid cell average component of near-road sources. Conversely, the receptor grid-average obtained from AERMOD is subtracted from the concentrations estimated by AERMOD at the monitor site, to calculate the NRI_{AERMOD} and avoid double counting of the grid cell average impacts from near-road sources. This approach is described in a 5-step process below.

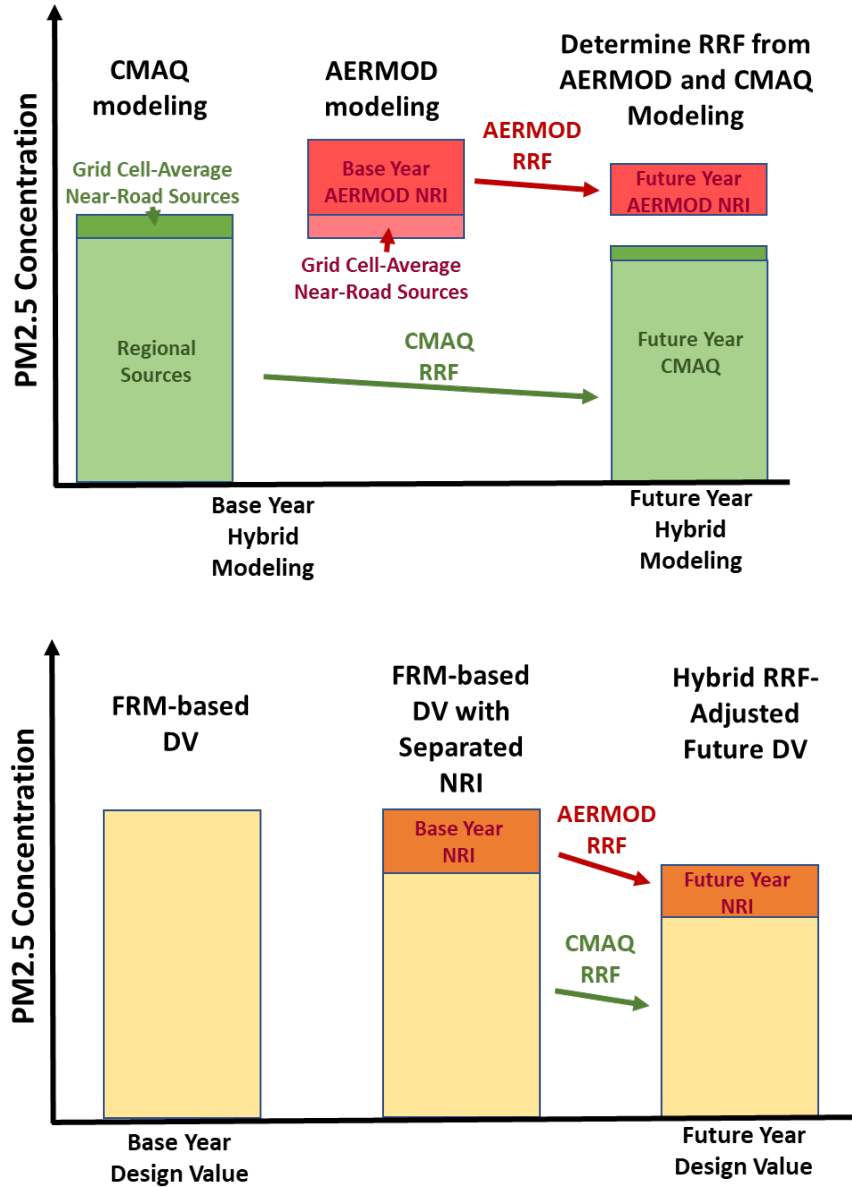


FIGURE II-6-3

DIAGRAM OF THE APPROACH TO PROJECT FUTURE PM2.5 CONCENTRATIONS USING RRF FOR REGIONAL MODELING AND DISPERSION MODELING OF NEAR-ROAD SOURCES

STEP 1: Conduct AERMOD dispersion modeling to determine the base year and attainment year speciated near-road increment.

The AERMOD modeling set-up is described in detail in the following section. The quarterly average contribution from near-road sources and the NRI_{AERMOD} for the base year is presented in Table II-6-1. Based on AERMOD modeling, the contribution from near-road sources averaged over the AERMOD receptor grid and averaged annually is $0.32 \mu\text{g}/\text{m}^3$, whereas the annual average contribution of near-road sources at the CA60NR monitor is $3.13 \mu\text{g}/\text{m}^3$. As a result, the estimated NRI_{AERMOD} annual average is $2.81 \mu\text{g}/\text{m}^3$. The future NRI and RRF calculated from the dispersion modeling are presented in Table II-6-2.

TABLE II-6-1

BASE YEAR QUARTERLY AVERAGE CONTRIBUTION OF NEAR-ROAD SOURCES AVERAGED OVER THE RECEPTOR GRID AND AT THE CA60NR MONITOR, AND NEAR-ROAD INCREMENT (\overline{NRI}_{AERMOD} , APPROACH #1), USING AERMOD

| AERMOD – Receptor Grid Average ($C_{AERMOD,grid}$) ($\mu\text{g}/\text{m}^3$) | | | | | |
|--|-----------|-----------|-----------|-----------|---------------|
| | Q1 | Q2 | Q3 | Q4 | Annual |
| Sulfate | 0.017 | 0.011 | 0.009 | 0.020 | 0.014 |
| Nitrate | 0.003 | 0.002 | 0.001 | 0.003 | 0.002 |
| Ammonium | 0.002 | 0.002 | 0.001 | 0.003 | 0.002 |
| OC | 0.068 | 0.042 | 0.037 | 0.078 | 0.056 |
| EC | 0.067 | 0.041 | 0.037 | 0.078 | 0.056 |
| Salt | 0.014 | 0.008 | 0.007 | 0.016 | 0.011 |
| Other | 0.223 | 0.135 | 0.119 | 0.252 | 0.182 |
| Total Near-Road | 0.39 | 0.24 | 0.21 | 0.45 | 0.32 |
| AERMOD – At Monitor ($C_{AERMOD,CA60NR}$) ($\mu\text{g}/\text{m}^3$) | | | | | |
| | Q1 | Q2 | Q3 | Q4 | Annual |
| Sulfate | 0.132 | 0.136 | 0.135 | 0.142 | 0.136 |
| Nitrate | 0.021 | 0.022 | 0.021 | 0.023 | 0.022 |
| Ammonium | 0.019 | 0.020 | 0.019 | 0.020 | 0.020 |
| OC | 0.518 | 0.536 | 0.529 | 0.549 | 0.533 |
| EC | 0.515 | 0.532 | 0.525 | 0.555 | 0.532 |
| Salt | 0.106 | 0.109 | 0.108 | 0.111 | 0.108 |
| Other | 1.737 | 1.797 | 1.776 | 1.818 | 1.782 |
| Total Near-Road | 3.05 | 3.15 | 3.11 | 3.22 | 3.13 |
| Near-Road Increment (\overline{NRI}_{AERMOD}) ($\mu\text{g}/\text{m}^3$) | | | | | |
| | Q1 | Q2 | Q3 | Q4 | Annual |
| Sulfate | 0.115 | 0.126 | 0.125 | 0.122 | 0.122 |
| Nitrate | 0.018 | 0.020 | 0.020 | 0.020 | 0.019 |
| Ammonium | 0.016 | 0.018 | 0.018 | 0.017 | 0.018 |
| OC | 0.450 | 0.494 | 0.493 | 0.471 | 0.477 |
| EC | 0.448 | 0.490 | 0.489 | 0.476 | 0.476 |
| Salt | 0.092 | 0.101 | 0.101 | 0.095 | 0.097 |
| Other | 1.515 | 1.662 | 1.658 | 1.565 | 1.600 |
| Total Near-Road | 2.65 | 2.91 | 2.90 | 2.77 | 2.81 |

TABLE II-6-2

FUTURE YEAR QUARTERLY NEAR-ROAD INCREMENT (NRI) AND RELATIVE REDUCTION FACTORS CALCULATED USING AERMOD.

| Future Year Near-Road Increment ($\mu\text{g}/\text{m}^3$) | | | | | |
|---|-----------|-----------|-----------|-----------|---------------|
| | Q1 | Q2 | Q3 | Q4 | Annual |
| Sulfate | 0.047 | 0.051 | 0.051 | 0.049 | 0.050 |
| Nitrate | 0.009 | 0.010 | 0.010 | 0.010 | 0.010 |
| Ammonium | 0.006 | 0.007 | 0.007 | 0.007 | 0.007 |
| OC | 0.253 | 0.279 | 0.278 | 0.261 | 0.268 |
| EC | 0.091 | 0.100 | 0.100 | 0.094 | 0.096 |
| Salt | 0.090 | 0.098 | 0.098 | 0.093 | 0.095 |
| Other | 1.475 | 1.617 | 1.612 | 1.533 | 1.559 |
| Total Near-Road | 1.97 | 2.16 | 2.16 | 2.05 | 2.08 |
| Relative Reduction Factors (RRF_{AERMOD}) (non-dimensional) | | | | | |
| | Q1 | Q2 | Q3 | Q4 | Annual |
| Sulfate | 0.408 | 0.408 | 0.408 | 0.404 | 0.407 |
| Nitrate | 0.518 | 0.518 | 0.518 | 0.515 | 0.517 |
| Ammonium | 0.377 | 0.377 | 0.377 | 0.371 | 0.375 |
| OC | 0.563 | 0.563 | 0.564 | 0.556 | 0.561 |
| EC | 0.204 | 0.204 | 0.204 | 0.197 | 0.202 |
| Salt | 0.972 | 0.972 | 0.972 | 0.978 | 0.974 |
| Other | 0.972 | 0.972 | 0.972 | 0.978 | 0.973 |
| Total Near-Road | 0.742 | 0.742 | 0.742 | 0.739 | 0.741 |

STEP 2: Determine the NRI.

As described above, we propose four alternatives to the calculation of NRI. Step 1 calculates the NRI_{AERMOD} used in the calculation of RRF_{AERMOD} .

The second alternative is to calculate the NRI using the grid cell-average near-road source contribution calculated with CMAQ. Two simulations are conducted to determine the contribution of near-road sources: (1) annual base year simulation with all emissions and (2) annual base year simulation that includes all emissions excluding the PM_{2.5} emissions from the near-road sources that are included in the AERMOD simulation. Then the difference in PM_{2.5} concentrations between the two simulations at the cell where CA60NR is located is the grid cell-average contribution of near-road sources, $C_{CMAQ,CA60NR}$. Then, the $NRI_{AERMOD-CMAQ}$ is calculated using equation II.6.4 using $C_{AERMOD,CA60NR}$ shown in Table II-6-1. The values for $C_{CMAQ,CA60NR}$ and $NRI_{AERMOD-CMAQ}$ are shown in Table II-6-3. The $NRI_{AERMOD-CMAQ}$ is larger than the NRI_{AERMOD} because the contribution from near-road sources estimated by CMAQ is smaller than the grid-cell average contribution calculated with AERMOD ($C_{AERMOD,grid}$).

TABLE II-6-3

**NEAR-ROAD SOURCE CONTRIBUTION ESTIMATED BY CMAQ AND NEAR ROAD INCREMENT
WITH GRID CELL AVERAGE CONTRIBUTION CALCULATED BY CMAQ ($NRI_{AERMOD-CMAQ}$)
APPROACH #2).**

| Near-Road Source Contribution ($C_{CMAQ,CA60NR}$) ($\mu\text{g}/\text{m}^3$) | | | | | |
|---|-----------|-----------|-----------|-----------|---------------|
| | Q1 | Q2 | Q3 | Q4 | Annual |
| Sulfate | 0.010 | 0.005 | 0.000* | 0.011 | 0.006 |
| Nitrate | 0.041 | 0.003 | 0.000* | 0.030 | 0.019 |
| Ammonium | 0.008 | 0.000* | 0.000* | 0.005 | 0.003 |
| OC | 0.028 | 0.012 | 0.024 | 0.030 | 0.023 |
| EC | 0.035 | 0.018 | 0.018 | 0.041 | 0.028 |
| Salt | 0.008 | 0.004 | 0.020 | 0.008 | 0.010 |
| Other | 0.093 | 0.050 | 0.016 | 0.102 | 0.065 |
| Total Near-Road | 0.22 | 0.09 | 0.08 | 0.23 | 0.15 |
| $NRI_{AERMOD-CMAQ}$ ($\mu\text{g}/\text{m}^3$) | | | | | |
| | Q1 | Q2 | Q3 | Q4 | Annual |
| Sulfate | 0.122 | 0.131 | 0.135 | 0.131 | 0.130 |
| Nitrate | 0.000* | 0.018 | 0.021 | 0.000* | 0.010 |
| Ammonium | 0.010 | 0.020 | 0.019 | 0.015 | 0.016 |
| OC | 0.490 | 0.524 | 0.506 | 0.519 | 0.510 |
| EC | 0.479 | 0.514 | 0.507 | 0.514 | 0.504 |
| Salt | 0.098 | 0.106 | 0.088 | 0.103 | 0.099 |
| Other | 1.645 | 1.747 | 1.760 | 1.716 | 1.717 |
| Total Near-Road | 2.84 | 3.06 | 3.04 | 3.00 | 2.98 |

*CMAQ estimated negative contribution to sulfate, nitrate, and ammonium, due to chemical interaction with organic aerosol precursors. Because AERMOD modeling only accounts for primary PM2.5, negative values are capped at 0.

The third alternative for the NRI is calculated using monitoring data. There are 19 PM2.5 FRM monitoring stations in the basin, although only four stations measure speciated PM. The basin includes distinct geographical features and localized sources that causes PM2.5 concentrations vary widely throughout the region. Because of the wide range of sources and PM2.5 concentrations across the basin, the NRI in this attainment demonstration is estimated by using observations at the CA60NR and the three closest monitors: Mira Loma, Fontana, and Rubidoux. These three monitors are located within a 20-kilometer radius from CA60NR. Out of the four monitors, only Rubidoux measures speciated PM2.5. Consequently, calculating speciated NRI is not possible from observations. Thus, the speciation of the NRI is based on the modeled speciated NRI using AERMOD. Table II-6-4 shows the quarterly average PM2.5 concentrations at the four monitors used to determine the NRI, the resulting NRI, and the quarterly speciation profiles calculated with AERMOD. The annual $NRI_{Monitors}$, estimated using monitoring data, is $1.64 \mu\text{g}/\text{m}^3$, which is 45% less than the $NRI_{AERMOD-CMAQ}$. Both estimates are subject to uncertainties and there is no direct way to determine the accuracy of the estimates due to the lack of direct measurements.

The validity of $NRI_{Monitors}$ relies on the assumption that all the neighboring monitors are surrounded by the similar regional sources, and the only difference between CA60NR and all other monitors is the presence of freeway CA-60. However, a brief inspection of the surroundings of the neighboring monitors reveals that the monitor at Fontana is 1 km from Fontana's Auto Speedway racetrack and close to industrial yards, and the Mira Loma monitor is less than 2 km downwind from a large Union Pacific railyard and within 500 meters from a railroad. Thus, it is gross assumption that the difference in PM_{2.5} between CA60NR and the rest of neighboring monitors expressed by the $NRI_{Monitors}$ is due to the contribution from freeway CA-60 alone.

TABLE II-6-4

NEAR-ROAD INCREMENT CALCULATED FROM OBSERVATIONS ($NRI_{Monitors}$, APPROACH #3) AND SPECIATION PROFILE FOR THE NRI BASED ON AERMOD MODELING.

| Monitor | Distance | Q1 | Q2 | Q3 | Q4 | Annual |
|--|----------|-------|-------|-------|-------|--------|
| Ontario-Route 60 Near Road | | 13.45 | 12.36 | 14.65 | 15.46 | 13.98 |
| Fontana | 13.5 km | 9.78 | 11.12 | 13.43 | 11.08 | 11.35 |
| Rubidoux | 18.8 km | 10.55 | 11.51 | 13.02 | 13.44 | 12.13 |
| Mira Loma | 12.2 km | 12.50 | 12.05 | 13.12 | 16.44 | 13.53 |
| Near-Road Increment ($\mu\text{g}/\text{m}^3$) | | 2.51 | 0.80 | 1.46 | 1.80 | 1.64 |
| Near-Road Increment Speciation | | | | | | |
| Sulfate | | 4.1% | 4.1% | 4.1% | 4.2% | 4.1% |
| Nitrate | | 0.7% | 0.7% | 0.7% | 0.7% | 0.7% |
| Ammonium | | 0.6% | 0.6% | 0.6% | 0.6% | 0.6% |
| OC | | 16.5% | 16.4% | 16.3% | 16.4% | 16.4% |
| EC | | 16.0% | 15.9% | 15.9% | 16.3% | 16.0% |
| Salt | | 3.5% | 3.5% | 3.5% | 3.5% | 3.5% |
| Other | | 58.7% | 58.9% | 59.0% | 58.3% | 58.7% |
| $NRI_{Monitors}$ ($\mu\text{g}/\text{m}^3$) | | | | | | |
| | | Q1 | Q2 | Q3 | Q4 | Annual |
| Sulfate | | 0.109 | 0.034 | 0.063 | 0.080 | 0.071 |
| Nitrate | | 0.017 | 0.005 | 0.010 | 0.013 | 0.011 |
| Ammonium | | 0.016 | 0.005 | 0.009 | 0.011 | 0.010 |
| OC | | 0.426 | 0.135 | 0.248 | 0.306 | 0.279 |
| EC | | 0.424 | 0.134 | 0.246 | 0.310 | 0.278 |
| Salt | | 0.087 | 0.028 | 0.051 | 0.062 | 0.057 |
| Other | | 1.434 | 0.455 | 0.836 | 1.018 | 0.936 |
| Total Near-Road | | 2.51 | 0.80 | 1.46 | 1.80 | 1.64 |

The fourth alternative is using the modeled NRI and CMAQ concentrations in relative terms to determine the portion of the design value that corresponds to the NRI, following equation II.6.6. The observed base year design value at the CA60NR monitor (DV_{CA60NR}) is shown in Table II-6-5. Equation II.6.6 requires the DV_{CA60NR} from Table II-6-5, the modeled concentrations by CMAQ at CA60NR shown in Table II-6-6 and the $NRI_{AERMOD-CMAQ}$ shown in Table II-6-3. The relative portion of PM2.5 species from $NRI_{AERMOD-CMAQ}$ with respect to total $NRI_{AERMOD-CMAQ}$ plus CMAQ concentrations, and the resulting $NRI_{RelativeModel}$ values are shown in Table II-6-6. The overall $NRI_{RelativeModel}$ is $1.80 \mu\text{g}/\text{m}^3$, which is 40% less than the $NRI_{AERMOD-CMAQ}$, and slightly higher than the $NRI_{Monitors}$. As discussed earlier, because of the lack of direct speciated measurements at the CA60NR monitor, it is not possible to ascertain which of the four alternatives to the NRI is the most accurate. However, the range of values for NRI can provide a sense of uncertainty bounds in the modeling of future design values at the CA60NR.

TABLE II-6-5
SPECIATED DESIGN VALUE AT THE CA60NR MONITOR (DV_{CA60NR})

| Base Year DV at CA60NR ($\mu\text{g}/\text{m}^3$) | Q1 | Q2 | Q3 | Q4 | Annual |
|---|--------------|--------------|--------------|--------------|--------------|
| Sulfate | 0.697 | 1.654 | 1.984 | 1.009 | 1.336 |
| Nitrate | 3.025 | 2.613 | 1.951 | 3.112 | 2.675 |
| Ammonium | 1.102 | 1.188 | 0.991 | 1.135 | 1.104 |
| OC | 4.933 | 3.961 | 6.002 | 4.628 | 4.881 |
| EC | 0.933 | 0.502 | 0.766 | 1.165 | 0.842 |
| Salt | 0.418 | 0.354 | 0.319 | 0.303 | 0.349 |
| Other | 1.513 | 1.182 | 1.706 | 3.201 | 1.901 |
| Water | 0.628 | 0.706 | 0.729 | 0.697 | 0.690 |
| Blank | 0.2 | 0.2 | 0.2 | 0.2 | 0.2 |
| Total | 13.45 | 12.36 | 14.65 | 15.45 | 13.98 |

TABLE II-6-6

NEAR-ROAD SOURCE CONTRIBUTION INCREMENT ($NRI_{RelativeModel}$, APPROACH #4) ESTIMATED BY CMAQ AND NEAR ROAD INCREMENT CALCULATED WITH GRID CELL AVERAGE CONTRIBUTION ESTIMATED BY CMAQ ($NRI_{AERMOD-CMAQ}$)

| CMAQ Baseline at CA60NR ($C_{CMAQ,Base}$) ($\mu\text{g}/\text{m}^3$) | | | | | |
|---|-----------|-----------|-----------|-----------|---------------|
| | Q1 | Q2 | Q3 | Q4 | Annual |
| Sulfate | 0.656 | 0.863 | 1.104 | 0.743 | 0.842 |
| Nitrate | 4.478 | 1.652 | 1.273 | 4.908 | 3.078 |
| Ammonium | 1.347 | 0.399 | 0.318 | 1.461 | 0.881 |
| OC | 6.500 | 4.404 | 5.697 | 7.604 | 6.051 |
| EC | 0.840 | 0.387 | 0.421 | 0.898 | 0.637 |
| Salt | 0.382 | 1.161 | 1.120 | 0.425 | 0.772 |
| Other | 2.505 | 1.611 | 1.740 | 2.959 | 2.204 |
| Total CMAQ | 16.71 | 10.48 | 11.67 | 19.00 | 14.46 |
| $NRI_{AERMOD-CMAQ}/(C_{CMAQ,Base}+NRI_{AERMOD-CMAQ})$ (non-dimensional) | | | | | |
| | Q1 | Q2 | Q3 | Q4 | Annual |
| Sulfate | 0.157 | 0.132 | 0.109 | 0.150 | 0.134 |
| Nitrate | 0.000 | 0.011 | 0.017 | 0.000 | 0.003 |
| Ammonium | 0.008 | 0.047 | 0.057 | 0.010 | 0.018 |
| OC | 0.070 | 0.106 | 0.082 | 0.064 | 0.078 |
| EC | 0.363 | 0.565 | 0.546 | 0.364 | 0.440 |
| Salt | 0.204 | 0.083 | 0.073 | 0.194 | 0.113 |
| Other | 0.377 | 0.423 | 0.495 | 0.367 | 0.410 |
| $NRI_{RelativeModel}$ ($\mu\text{g}/\text{m}^3$) | | | | | |
| | Q1 | Q2 | Q3 | Q4 | Annual |
| Sulfate | 0.109 | 0.218 | 0.216 | 0.152 | 0.174 |
| Nitrate | 0.000 | 0.029 | 0.032 | 0.000 | 0.015 |
| Ammonium | 0.008 | 0.056 | 0.057 | 0.012 | 0.033 |
| OC | 0.346 | 0.421 | 0.489 | 0.296 | 0.388 |
| EC | 0.339 | 0.283 | 0.419 | 0.424 | 0.366 |
| Salt | 0.085 | 0.030 | 0.023 | 0.059 | 0.049 |
| Other | 0.570 | 0.500 | 0.845 | 1.175 | 0.772 |
| Total Near-Road | 1.46 | 1.54 | 2.08 | 2.12 | 1.80 |

In summary, the four alternatives described above span the range of NRI from 1.64 $\mu\text{g}/\text{m}^3$ to 2.98 $\mu\text{g}/\text{m}^3$. While there are no direct measurements or any comprehensive study near the CA60NR that could provide a better estimate of the contribution of near-road sources to observed PM2.5, a recent study collected PM2.5 filter samples near two other southern California highways (I-5 and I-710), placing the samplers both upwind and downwind from the freeways.² Measurements over two weeks showed overall differences between upwind and downwind measurements ranging from 1 $\mu\text{g}/\text{m}^3$ to 3 $\mu\text{g}/\text{m}^3$, which are in the same range as the four alternatives for NRI.

STEP 3: Separate the NRI portion from the measured quarterly base year design value.

The quarterly averages of the base year design value are calculated following the methodology described in the U.S. EPA modeling guidance. Speciation at CA60NR is derived by interpolating the speciation profiles from the four CSN monitors in the basin. Then, the NRI is subtracted from the speciated base year design value to obtain RDV. In this example, $NRI_{AERMOD-CMAQ}$ is used, and the breakdown between NRI and RDV is shown in Table II-6-7. Note that the estimated NRI for crustal component Other is larger than the estimated portion from the calculated base year design value in quarters 2 and 3. Thus, the values for Other in $NRI_{AERMOD-CMAQ}$ in quarter 2 and quarter 3 are capped at the magnitude in the base year design value.

² Wang X., Gronstal S., Lopez B., Jung H., Chen A.L.-H., Wu G., Ho S.S.H., Chow J.C., Watson J.G., Yao Q., Yoon S., 2023. Evidence of non-tailpipe emission contributions to PM2.5 and PM10 near southern California highways. *Environmental Pollution*, 3017, 120691.
<https://doi.org/10.1016/j.envpol.2022.120691>

TABLE II-6-7

**DISAGGREGATION OF NEAR-ROAD INCREMENT FROM REGIONAL COMPONENT OF THE BASE
YEAR DESIGN VALUE**

| Speciated Base Year DV ($\mu\text{g}/\text{m}^3$) | Q1 | Q2 | Q3 | Q4 | Annual |
|---|--------------|--------------|--------------|--------------|---------------|
| Sulfate | 0.697 | 1.654 | 1.984 | 1.009 | 1.336 |
| Nitrate | 3.025 | 2.613 | 1.951 | 3.112 | 2.675 |
| Ammonium | 1.102 | 1.188 | 0.991 | 1.135 | 1.104 |
| OC | 4.933 | 3.961 | 6.002 | 4.628 | 4.881 |
| EC | 0.933 | 0.502 | 0.766 | 1.165 | 0.842 |
| Salt | 0.418 | 0.354 | 0.319 | 0.303 | 0.349 |
| Other | 1.513 | 1.182 | 1.706 | 3.201 | 1.901 |
| Water | 0.628 | 0.706 | 0.729 | 0.697 | 0.690 |
| Blank | 0.2 | 0.2 | 0.2 | 0.2 | 0.2 |
| Total | 13.45 | 12.36 | 14.65 | 15.45 | 13.98 |
| | | | | | |
| NRI_{AERMOD-CMAQ} ($\mu\text{g}/\text{m}^3$) | Q1 | Q2 | Q3 | Q4 | Annual |
| Sulfate | 0.122 | 0.131 | 0.135 | 0.131 | 0.130 |
| Nitrate | 0.000 | 0.018 | 0.021 | 0.000 | 0.010 |
| Ammonium | 0.010 | 0.020 | 0.019 | 0.015 | 0.016 |
| OC | 0.490 | 0.524 | 0.506 | 0.519 | 0.510 |
| EC | 0.479 | 0.502 | 0.507 | 0.514 | 0.501 |
| Salt | 0.098 | 0.106 | 0.088 | 0.103 | 0.099 |
| Other | 1.513 | 1.182* | 1.706* | 1.716 | 1.529 |
| Total Near-Road | 2.71 | 2.48 | 2.98 | 3.00 | 2.79 |
| | | | | | |
| Regional Component (RDV) ($\mu\text{g}/\text{m}^3$) | Q1 | Q2 | Q3 | Q4 | Annual |
| Sulfate | 0.575 | 1.523 | 1.849 | 0.878 | 1.206 |
| Nitrate | 3.025 | 2.595 | 1.930 | 3.112 | 2.665 |
| Ammonium | 1.092 | 1.168 | 0.972 | 1.120 | 1.088 |
| OC | 4.443 | 3.437 | 5.496 | 4.109 | 4.371 |
| EC | 0.454 | 0.000 | 0.259 | 0.651 | 0.341 |
| Salt | 0.320 | 0.248 | 0.231 | 0.200 | 0.250 |
| Other | 0.000 | 0.000 | 0.000 | 1.485 | 0.371 |
| Water | 0.628 | 0.706 | 0.729 | 0.697 | 0.69 |
| Blank | 0.2 | 0.2 | 0.2 | 0.2 | 0.2 |
| Total Regional | 10.74 | 9.88 | 11.67 | 12.45 | 11.18 |

*Values capped at the values of Other in the speciated DV in quarters 2 and 3

STEP 4: Project future DV by applying AERMOD-based RRF to NRI and CMAQ-based RRF to the regional component RDV.

The AERMOD-based RRF is calculated in Step 1 and is presented in Table II-6-2. The CMAQ-based RRF is calculated following the same methodology used in the traditional attainment demonstration approach, as described in the U.S. EPA modeling guidance. Namely, the quarterly average of modeled concentrations for the base year and the attainment scenario are averaged over a 3-by-3 grid centered at the grid cell where the monitor is located. The quarterly average value for each PM2.5 species in the attainment case divided by the quarterly average for the base year is the RRF for each PM2.5 species. The calculated RRF values are shown in Table II-6-8.

TABLE II-6-8

CMAQ-BASED RELATIVE REDUCTION FACTORS (RRF) FOR THE MONITOR AT CA60NR

| | Q1 | Q2 | Q3 | Q4 | Annual |
|----------|-------|-------|-------|-------|--------|
| Sulfate | 1.053 | 1.013 | 1.007 | 1.023 | 1.017 |
| Nitrate | 0.518 | 0.622 | 0.688 | 0.477 | 0.571 |
| Ammonium | 0.532 | 0.559 | 0.672 | 0.482 | 0.566 |
| OC | 1.112 | 0.963 | 0.931 | 1.081 | 1.018 |
| EC | 0.71 | 0.644 | 0.654 | 0.696 | 0.686 |
| Salt | 1.015 | 1.044 | 1.053 | 1.031 | 1.034 |
| Other | 1.095 | 1.064 | 1.058 | 1.091 | 1.080 |

The AERMOD-based RRF is applied to the base year NRI and the CMAQ-based RRF is applied to the base year RDV. The resulting speciated concentrations, shown in Table II-6-9, represent the PM2.5 concentrations in the attainment scenario.

TABLE II-6-9

PROJECTED NRI (BASED ON $NRI_{AERMOD-CMAQ}$, APPROACH #2) AND REGIONAL COMPONENT IN THE ATTAINMENT SCENARIO

| | Q1 | Q2 | Q3 | Q4 | Annual |
|--|-------|-------|-------|-------|--------|
| Near-Road Increment (NRI) ($\mu\text{g}/\text{m}^3$) | | | | | |
| Sulfate | 0.050 | 0.054 | 0.055 | 0.053 | 0.053 |
| Nitrate | 0.000 | 0.010 | 0.011 | 0.000 | 0.005 |
| Ammonium | 0.004 | 0.007 | 0.007 | 0.006 | 0.006 |
| OC | 0.276 | 0.295 | 0.285 | 0.288 | 0.286 |
| EC | 0.097 | 0.102 | 0.104 | 0.101 | 0.101 |
| Salt | 0.095 | 0.103 | 0.086 | 0.100 | 0.096 |
| Other | 1.473 | 1.150 | 1.659 | 1.680 | 1.491 |
| Total Near-Road | 2.00 | 1.72 | 2.21 | 2.23 | 2.04 |
| Regional Component (RDV) ($\mu\text{g}/\text{m}^3$) | | | | | |
| Sulfate | 0.605 | 1.543 | 1.862 | 0.898 | 1.227 |
| Nitrate | 1.567 | 1.614 | 1.328 | 1.484 | 1.498 |
| Ammonium | 0.581 | 0.653 | 0.653 | 0.540 | 0.607 |
| OC | 4.940 | 3.310 | 5.117 | 4.442 | 4.452 |
| EC | 0.322 | 0.000 | 0.169 | 0.453 | 0.236 |
| Salt | 0.325 | 0.259 | 0.243 | 0.207 | 0.258 |
| Other | 0.000 | 0.000 | 0.000 | 1.621 | 0.405 |
| Total Regional | 8.34 | 7.38 | 9.37 | 9.64 | 8.68 |

STEP 5: Add the future NRI and RDV components, calculate particle bound water and add blank to determine the future design value.

The future NRI and RDV components calculated in step 4 are added. Particle bound water is calculated following U.S. EPA modeling guidance, using a polynomial regression equation fitted to the equilibrium model Aerosol Inorganic Matter (AIM) as a function of sulfate, nitrate, and ammonium concentrations. The standard blank of $0.2 \mu\text{g}/\text{m}^3$ is added to the sum of all components to obtain the quarterly averages. The future annual design value is calculated as the average of the quarterly values. Table II-6-10 shows the calculated values, showing that the annual design value is $11.59 \mu\text{g}/\text{m}^3$, and thus demonstrating attainment of the annual PM_{2.5} standard.

TABLE II-6-10

PROJECTED ANNUAL PM2.5 DESIGN VALUE IN THE ATTAINMENT SCENARIO

| | Q1 | Q2 | Q3 | Q4 | Annual |
|--|-------|-------|-------|-------|--------------|
| Future DV with $NRI_{AERMOD-CMAQ}$ ($\mu\text{g}/\text{m}^3$) | | | | | |
| Sulfate | 0.655 | 1.596 | 1.917 | 0.951 | 1.280 |
| Nitrate | 1.567 | 1.623 | 1.339 | 1.484 | 1.503 |
| Ammonium | 0.585 | 0.661 | 0.660 | 0.545 | 0.613 |
| OC | 5.216 | 3.605 | 5.402 | 4.730 | 4.739 |
| EC | 0.419 | 0.102 | 0.273 | 0.554 | 0.337 |
| Salt | 0.420 | 0.362 | 0.329 | 0.307 | 0.355 |
| Other | 1.473 | 1.150 | 1.659 | 3.301 | 1.896 |
| Water | 0.409 | 0.839 | 0.855 | 0.557 | 0.665 |
| Blank | 0.2 | 0.2 | 0.2 | 0.2 | 0.200 |
| Total | 10.94 | 10.14 | 12.63 | 12.63 | 11.59 |

The future design value calculated using this hybrid approach is sensitive to the magnitude of NRI. Because emissions from on-road sources are expected to decline faster than the overall emissions in the basin, the NRI portion is projected to decline faster than the RDV. Table II-6-11 shows the future design value calculated using $NRI_{Monitors}$, which is the smallest among the four alternative NRI values. Since the magnitude of $NRI_{Monitors}$ is smaller than $NRI_{AERMOD-CMAQ}$, the overall future DV increases. As a result, the DV calculated using $NRI_{Monitors}$ is $11.91 \mu\text{g}/\text{m}^3$, higher than the DV calculated using $NRI_{AERMOD-CMAQ}$. Even though the DV calculated with a more conservative estimate of NRI is higher, this hybrid modeling approach demonstrates attainment of the annual PM2.5 standard.

TABLE II-6-11

PROJECTED ANNUAL PM2.5 DESIGN VALUE IN THE ATTAINMENT SCENARIO USING ALTERNATIVE $NRI_{Monitors}$ (**APPROACH #3**)

| | Q1 | Q2 | Q3 | Q4 | Annual |
|---|--------------|--------------|--------------|--------------|--------------|
| Future DV with $NRI_{Monitors}$ ($\mu\text{g}/\text{m}^3$) | | | | | |
| Sulfate | 0.664 | 1.655 | 1.960 | 0.983 | 1.315 |
| Nitrate | 1.567 | 1.625 | 1.341 | 1.485 | 1.504 |
| Ammonium | 0.584 | 0.663 | 0.663 | 0.546 | 0.614 |
| OC | 5.252 | 3.760 | 5.497 | 4.842 | 4.838 |
| EC | 0.448 | 0.264 | 0.390 | 0.656 | 0.440 |
| Salt | 0.421 | 0.368 | 0.332 | 0.309 | 0.357 |
| Other | 1.483 | 1.216 | 1.733 | 3.379 | 1.953 |
| Water | 0.413 | 0.877 | 0.881 | 0.576 | 0.687 |
| Blank | 0.2 | 0.2 | 0.2 | 0.2 | 0.2 |
| Total | 11.03 | 10.63 | 13.00 | 12.98 | 11.91 |

AERMOD Dispersion Modeling Set-Up

The dispersion modeling set-up is based on the American Meteorological society (AMS) and U.S. EPA Regulatory Model–AERMOD (Cimorelli et al., 2005)³. AERMOD is one of the official EPA dispersion models required to be used for State Implementation Plan (SIP) revisions for existing sources and for New Source Review (NSR) and Prevention of Significant Deterioration (PSD) programs (U.S. EPA, 2017⁴). It has been widely employed in environmental science and air quality management (e.g., Gibson et al., 2013,⁵ Rood 2014⁶).

AERMOD incorporates air dispersion based on planetary boundary layer turbulence structure and scaling concepts, including treatment of both surface and elevated sources, and both simple and complex terrain. The AERMOD modeling system consists of several key components, including (1) AERMET, a meteorological data preprocessor; (2) AERMAP, a terrain data preprocessor that incorporates complex terrain using USGS Digital Elevation Data; (3) AERSCREEN, a screening version of AERMOD; (4) AERSURFACE, a surface characteristics preprocessor; and (5) BPIPPRIM, a multi-building dimensions program incorporating the GEP (Good Engineering Practice) technical procedures for PRIME (Plume Rise Model Enhancements) applications (U.S. EPA, 2017).

The meteorological data used in AERMOD to simulate the dispersion of pollutants was from the Weather Research and Forecasting (WRF) model version 4.4.2, which was run at a spatial resolution of 4 km by 4 km. Extensive evaluation of the meteorological modeling performance is presented in Chapter 3 of Appendix II of this plan. The meteorological data was processed with Meteorological Model Input Formulator (MMIF) version 4.0, which prepares the data for input into AERMOD. The data was then further processed and adjusted by the AERMET preprocessor to prepare the meteorological data specifically for AERMOD. Mixing heights, which are crucial for the vertical dispersion of air pollutants, were calculated by AERMET. AERMET was run with the Bulk Richardson number option to estimate the

³ Cimorelli, A. J., Perry, S. G., Venkatram, A., Weil, J. C., Paine, R. J., Wilson, R. B., ... & Brode, R. W. (2005). AERMOD: A dispersion model for industrial source applications. Part I: General model formulation and boundary layer characterization. *Journal of Applied Meteorology and Climatology*, 44(5), 682-693. <https://doi.org/10.1175/JAM2227.1>

⁴ U.S. EPA, 2017, Air Quality Dispersion Modeling - Preferred and Recommended Models, Support Center for Regulatory Atmospheric Modeling (SCRAM), <https://www.epa.gov/scram/air-quality-dispersion-modeling-preferred-and-recommended-models>

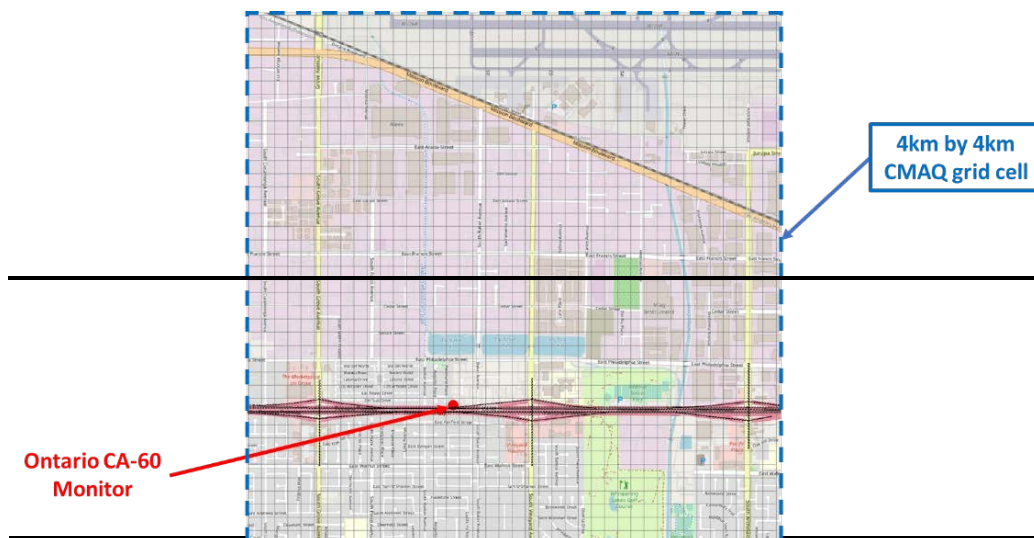
⁵ Gibson, M. D., Kundu, S., & Satish, M. (2013). Dispersion model evaluation of PM_{2.5}, NO_x and SO₂ from point and major line sources in Nova Scotia, Canada using AERMOD Gaussian plume air dispersion model. *Atmospheric Pollution Research*, 4(2), 157-167. <https://doi.org/10.5094/APR.2013.016>

⁶ Rood, A. S. (2014). Performance evaluation of AERMOD, CALPUFF, and legacy air dispersion models using the Winter Validation Tracer Study dataset. *Atmospheric Environment*, 89, 707-720. <https://doi.org/10.1016/j.atmosenv.2014.02.054>

vertical mixing height and it was configured to adjust the friction velocity (u^*) but without any wind direction randomization.

AERMAP was used to process terrain data. In the case of the Drat PM2.5 Plan, 1 arcsecond National Elevation Dataset (NED) was used as the terrain data. Receptors are points where pollutant concentrations are calculated to assess the impact of emissions. In this setup, receptors were placed at 100-meter intervals over one CMAQ grid (4 km by 4 km). Additionally, there was one discrete receptor located at the CA60NR monitor. The receptors were positioned at a height of 4.9 meters above the ground, which matches the probe height of the CA60NR monitor. This ensures consistency in the measurements. Figure II-6-4 shows the receptor grid and location of CA60NR.

The modeling emission set-up only includes the emission sources along freeway CA-60 and its on- and off-ramps. Emission sources are grouped into 10 groups so that each category is modeled using distinctive emissions temporal and chemical profiles that can be tracked throughout the modeling. These emissions are derived from SCAG's vehicle activity dataset, which is also used in the regional modeling set-up. SCAG's dataset includes vehicle activity for 5 different vehicle classes: light and medium duty vehicles, light heavy-duty trucks, medium heavy-duty trucks, heavy heavy-duty trucks, and buses. EMFAC 2021 is used to calculate an aggregated emissions factor on a per-mile basis for these 5 groupings that includes exhaust, and tire and brake wear emissions. In addition, road dust emissions are estimated by using SCAG's vehicle activity and road information dataset and by using the road dust methodology described in Attachment H of Appendix III from the 2022 AQMP. In total, five vehicle categories and two emission processes per vehicle class for a total of ten sources of emissions. Figure II-6-5 shows the distribution of the primary PM2.5 emissions along the freeway CA-60 within the dispersion modeling domain.



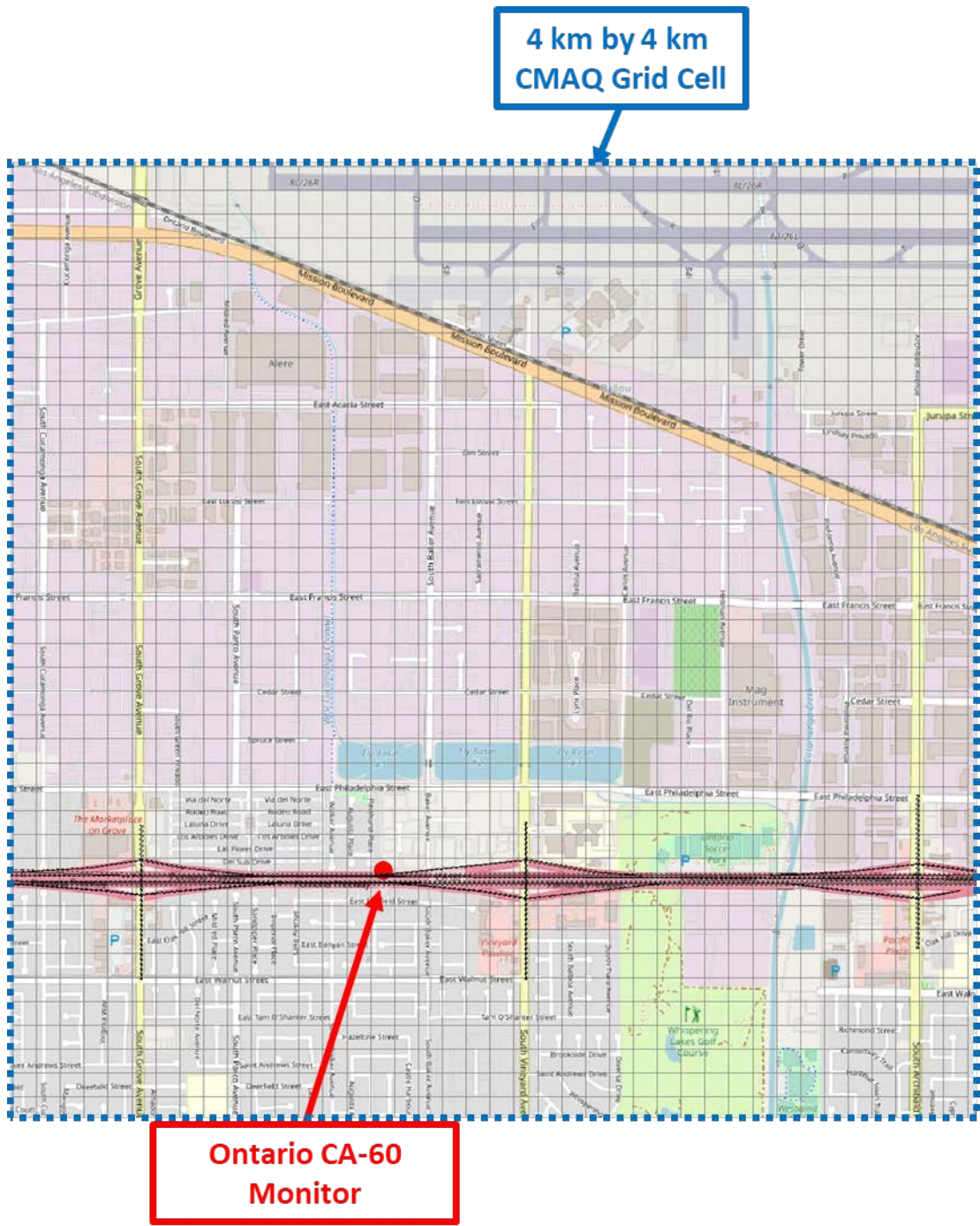
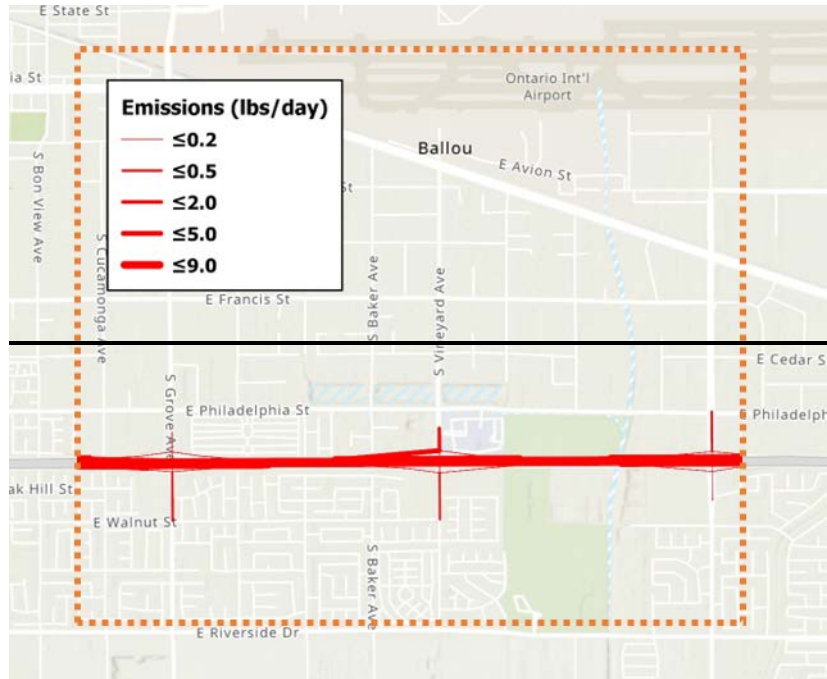


FIGURE II-6-4

DISPERSION MODELING DOMAIN SET-UP

South Coast Air Basin Attainment Plan for the 2012 Annual PM2.5 Standard



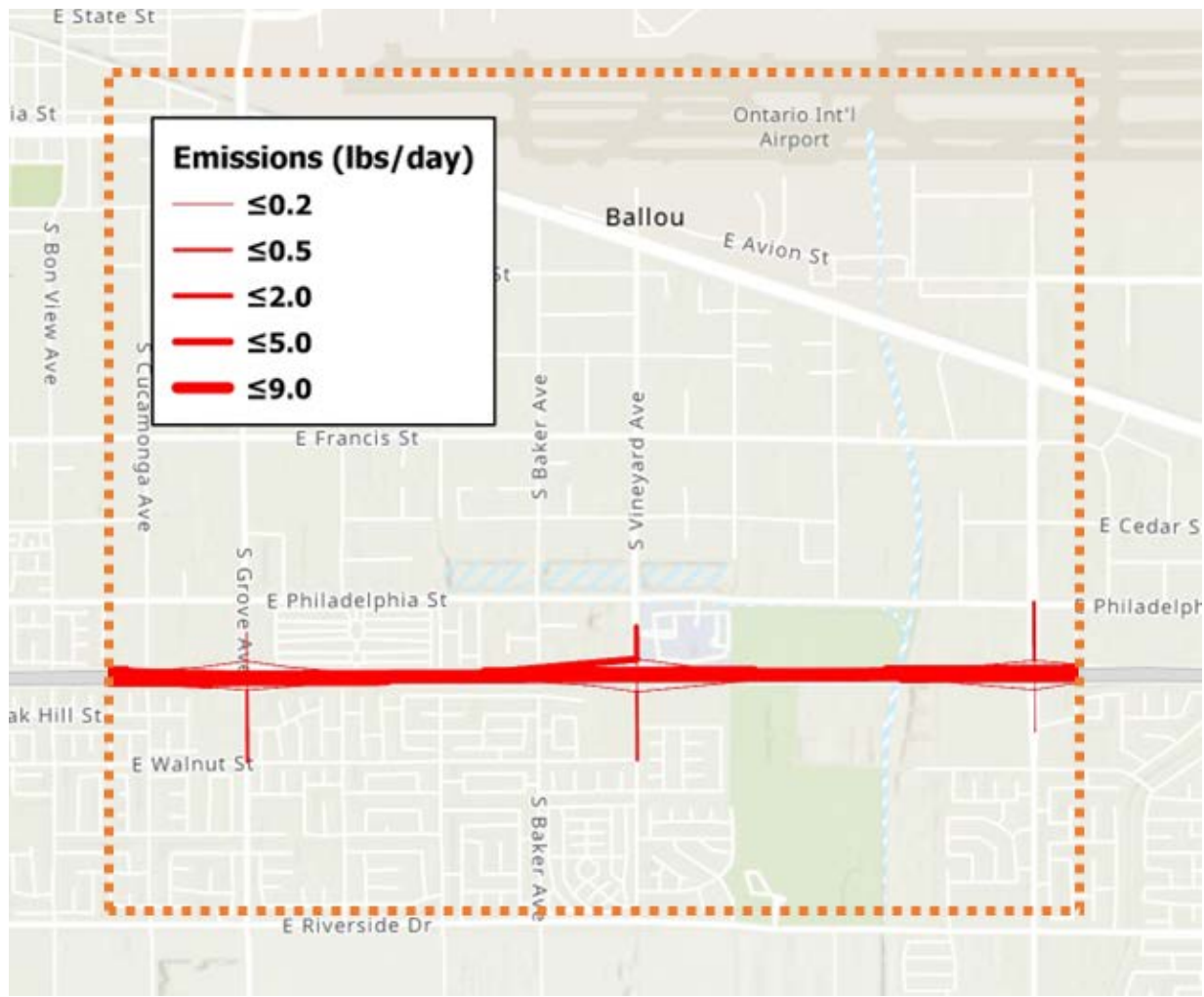


FIGURE II-6-5

SPATIAL DISTRIBUTION OF ON-ROAD PRIMARY PM_{2.5} EMISSIONS IN THE DISPERSION MODELING DOMAIN

Concentrations of total PM_{2.5} for all 10 emission sources are calculated on an hourly basis for the entire year of 2018. Daily emissions are calculated using average-day emission factors for the total PM_{2.5}. Temporal and chemical speciation profiles are applied as a post-processing step because both profiles are multipliers to the emissions. Because dispersion of pollutants is directly proportional to the emission flux, concentrations at different times and for different species are the product of the hourly estimated concentration and the temporal and chemical profile factors.

All emission sources were modeled as lines with constant emission rates. The initial vertical dimension for vehicle emissions was set at 5.1 meters, following examples from U.S. EPA's Conformity Hotspot

Guidance, Appendix J.3.⁷ The release height of vehicle emissions was set at 2.6 meters per the guidance suggestion, whereas road dust emissions release height was set at 0.5 meters above ground level. Hourly POST files (Post-Processing File) were generated for different source groups. These files contain detailed information about pollutant concentrations and dispersion patterns over time and space and are used for subsequent temporal scaling and analysis.

Table II-6-12 lists the annual average PM2.5 emissions from vehicle exhausts and paved road dust along the CA-60 freeway within the 4km-by-4km CMAQ model grid cell where the monitoring station is located. The total PM2.5 emissions from vehicle exhaust significantly drop from 39.31 lbs/day in the base year 2018 to 20.11 lbs/year in the 2030 attainment scenario primarily due to the adoption of cleaner vehicles. In contrast, PM2.5 emissions from paved-road dust slightly increase from 25.73 lbs/day in 2018 to 27.29 lbs/day in 2030 because of higher vehicle activity rates in the future.

TABLE II-6-12. ANNUAL AVERAGE PM2.5 EMISSIONS ALONG CA-60 FREEWAY IN THE DISPERSION MODELING DOMAIN

| Source | Annual Average PM2.5 Emissions (pounds per day) | |
|--|--|-----------------|
| | Base Year 2018 | 2030 Attainment |
| Road Dust | | |
| Light and Medium Duty Vehicles | 11.3 | 9.8 |
| Light Heavy-Duty Trucks | 1.2 | 0.7 |
| Medium Heavy-Duty Trucks | 2.3 | 2.9 |
| Heavy Heavy-Duty Trucks | 10.8 | 13.9 |
| Buses | 0.0 | 0.0 |
| Total Road Dust | 25.7 | 27.3 |
| Vehicle Emissions, Exhaust + Tire and Brake Wear | | |
| Light and Medium Duty Vehicles | 10.9 | 8.5 |
| Light Heavy-Duty Trucks | 3.1 | 1.9 |
| Medium Heavy-Duty Trucks | 7.6 | 1.5 |
| Heavy Heavy-Duty Trucks | 17.7 | 8.3 |
| Buses | 0.0 | 0.0 |
| Total Vehicle Emissions | 39.3 | 20.1 |
| Total Emissions | 65.0 | 47.4 |

⁷ PM Hot-spot Guidance. Transportation Conformity Guidance for Quantitative Hot-spot Analyses in PM2.5 and PM10 Nonattainment and Maintenance Areas, Office of Transportation and Air Quality, U.S. Environmental Protection Agency, EPA-420-B-21-037

Figure II-6-6 presents the mass fractions of primary PM_{2.5} speciation in the near-road emission sources. Speciation for vehicle emissions changes from 2018 to the 2030 attainment scenario, because exhaust emissions decline and tire and brake wear emissions become a relatively larger contributor to total vehicle emissions. As shown, crustal components (including primary particulates containing silicon, calcium, aluminum, iron, and titanium) dominate emissions from paved road dust, accounting for approximately 90% of the total mass of paved road dust emissions and contribute significantly to emissions from light-duty vehicles, accounting for approximately 50%. Following crustal components, organic carbon (OC) is the next significant contributor to light-duty vehicle emissions, accounting for over 25%. In heavy-duty vehicle emissions, elemental carbon (EC) is the largest contributor in 2018, followed by crustal components and OC. Because exhaust emissions from heavy-duty vehicles are substantially reduced in the future, the EC fraction declines substantially, and the tire and break wear contribution in the 2030 attainment becomes more prominent, increasing the crustal fraction.

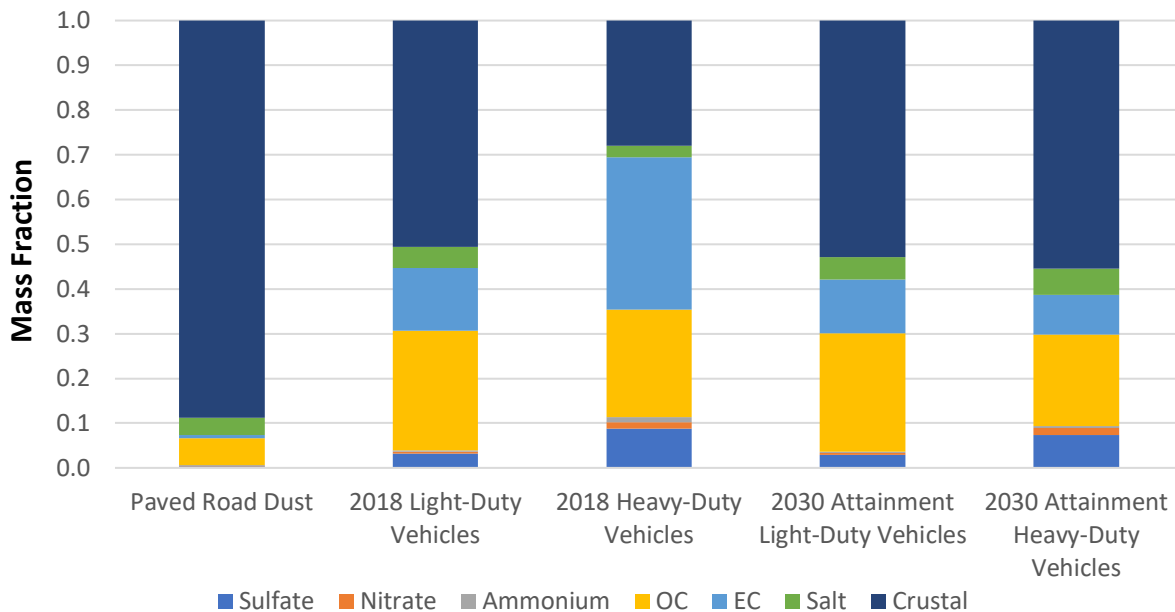


FIGURE II-6-6

SPECIATION OF NEAR-ROAD EMISSION SOURCES

PM_{2.5} simulation with AERMOD

Figure II-6-7 shows the average PM_{2.5} concentration map calculated by AERMOD that represents the contribution of the direct PM_{2.5} emissions from on-road sources. The results indicate that the most significant impacts of on-road emissions are concentrated along the freeway near off-ramps, and the dispersion of PM_{2.5} is highly localized within a 300-meter radius from the freeway. Specifically, on-road

sources contribute $3.13 \mu\text{g}/\text{m}^3$ to PM2.5 levels at the monitoring site, while the average contribution across the entire 4 km-by-4 km grid cell is $0.32 \mu\text{g}/\text{m}^3$ (Figure II-6-8).

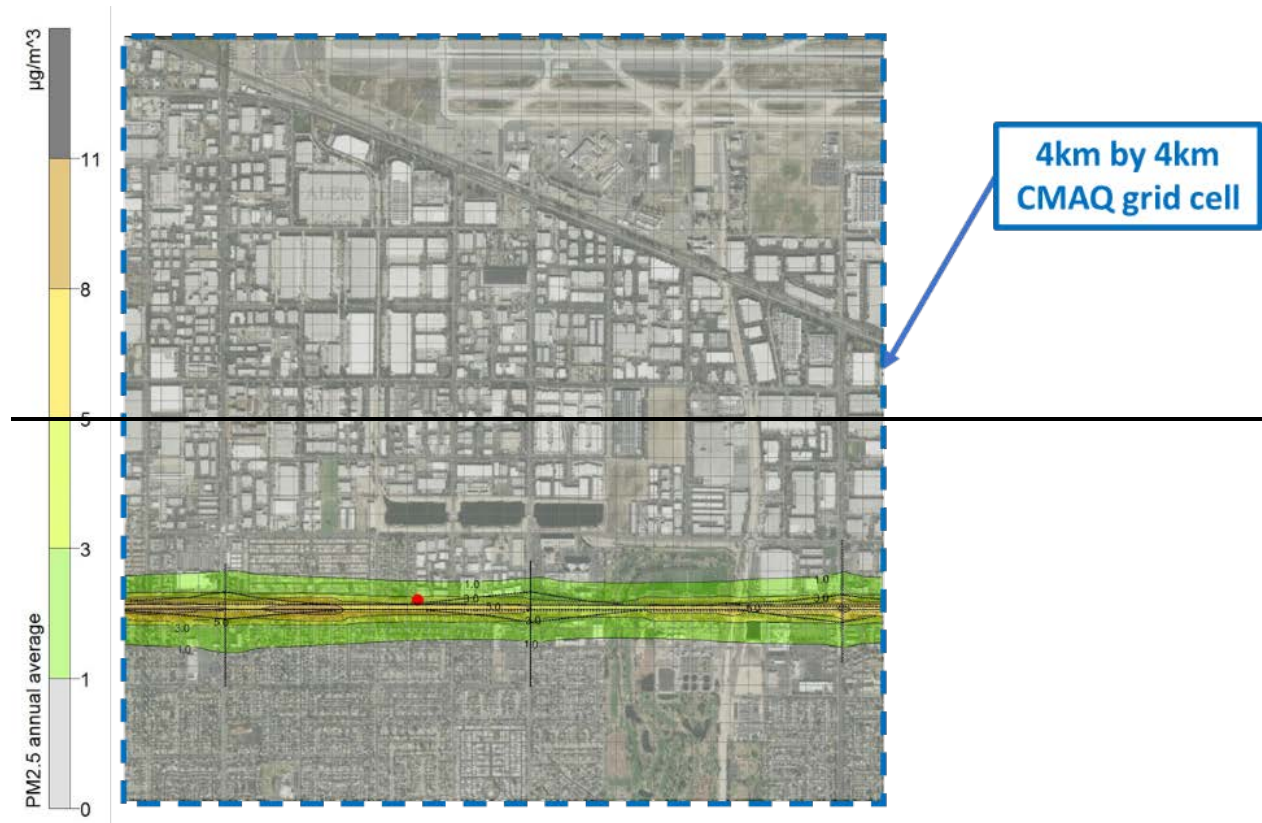
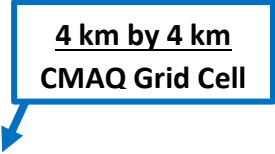


FIGURE II-6-7

ESTIMATES BASED ON DISPERSION MODELING OF THE CONTRIBUTION OF DIRECT PM2.5 EMISSIONS FROM CA-60 FREEWAY TO ANNUAL PM2.5 AROUND THE CA-60 NEAR ROAD MONITOR

Figure II-6-8 shows the contribution of on-road sources to annual PM2.5 at the monitoring station and as a grid-wide average across the 4 km-by-4 km grid cell where the monitor is located. The difference between the contribution at the monitor and the grid average contribution is the near-road increment calculated by AERMOD (NRI_{AERMOD}). The contribution is disaggregated by chemical components, showing that primary PM2.5 species are the dominant contributors. Crustal species are emitted largely from dust resuspension, whereas OC and EC are emitted from vehicle exhaust. Projections for the future year 2030 with the addition of emission controls targeting vehicle exhaust emissions are also shown in Figure II-6-8. Because of the introduction of cleaner vehicles in the future, the contribution of vehicle exhaust to OC and EC is substantially reduced by 2030. However, the contribution to crustal species, which is proportional to vehicle activities, increases slightly due to increased vehicle miles travelled (VMT) from 2018 through 2030.



4 km by 4 km
CMAQ Grid Cell

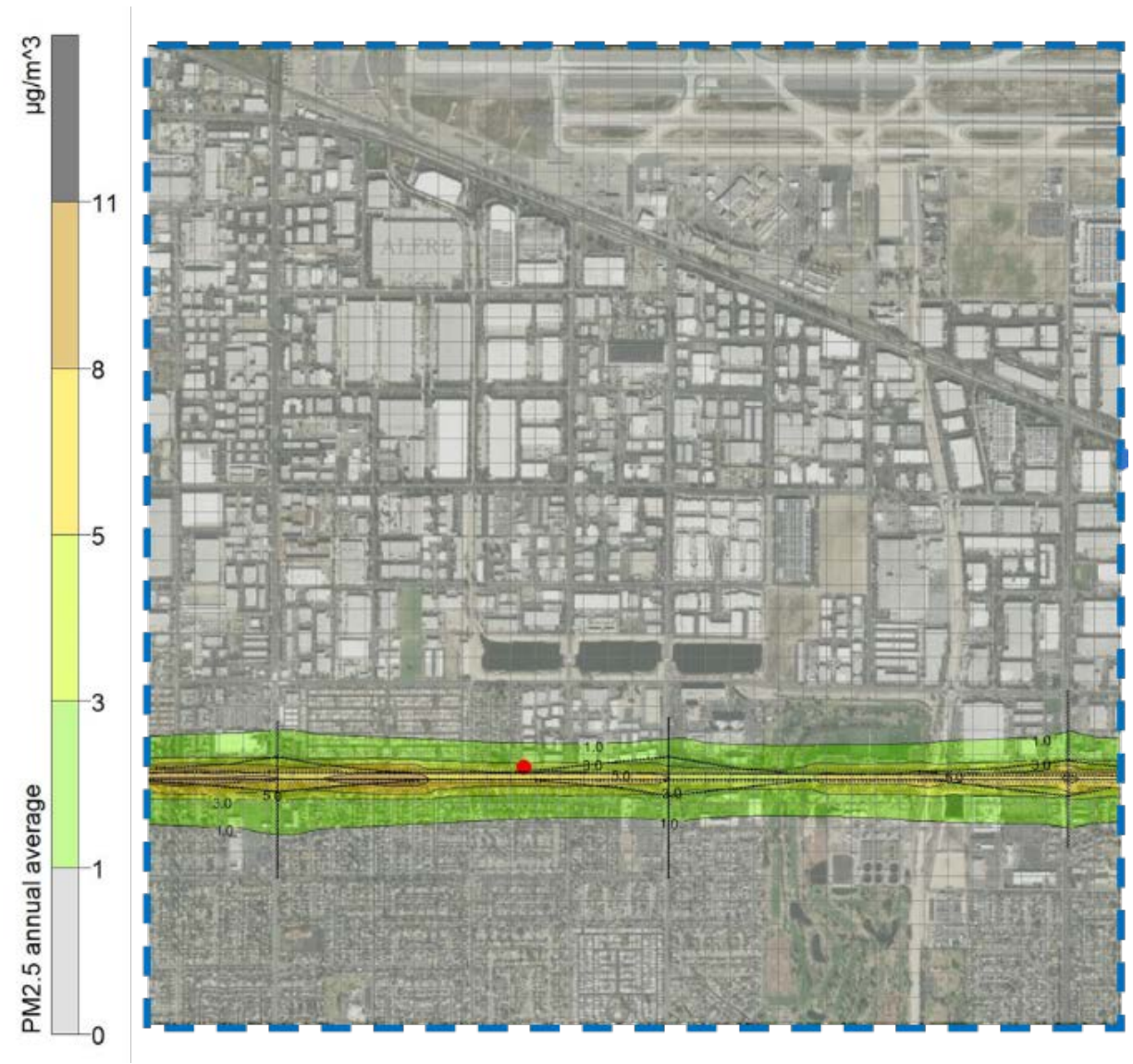


FIGURE II-6-7

ESTIMATES BASED ON DISPERSION MODELING OF THE CONTRIBUTION OF DIRECT PM2.5 EMISSIONS FROM CA-60 FREEWAY TO ANNUAL PM2.5 AROUND THE CA-60 NEAR-ROAD MONITOR

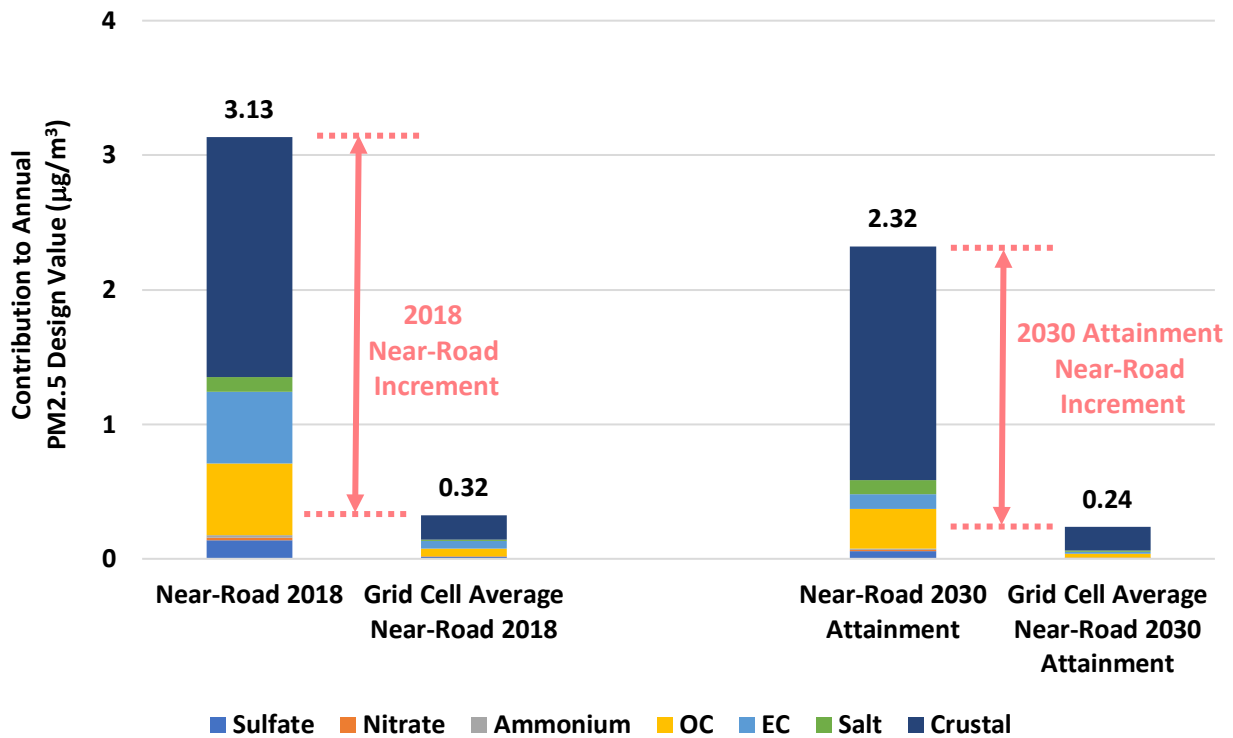


FIGURE II-6-8

CONTRIBUTION OF DIRECT PM2.5 EMISSIONS ESTIMATED BY DISPERSION MODELING FROM CA-60 FREEWAY TO ANNUAL PM2.5 AT THE CA-60 NEAR-ROAD MONITOR AND GRID AVERAGE, FOR BASE YEAR 2018 AND FUTURE YEAR 2030 CONTROL SCENARIO

Model Evaluation of Hybrid Model

The use of the combination of regional modeling with CMAQ and local source dispersion modeling with AERMOD is motivated by the fact that the regional model CMAQ can only predict changes in concentrations averaged over a 4 km-by-4 km cell, whereas AERMOD can model the steep gradients in primary PM2.5 that occur between the freeway and the nearby monitor. As described above, AERMOD is used to determine the near-road increment in PM2.5 that is caused by the monitor being close to route CA60. To assess the performance of this hybrid approach, observations at the monitor are compared to hybrid modeling results (C_{Hybrid}) defined as the CMAQ modeled PM2.5 plus the NRI calculated with AERMOD:

$$C_{Hybrid} = C_{CMAQ,Base} + NRI_{AERMOD-CMAQ} \quad (II.6.9)$$

Equation II.6.9 is equivalent to the following expression:

$$C_{Hybrid} = C_{CMAQ,NoCA60NR} + C_{AERMOD,CA60NR} \quad (II.6.10)$$

Where $C_{CMAQ, NoCA60NR}$ is the modeled concentrations from the simulation with all the near-road source emissions included in the AERMOD setup removed from base year emissions. The difference between $C_{CMAQ, Base}$ and $C_{CMAQ, NoCA60NR}$ represents the contribution of near-road sources estimated by CMAQ, $C_{CMAQ, CA60NR}$. The annual average contribution from CA60NR near-road sources to total PM_{2.5} estimated by CMAQ is shown in Figure II-6-9. The impact of those sources is limited within the grid cells surrounding the CA60NR station and ranging from 0.01 to 0.15 $\mu\text{g}/\text{m}^3$.

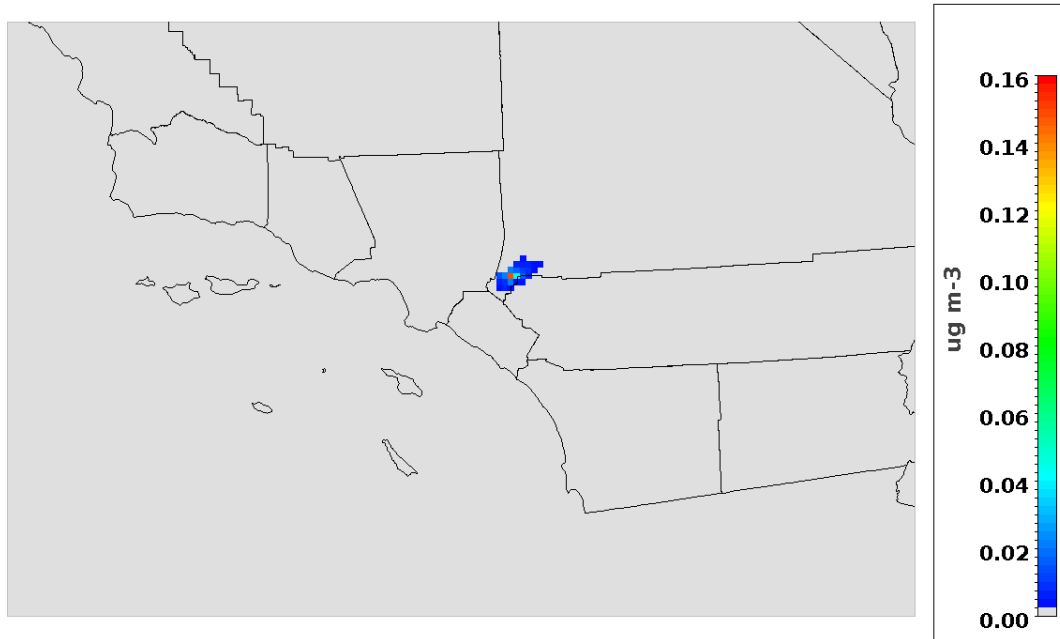


FIGURE II-6-9

CONTRIBUTION OF DIRECT PM_{2.5} EMISSIONS FROM NEAR-ROAD SOURCES AROUND CA60NR TO ANNUAL PM_{2.5} CONCENTRATIONS ESTIMATED BY CMAQ FOR BASE YEAR 2018

Figure II-6-10 shows the time series of daily PM_{2.5} comparing observations with modeled concentrations obtained with CMAQ and the hybrid modeling approach. In general, both CMAQ and the hybrid modeling approach capture the seasonal variation, showing higher concentrations in the first and fourth quarters of the month, and lower concentrations in spring and summer. Figure II-6-11 shows the daily near-road source contribution to CA60NR PM_{2.5} concentrations as modeled by AERMOD. As in the case of CMAQ modeling, PM_{2.5} concentrations modeled with AERMOD show higher peaks in the first and fourth quarters, due to stagnation that happens in colder months.

While seasonal trends are modeled reasonably well, the base CMAQ model overestimates PM_{2.5} concentrations, especially in the colder months. These biases may be attributed to biases in seasonal variations of emissions and/or mixing layer heights in the model. Because hybrid modeling adds approximately 3 $\mu\text{g}/\text{m}^3$ to the CMAQ base modeling to account for the contribution of the NRI, the hybrid modeling approach further overestimate PM_{2.5} concentrations, compared to CMAQ base modeling. As a

result, hybrid modeling shows higher bias and error than the CMAQ base modeling. However, CMAQ underestimates PM_{2.5} concentrations in spring and summer, and the hybrid modeling approach shows improvements by narrowing the gaps between modeling and observations during the spring and summer seasons. Table II-6-13 shows the modeling performance metrics for both CMAQ and the hybrid modeling approach. The metric definitions are included in Chapter 5 of Appendix II.

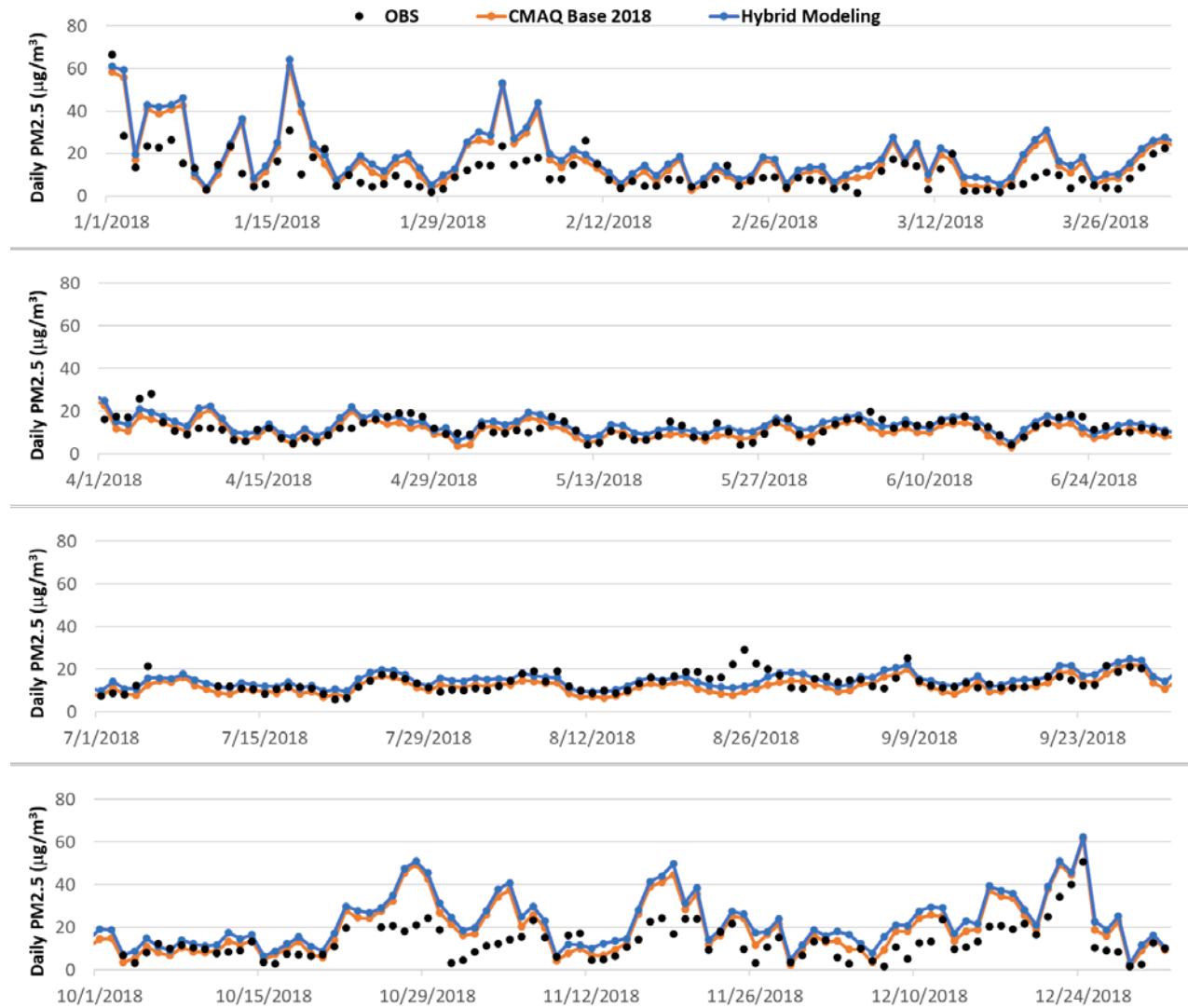


FIGURE II-6-10

DAILY PM_{2.5} AS OBSERVED AND SIMULATED WITH THE CMAQ AND AERMOD-CMAQ HYBRID MODELING SYSTEMS AT THE CA60NR MONITORING STATION IN 2018

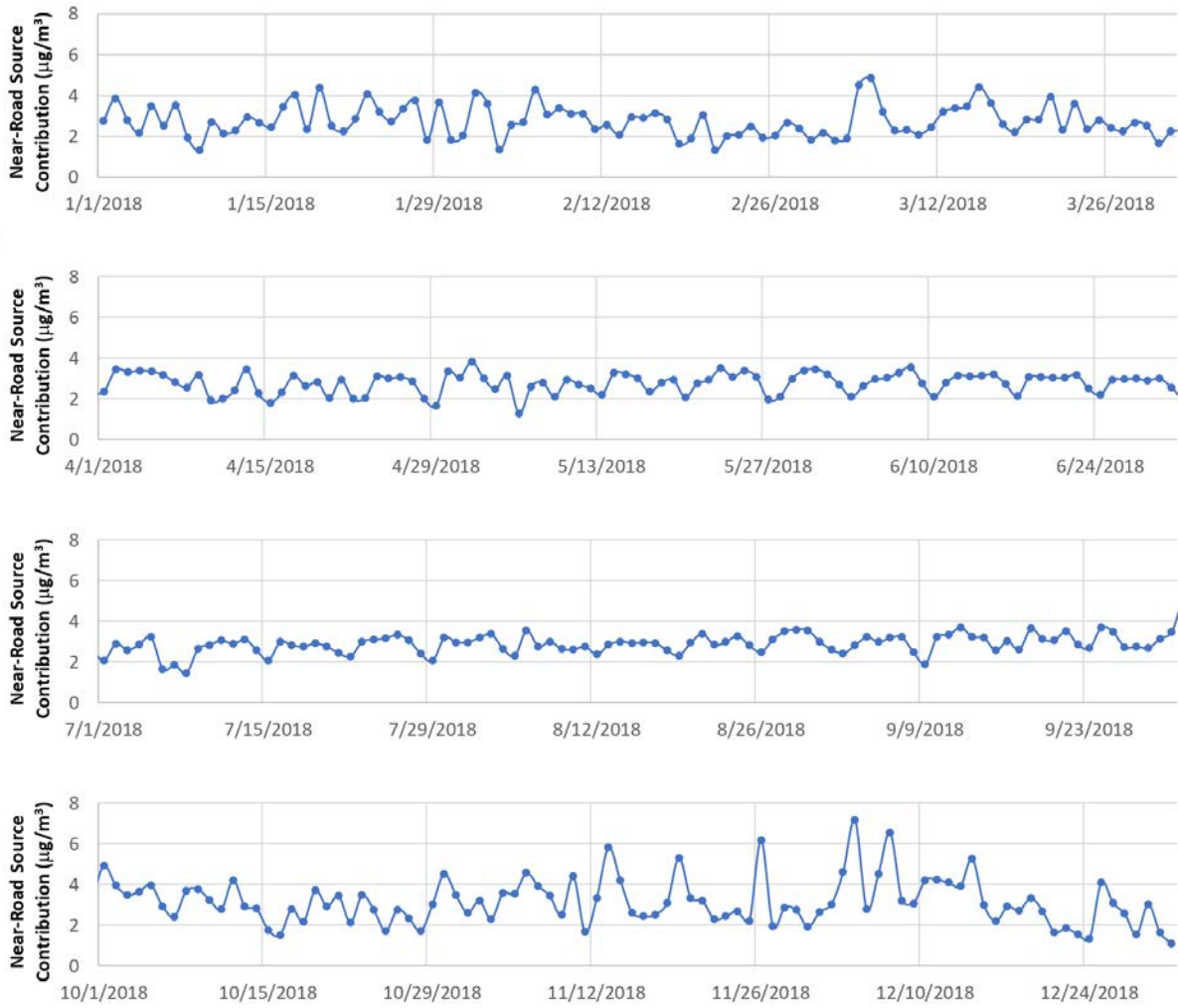


FIGURE II-6-11

DAILY CONTRIBUTION FROM NEAR-ROAD SOURCES TO DAILY PM2.5 AT THE CA60NR MONITOR AS MODELED BY AERMOD.

TABLE II-6-13. MODELING PERFORMANCE EVALUATION OF CMAQ AND HYBRID MODELING AT THE CA60NR MONITOR

| CMAQ | | | | | | |
|---------------|------------|--|--|--------------------|---|--------------------|
| Period | Obs | Average ($\mu\text{g}/\text{m}^3$) | Mean Bias ($\mu\text{g}/\text{m}^3$) | NMB (%) | Mean Error ($\mu\text{g}/\text{m}^3$) | NME (%) |
| Annual | 12.5 | 15.0 | 2.4 | 19% | 5.1 | 41% |
| Q1 | 11.2 | 17.2 | 6.0 | 54% | 7.1 | 63% |
| Q2 | 12.1 | 11.0 | -1.1 | -9% | 2.8 | 23% |
| Q3 | 13.8 | 12.1 | -1.8 | -13% | 3.0 | 22% |
| Q4 | 13.1 | 19.6 | 6.5 | 50% | 7.4 | 57% |
| Hybrid | | | | | | |
| Period | Obs | Average ($\mu\text{g}/\text{m}^3$) | Mean Bias ($\mu\text{g}/\text{m}^3$) | NMB (%) | Mean Error ($\mu\text{g}/\text{m}^3$) | NME (%) |
| Annual | 12.5 | 17.7 | 5.2 | 41% | 6.2 | 50% |
| Q1 | 11.2 | 19.7 | 8.5 | 76% | 9.0 | 81% |
| Q2 | 12.1 | 13.7 | 1.6 | 13% | 3.1 | 26% |
| Q3 | 13.8 | 14.9 | 1.1 | 8% | 3.0 | 22% |
| Q4 | 13.1 | 22.5 | 9.5 | 73% | 9.7 | 75% |

Annual PM_{2.5} Design Values using the Hybrid Approach

The resulting future design values using the four different NRI estimates are compared to the DV calculated using the traditional approach and are shown in Figure II-6-12. While the traditional approach suggests that the CA-60 near-road monitor fails to attain the standard under the 2030 control scenario, the hybrid approach, designed to capture the steep gradients in direct PM_{2.5} concentrations around the freeway, shows that the projected annual PM_{2.5} concentration will be below the NAAQS of 12 $\mu\text{g}/\text{m}^3$. The hybrid approach using the $NRI_{AERMOD-CMAQ}$ based on AERMOD and CMAQ modeling projects the DV at 11.59 $\mu\text{g}/\text{m}^3$, demonstrating that CA60NR would meet the annual PM_{2.5} by a wide margin. The DV calculated using the NRI_{AERMOD} estimated purely from AERMOD modeling is projected to be 11.63 $\mu\text{g}/\text{m}^3$. The DV calculated using $NRI_{RelativeModel}$, based on combining both AERMOD and CMAQ modeling in relative terms to determine the NRI, is 11.75 $\mu\text{g}/\text{m}^3$. Even with the most conservative estimate of NRI based on monitoring data at neighboring sites, $NRI_{Monitor}$, the hybrid approach still shows that the DV at CA60NR would be 11.91 $\mu\text{g}/\text{m}^3$, well below the annual PM_{2.5} standard.

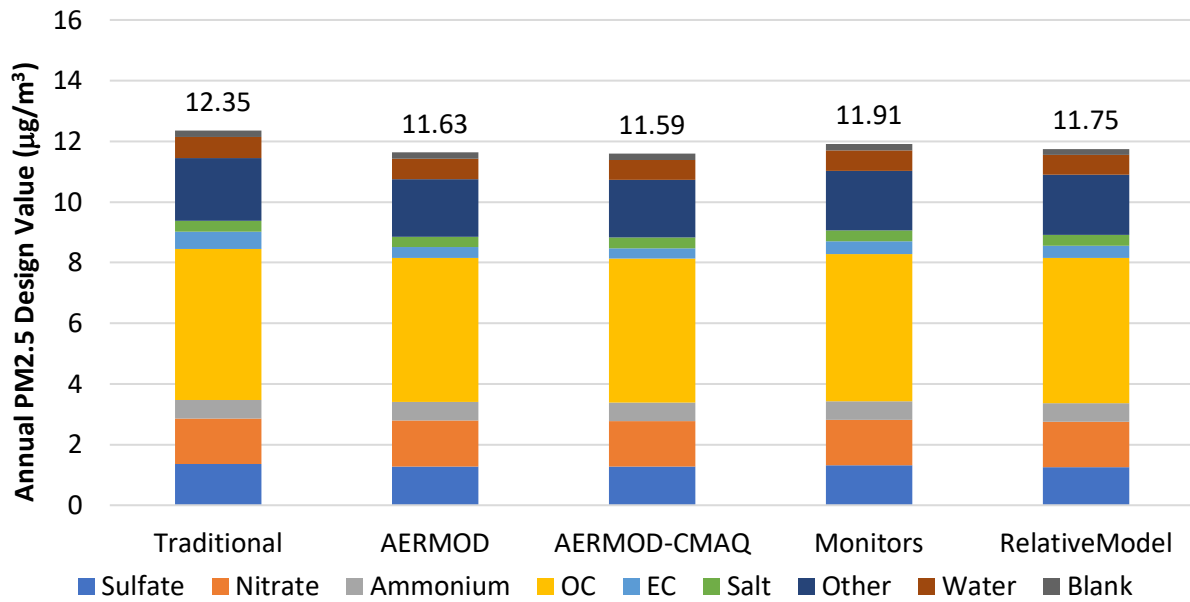


FIGURE II-6-12

COMPARISON OF DESIGN VALUE PROJECTIONS BETWEEN THE TRADITIONAL APPROACH AND THE HYBRID APPROACH USING DIFFERENT NRI ESTIMATES

Summary

The near-road monitoring site in Ontario (CA60NR) has recorded elevated PM_{2.5} levels since its data has been used for design value calculations in 2015. Annual PM_{2.5} concentrations at this near-road site consistently exceed those at the previous design site in Mira Loma, making CA60NR the new design site for annual PM_{2.5} in the South Coast Air Basin. However, accurately simulating PM_{2.5} and demonstrating potential future PM_{2.5} attainment at this near-road site are challenging due to substantial influence from nearby road-related sources and sub-grid scale spatial variation. This chapter focuses on the methodology and findings of PM_{2.5} attainment assessment at CA60NR by using a hybrid modeling system that combines a regional model (CMAQ) with a dispersion model (AERMOD). To address the unique challenges posed by near-road sites, a novel hybrid methodology is developed to quantify the contribution of PM_{2.5} emissions from vehicles and road dust to the near-road monitor's PM_{2.5} concentrations and to calculate the future annual PM_{2.5} design values using the hybrid approach. Results show that the hybrid approach estimates the future design value at the CA-60 near-road site is 11.59 µg/m³. Taking uncertainties into account to quantify the near-road increment, projections of design values at the Ontario CA-60 near-road site range between 11.59 and 11.91 µg/m³, and even with the most conservative NRI, the Ontario CA-60 near-road site is expected to attain the annual PM_{2.5} standard. This affirms that with the controls proposed in the Plan, all the locations including Ontario CA-60 near-road in the South Coast Air Basin will attain the 2012 annual PM_{2.5} NAAQS in 2030.

Chapter 7

~~EXCEPTIONAL EVENT DEMONSTRATION~~

ATYPICAL EVENTS ANALYSIS

Introduction

Fireworks Emissions

Professional Fireworks

Historical Analysis

Fireworks Summary for 2016-07-05

Fireworks Summary for 2017-07-04 and 2017-07-05

Fireworks Summary for 2018-07-05

Fireworks Summary for 2019-07-05

Conclusions

Introduction

The EPA Memorandum “Additional Methods, Determinations, and Analyses to Modify Air Quality Data Beyond Exceptional Events” (U.S. EPA, 2019)¹ published in 2019 establishes that ambient data that is not representative to characterize the base year design value may be excluded for the purposes of attainment demonstrations.

This report describes five 24-hour PM2.5 exceedances at the 60 Near Road monitor caused by Independence Day Fireworks that meet the exceptional event criteria established by the U.S. EPA (U.S. EPA, 2016²; U.S. EPA 2007³). The events occurred in the South Coast Air Basin, within the jurisdiction of the South Coast Air Quality Management District (South Coast AQMD). The table below shows a list of exceedances described in this report.

¹ Clarification Memo on Additional Methods, Determinations, and Analyses to Modify Air Quality Data Beyond Exceptional Events. 2019. Environmental Protection Agency. <https://www.epa.gov/air-quality-analysis/clarification-memo-additional-methods-determinations-and-analyses-modify-air>.

² October 3, 2016. “Treatment of Data Influenced by Exceptional Events.” Fed. Reg. 68216 (40 C.F.R. pts 50 & 51): Vol. 81. https://www.epa.gov/sites/default/files/2018-10/documents/exceptional_events_rule_revisions_2060-as02_final.pdf.

³ Environmental Protection Agency. March 22, 2007. “Treatment of Data Influenced by Exceptional Events.” Fed. Reg. 13560 (40 C.F.R. pts 50 & 51): Vol. 72. <https://www.govinfo.gov/content/pkg/FR-2007-03-22/pdf/E7-5156.pdf>.

**TABLE II-7-1:
EXCEEDANCES FOR 2016-2019 INDEPENDENCE DAY FIREWORKS.**

| Date | Local Site Name | AQS Site ID | POC | Parameter Code | Conc.* |
|---|----------------------------|-------------|-----|----------------|--------|
| 2016-07-05 | Ontario-Route 60 Near Road | 06-071-0027 | 1 | 88101 | 49.5 |
| 2016-07-05 | Ontario-Route 60 Near Road | 06-071-0027 | 3 | 88101 | 55.9 |
| 2017-07-04 | Ontario-Route 60 Near Road | 06-071-0027 | 1 | 88101 | 39.2 |
| 2017-07-05 | Ontario-Route 60 Near Road | 06-071-0027 | 1 | 88101 | 67.8 |
| 2018-07-05 | Ontario-Route 60 Near Road | 06-071-0027 | 1 | 88101 | 55.7 |
| 2018-07-05 | Ontario-Route 60 Near Road | 06-071-0027 | 3 | 88101 | 70.6 |
| 2019-07-05 | Ontario-Route 60 Near Road | 06-071-0027 | 1 | 88101 | 57.7 |
| 2019-07-05 | Ontario-Route 60 Near Road | 06-071-0027 | 3 | 88101 | 71.2 |
| *Conc. = Concentration ($\mu\text{g}/\text{m}^3$) | | | | | |

Emissions from the 4th and 5th of July fireworks lead to high PM_{2.5} concentrations region-wide. Exceedances occurred at other monitors throughout the South Coast Air Basin on the same days that the exceedances that occurred at the Route 60 Near Road station. While these exceedances also increased annual PM_{2.5} design values at these other monitors, exclusion of these exceedances would not result in a reduced carrying capacity.

Fireworks Emissions

Fireworks use is ubiquitous across Southern California on Independence Day. Many municipalities host professional fireworks displays on the evening of July 4th to commemorate the holiday. In addition, there is a strong culture of using personal-use “backyard” fireworks on Independence Day, which are likely the dominant source of fireworks emissions throughout the region based on video evidence from aerial observations. For example, see KCAL News, “Fourth of July: Residents celebrate America’s birthday with fireworks of their own”

<https://youtu.be/e08V6Sw0L4I>. Transcript of KCAL news story from July 4, 2023:

“Welcome back, I’m Suzie Suh. Now at 9:30, illegal fireworks going off all over the Southland, as you can see from our picture. Desmond Shaw is live in Skycal tonight, Desmond. Well Suzie, Happy 4th of July. I’ll put up the Map Tracker for a bit to show where we are. At the 405 and 710 right now, looking to north towards Lynwood, Compton, South L.A., and look at this in the distance. It almost looks like a giant lightning storm. Those are all fireworks almost exclusively from illegal variety here. It’s always so amazing to see this every year. Must be hundreds of thousands of pounds worth of illegal fireworks going off. I’m always reminded when LAPD or another agency discovers a big stash of fireworks that they haul offsite, it makes you wonder how many other stashes there must be out there to be able to ignite this many fireworks here. This has been going on for an hour; it’s going to be going on for at least another couple hours. And of course, this layer is getting so thick you can practically taste the gunpowder in the air. This will be with us into the early morning hours. So, unfortunate for our air quality. Very impressive to look at, but don’t forget that about 90% of this is not of the legal variety on this Independence Day evening. Live at Skycal overhead, I’m Desmond Shaw. Suzie, back to you in the studio”.

Personal-use fireworks are illegal in Ontario, CA, and several neighboring cities, see

Table II-7-2. Personal-use fireworks are also illegal in several upwind cities throughout the Basin including the City of Los Angeles, the largest city in the region with nearly 4 million residents. However, ordinances prohibiting the use of these fireworks are difficult to enforce. Data are not available to quantify the use of illegal fireworks in the city of Ontario, CA or upwind areas. However, the city of Ontario, CA held a takeback event in June 2021 encouraging citizens to turn in illegal fireworks with no questions asked and a house exploded in March of 2021 due to illegal fireworks <https://abc7.com/illegal-fireworks-ontario-takeback-explosion/10810827/>, which suggests that citizens might not always abide by the fireworks ban. Personal-use fireworks are widely available to purchase in cities that do allow fireworks.

**TABLE II-7-2:
EXAMPLE OF CITIES NEAR ONTARIO WITH PROHIBITION LAWS REGARDING CONSUMER-
GRADE FIREWORKS.**

| City | Distance to 06-071-0027 site (miles)* | Link |
|----------------------|---------------------------------------|---|
| Ontario, CA | 0 | https://www.ontarioca.gov/NoFireworks |
| Montclair, CA | 5.3 | https://www.cityofmontclair.org/fireworks/ |
| Rancho Cucamonga, CA | 5.4 | https://www.cityofrc.us/news/all-fireworks-are-illegal-rancho-cucamonga |
| Jurupa Valley, CA | 8.9 | https://www.jurupavalley.org/467/Fireworks |

* approximate distance

Professional Fireworks

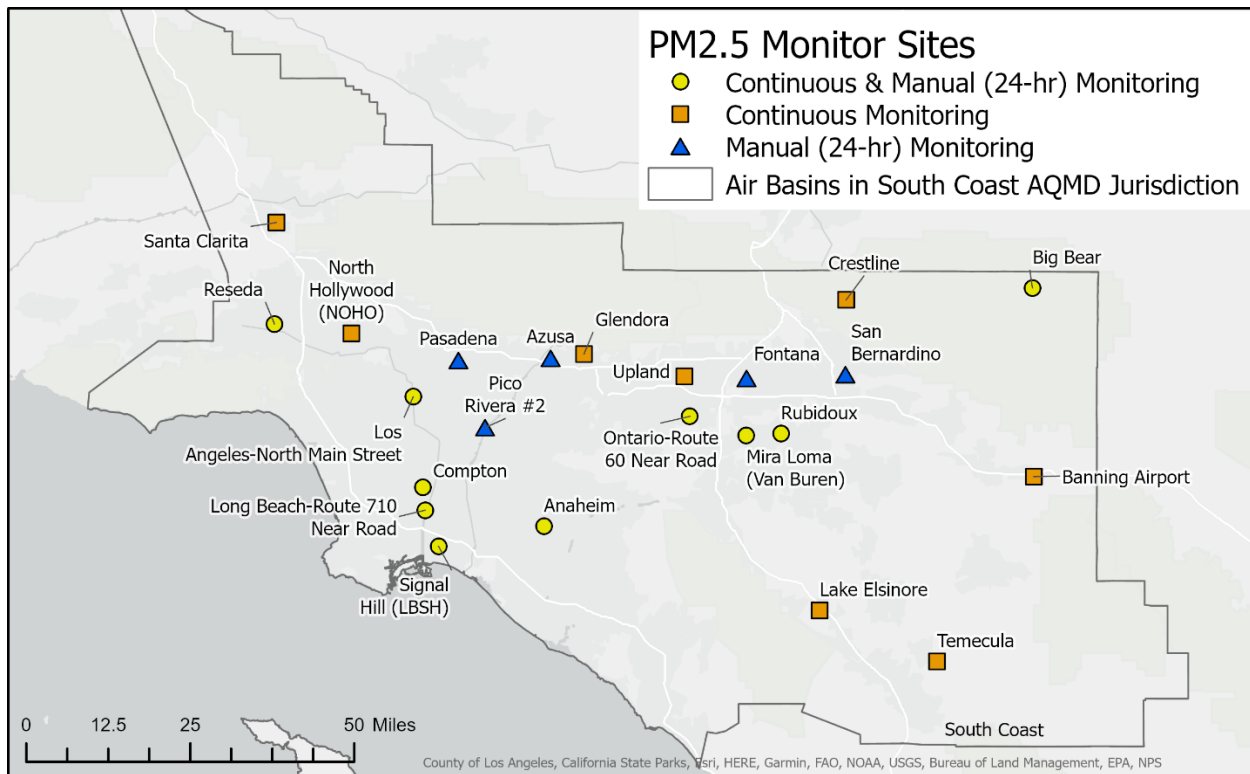
Table II-7-3 shows several examples of professional fireworks displays in Ontario, CA and neighboring cities planned for 2023 and in recent years. While we don't have complete records for professional grade fireworks events for 2016-2019, such events are typically an annual event around July 4. The Fontana Herald News reported in June 2020 that Rancho Cucamonga would still launch fireworks despite no spectators being allowed to gather due to the COVID-19 pandemic, https://www.fontanaheraldnews.com/entertainment/rancho-cucamonga-will-have-fireworks-show-on-july-4/article_6eb09f5e-afec-11ea-b6cc-e325e7aee8a6.html. The article indicates that Rancho Cucamonga's fireworks typically occur at the LoanMart Field, which is located approximately 6.3 miles from the Ontario-Route 60 Near Road monitoring station. In addition to the professional fireworks displays near the monitoring station, professional fireworks displays are common throughout upwind areas in the Los Angeles metropolitan area.

**TABLE II-7-3:
EXAMPLE PAST PROFESSIONAL FIREWORKS DISPLAYS.**

| Date | Location | Distance to 06-071-0027 site (miles)* | Link |
|---|---|---------------------------------------|---|
| 2023-07-04 | Westwind Park (Ontario, CA) | 1.3 | https://www.ontarioca.gov/independenceDay |
| 2023-07-01 | Ruben S. Ayala Park (Chino, CA) | 4.8 | https://www.cityofchino.org/346/Fireworks-Spectacular |
| 2023-07-04 | Fairplex (Pomona, CA) | 9.4 | https://fairplex.com/kaboom/ |
| 2023-07-05 | Cable Airport (Upland, CA) | 6.8 | https://www.uplandca.gov/4th-of-july-festivities |
| 2022-07-04 | LoanMart Field (Rancho Cucamonga, CA) | 6.3 | https://patch.com/california/banning-beaumont/calendar/event/20220704/1869836/4th-of-july-concert-fireworks-spectacular-2022-rancho-cucamonga |
| 2022-07-04 | Miller Park Amphitheater (Fontana, CA) | 11.6 | https://www.fontanaca.gov/2158/4th-of-July-Celebration |
| 2022-06-25 | Eastvale Community Park | 6.5 | https://patch.com/california/banning-beaumont/calendar/event/20220625/1873637/picnic-in-the-park-carnival-fireworks-2022-eastvale |
| <u>2019-07-04</u> | <u>Los Angeles area</u> | | https://www.nbclosangeles.com/the-scene/fourth-of-july-fireworks-2019/133056/ |
| <u>2019-07-04</u> & <u>2019-07-05</u> | <u>Areas throughout the South Coast Air Basin and in the Coachella Valley</u> | | https://www.coronaca.gov/Home/Components/News/News/4066/17 |
| <u>2019-07-04</u> | <u>Throughout Los Angeles County</u> | | https://ktla.com/news/local-news/socal-air-pollution-spikes-amid-haze-of-july-4-fireworks-air-quality-advisory-issued/ |
| <u>2017-07-04</u> | <u>Inland Empire (CA)</u> | | https://iecn.com/4th-july-inland-empire-2017-watch-fireworks/ |

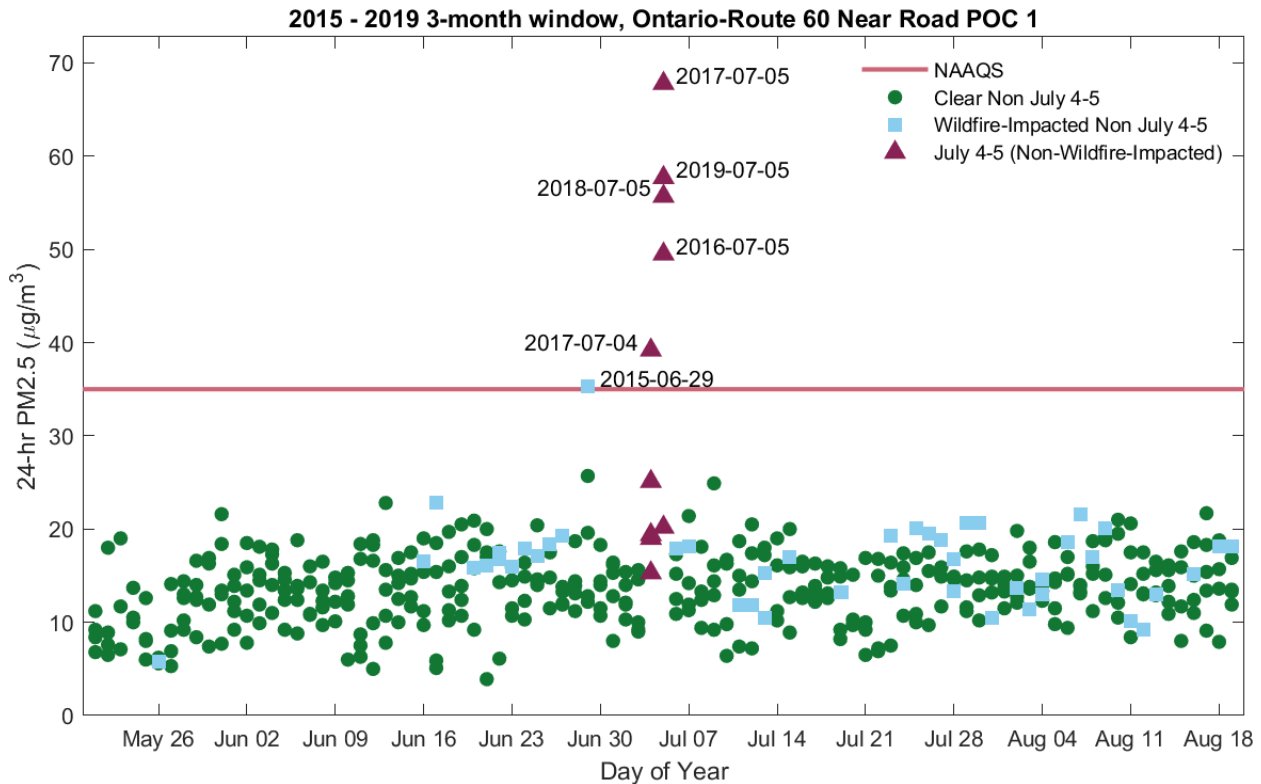
Historical Analysis

Figure II-7-1 shows a map of the regulatory PM2.5 monitors in the South Coast Air Basin. Figure II-7-2 through Figure II-7-13 show historical data during the 3-month period centered on July 4 and 5 for 2015-2019 for the Ontario-Route 60 Near Road, Mira Loma (Van Buren), Rubidoux, Anaheim, and Los Angeles-North Main monitoring stations. Data from stations other than Ontario-Route 60 Near Road are included to demonstrate the regional nature of these events. The data are plotted as both time series and boxplots. The lengths of the whiskers in the boxplots indicate the 1st and 99th percentiles. The exceedances in Table 1 are all anomalously high; all of the five exceedance events at the Ontario-Route 60 Near Road monitor are squarely above the 99th percentile. Hazard Mapping System (HMS)⁴ and NASA Worldview were used to categorize the data as wildfire-impacted and non-wildfire impacted; the data were also categorized as July 4 or 5 and other days, leading to four groupings of data. Note that the data used to calculate the boxplots do not include any July 4 or 5 data. This set of figures demonstrate that across multiple years, exceedances during the summer predominantly occur on July 4 and July 5 or on days with evidence of wildfire impacts.



⁴ National Oceanic and Atmospheric Administration, Office of Satellite and Product Operations, National Environmental Satellite, Data, and Information Service. 2023. "Hazard Mapping System Fire and Smoke Product." <https://www.ospo.noaa.gov/Products/land/hms.html>.

**FIGURE II-7-1:
LOCATION OF ALL REGULATORY PM_{2.5} MONITORS IN THE SOUTH COAST AIR BASIN.**



**FIGURE II-7-2:
HISTORICAL DAILY PM_{2.5} DATA DURING THE 3-MONTH PERIOD CENTERED ON JULY 4 AND 5
FOR 2015-2019 AT THE 60 NEAR ROAD STATION (POC 1).**

(THE FIVE EXCEEDANCE EVENTS THAT ARE THE SUBJECT OF THIS REPORT ARE LABELED WITH THE DATE OF THE EVENT AND INDICATED WITH A MAROON TRIANGLE. THE DATA ARE SEPARATED BY WILDFIRE/NON-WILDFIRE IMPACTS AND JULY 4 AND 5 OR OTHER DAYS. THE LINE IDENTIFIED AS "NAAQS" INDICATES THE 2006 24-HOUR PM_{2.5} STANDARD. HMS DID NOT IDENTIFY A SMOKE PLUME DURING THE ELEVATED VALUE RECORDED ON JUNE 29, 2015 POTENTIALLY DUE TO WIDESPREAD CLOUD COVER ACROSS THE REGION, HOWEVER, A LARGE WILDFIRE NEARBY IN THE SAN BERNARDINO MOUNTAINS CALLED THE LAKE FIRE LIKELY IMPACTED AIR QUALITY ON THIS DATE.)

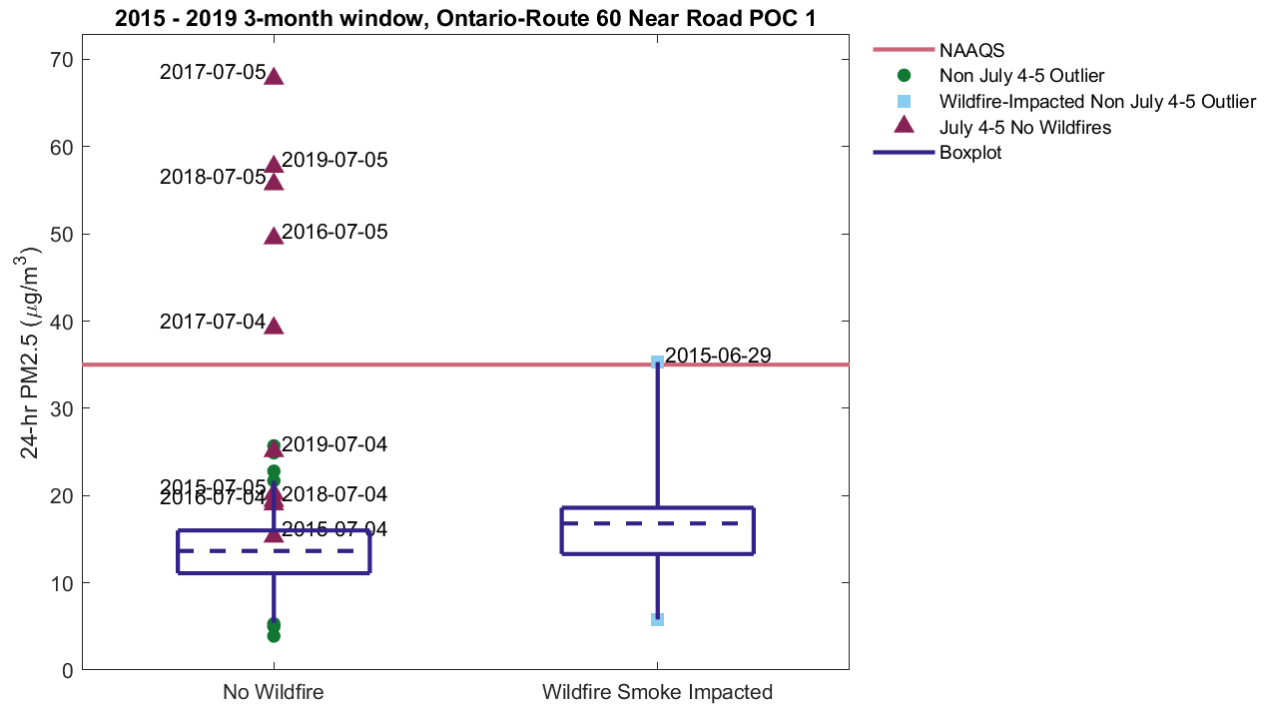


**FIGURE II-7-3:
BOXPLOTS OF HISTORICAL DAILY PM2.5 DATA DURING THE 3-MONTH PERIOD CENTERED ON JULY 4 AND 5 FOR 2015-2019 AT THE 60 NEAR ROAD STATION (POC 1).**

(THE DATA ARE SEPARATED BY WILDFIRE/NON-WILDFIRE IMPACTS AND JULY 4 AND 5 OR OTHER DAYS. NOTE THAT THE JULY 4 AND 5 DATA WERE NOT INCLUDED IN THE CALCULATION OF THE BOXPLOTS. THE LENGTHS OF THE WHISKERS INDICATE THE 1ST AND 99TH PERCENTILES OF THE NON-JULY-4/5 DATA. HMS DID NOT IDENTIFY A SMOKE PLUME DURING THE ELEVATED VALUE RECORDED ON JUNE 29, 2015 POTENTIALLY DUE TO WIDESPREAD CLOUD COVER ACROSS THE REGION, HOWEVER, A LARGE WILDFIRE NEARBY IN THE SAN BERNARDINO MOUNTAINS CALLED THE LAKE FIRE LIKELY IMPACTED AIR QUALITY ON THIS DATE)

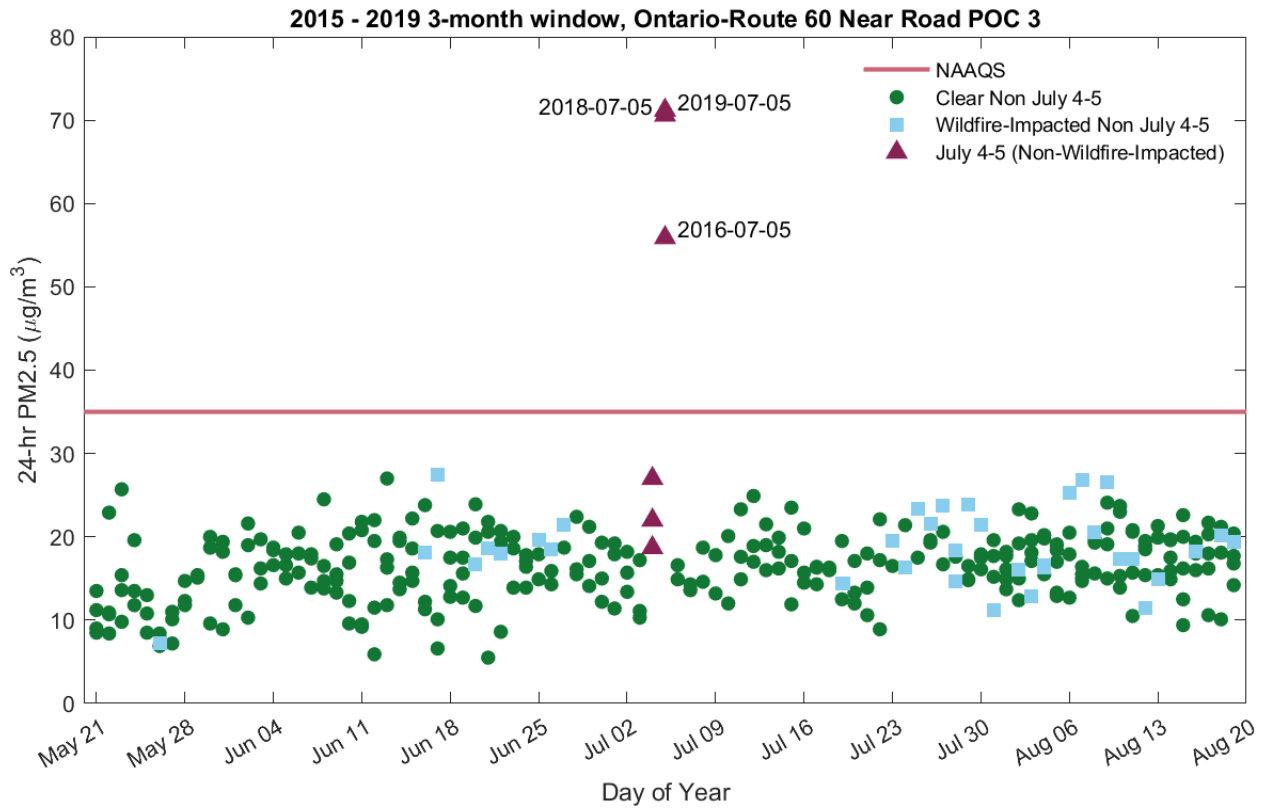


FIGURE II-7-4:
HISTORICAL DAILY PM2.5 DATA DURING THE 3-MONTH PERIOD CENTERED ON JULY 4 AND 5
FOR 2015-2019 AT THE 60 NEAR ROAD STATION (POC 3).
 (THE DATA ARE SEPARATED BY WILDFIRE/NON-WILDFIRE IMPACTS AND JULY 4 AND 5 OR
 OTHER DAYS)

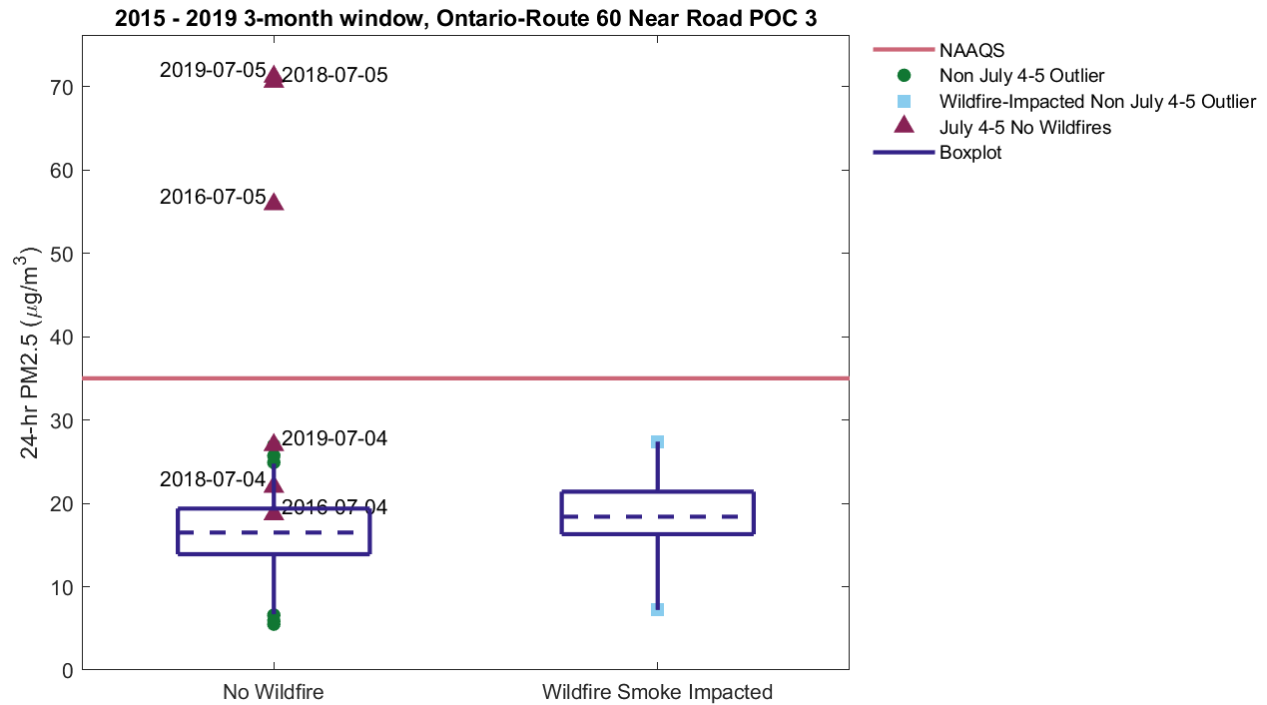


FIGURE II-7-5:
BOXPLOTS OF HISTORICAL DAILY PM2.5 DATA DURING THE 3-MONTH PERIOD CENTERED ON JULY 4 AND 5 FOR 2015-2019 AT THE 60 NEAR ROAD STATION (POC 3).
 (THE DATA ARE SEPARATED BY WILDFIRE/NON-WILDFIRE IMPACTS AND JULY 4 AND 5 OR OTHER DAYS. NOTE THAT THE JULY 4 AND 5 DATA WERE NOT INCLUDED IN THE CALCULATION OF THE BOXPLOTS. THE LENGTHS OF THE WHISKERS INDICATE THE 1ST AND 99TH PERCENTILES OF THE NON-JULY-4/5 DATA)

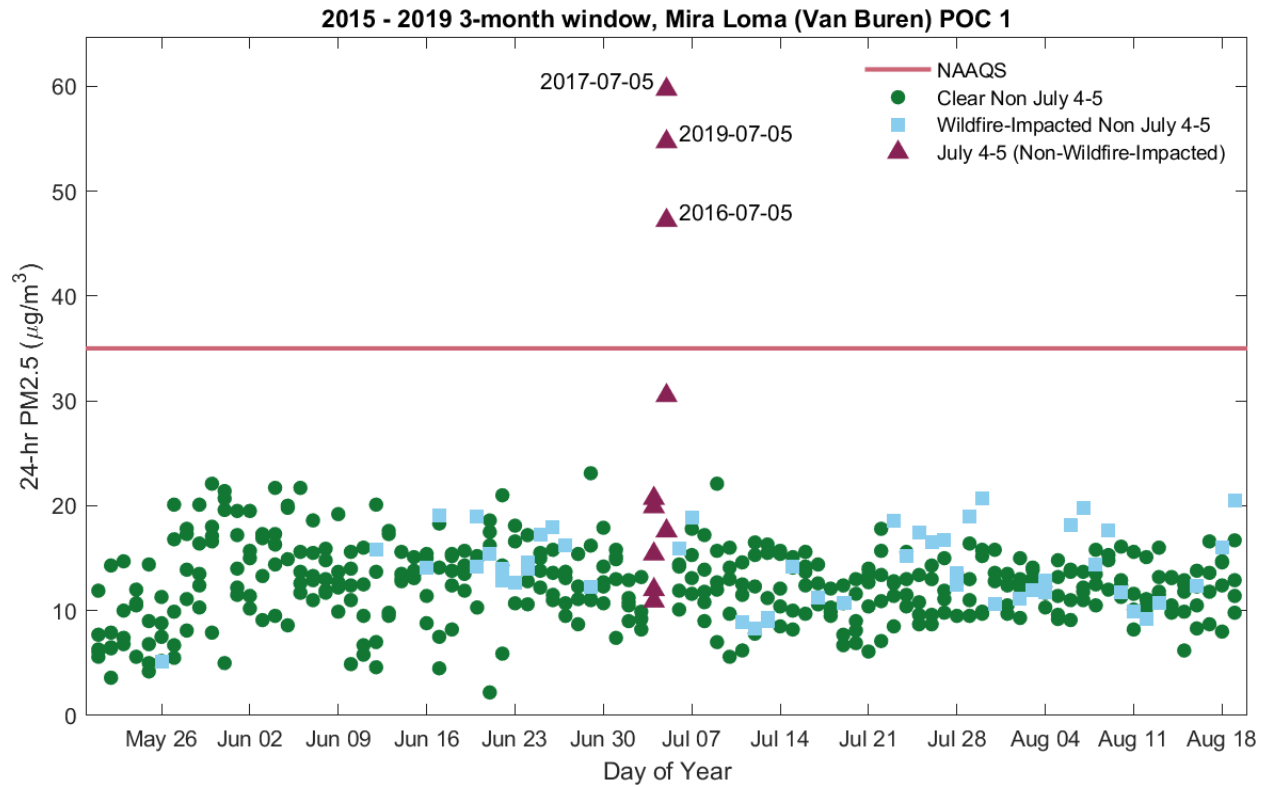


FIGURE II-7-6:
HISTORICAL DAILY PM2.5 DATA DURING THE 3-MONTH PERIOD CENTERED ON JULY 4 AND 5
FOR 2015-2019 AT THE MIRA LOMA (VAN BUREN) STATION (POC 1).
 (THE DATA ARE SEPARATED BY WILDFIRE/NON-WILDFIRE IMPACTS AND JULY 4 AND 5 OR
 OTHER DAYS)

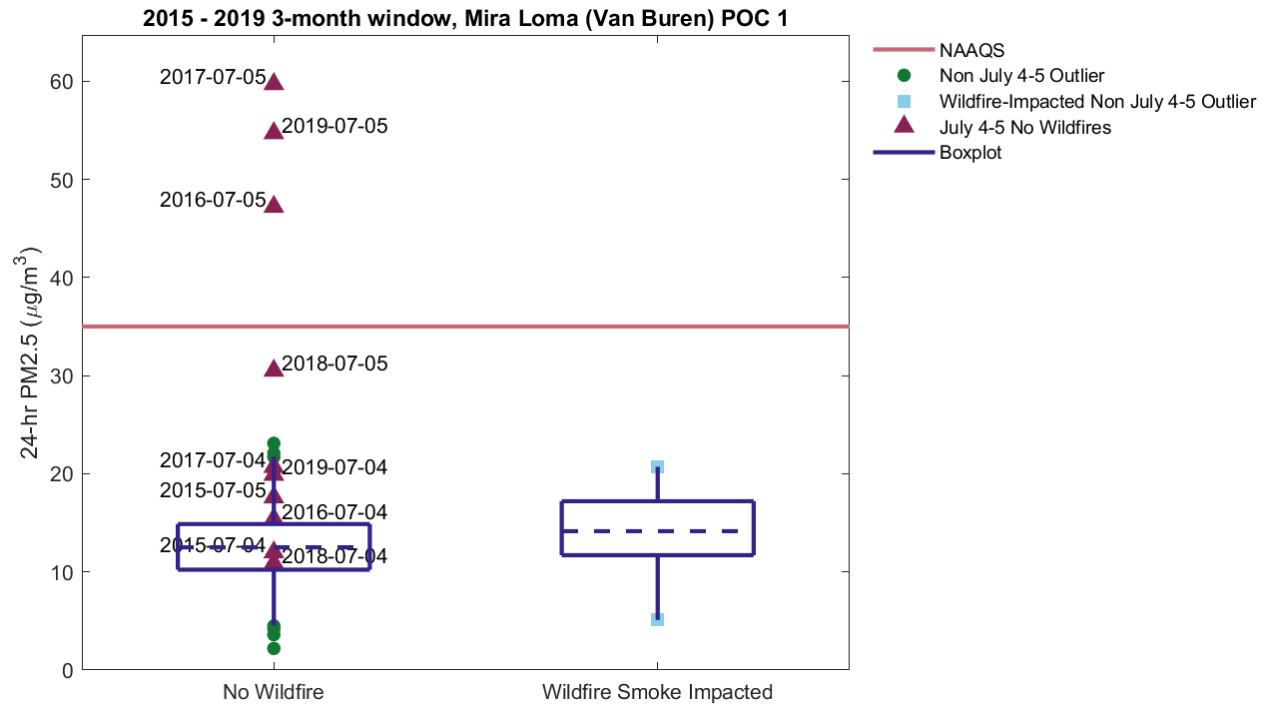


FIGURE II-7-7:
BOXPLOTS OF HISTORICAL DAILY PM2.5 DATA DURING THE 3-MONTH PERIOD CENTERED ON JULY 4 AND 5 FOR 2015-2019 AT THE MIRA LOMA (VAN BUREN) STATION (POC 1).
 (THE DATA ARE SEPARATED BY WILDFIRE/NON-WILDFIRE IMPACTS AND JULY 4 AND 5 OR OTHER DAYS. NOTE THAT THE JULY 4 AND 5 DATA WERE NOT INCLUDED IN THE CALCULATION OF THE BOXPLOTS. THE LENGTHS OF THE WHISKERS INDICATE THE 1ST AND 99TH PERCENTILES OF THE NON-JULY-4/5 DATA)

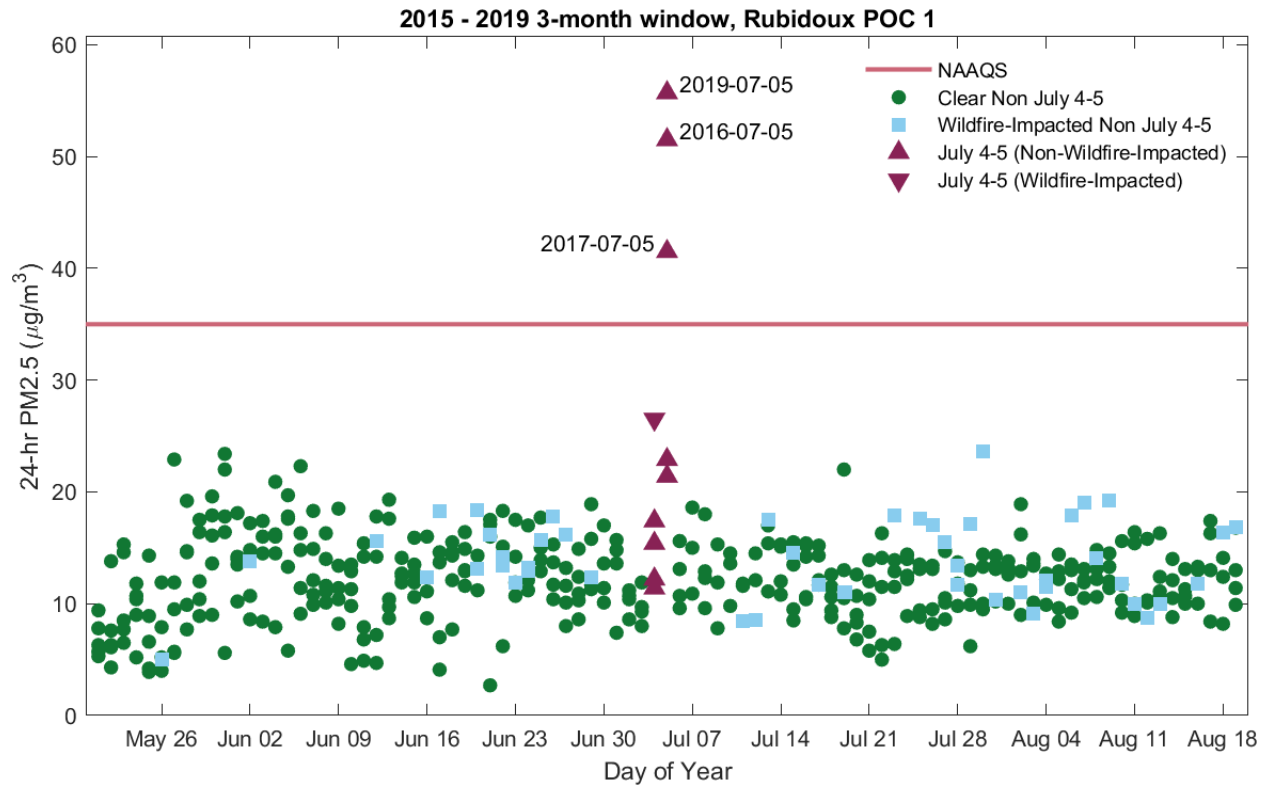


FIGURE II-7-8:
HISTORICAL DAILY PM_{2.5} DATA DURING THE 3-MONTH PERIOD CENTERED ON JULY 4 AND 5 FOR 2015-2019 AT THE RUBIDOUX STATION (POC 1).
 (THE DATA ARE SEPARATED BY WILDFIRE/NON-WILDFIRE IMPACTS AND JULY 4 AND 5 OR OTHER DAYS)

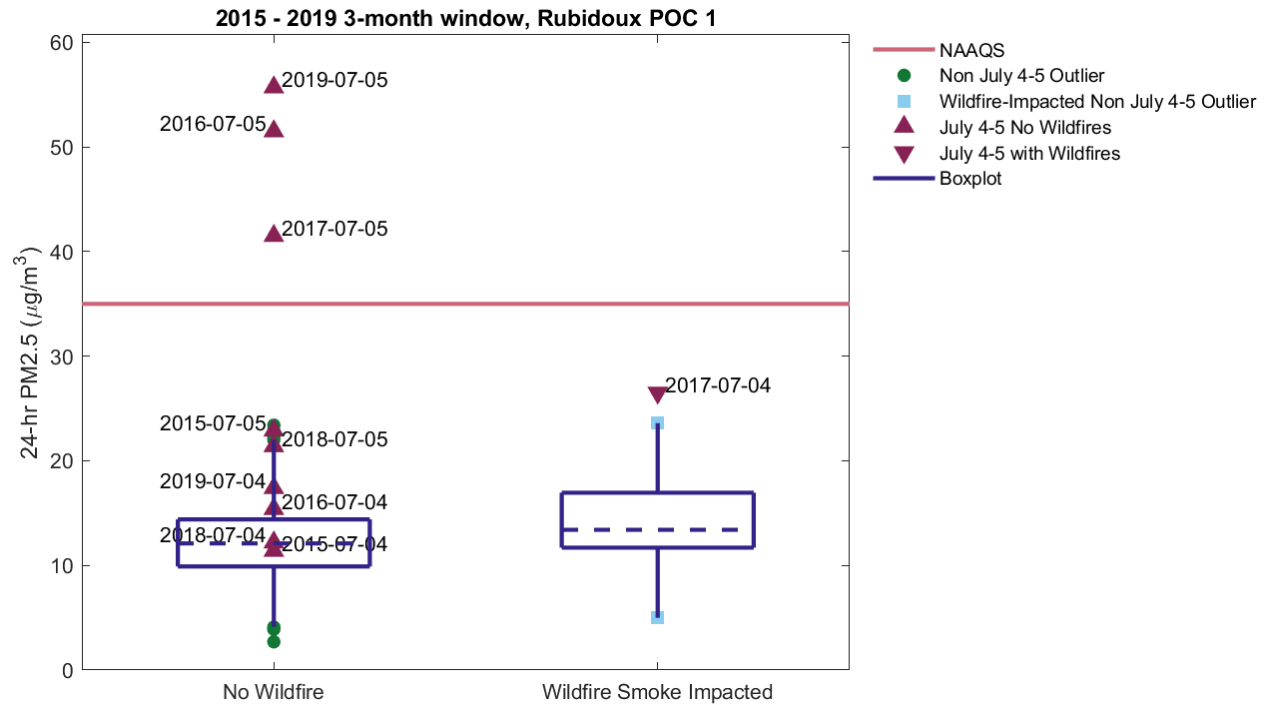


FIGURE II-7-9:
BOXPLOTS OF HISTORICAL DAILY PM2.5 DATA DURING THE 3-MONTH PERIOD CENTERED ON JULY 4 AND 5 FOR 2015-2019 AT THE RUBIDOUX STATION (POC 1).
 (THE DATA ARE SEPARATED BY WILDFIRE/NON-WILDFIRE IMPACTS AND JULY 4 AND 5 OR OTHER DAYS. NOTE THAT THE JULY 4 AND 5 DATA WERE NOT INCLUDED IN THE CALCULATION OF THE BOXPLOTS. THE LENGTHS OF THE WHISKERS INDICATE THE 1ST AND 99TH PERCENTILES OF THE NON-JULY-4/5 DATA)

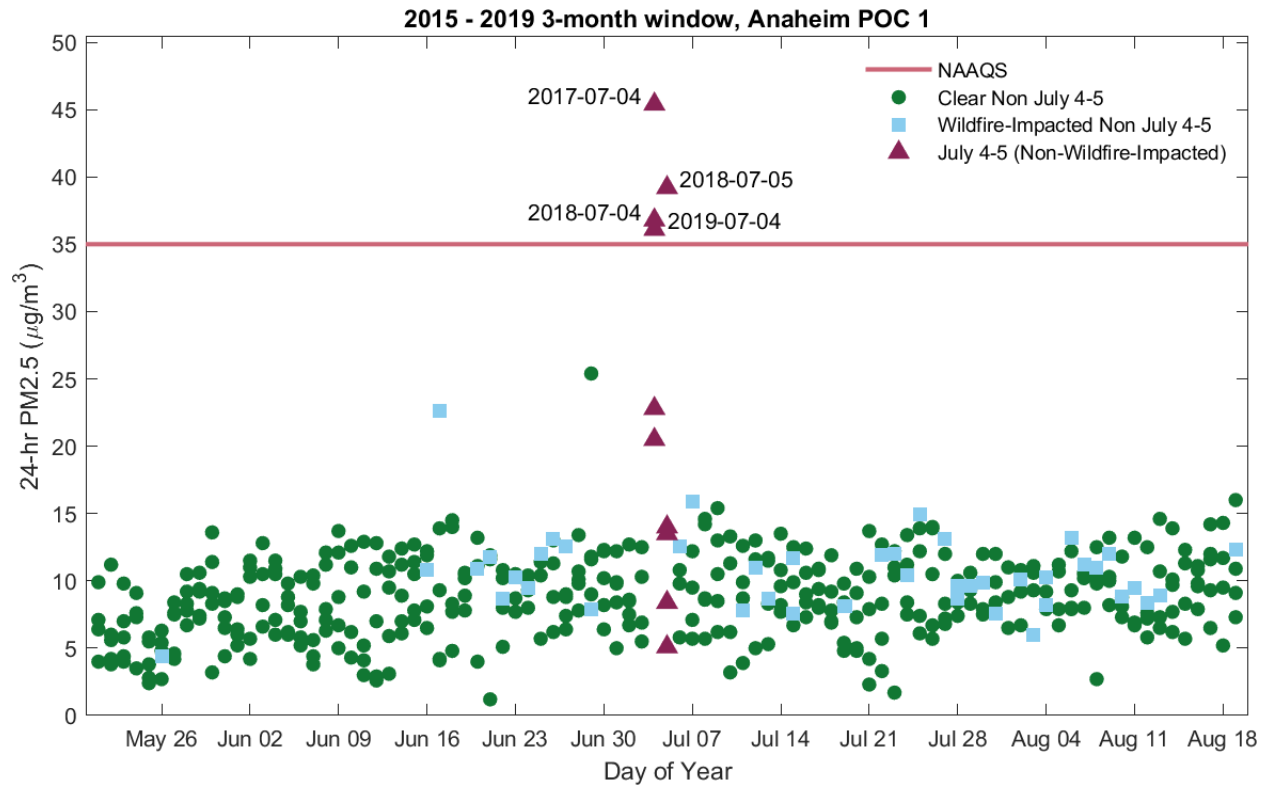


FIGURE II-7-10:
HISTORICAL DAILY PM2.5 DATA DURING THE 3-MONTH PERIOD CENTERED ON JULY 4 AND 5
FOR 2016-2019 AT THE ANAHEIM STATION (POC 1).
 (THE DATA ARE SEPARATED BY WILDFIRE/NON-WILDFIRE IMPACTS AND JULY 4 AND 5 OR
 OTHER DAYS)

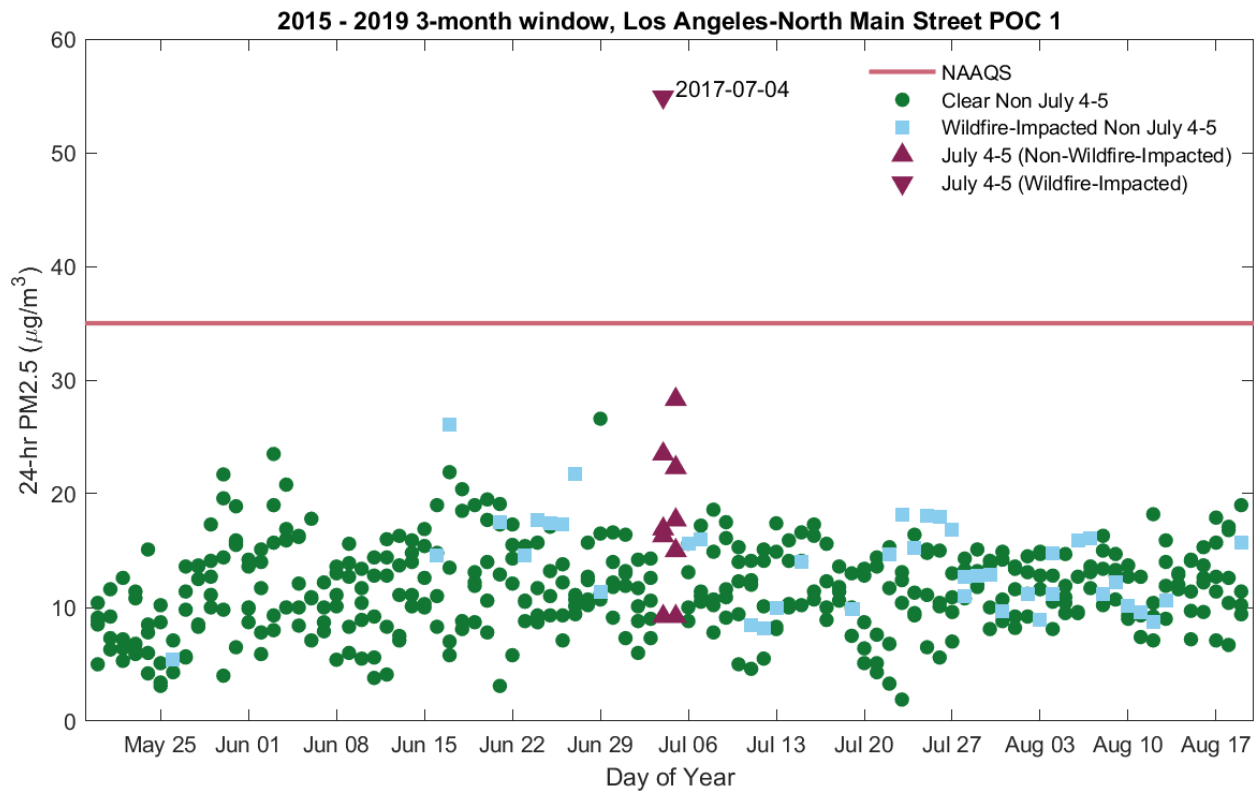


FIGURE II-7-12:
HISTORICAL DAILY PM2.5 DATA DURING THE 3-MONTH PERIOD CENTERED ON JULY 4 AND 5
FOR 2016-2019 AT THE LOS ANGELES-NORTH MAIN STATION (POC 1).
 (THE DATA ARE SEPARATED BY WILDFIRE/NON-WILDFIRE IMPACTS AND JULY 4 AND 5 OR
 OTHER DAYS)

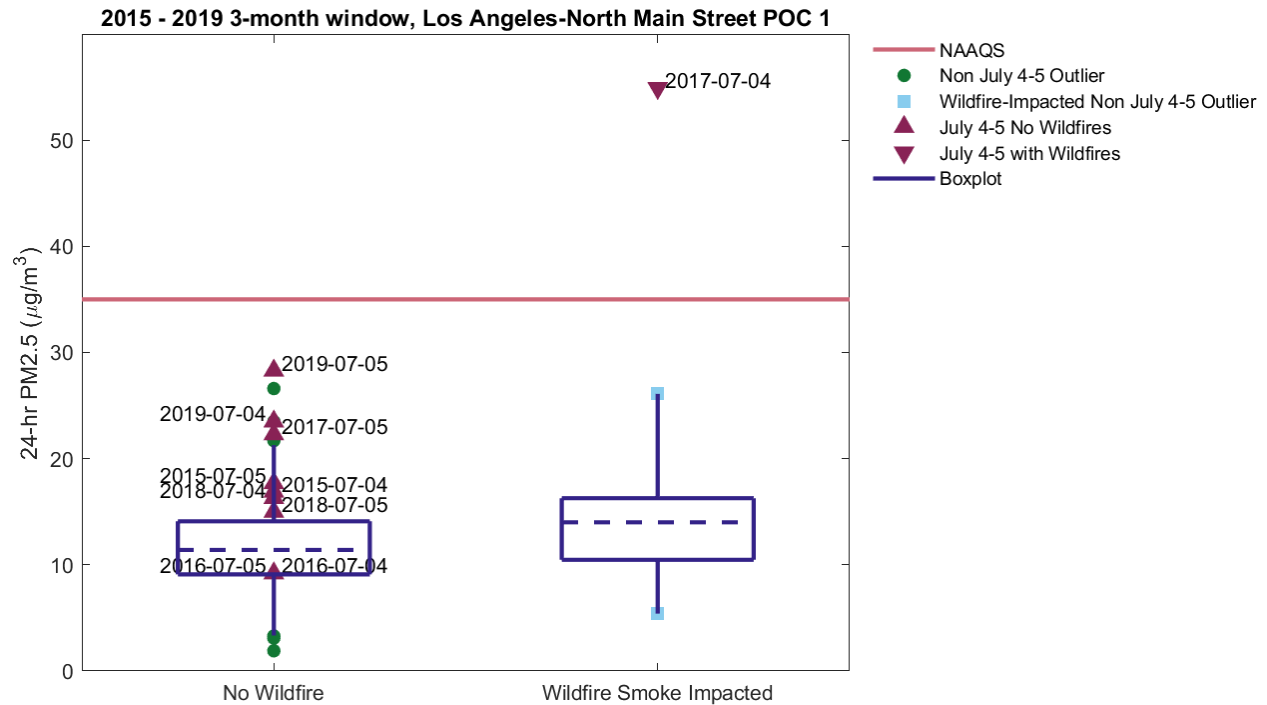


FIGURE II-7-13: BOXPLOTS OF HISTORICAL DAILY PM2.5 DATA DURING THE 3-MONTH PERIOD CENTERED ON JULY 4 AND 5 FOR 2016-2019 AT THE LOS ANGELES-NORTH MAIN STATION (POC 1).

(THE DATA ARE SEPARATED BY WILDFIRE/NON-WILDFIRE IMPACTS AND JULY 4 AND 5 OR OTHER DAYS. NOTE THAT THE JULY 4 AND 5 DATA WERE NOT INCLUDED IN THE CALCULATION OF THE BOXPLOTS. THE LENGTHS OF THE WHISKERS INDICATE THE 1ST AND 99TH PERCENTILES OF THE NON-JULY-4/5 DATA)

Fireworks Summary for 2016-07-05

As is documented earlier in this report, the use of personal fireworks is widespread throughout the Basin. Since personal fireworks are predominantly used in residential neighborhoods, residential land use serves as a proxy for locations of fireworks emissions. Residential land use from the 2019 annual land use dataset from the Southern California Association of Governments (SCAG;

https://hub.scag.ca.gov/datasets/ea9fda878c1947d2afac5142fd5cb658_0/about) is shown in Figure II-7-14. Residential land use, along with mixed residential and commercial land use are shown in the map. HYSPLIT⁵ back-trajectories using the National Oceanic and Atmospheric Administration (NOAA) High Resolution Rapid Refresh (HRRR) 3km meteorological model arriving 50m above the 60 Near Road monitoring station for July 4-5, 2016 are also shown in

⁵ HYSPLIT Trajectories. 2023. NOAA Air Resources Laboratory. https://www.ready.noaa.gov/HYSPLIT_traj.php.

Figure II-7-14. All the back-trajectories originate over the Pacific Ocean and cross large residential areas of the South Coast Air Basin. Figure II-7-15 shows wind roses throughout the South Coast Air Basin for 9 PM on July 4 through 2 PM on July 5, 2016 using wind data from South Coast AQMD monitoring stations and local airports. The wind roses in Figure II-7-15 confirm the onshore wind pattern shown in the HYSPLIT back-trajectories in Figure II-7-14.

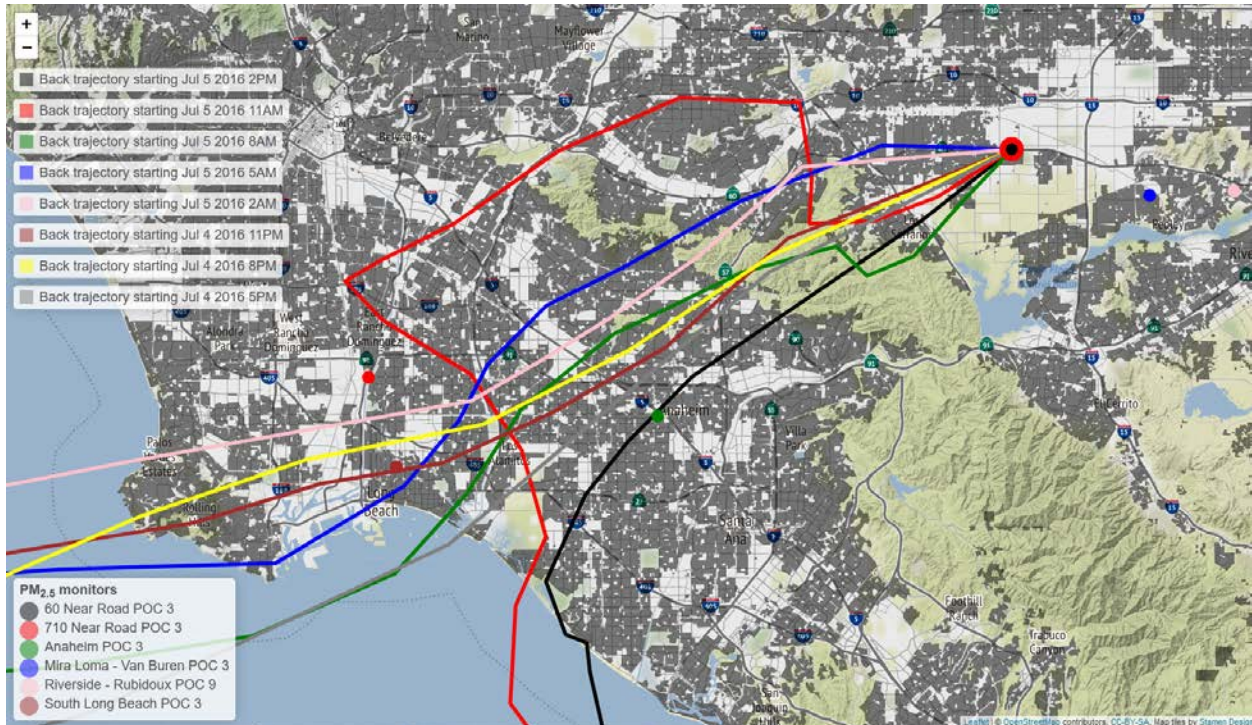


FIGURE II-7-14:
HYSPLIT BACK-TRAJECTORIES FROM 60 NEAR ROAD FOR JULY 4-5, 2016 OVERLAID ON A MAP OF THE SOUTH COAST AIR BASIN SHOWING RESIDENTIAL LAND USE (SHOWN IN GRAY).

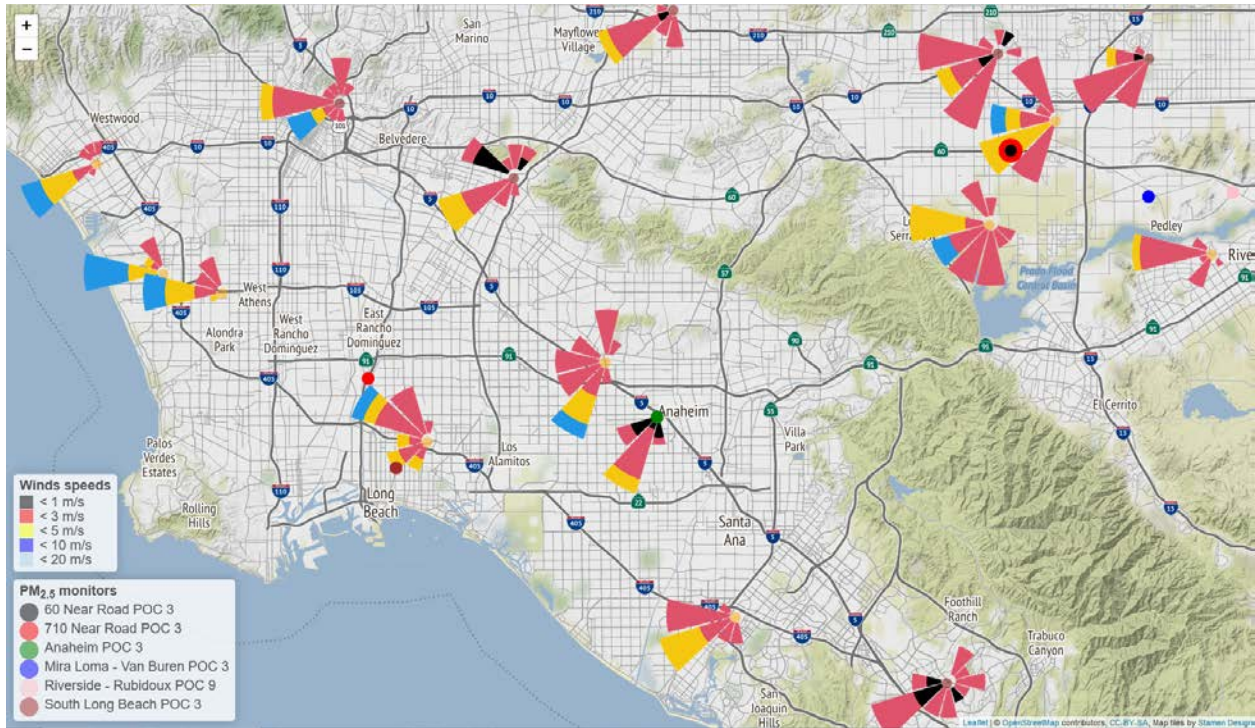


FIGURE II-7-15:
WIND ROSES FOR 9 PM ON JULY 4 THROUGH 2 PM ON JULY 5, 2016 THROUGHOUT THE SOUTH COAST AIR BASIN.

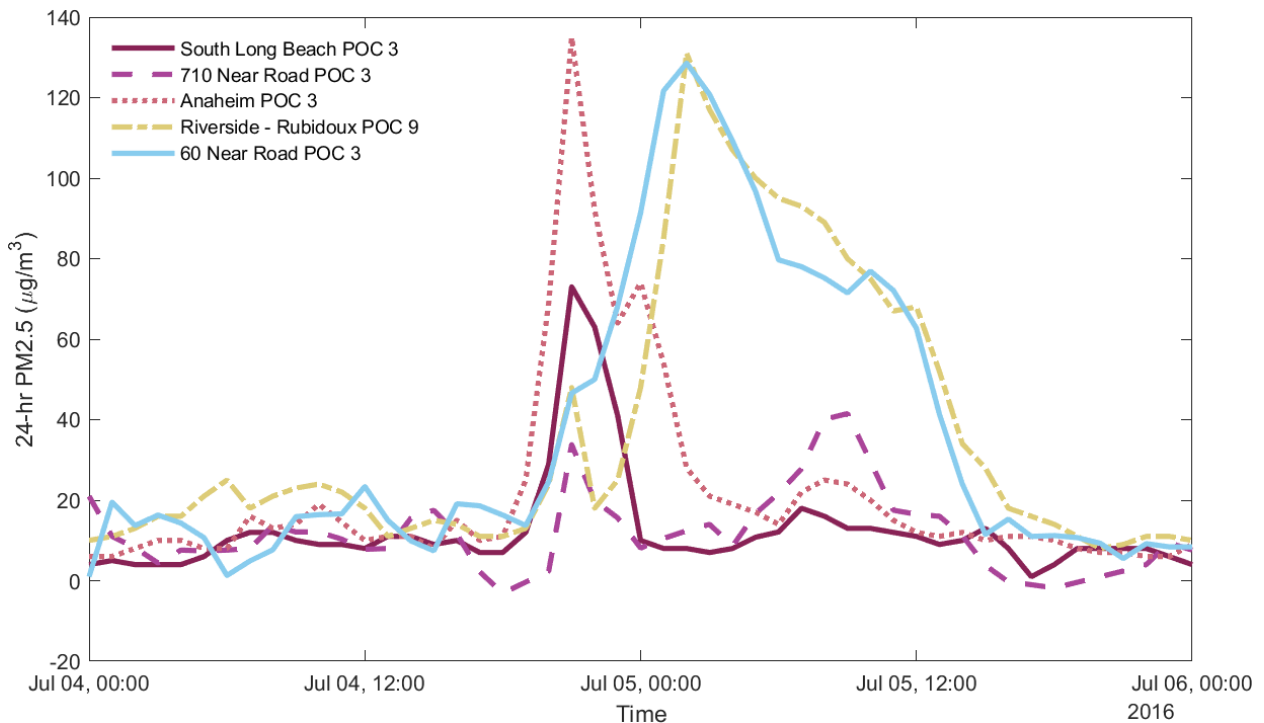


Figure II-7-16 shows time series plots of hourly PM2.5 data at selected stations with continuous PM2.5 instruments within the South Coast Air Basin for July 4-5, 2016. The concentrations peak

at stations closer to the coast earlier than in inland areas (see Figure II-7-14 for monitor locations). This is consistent with the combination of 1) extensive fireworks use across the Basin, especially the most populated areas closer to the coast and 2) the dominant onshore flow that transports these emissions inland. The inland areas have local emissions as well as transported emissions from upwind areas.

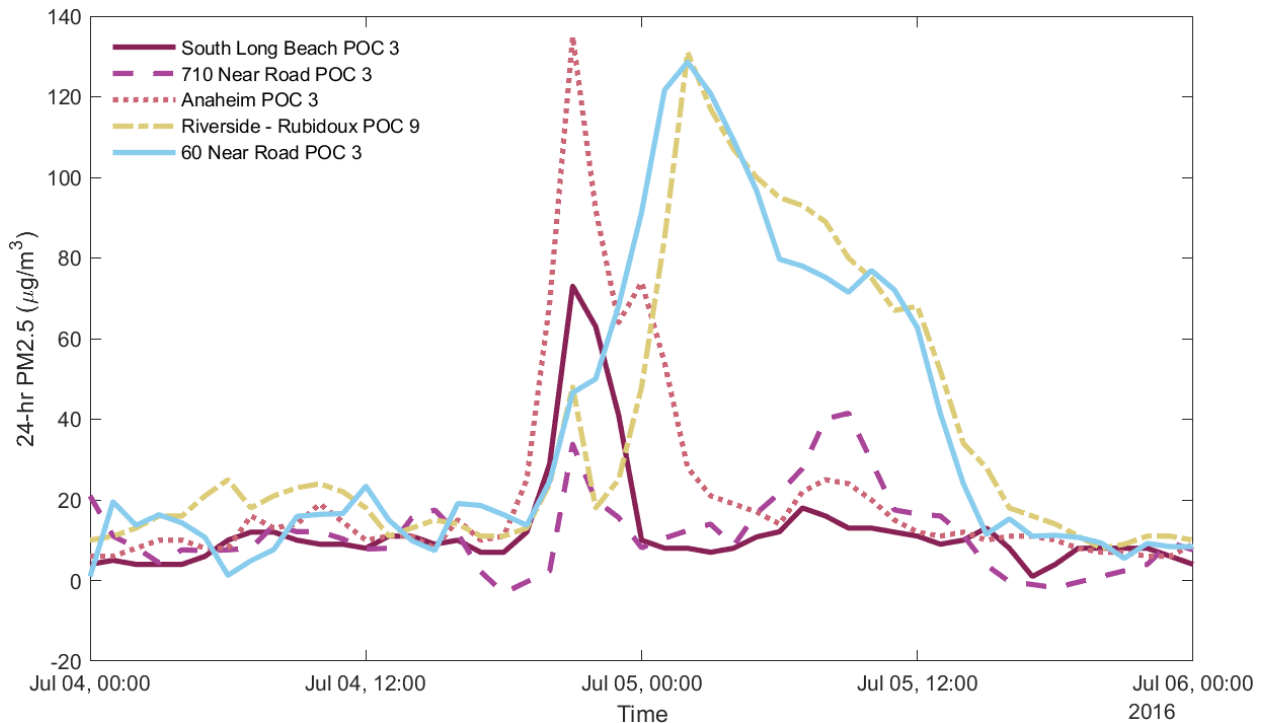


FIGURE II-7-16:
HOURLY TIME SERIES FOR JULY 4-5, 2016 FOR PM_{2.5} MONITORING STATIONS IN THE SOUTH COAST AIR BASIN.

Fireworks Summary for 2017-07-04 and 2017-07-05

Residential land use (a proxy for fireworks emissions locations) and HYSPLIT back-trajectories using the NOAA HRRR meteorological model arriving at the 60 Near Road monitoring station for July 4-5, 2017 are shown in Figure II-7-17. All the back-trajectories originate over the Pacific Ocean and cross large residential areas of the South Coast Air Basin. Figure II-7-18 shows wind roses throughout the South Coast Air Basin for 9 PM on July 4 through 2 PM on July 5, 2017 using wind data from South Coast AQMD monitoring stations and local airports. The wind roses in Figure II-7-18 confirm the onshore wind pattern shown in the HYSPLIT back-trajectories in Figure II-7-17.

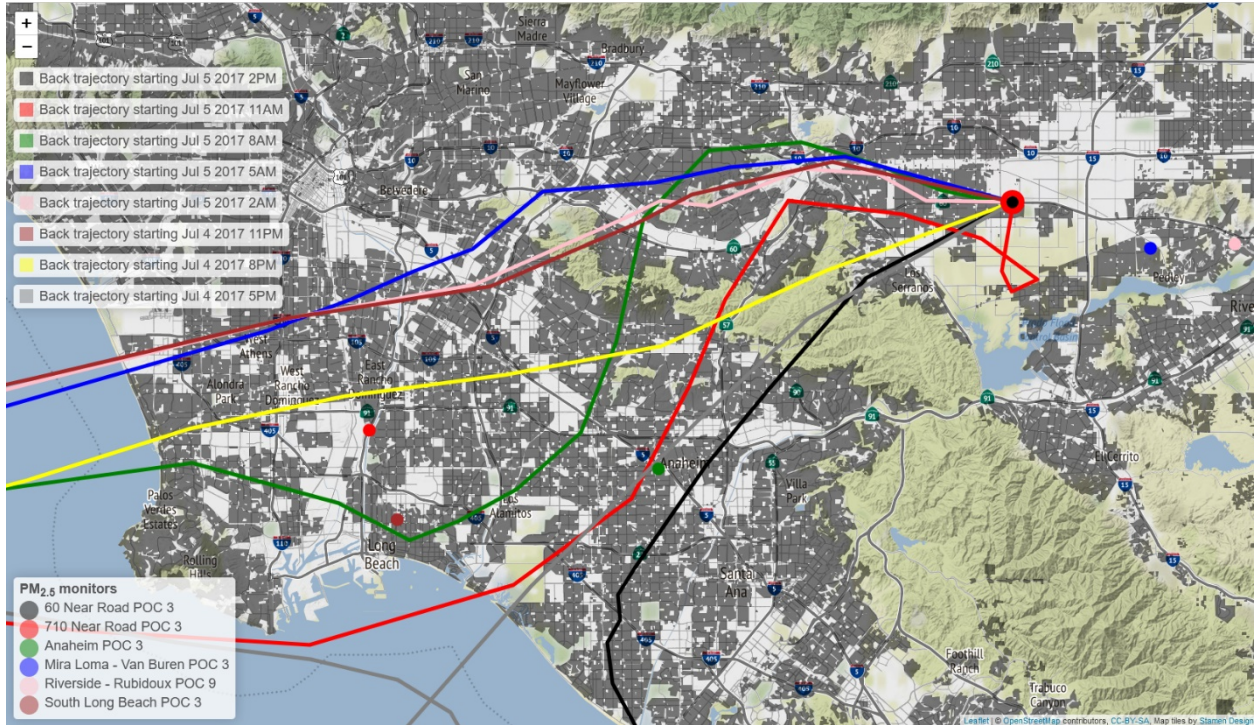
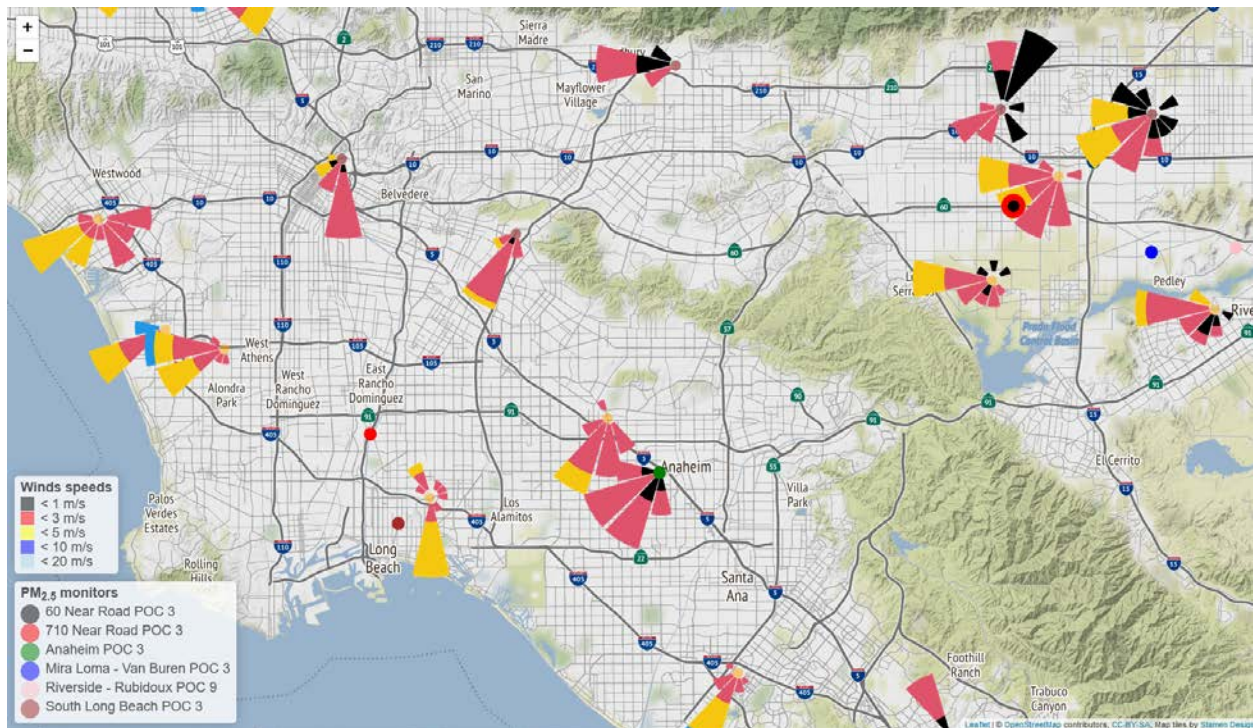
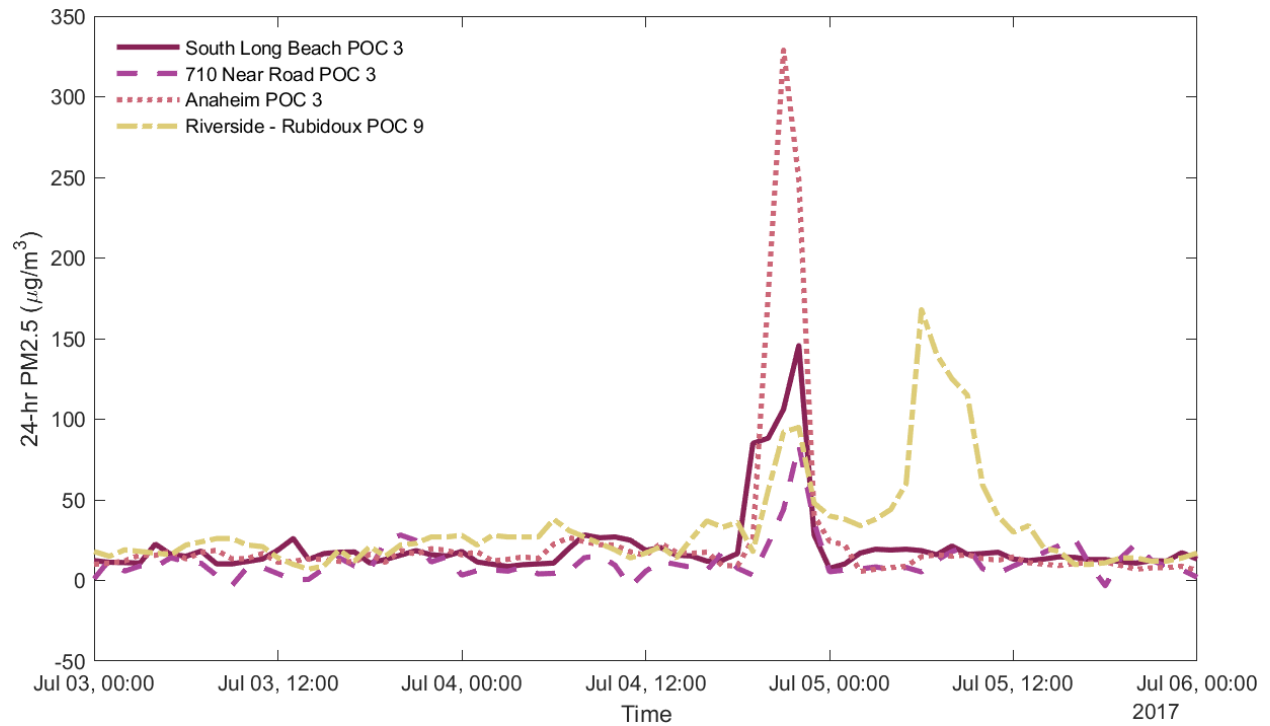


FIGURE II-7-17:
HYSPLIT BACK-TRAJECTORIES FROM 60 NEAR ROAD FOR JULY 4-5, 2017 OVERLAID ON A MAP OF THE SOUTH COAST AIR BASIN SHOWING RESIDENTIAL LAND USE (SHOWN IN GRAY).



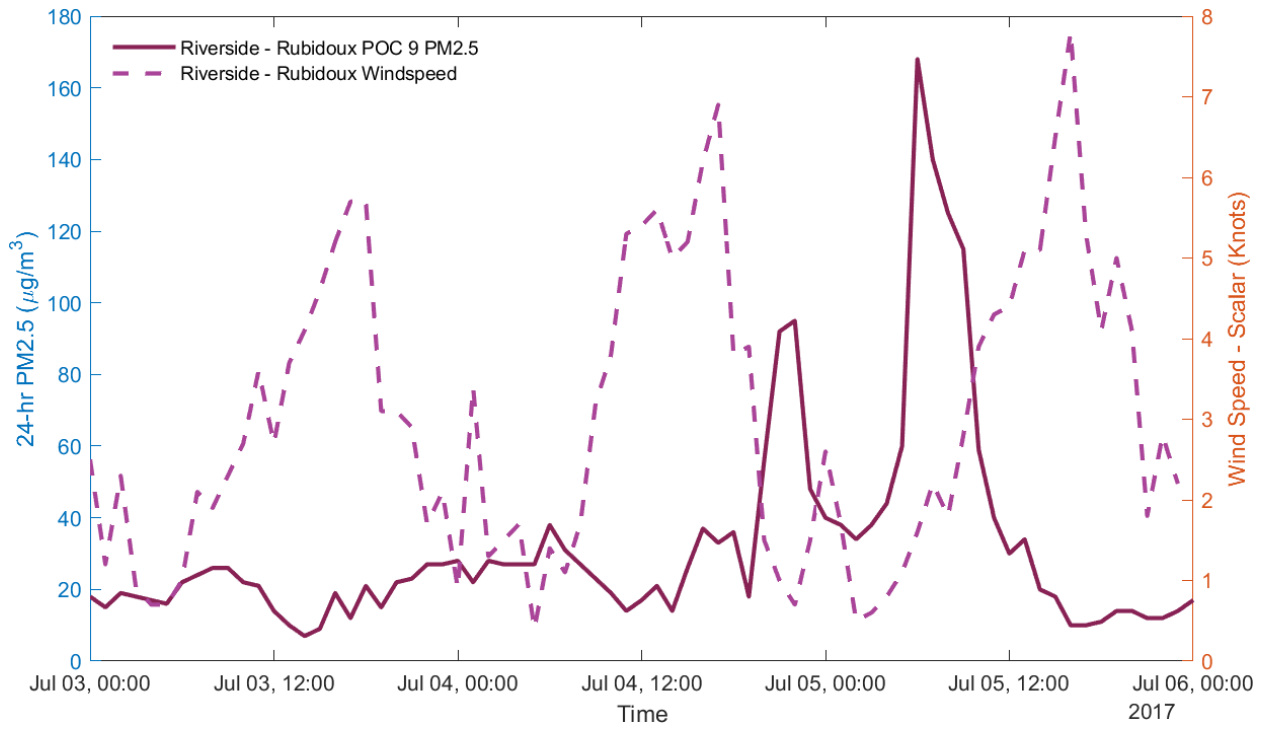
**FIGURE II-7-18:
WIND ROSES FOR 9 PM ON JULY 4 THROUGH 2 PM ON JULY 5, 2017 THROUGHOUT THE
SOUTH COAST AIR BASIN.**

Figure II-7-19 shows time series plots of hourly PM_{2.5} data at selected stations with continuous PM_{2.5} instruments within the South Coast Air Basin for July 3-5, 2017. The concentrations peak at stations closer to the coast earlier than in inland areas (see Figure II-7-17 for monitor locations). This is consistent with the combination of 1) extensive fireworks use across the Basin, especially the most populated areas closer to the coast and 2) the dominant onshore flow that transports these emissions inland. The inland areas have local emissions as well as transported emissions from upwind areas.



**FIGURE II-7-19:
HOURLY TIME SERIES FOR JULY 3-5, 2017 FOR PM_{2.5} MONITORING STATIONS IN THE SOUTH
COAST AIR BASIN.**

Figure II-7-20 through Figure II-7-21 show time series plots of PM_{2.5} (left axes) and windspeed (right axes) for the stations shown in Figure II-7-19 that have co-located wind data. The PM_{2.5} concentrations tend to be the highest during the periods with lowest windspeeds. This is consistent with elevated nearby emissions, such as fireworks and reflects the emission patterns of fireworks, which are typically used at nightfall.



**FIGURE II-7-20:
HOURLY PM2.5 AND WINDSPEED FOR JULY 3-5, 2017 AT THE RIVERSIDE - RUBIDOUX
STATION.**

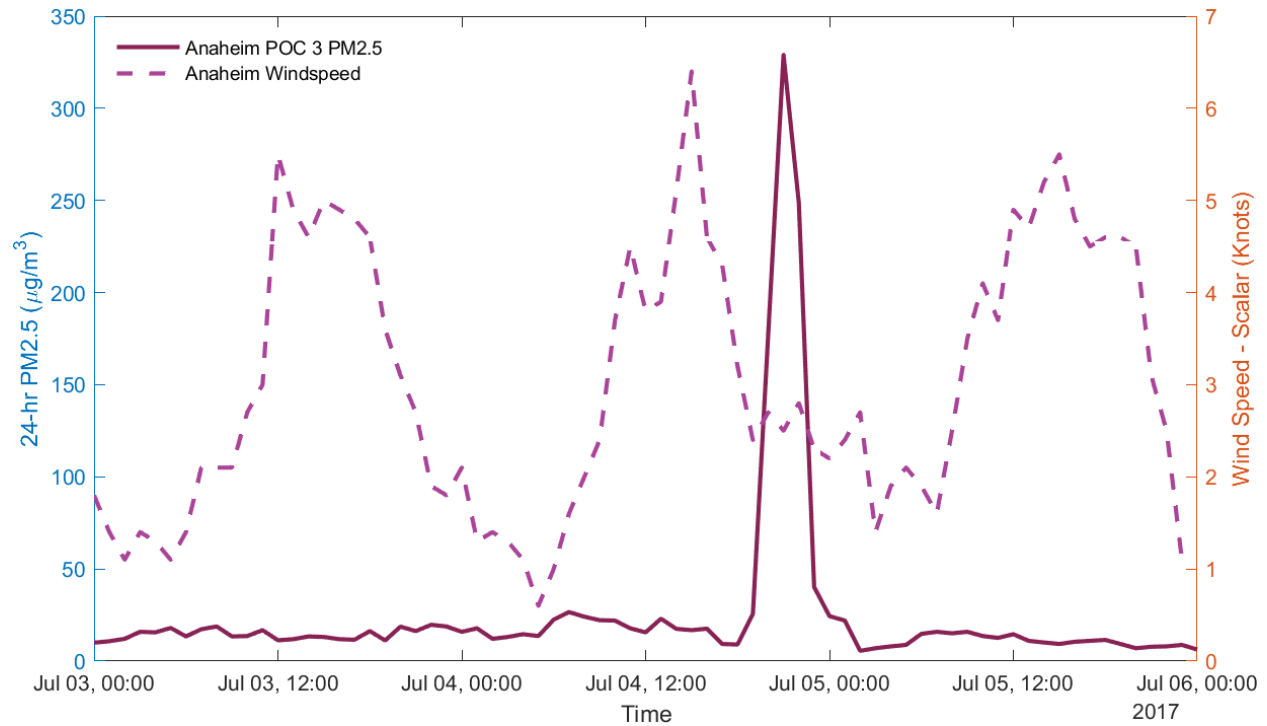


**FIGURE II-7-21:
HOURLY PM2.5 AND WINDSPEED FOR JULY 3-5, 2017 AT THE ANAHEIM STATION.**

Figure II-7-22 through Figure II-7-23 show scatter plots of PM2.5 versus hourly windspeed. This is the same data as shown in Figure II-7-20 through Figure II-7-21, except that the data are limited to 9 PM on July 4 through 5 PM on July 5, 2017 when we expect the greatest impacts from fireworks emissions. The NAAQS value (35 µg/m³) is shown as a horizontal line. Most PM2.5 measurements were below the NAAQS value whenever the winds were above approximately 5 knots, with the highest concentrations occurring at lower wind speeds. This pattern is consistent with elevated nearby emissions from fireworks accumulating to high concentrations during periods of lower ventilation and then diluting during periods of increased ventilation at higher windspeeds.

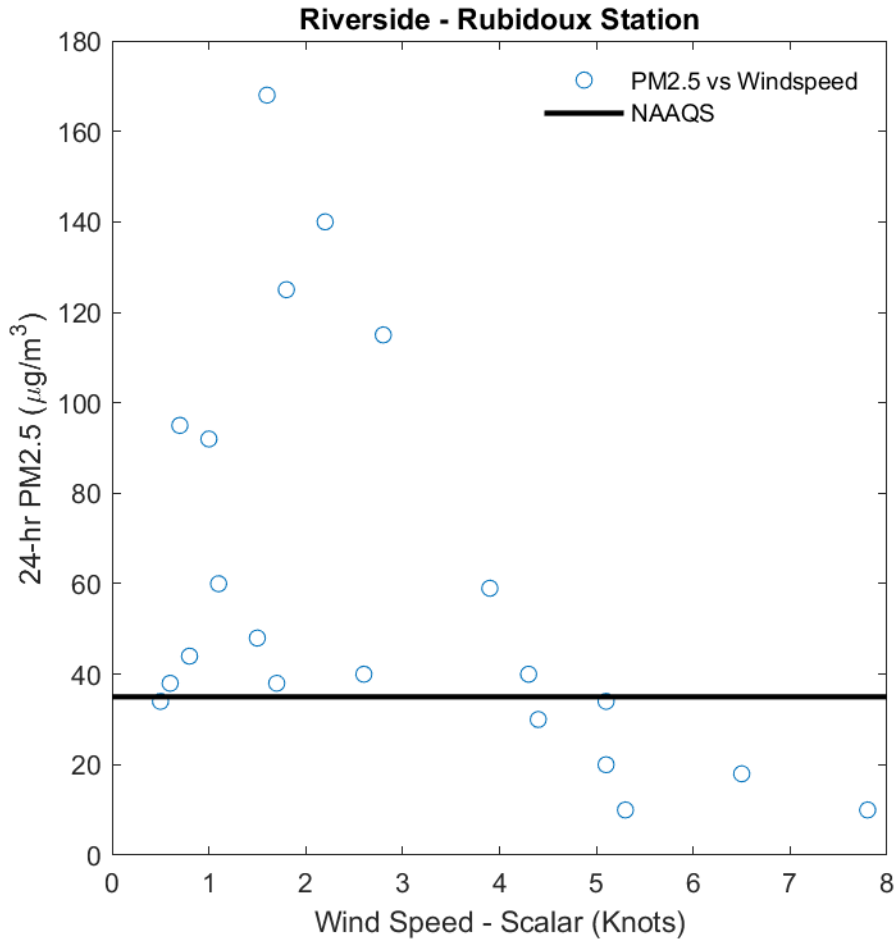


FIGURE II-7-22:
HOURLY PM2.5 VERSUS WINDSPEED FOR 9 PM ON JULY 4 THROUGH 5 PM ON JULY 5, 2017
AT THE RIVERSIDE - RUBIDOUX STATION.

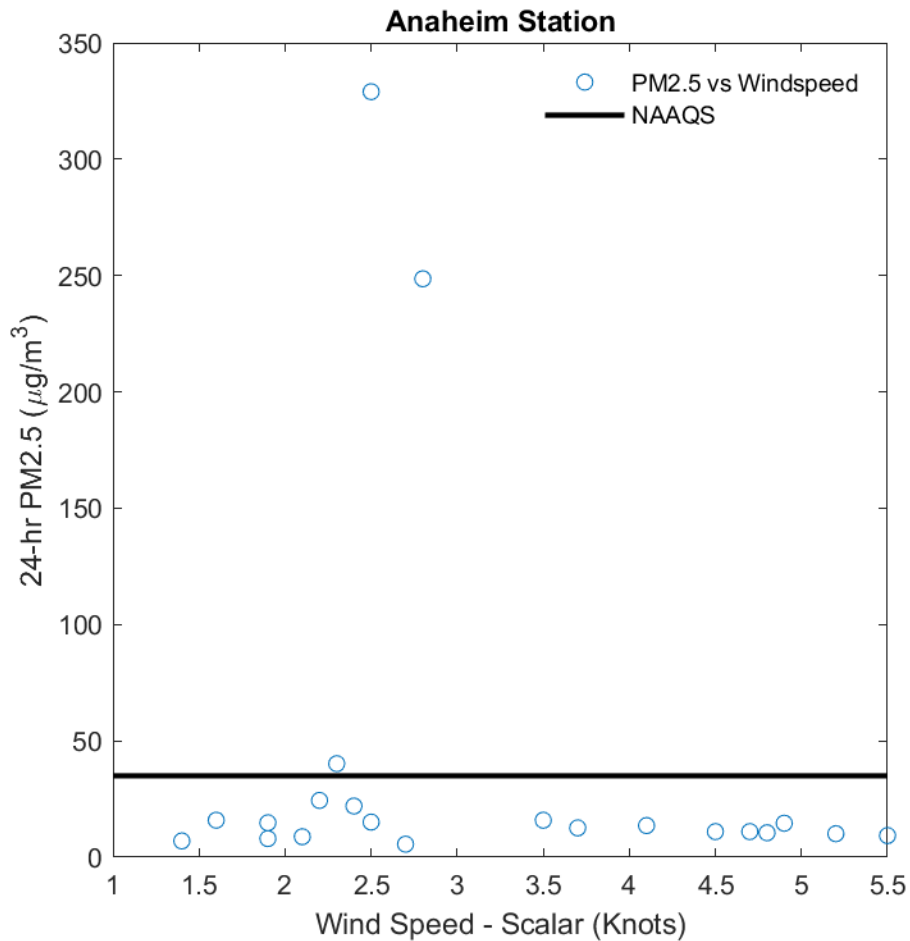


FIGURE II-7-23:
HOURLY PM2.5 VERSUS WINDSPEED FOR 9 PM ON JULY 4 THROUGH 5 PM ON JULY 5, 2017
AT THE ANAHEIM STATION.

Fireworks Summary for 2018-07-05

Residential land use (a proxy for fireworks emissions locations) and HYSPLIT back-trajectories using the NOAA HRRR meteorological model arriving at the 60 Near Road monitoring station for July 4-5, 2018 are shown in Figure II-7-24. All the back-trajectories originate over the Pacific Ocean or locally within the South Coast Air Basin and cross large residential areas of the South Coast Air Basin. Figure II-7-25 shows wind roses throughout the South Coast Air Basin for 9 PM on July 4 through 2 PM on July 5, 2018 using wind data from South Coast AQMD monitoring stations and local airports. The low windspeeds and onshore components shown in the wind roses in Figure II-7-25 are consistent with the meandering and ocean-sourced HYSPLIT back-trajectories in Figure II-7-24.

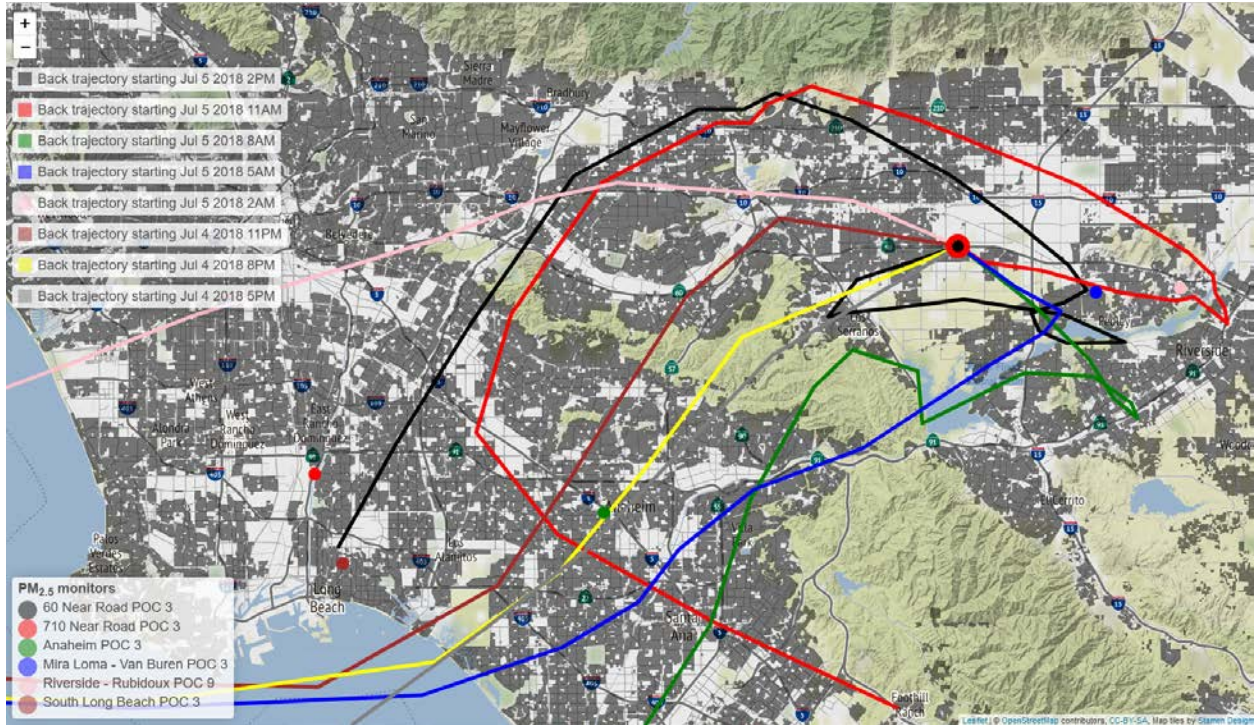
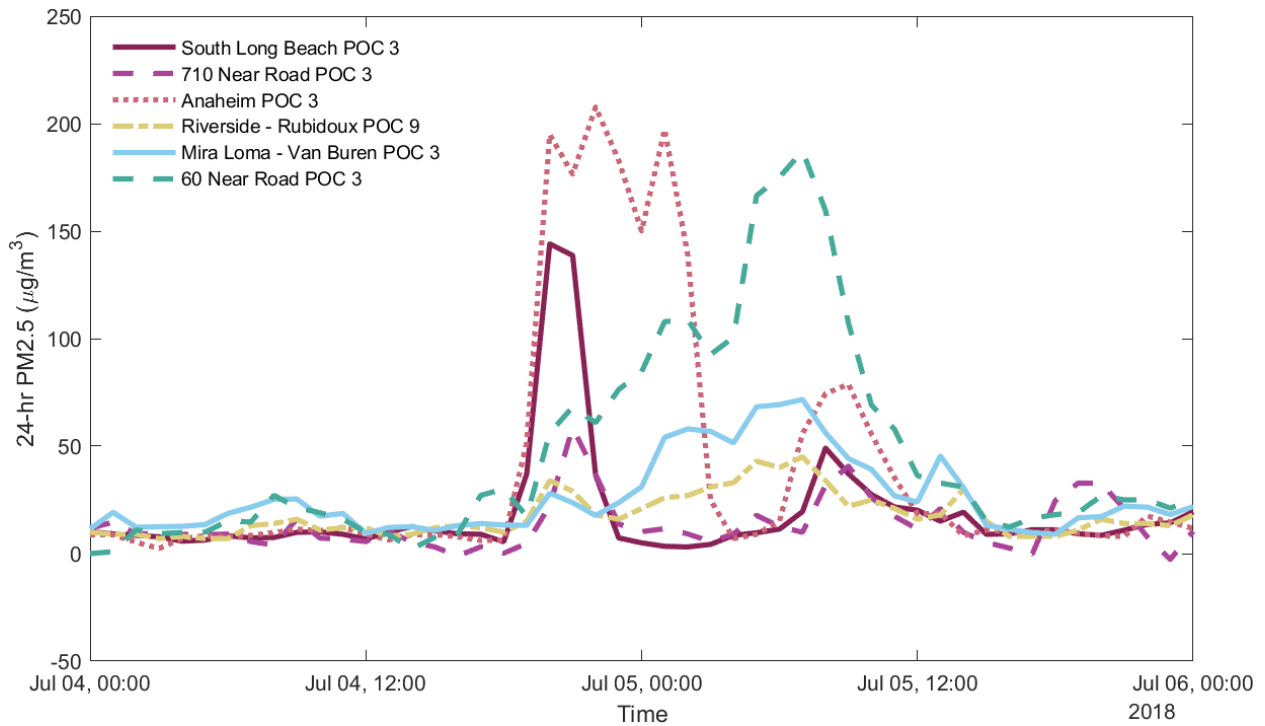
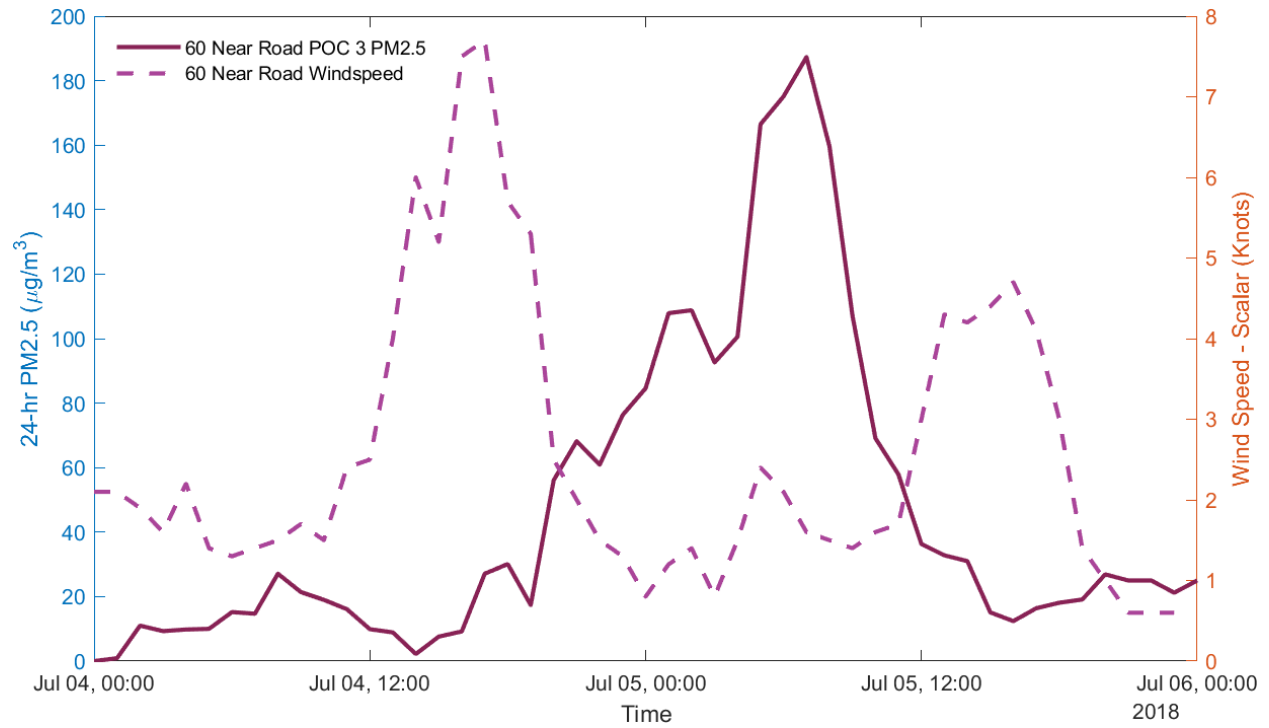


FIGURE II-7-24:
HYSPLIT BACK-TRAJECTORIES FROM 60 NEAR ROAD FOR JULY 4-5, 2018 OVERLAID ON A MAP OF THE SOUTH COAST AIR BASIN SHOWING RESIDENTIAL LAND USE (SHOWN IN GRAY).



**FIGURE II-7-26:
HOURLY TIME SERIES FOR JULY 4-5, 2018 FOR PM_{2.5} MONITORING STATIONS IN THE SOUTH COAST AIR BASIN.**

Figure II-7-27 through Figure II-7-29 show time series plots of PM_{2.5} (left axes) and windspeed (right axes) for the stations shown in Figure II-7-26 that have co-located wind data. The PM_{2.5} concentrations tend to be the highest during the periods with lowest windspeeds. This is consistent with elevated nearby emissions, such as fireworks and reflects the emission patterns of fireworks, which are typically used at nightfall.



**FIGURE II-7-27:
HOURLY PM2.5 AND WINDSPEED FOR JULY 4-5, 2018 AT THE 60 NEAR ROAD STATION.**

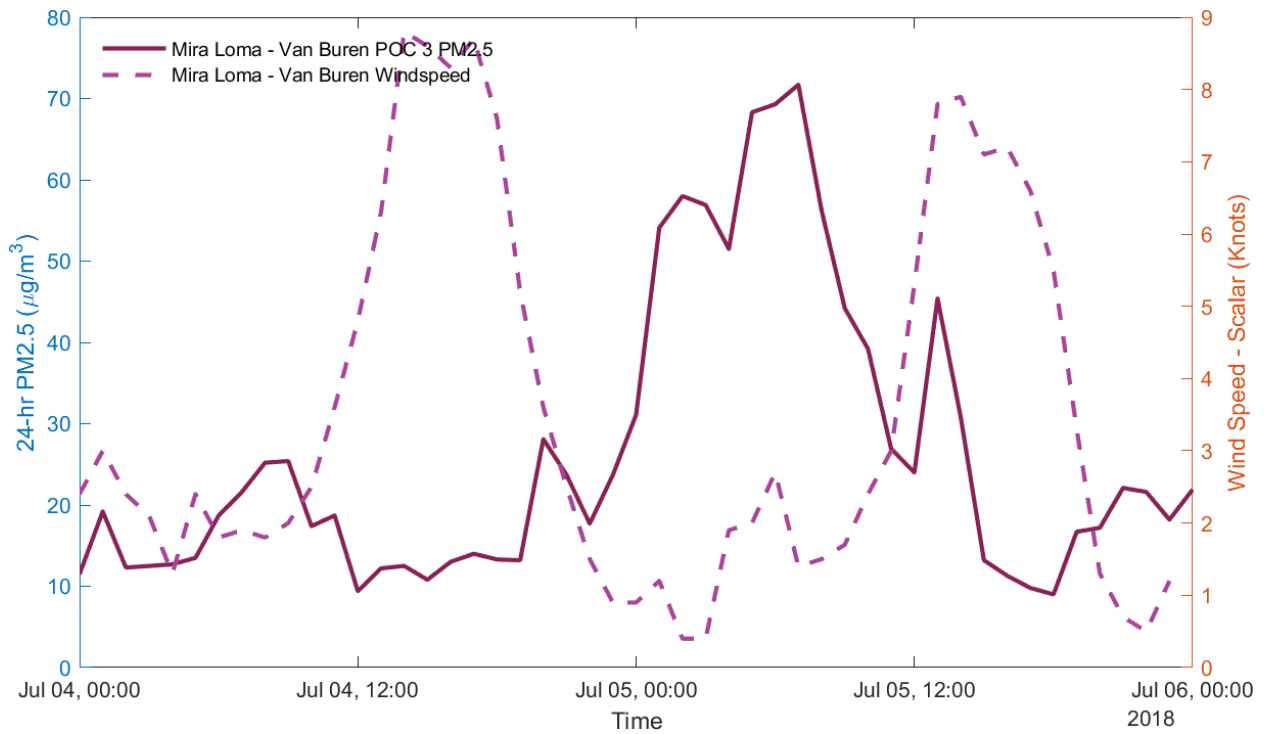
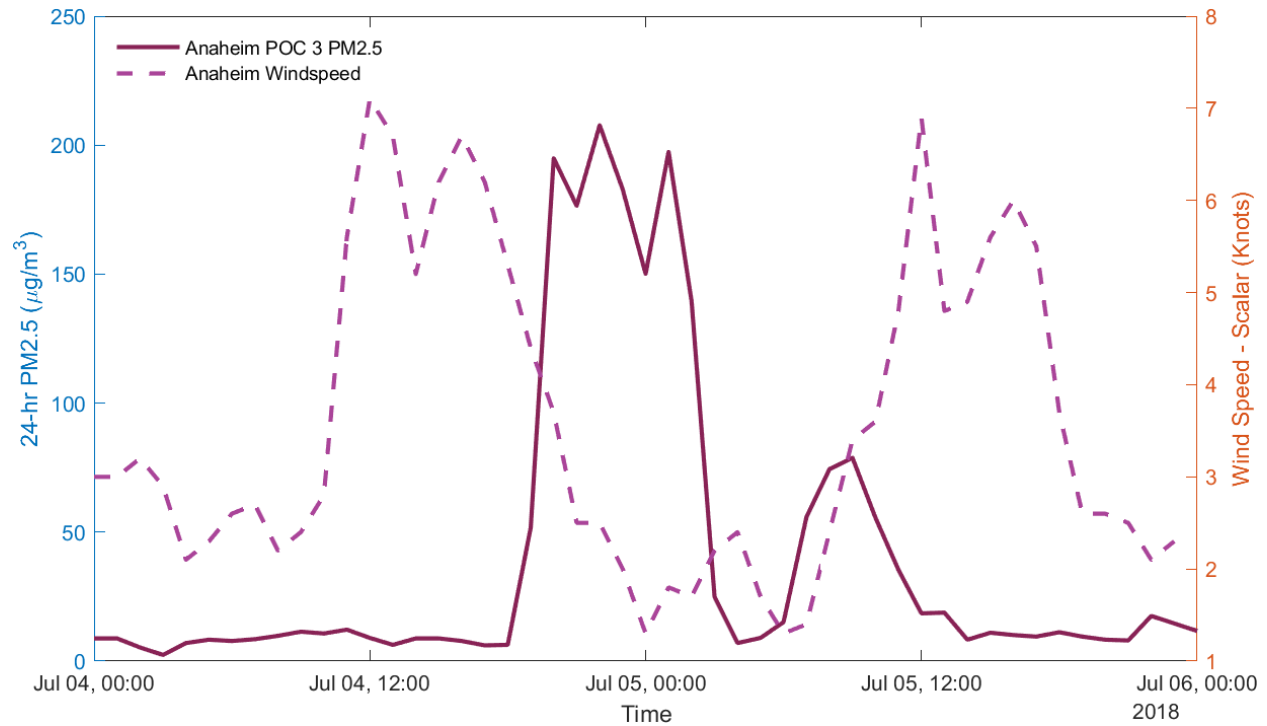


FIGURE II-7-28:
HOURLY PM2.5 AND WINDSPEED FOR JULY 4-5, 2018 AT THE MIRA LOMA – VAN BUREN STATION.



**FIGURE II-7-29:
HOURLY PM2.5 AND WINDSPEED FOR JULY 4-5, 2018 AT THE ANAHEIM STATION.**

Figure II-7-30 through Figure II-7-32 show scatter plots of PM2.5 versus hourly windspeed. This is the same data as shown in Figure II-7-27 through Figure II-7-29, except that the data are limited to 9 PM on July 4 through 5 PM on July 5, 2018 when we expect the greatest impacts from fireworks emissions. The NAAQS value (35 µg/m³) is shown as a horizontal line. Most PM2.5 measurements were below the NAAQS value whenever the winds were above approximately 5 knots, with the highest concentrations occurring at lower wind speeds. This pattern is consistent with elevated nearby emissions from fireworks accumulating to high concentrations during periods of lower ventilation and then diluting during periods of increased ventilation at higher windspeeds.

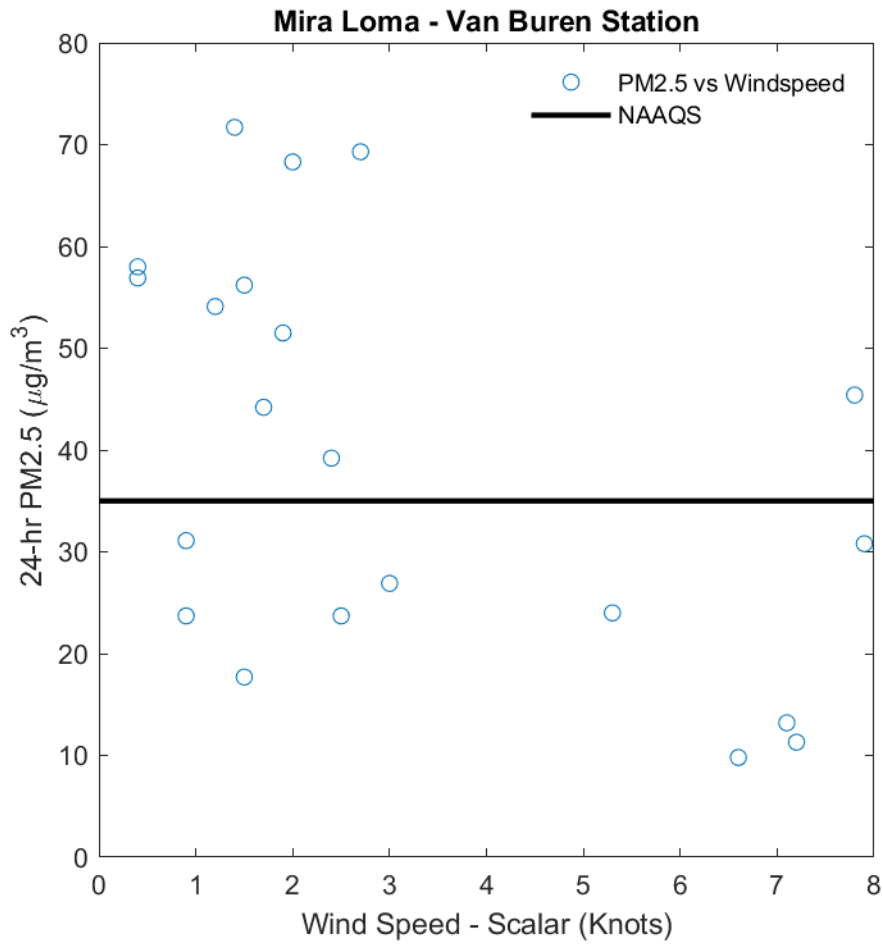


FIGURE II-7-31:
HOURLY PM2.5 VERSUS WINDSPEED FOR 9 PM ON JULY 4 THROUGH 5 PM ON JULY 5, 2018
AT THE MIRA LOMA – VAN BUREN STATION.

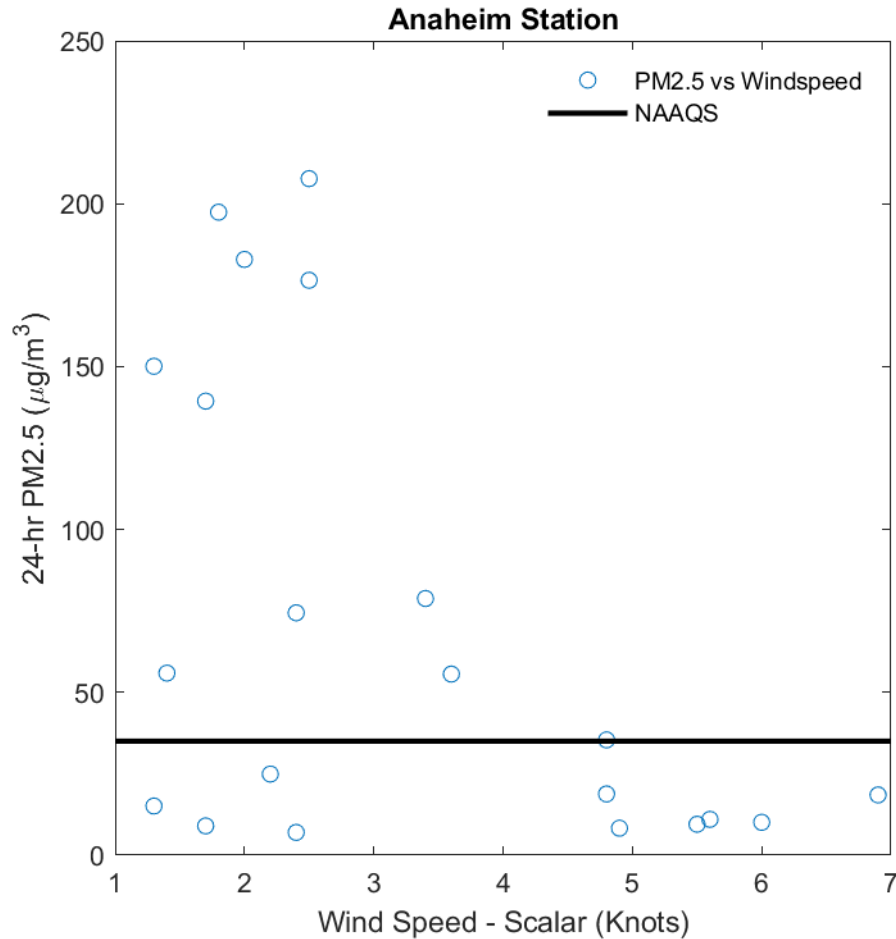


FIGURE II-7-32:
HOURLY PM2.5 VERSUS WINDSPEED FOR 9 PM ON JULY 4 THROUGH 5 PM ON JULY 5, 2018
AT THE ANAHEIM STATION.

Fireworks Summary for 2019-07-05

Residential land use (a proxy for fireworks emissions locations) and HYSPLIT back-trajectories using the NOAA HRRR meteorological model arriving at the 60 Near Road monitoring station for July 4-5, 2019 are shown in Figure II-7-33. All the back-trajectories originate over the Pacific Ocean and cross large residential areas of the South Coast Air Basin. Figure II-7-34 shows wind roses throughout the South Coast Air Basin for 9 PM on July 4 through 2 PM on July 5, 2019 using wind data from South Coast AQMD monitoring stations and local airports. The wind roses in Figure II-7-34 confirm the onshore wind pattern shown in the HYSPLIT back-trajectories in Figure II-7-33.

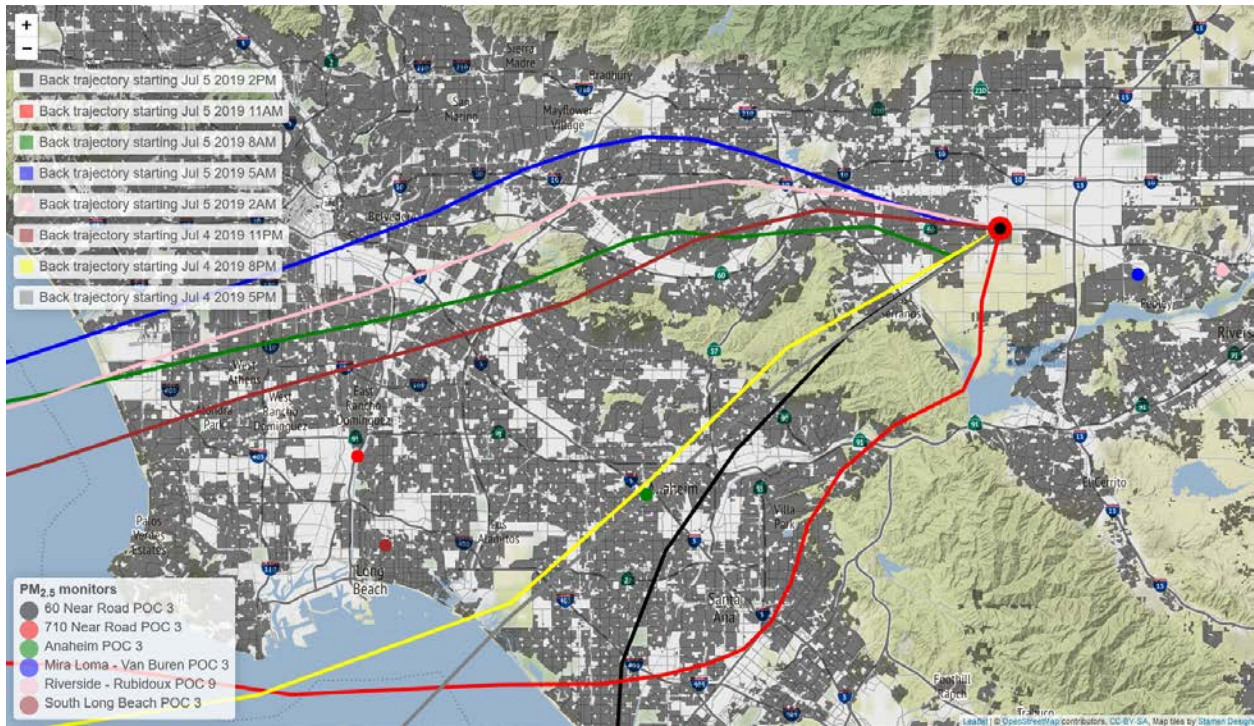


FIGURE II-7-33:
HYSPLIT BACK-TRAJECTORIES FROM 60 NEAR ROAD FOR JULY 4-5, 2019 OVERLAID ON A MAP OF THE SOUTH COAST AIR BASIN SHOWING RESIDENTIAL LAND USE (SHOWN IN GRAY).

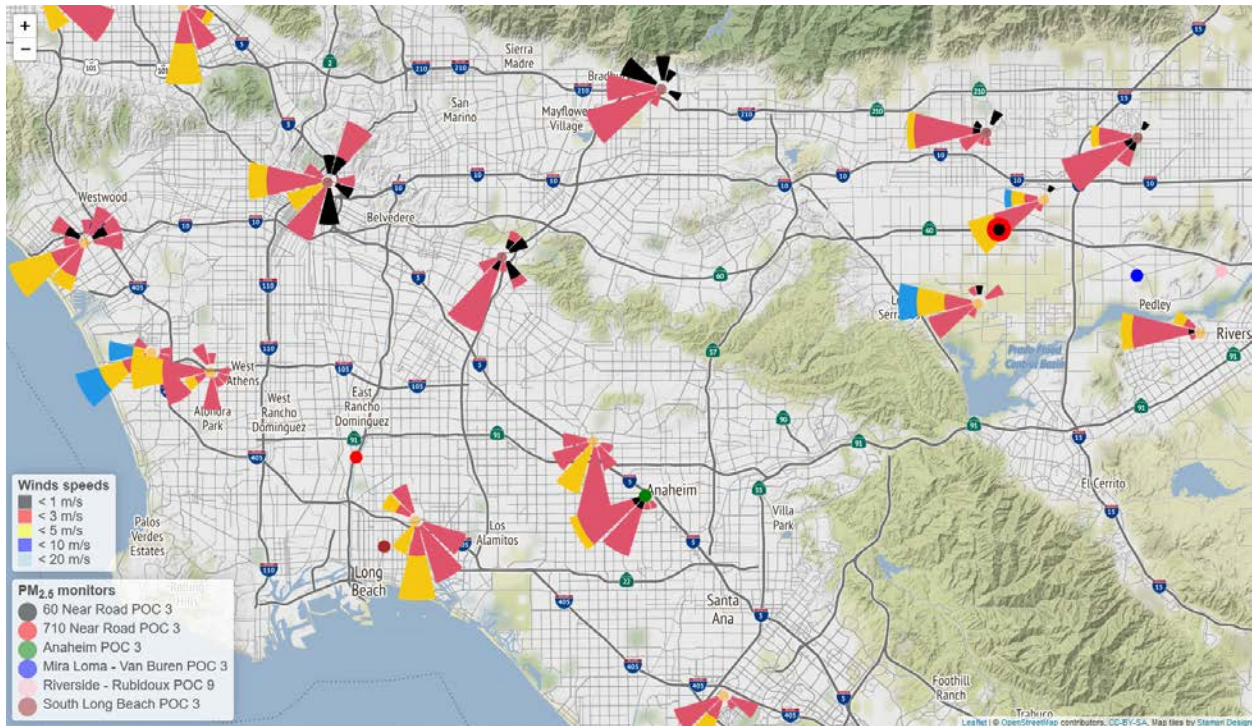
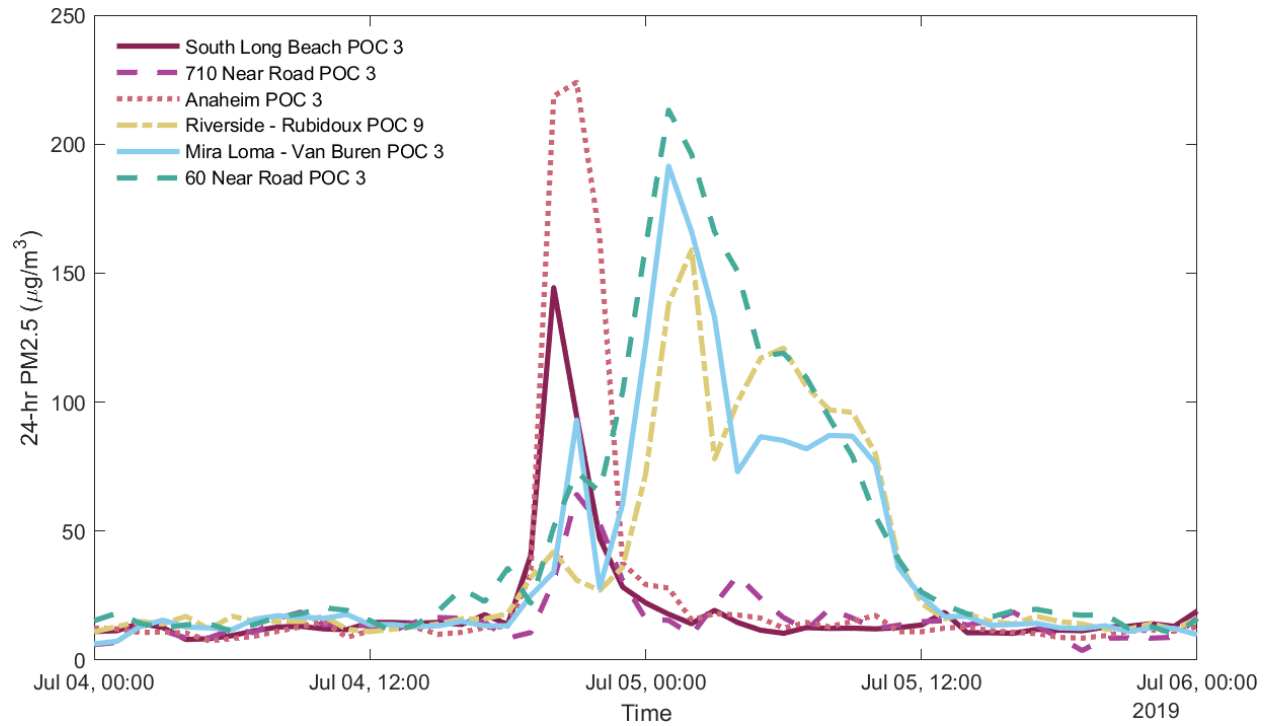


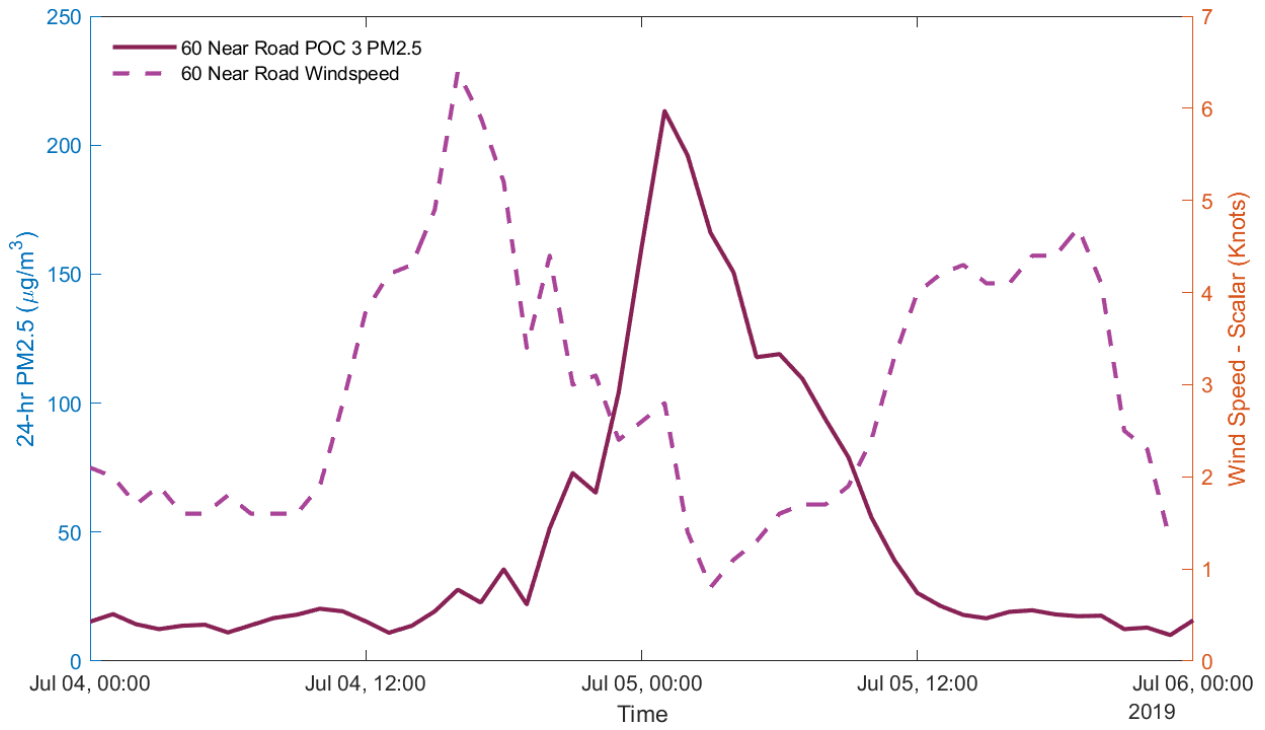
FIGURE II-7-34:
WIND ROSES FOR 9 PM ON JULY 4 THROUGH 2 PM ON JULY 5, 2019 THROUGHOUT THE SOUTH COAST AIR BASIN.

Figure II-7-35 shows time series plots of hourly PM_{2.5} data at selected stations with continuous PM_{2.5} instruments within the South Coast Air Basin for July 4-5, 2019. The concentrations peak at stations closer to the coast earlier than in inland areas (see Figure II-7-33 for monitor locations). This is consistent with the combination of 1) extensive fireworks use across the Basin, especially the most populated areas closer to the coast and 2) the dominant onshore flow that transports these emissions inland. The inland areas have local emissions as well as transported emissions from upwind areas.



**FIGURE II-7-35:
HOURLY TIME SERIES FOR JULY 4-5, 2019 FOR PM_{2.5} MONITORING STATIONS IN THE SOUTH COAST AIR BASIN.**

Figure II-7-36 through Figure II-7-39 show time series plots of PM_{2.5} (left axes) and windspeed (right axes) for the stations shown in Figure II-7-35 that have co-located wind data. The PM_{2.5} concentrations tend to be the highest during the periods with lowest windspeeds. This is consistent with elevated nearby emissions, such as fireworks and reflects the emission patterns of fireworks, which are typically used at nightfall.



**FIGURE II-7-36:
HOURLY PM2.5 AND WINDSPEED FOR JULY 4-5, 2019 AT THE 60 NEAR ROAD STATION.**

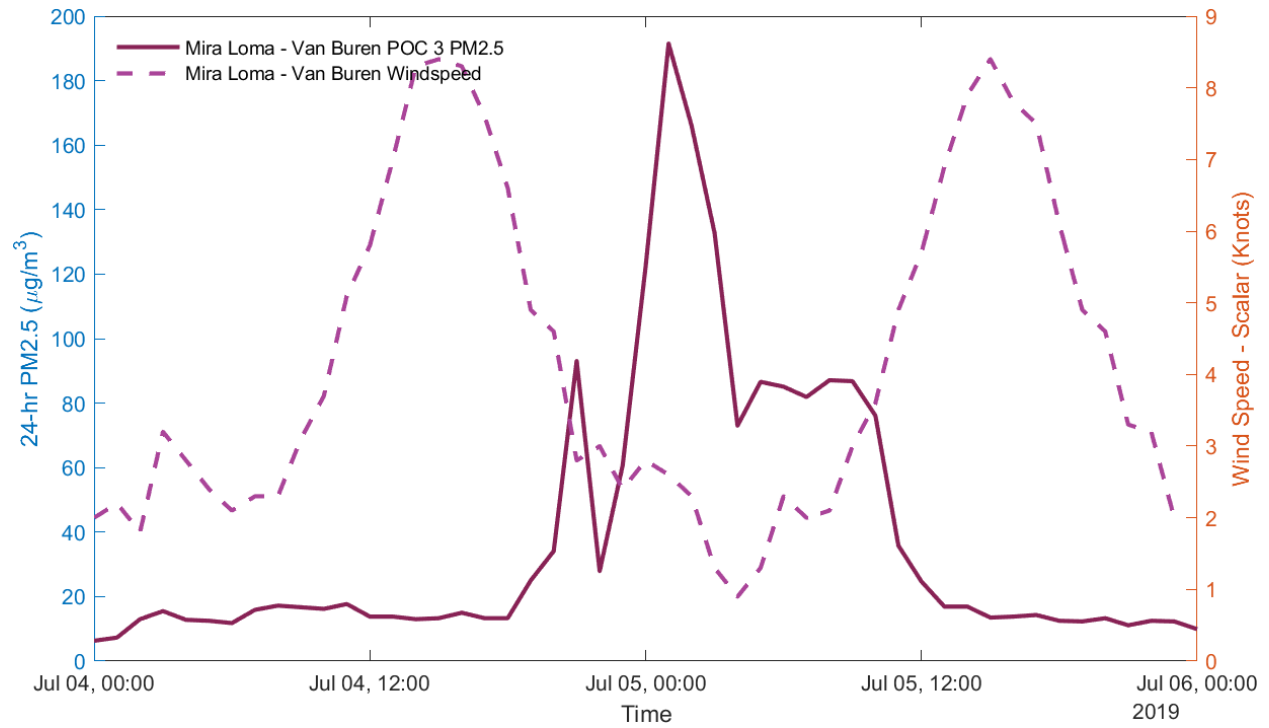


**FIGURE II-7-37:
HOURLY PM2.5 AND WINDSPEED FOR JULY 4-5, 2019 AT THE MIRA LOMA – VAN BUREN
STATION.**

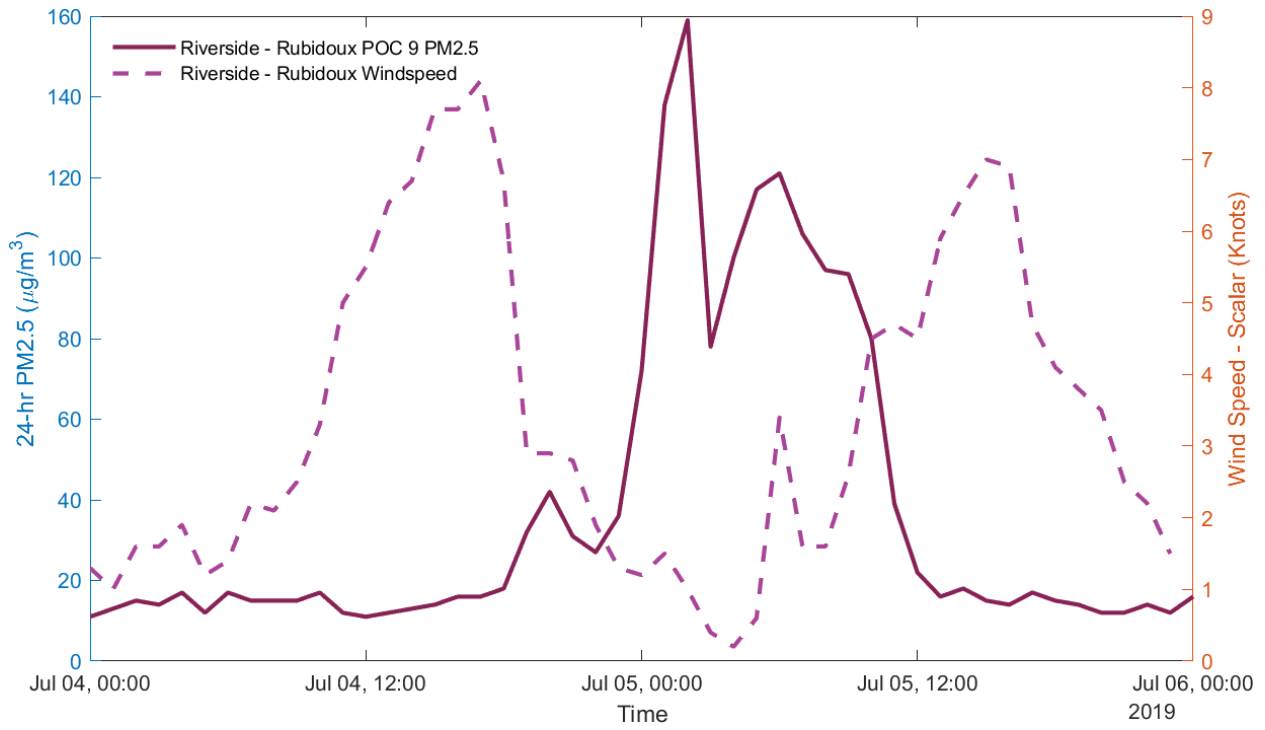


**FIGURE II-7-38:
HOURLY PM2.5 AND WINDSPEED FOR JULY 4-5, 2019 AT THE RIVERSIDE - RUBIDOUX
STATION.**

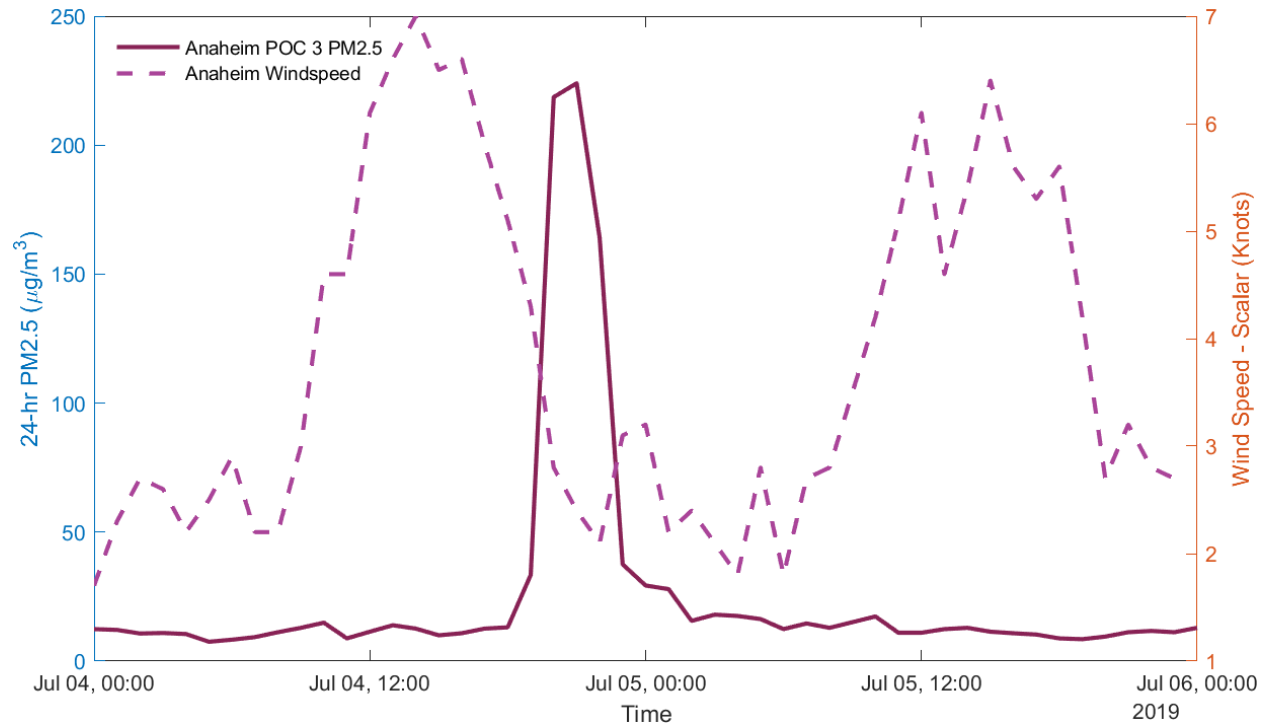


**FIGURE II-7-39:
HOURLY PM_{2.5} AND WINDSPEED FOR JULY 4-5, 2019 AT THE ANAHEIM STATION.**

Figure II-7-40 through Figure II-7-43 show scatter plots of PM_{2.5} versus hourly windspeed. This is the same data as shown in Figure II-7-36 through Figure II-7-39, except that the data are limited to 9 PM on July 4 through 5 PM on July 5, 2019 when we expect the greatest impacts from fireworks emissions. The NAAQS value (35 µg/m³) is shown as a horizontal line. Most PM_{2.5} measurements were below the NAAQS value whenever the winds were above approximately 5 knots, with the highest concentrations occurring at lower wind speeds. This pattern is consistent with elevated nearby emissions from fireworks accumulating to high concentrations during periods of lower ventilation and then diluting during periods of increased ventilation at higher windspeeds.

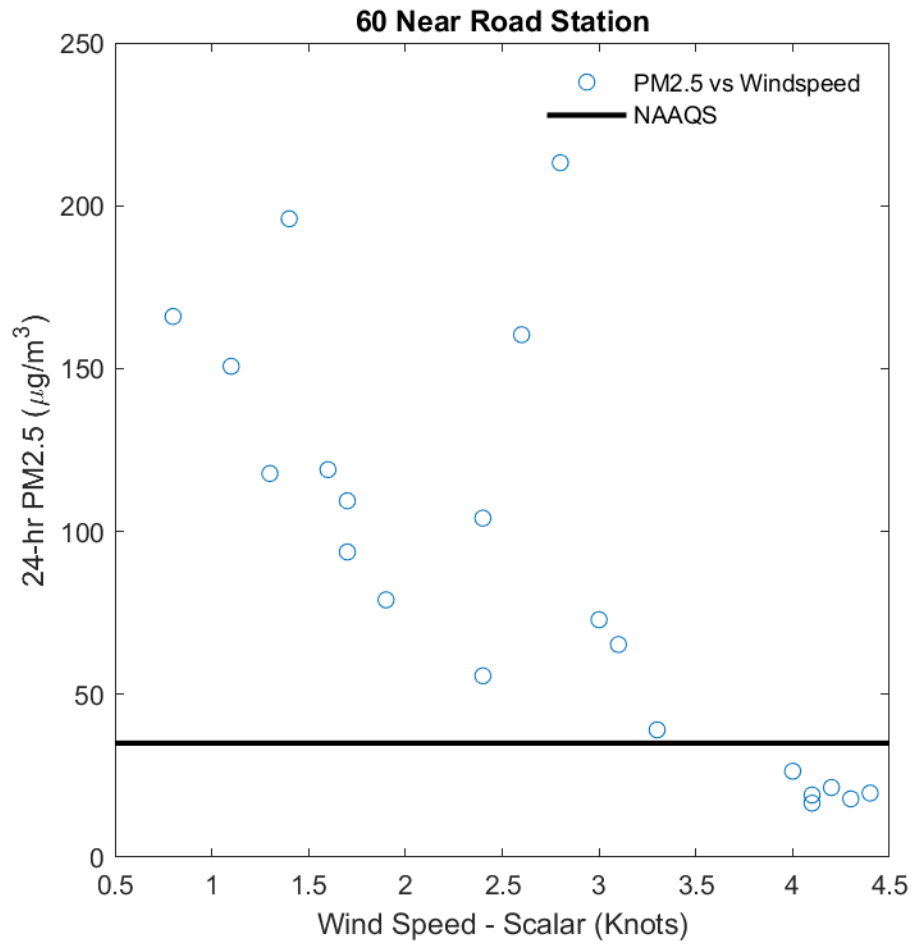


FIGURE II-7-40:
HOURLY PM2.5 VERSUS WINDSPEED FOR 9 PM ON JULY 4 THROUGH 5 PM ON JULY 5, 2019
AT THE 60 NEAR ROAD STATION.

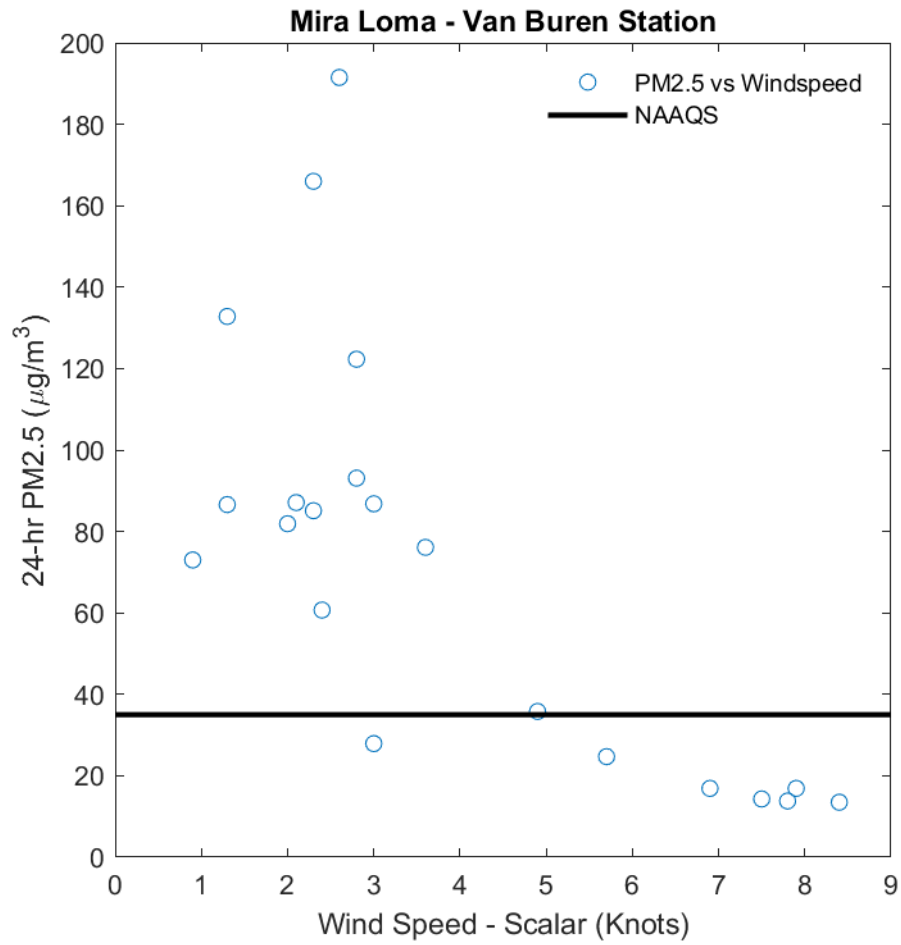


FIGURE II-7-41:
HOURLY PM2.5 VERSUS WINDSPEED FOR 9 PM ON JULY 4 THROUGH 5 PM ON JULY 5, 2019
AT THE MIRA LOMA – VAN BUREN STATION.

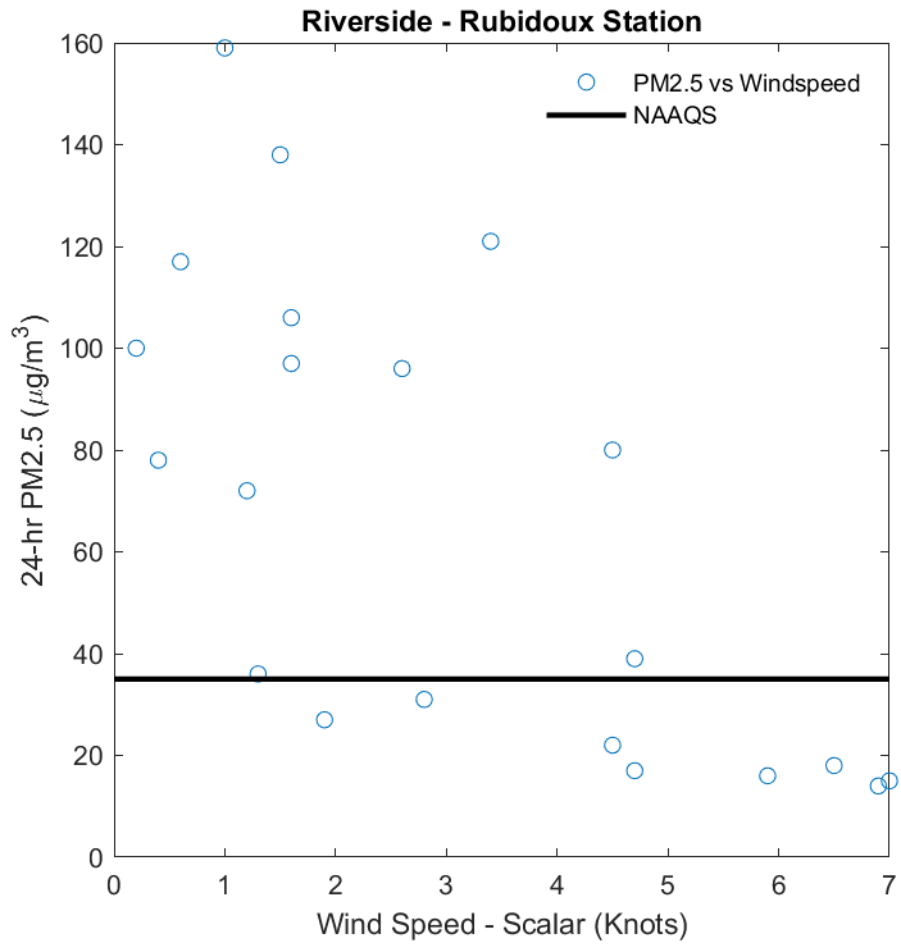
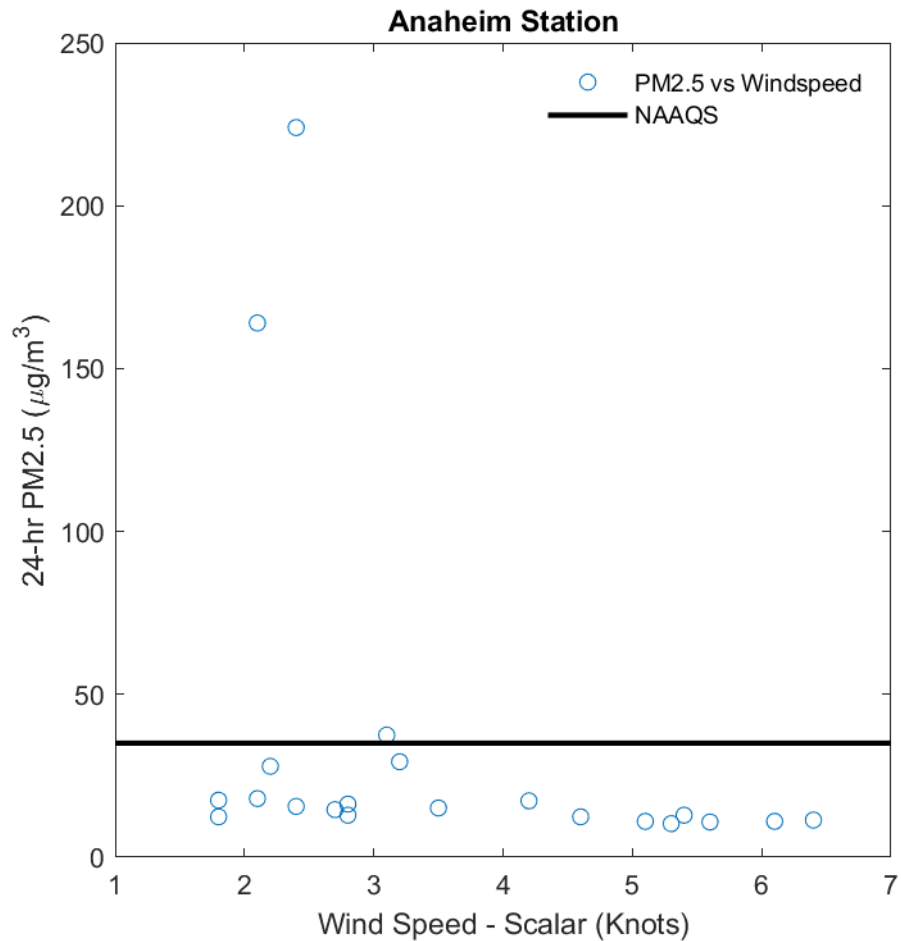


FIGURE II-7-42:
HOURLY PM2.5 VERSUS WINDSPEED FOR 9 PM ON JULY 4 THROUGH 5 PM ON JULY 5, 2019
AT THE RIVERSIDE - RUBIDOUX STATION.



**FIGURE II-7-43:
HOURLY PM2.5 VERSUS WINDSPEED FOR 9 PM ON JULY 4 THROUGH 5 PM ON JULY 5, 2019
AT THE ANAHEIM STATION.**

Conclusion

South Coast AQMD posits that the 24-hour PM2.5 exceedances listed in Table II-7-1 in this report qualify for exclusion for analyses estimating base and future year design values for the PM2.5 attainment demonstration because the ambient data are not representative to characterize base period concentrations (see Table 1 of U.S. EPA, 2019). The annual fireworks emissions during Independence Day celebrations throughout the South Coast Air Basin impacting PM2.5 concentrations on July 4-5 are atypical, extreme, and unrepresentative events compared to typical summer days.

Attachment 1

WRF MODEL PERFORMANCE TIME SERIES

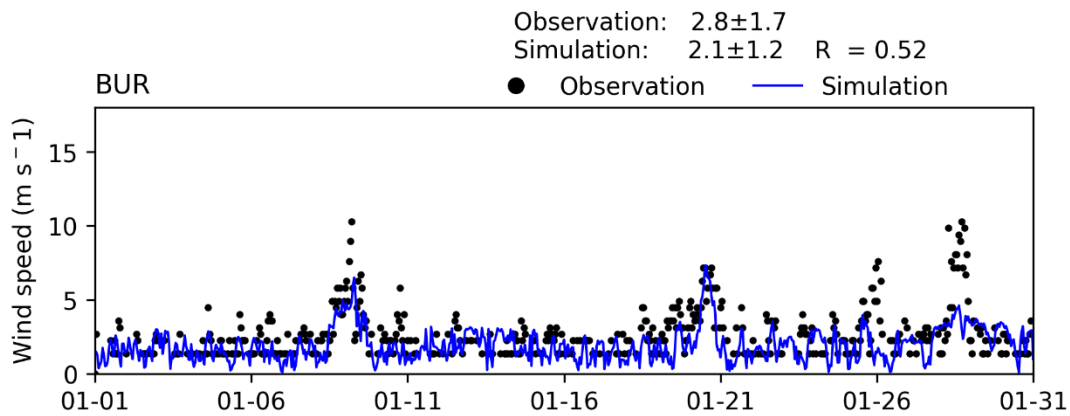
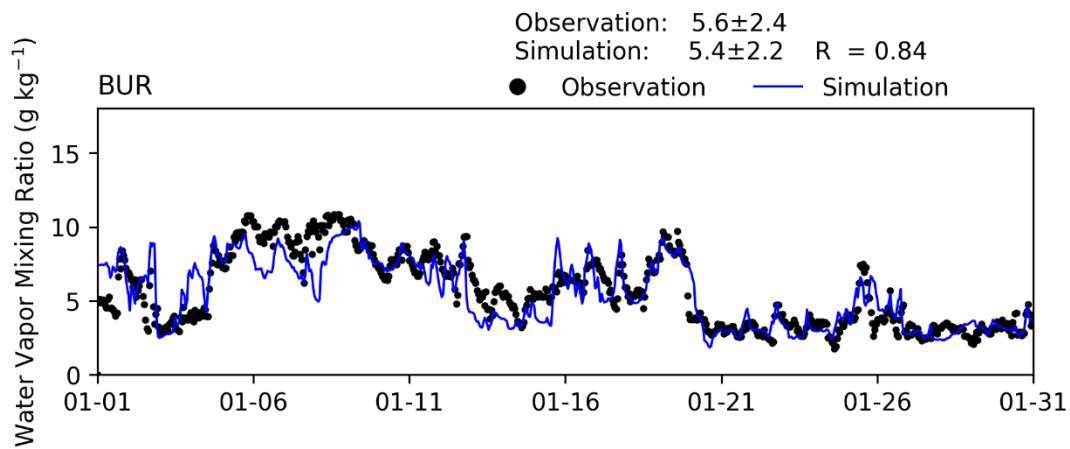
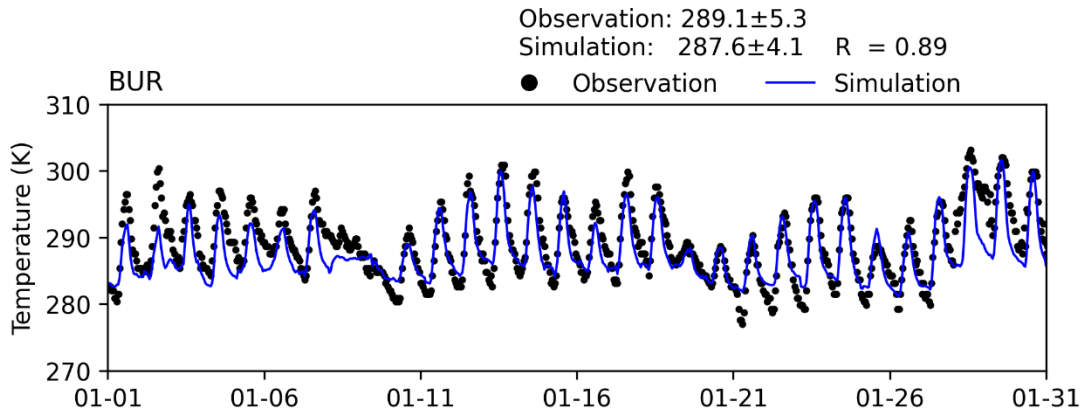


FIGURE V-A1
TIME SERIES OF HOURLY MEASUREMENTS AND WRF SIMULATIONS AT BURBANK AIRPORT (BUR) FOR
JANUARY 2018

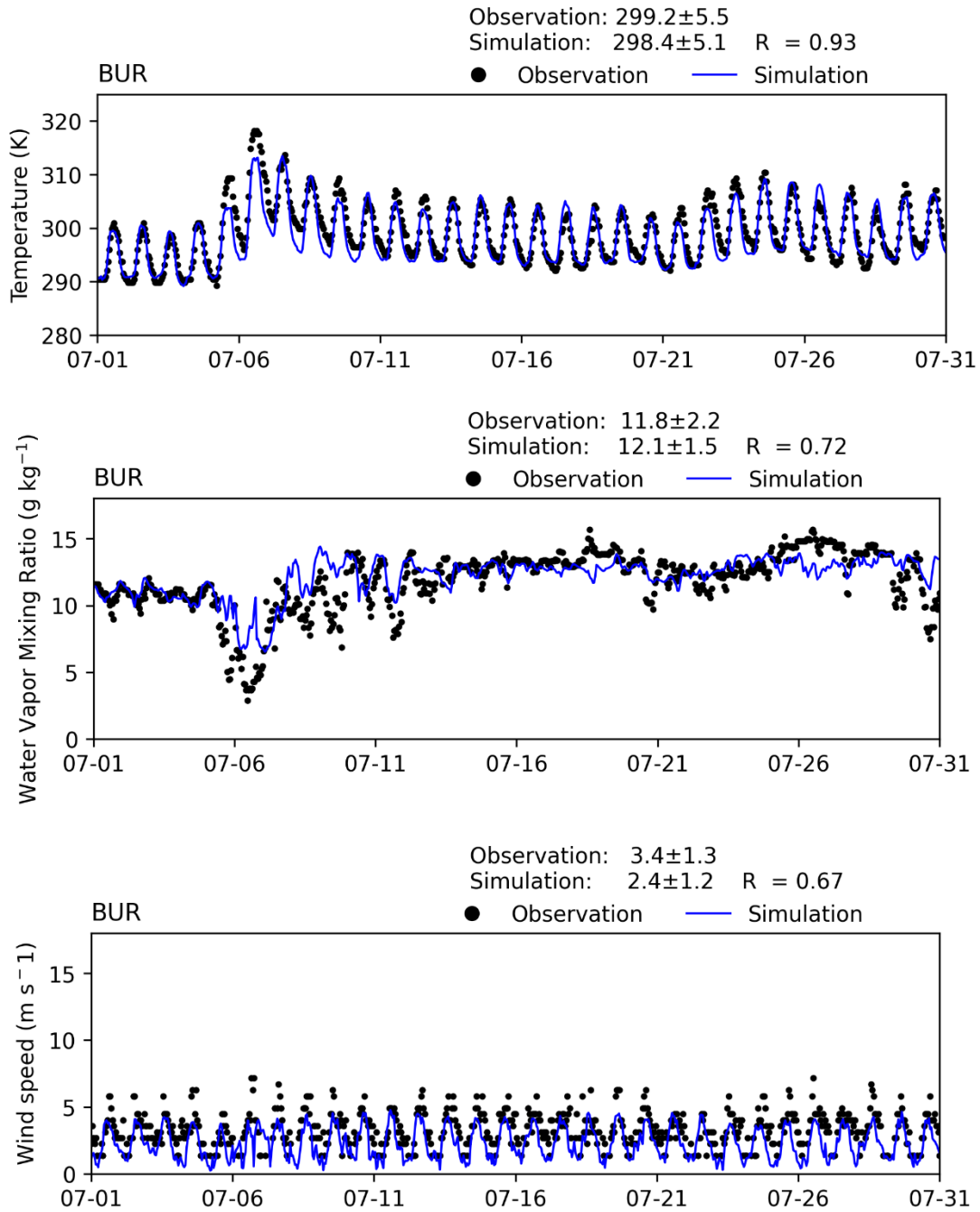


FIGURE V-A2
TIME SERIES OF HOURLY MEASUREMENTS AND WRF SIMULATIONS AT BURBANK AIRPORT (BUR) FOR JULY 2018

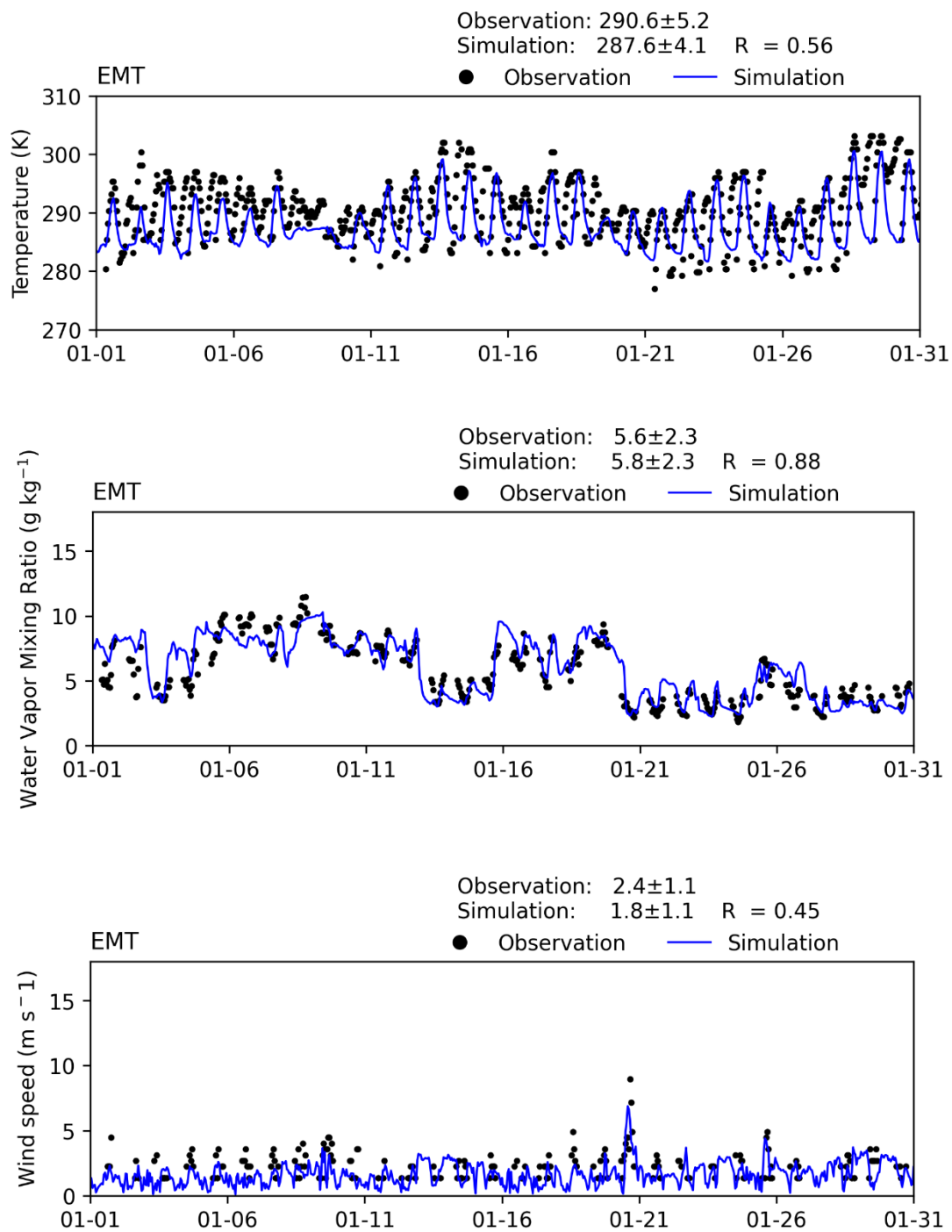


FIGURE V-A3
TIME SERIES OF HOURLY MEASUREMENTS AND WRF SIMULATIONS AT EI MONTE (EMT) FOR JANUARY 2018

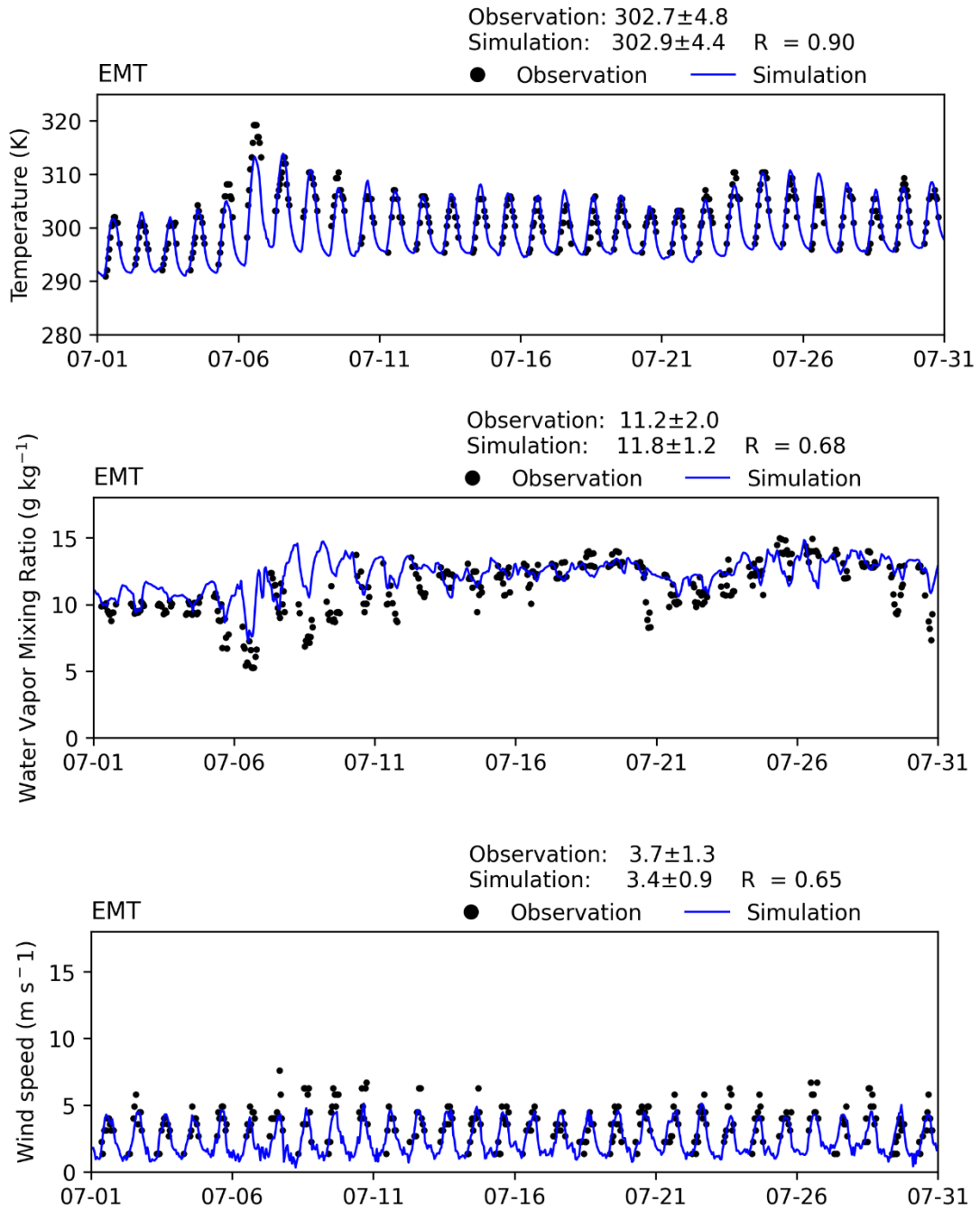


FIGURE V-A4
TIME SERIES OF HOURLY MEASUREMENTS AND WRF SIMULATIONS AT EI MONTE (EMT) FOR JULY 2018

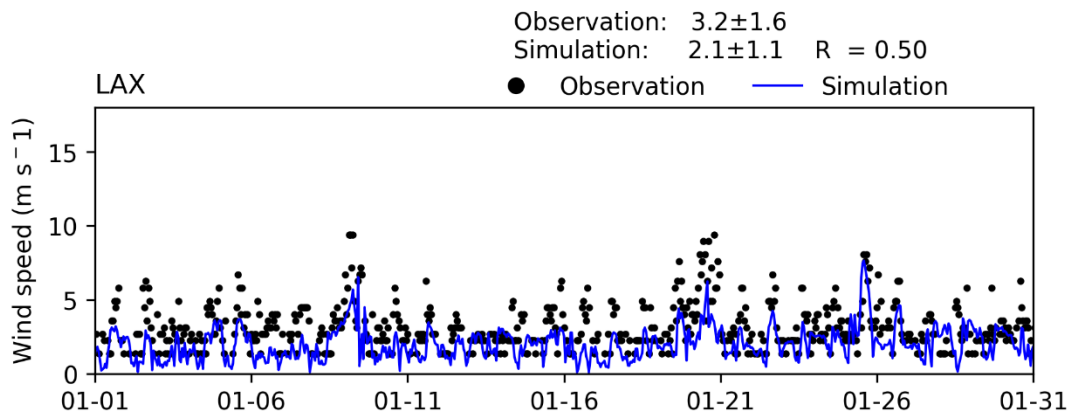
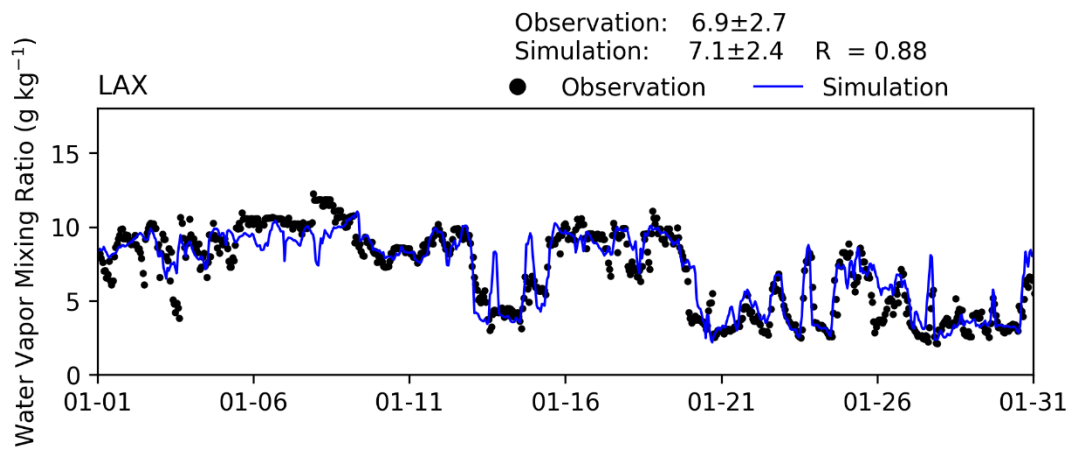
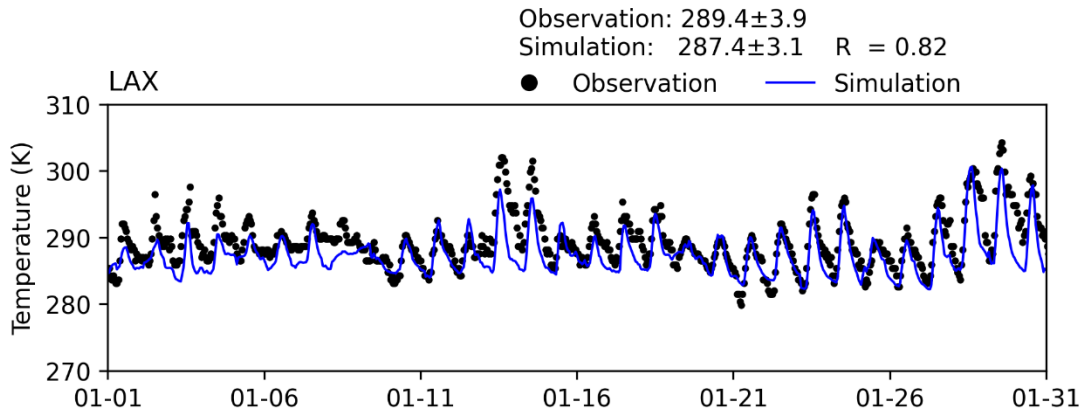


FIGURE V-A5
TIME SERIES OF HOURLY MEASUREMENTS AND WRF SIMULATIONS AT LOS ANGELES AIRPORT (LAX)
FOR JANUARY 2018

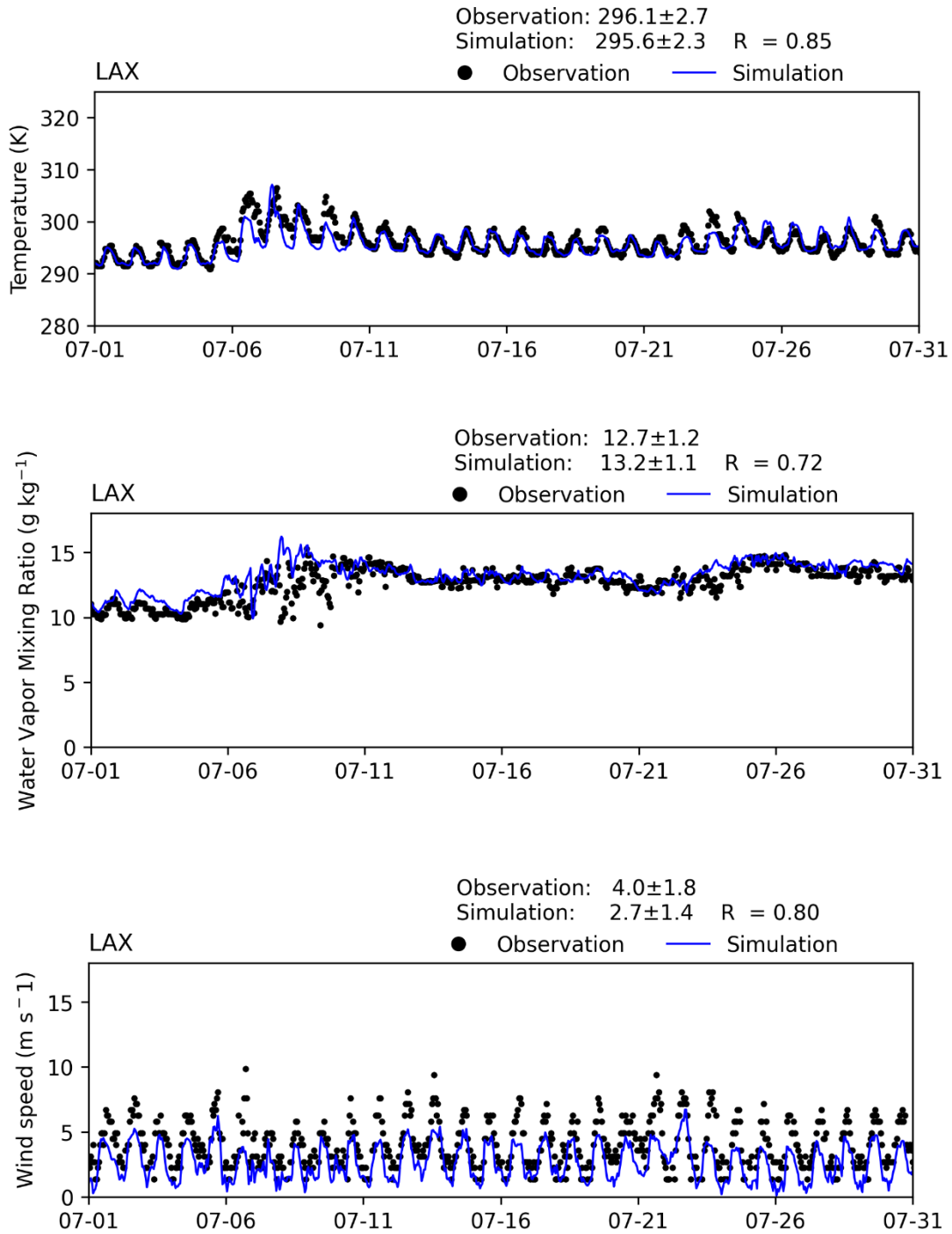


FIGURE V-A6
TIME SERIES OF HOURLY MEASUREMENTS AND WRF SIMULATIONS AT LOS ANGELES AIRPORT (LAX)
FOR JULY 2018

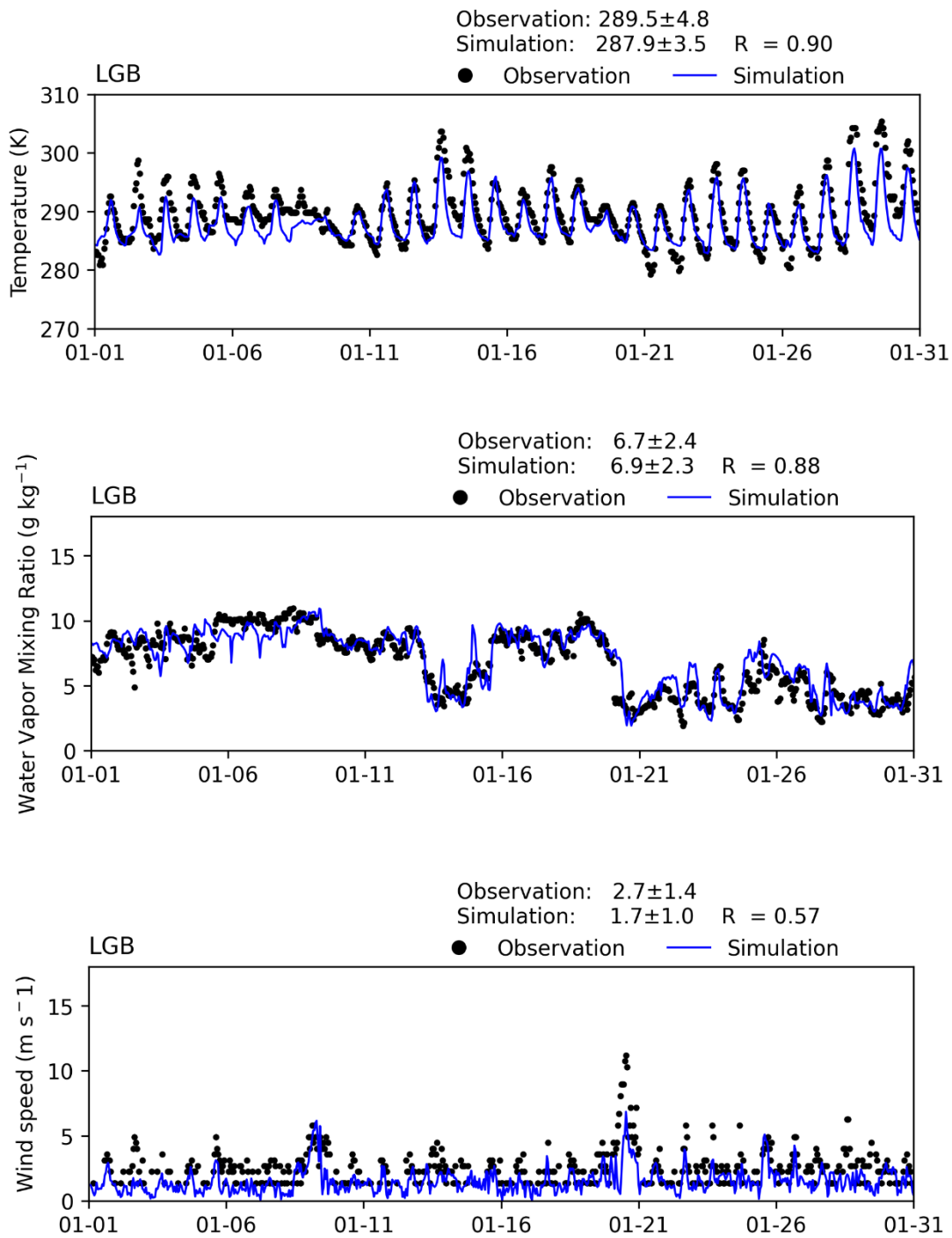


FIGURE V-A7
TIME SERIES OF HOURLY MEASUREMENTS AND WRF SIMULATIONS AT LONG BEACH AIRPORT (LGB)
FOR JANUARY 2018

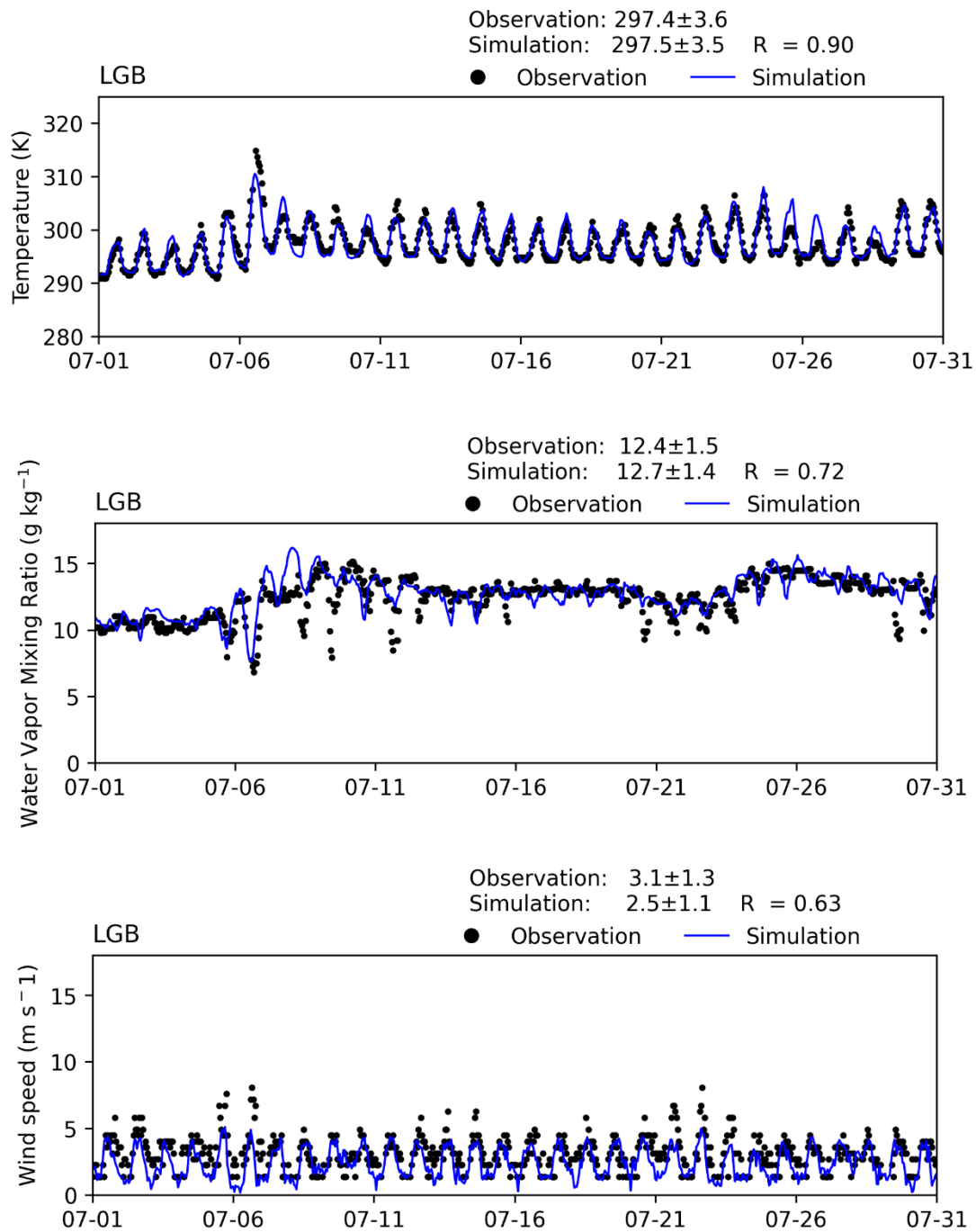


FIGURE V-A8
TIME SERIES OF HOURLY MEASUREMENTS AND WRF SIMULATIONS AT LONG BEACH AIRPORT (LGB)
FOR JULY 2018

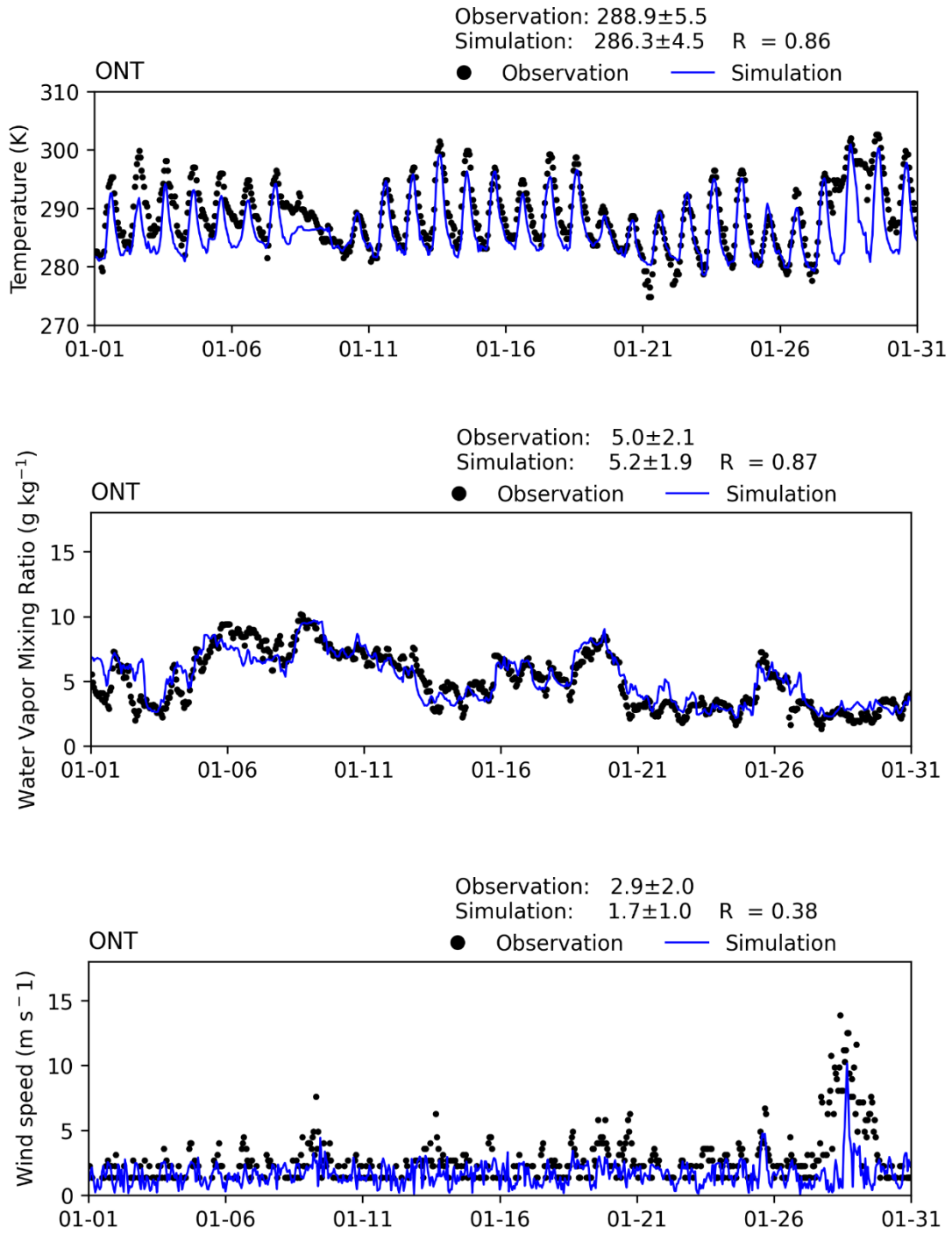


FIGURE V-A9
TIME SERIES OF HOURLY MEASUREMENTS AND WRF SIMULATIONS AT ONTARIO INTERNATIONAL AIRPORT (ONT) FOR JANUARY 2018

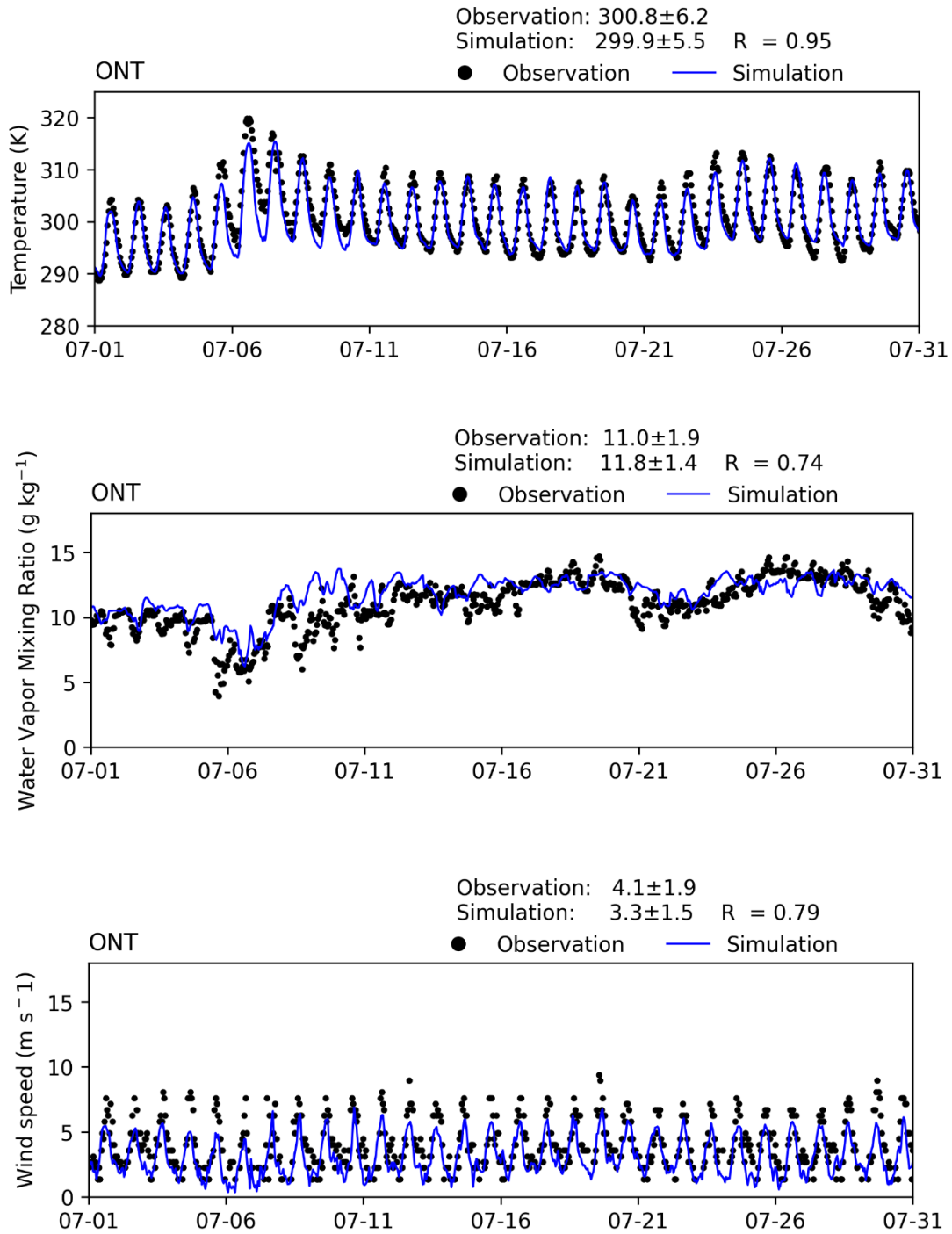


FIGURE V-A10
TIME SERIES OF HOURLY MEASUREMENTS AND WRF SIMULATIONS AT ONTARIO INTERNATIONAL AIRPORT (ONT) FOR JULY 2018

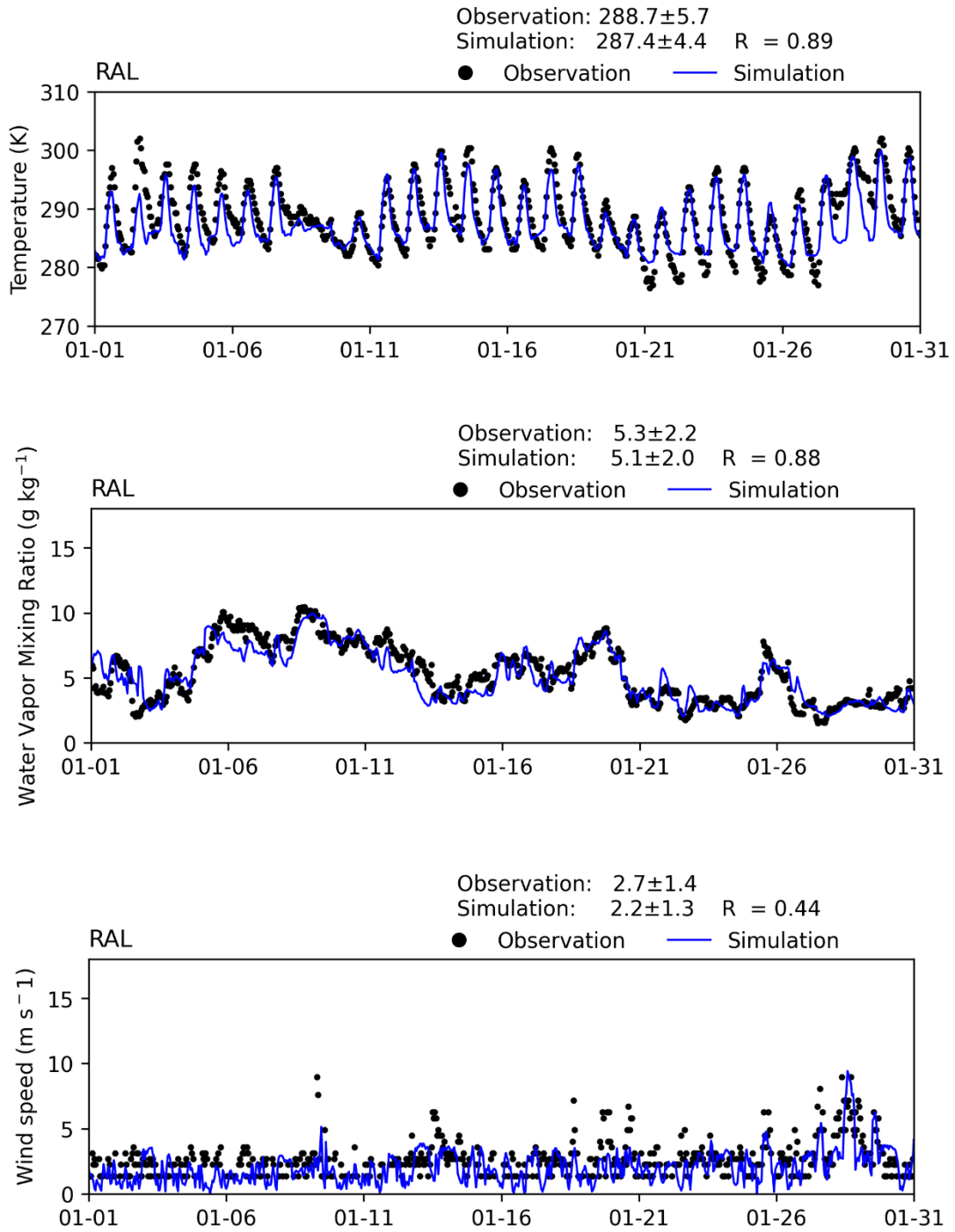


FIGURE V-A11
TIME SERIES OF HOURLY MEASUREMENTS AND WRF SIMULATIONS AT RIVERSIDE MUNICIPAL AIRPORT (RAL) FOR JANUARY 2018

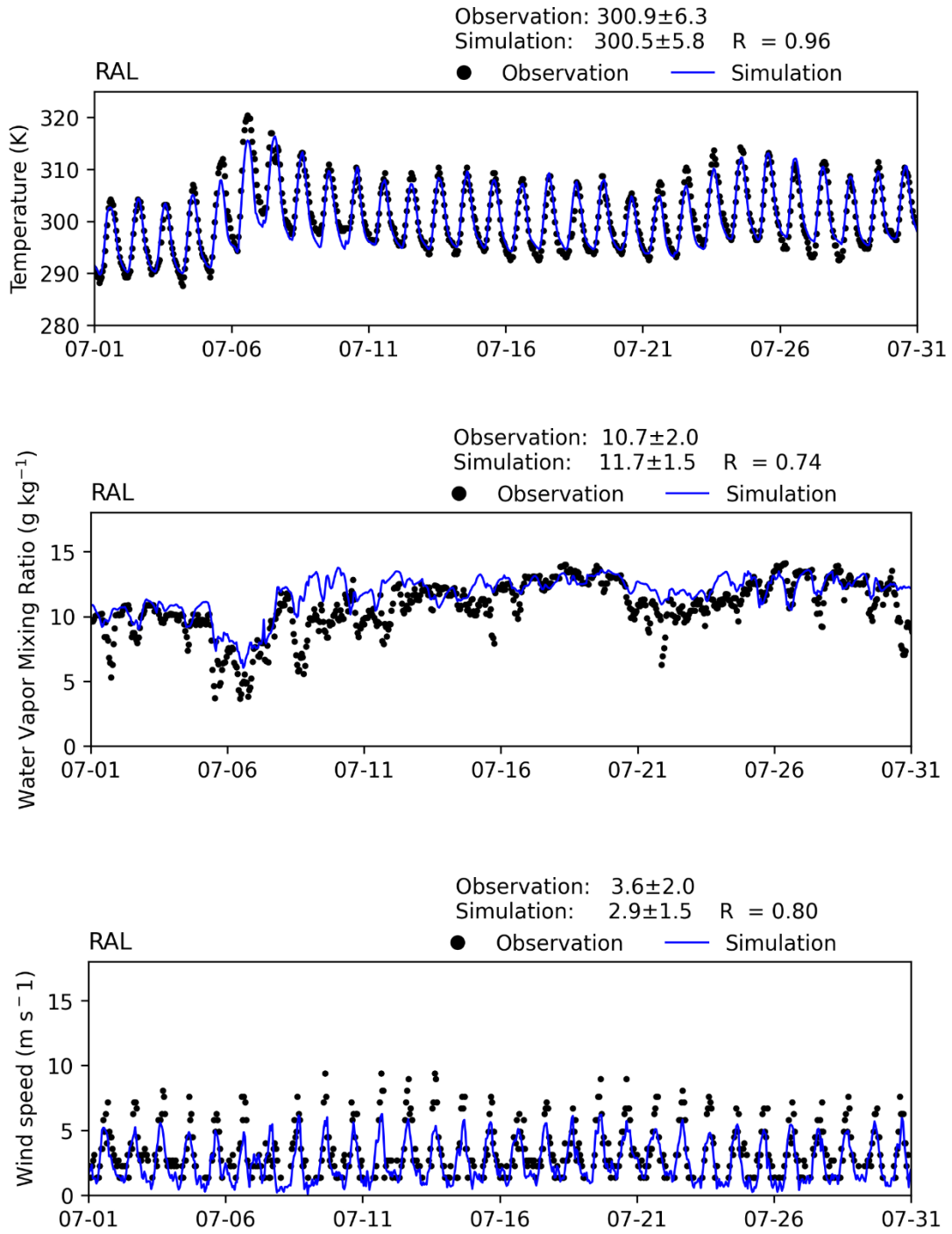


FIGURE V-A12
TIME SERIES OF HOURLY MEASUREMENTS AND WRF SIMULATIONS AT RIVERSIDE MUNICIPAL AIRPORT (RAL) FOR JULY 2018

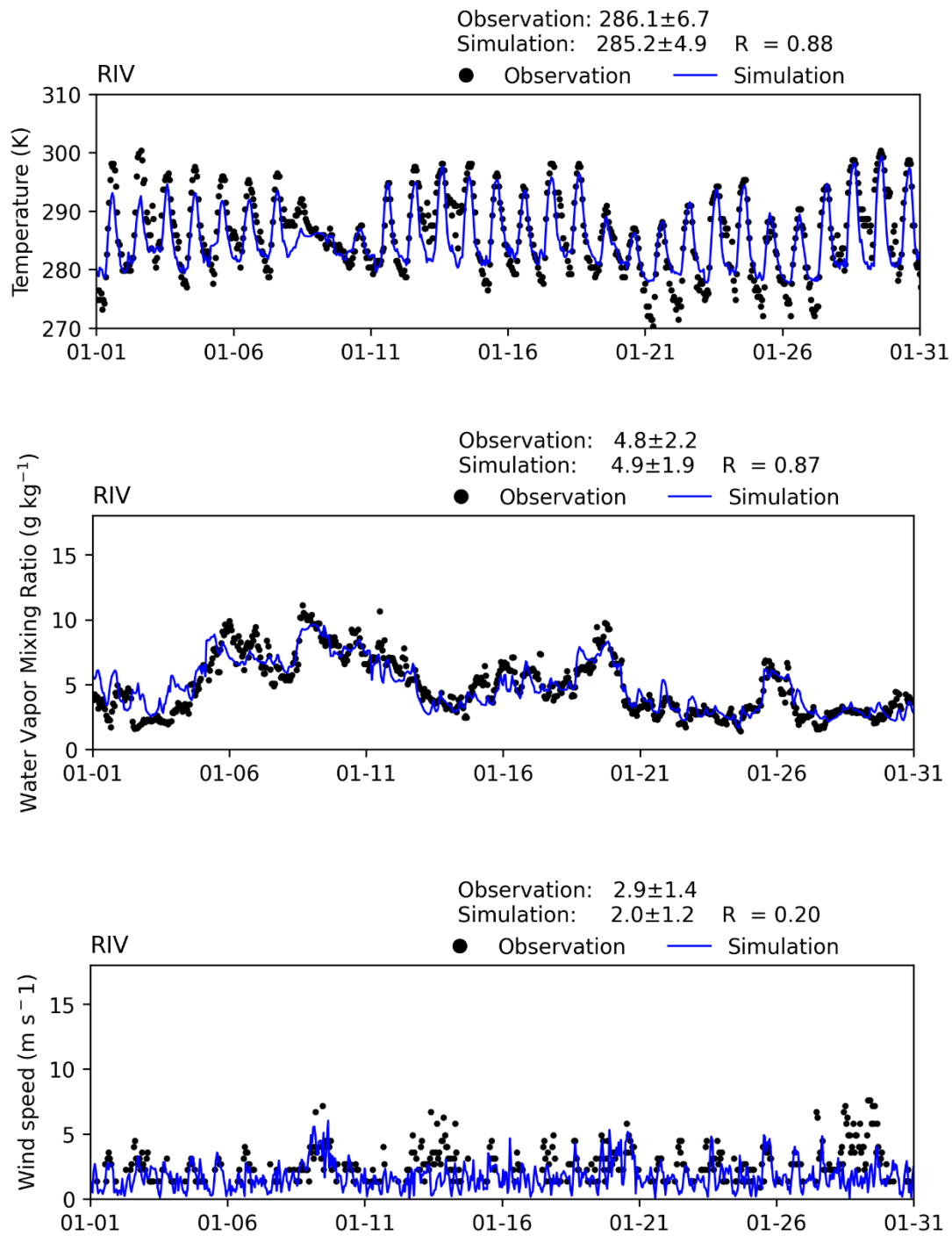


FIGURE V-A13
TIME SERIES OF HOURLY MEASUREMENTS AND WRF SIMULATIONS AT MARCH AIR RESERVE AIRPORT (RIV) FOR JANUARY 2018

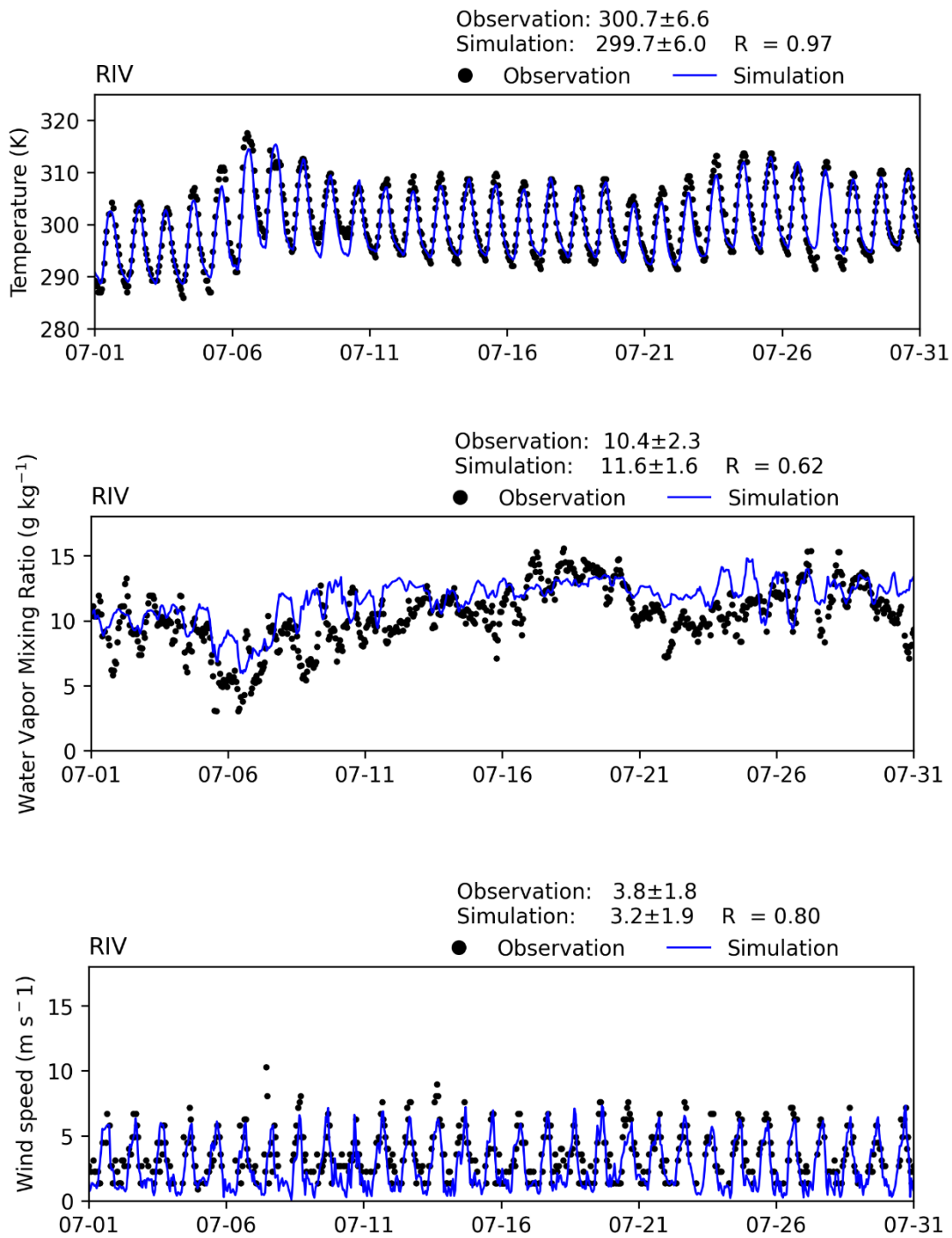


FIGURE V-A14
TIME SERIES OF HOURLY MEASUREMENTS AND WRF SIMULATIONS AT MARCH AIR RESERVE AIRPORT (RIV) FOR JULY 2018

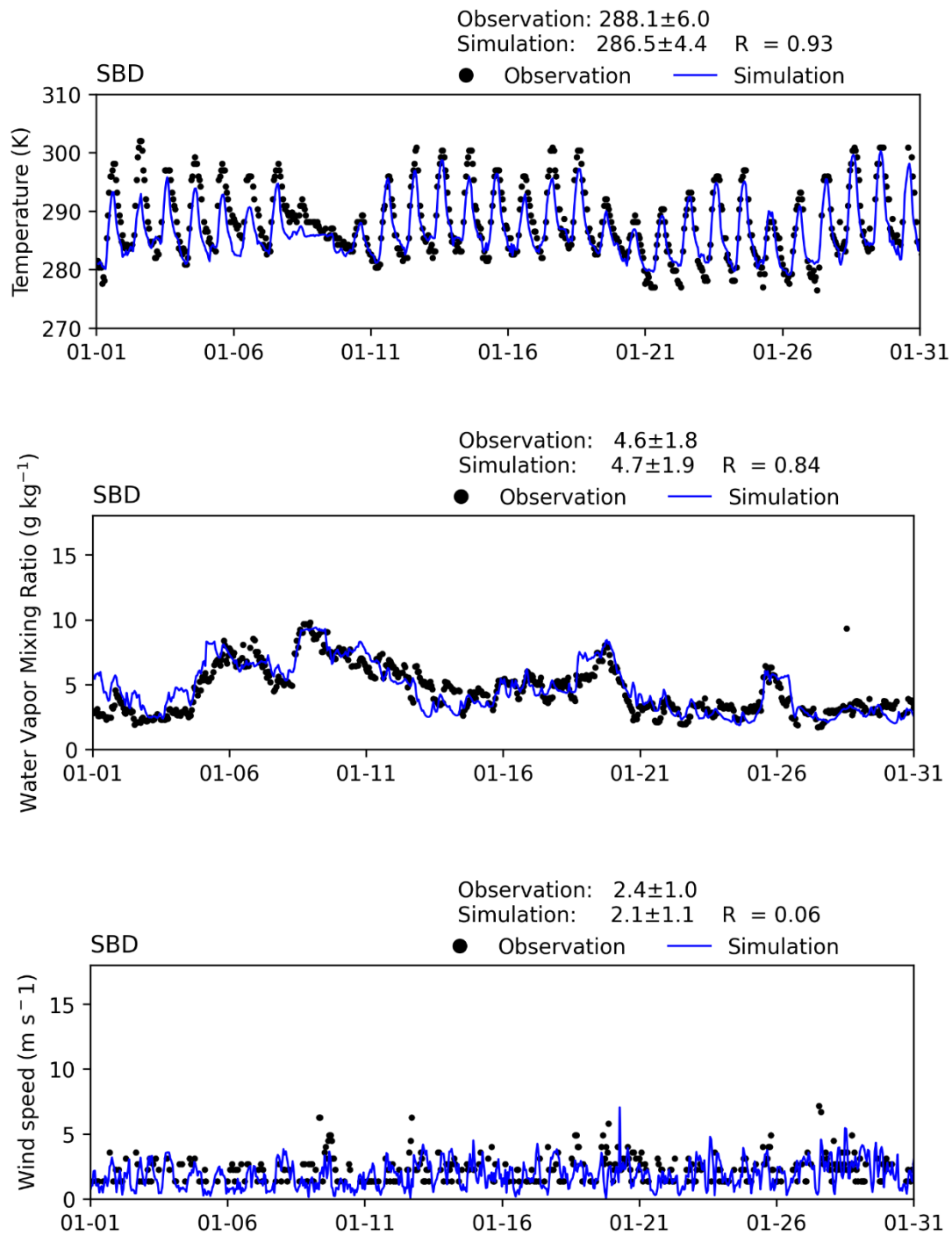


FIGURE V-A15
TIME SERIES OF HOURLY MEASUREMENTS AND WRF SIMULATIONS AT SAN BERNARDINO INTERNATIONAL AIRPORT (SBD) FOR JANUARY 2018

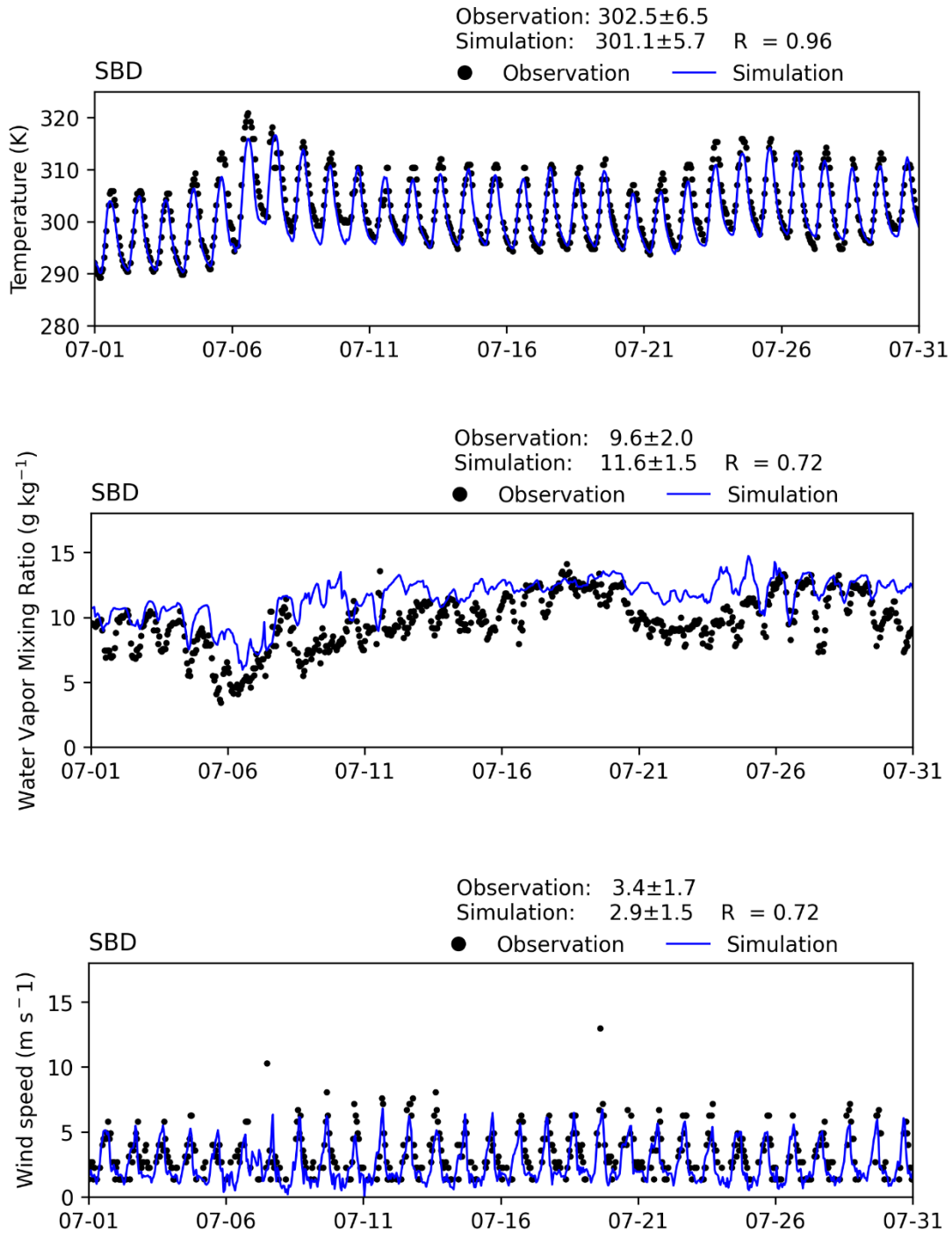


FIGURE V-A16
TIME SERIES OF HOURLY MEASUREMENTS AND WRF SIMULATIONS AT SAN BERNARDINO INTERNATIONAL AIRPORT (SBD) FOR JULY 2018

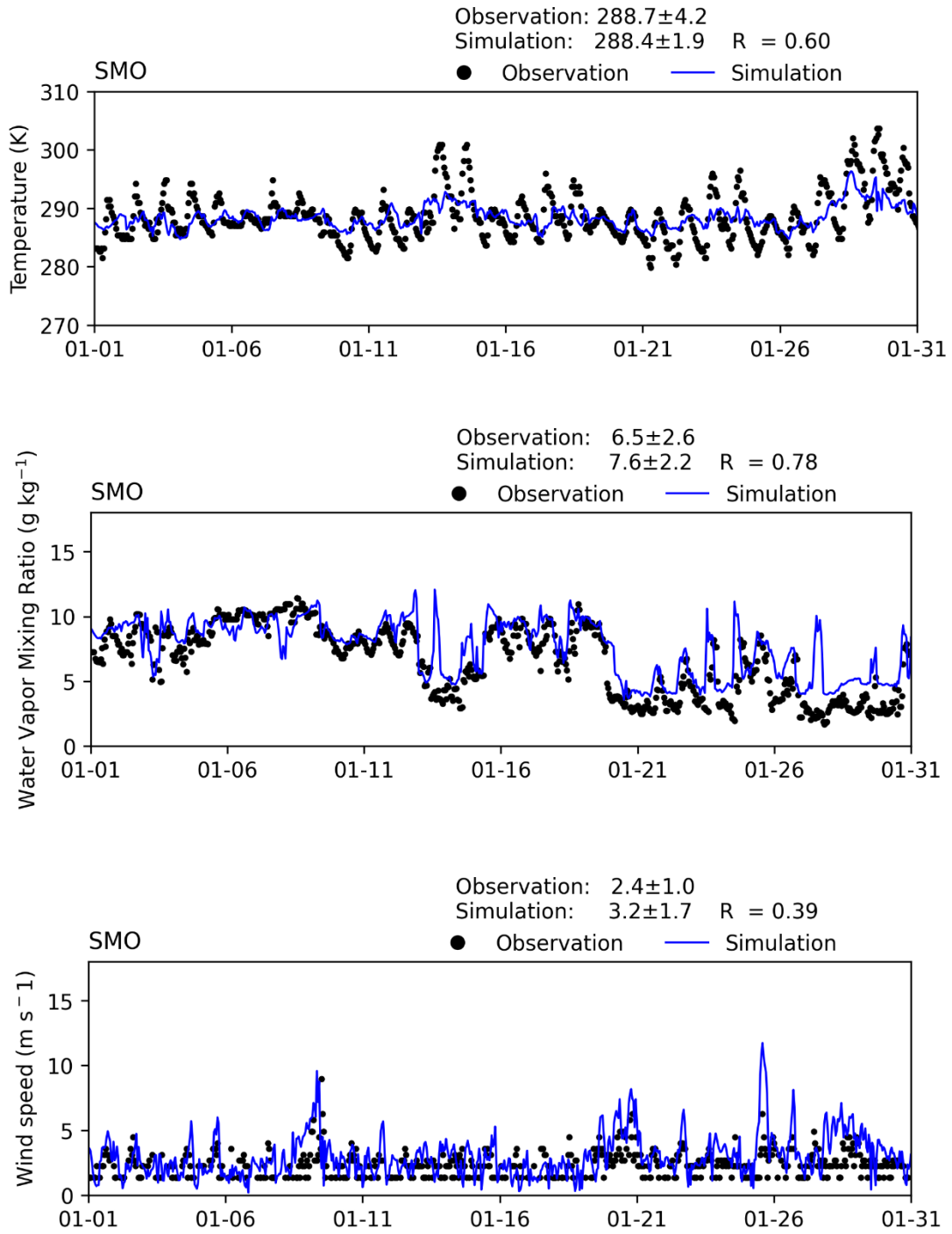


FIGURE V-A17
TIME SERIES OF HOURLY MEASUREMENTS AND WRF SIMULATIONS AT SANTA MONICA AIRPORT (SMO) FOR JANUARY 2018

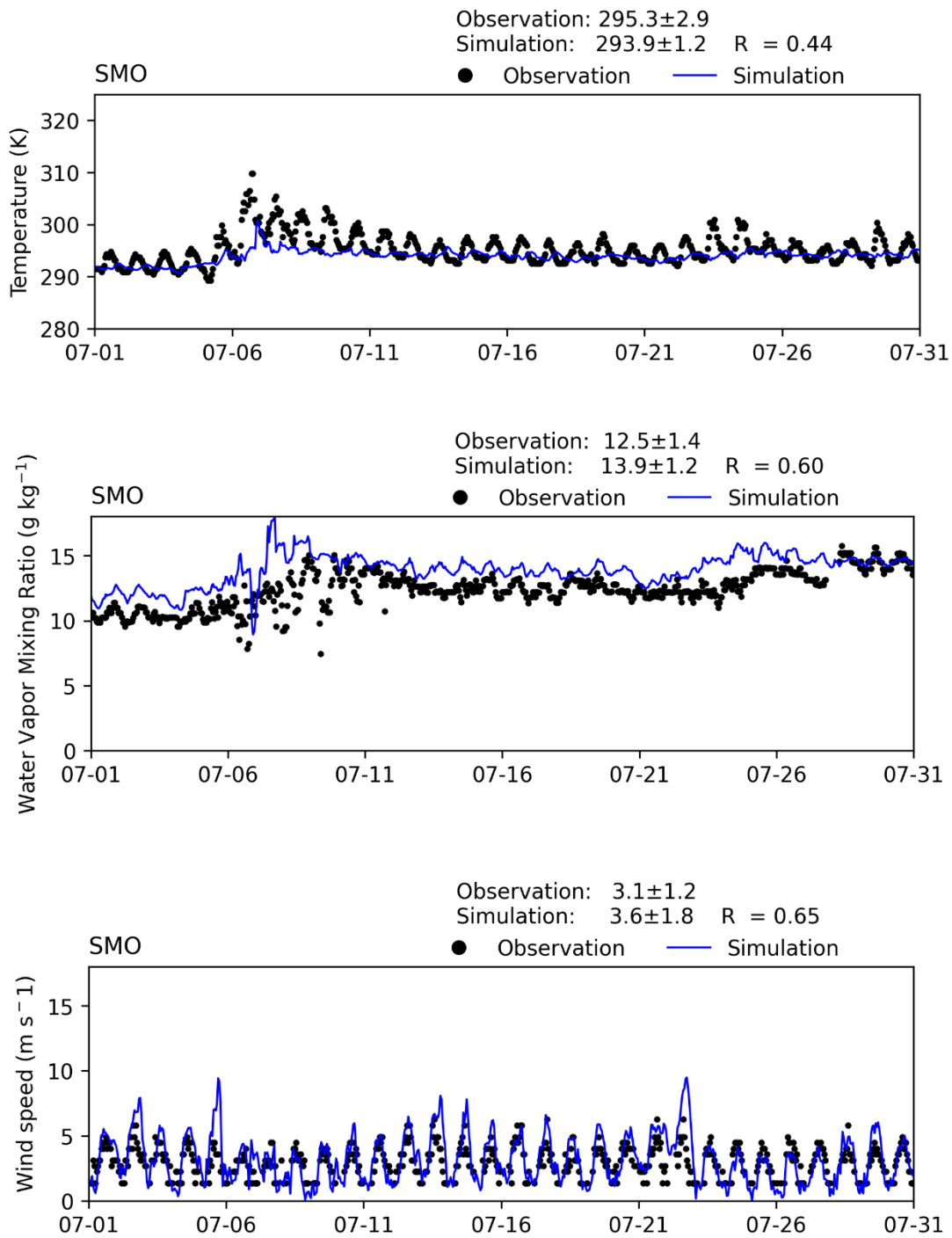


FIGURE V-A18
TIME SERIES OF HOURLY MEASUREMENTS AND WRF SIMULATIONS AT SANTA MONICA AIRPORT (SMO) FOR JULY 2018

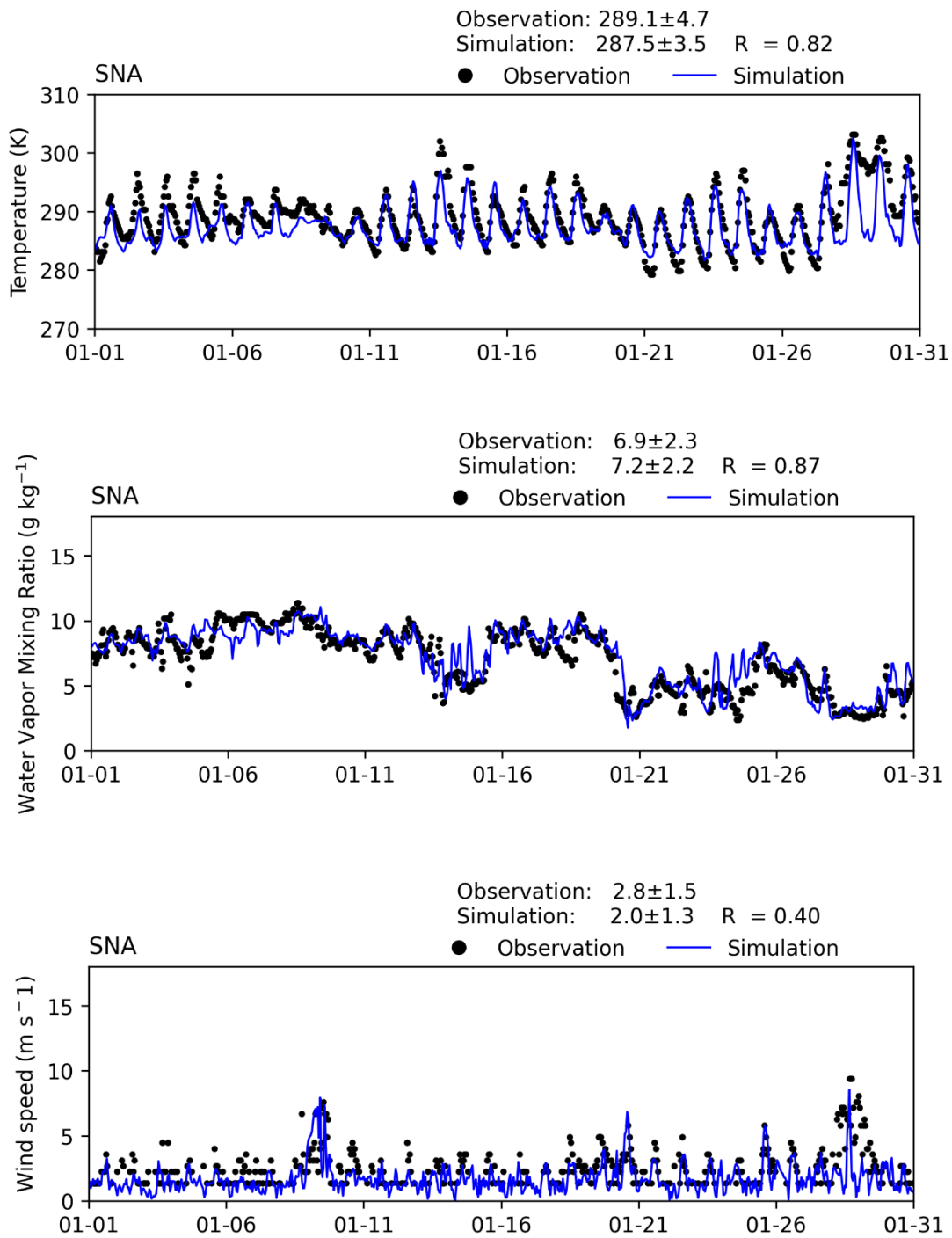


FIGURE V-A19
TIME SERIES OF HOURLY MEASUREMENTS AND WRF SIMULATIONS AT SANTA ANA JOHN WAYNE AIRPORT (SNA) FOR JANUARY 2018

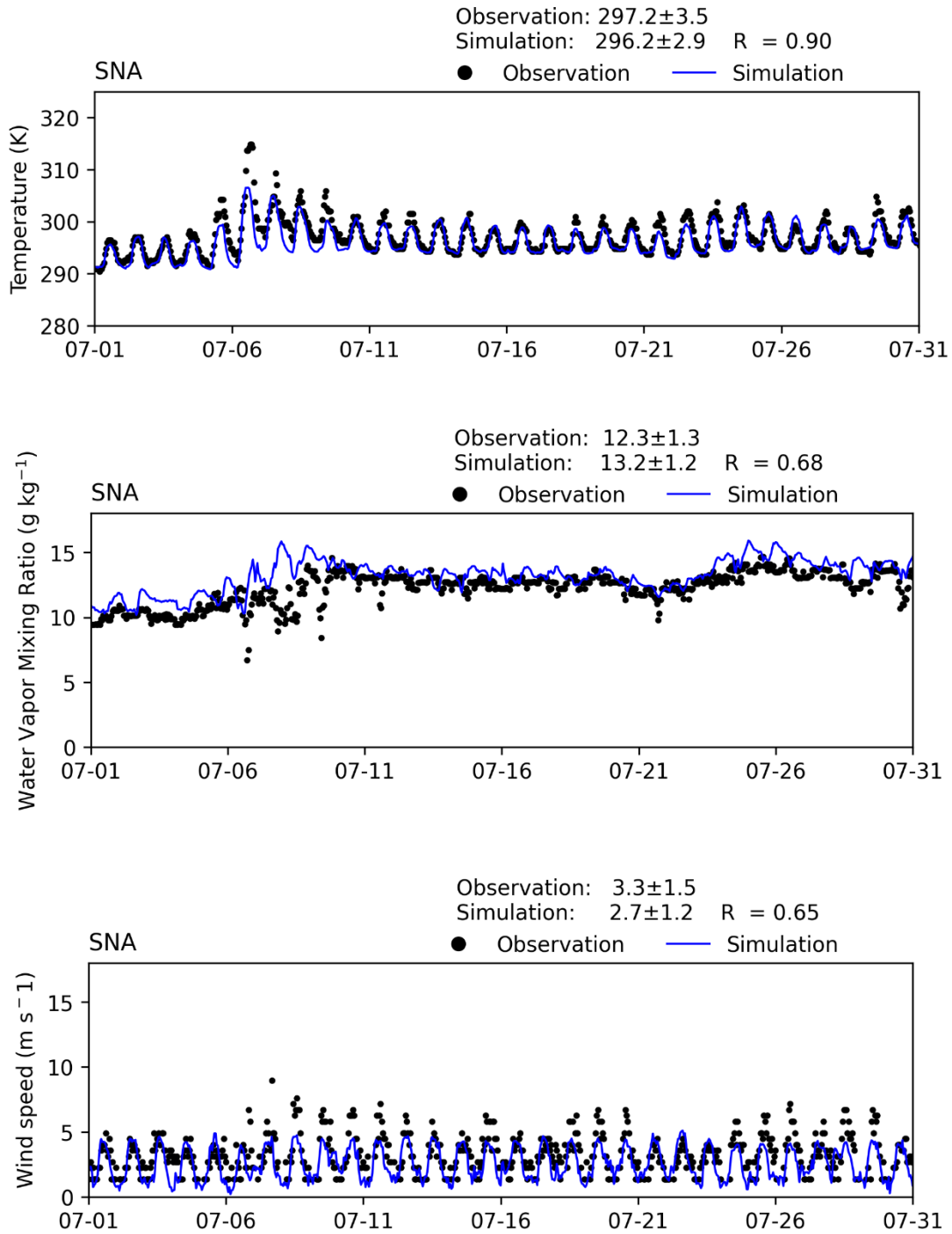


FIGURE V-A20
TIME SERIES OF HOURLY MEASUREMENTS AND WRF SIMULATIONS AT SANTA ANA JOHN WAYNE AIRPORT (SNA) FOR JULY 2018

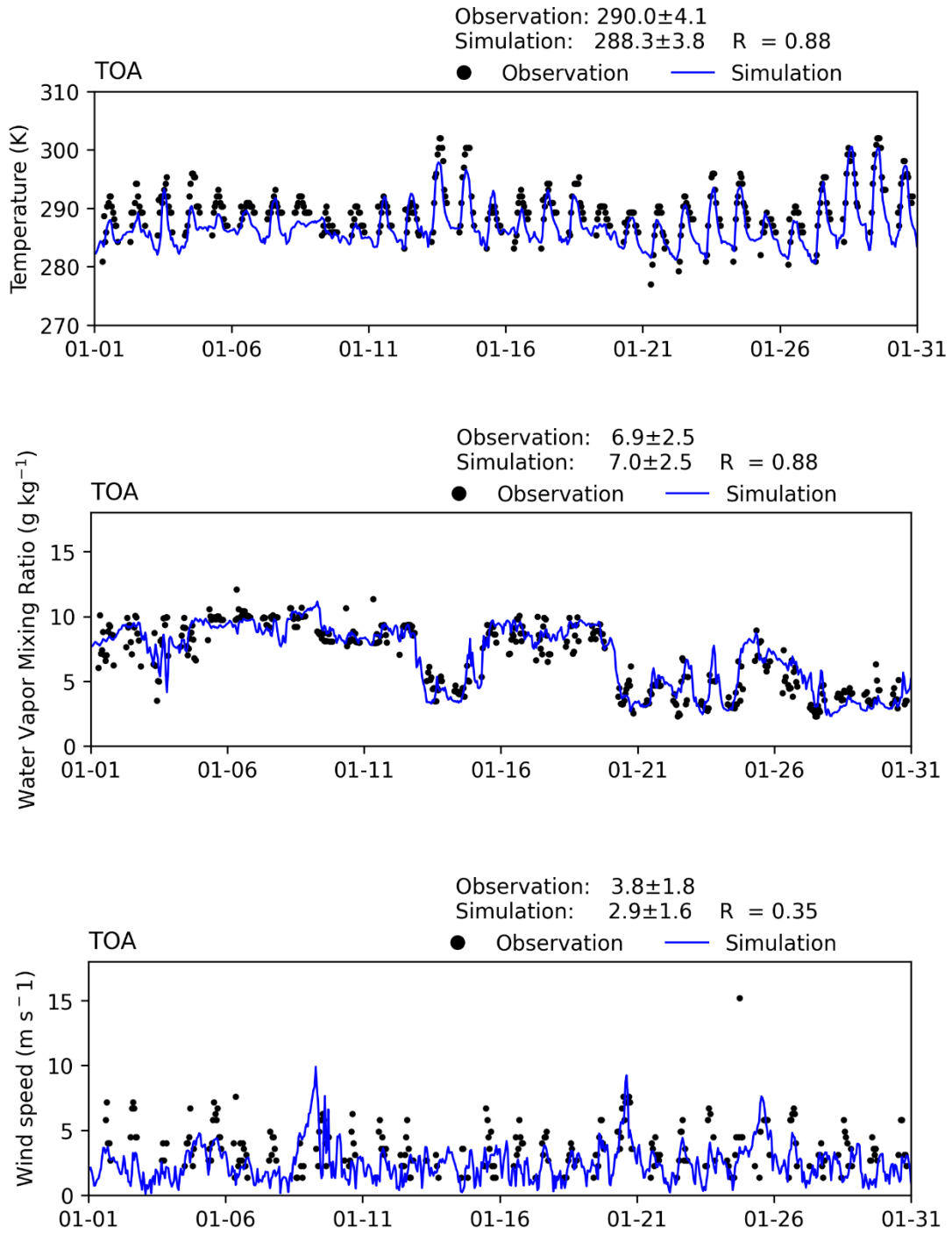


FIGURE V-A21
TIME SERIES OF HOURLY MEASUREMENTS AND WRF SIMULATIONS AT TORRANCE (TOA) FOR
JANUARY 2018

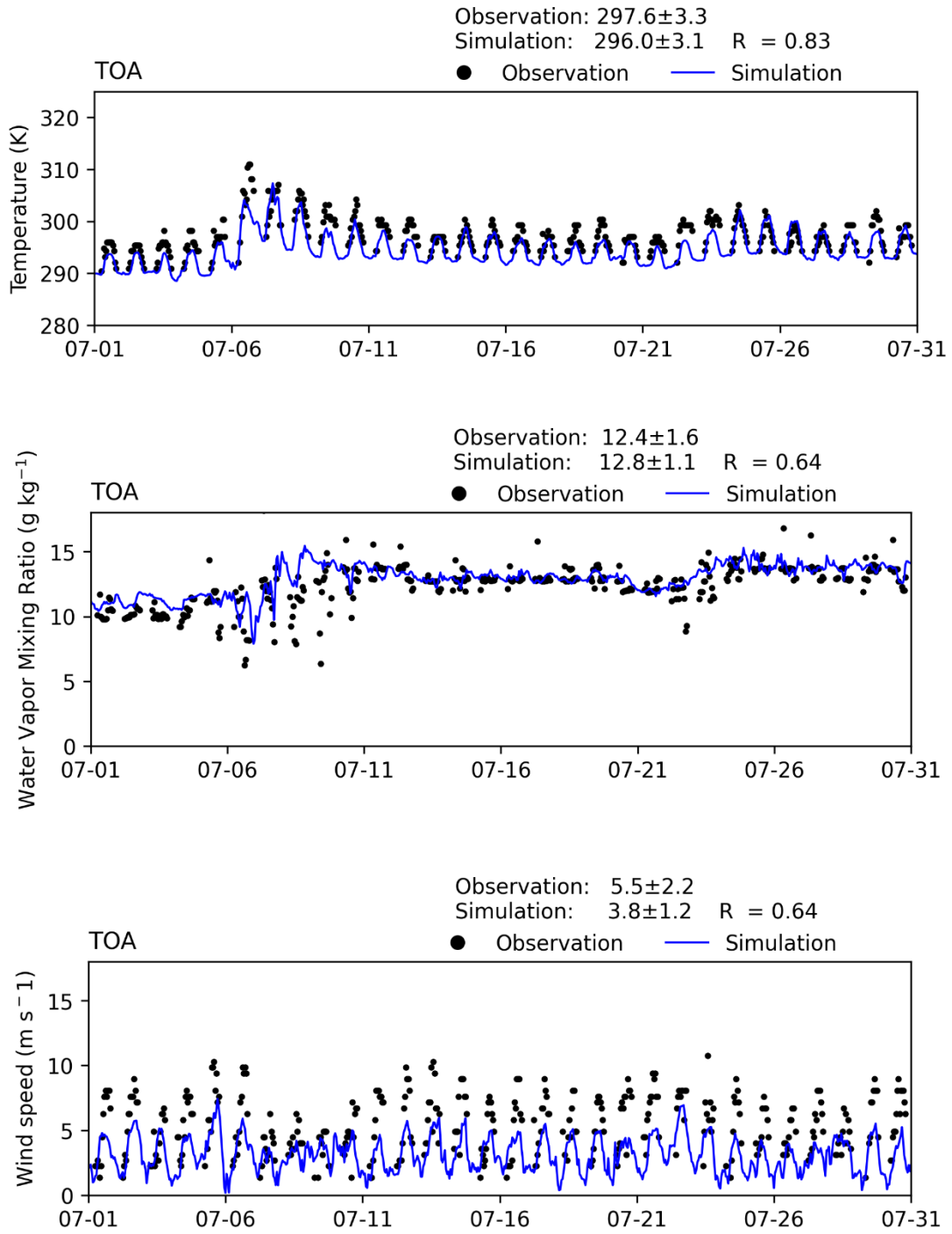


FIGURE V-A22
TIME SERIES OF HOURLY MEASUREMENTS AND WRF SIMULATIONS AT TORRANCE (TOA) FOR JULY 2018

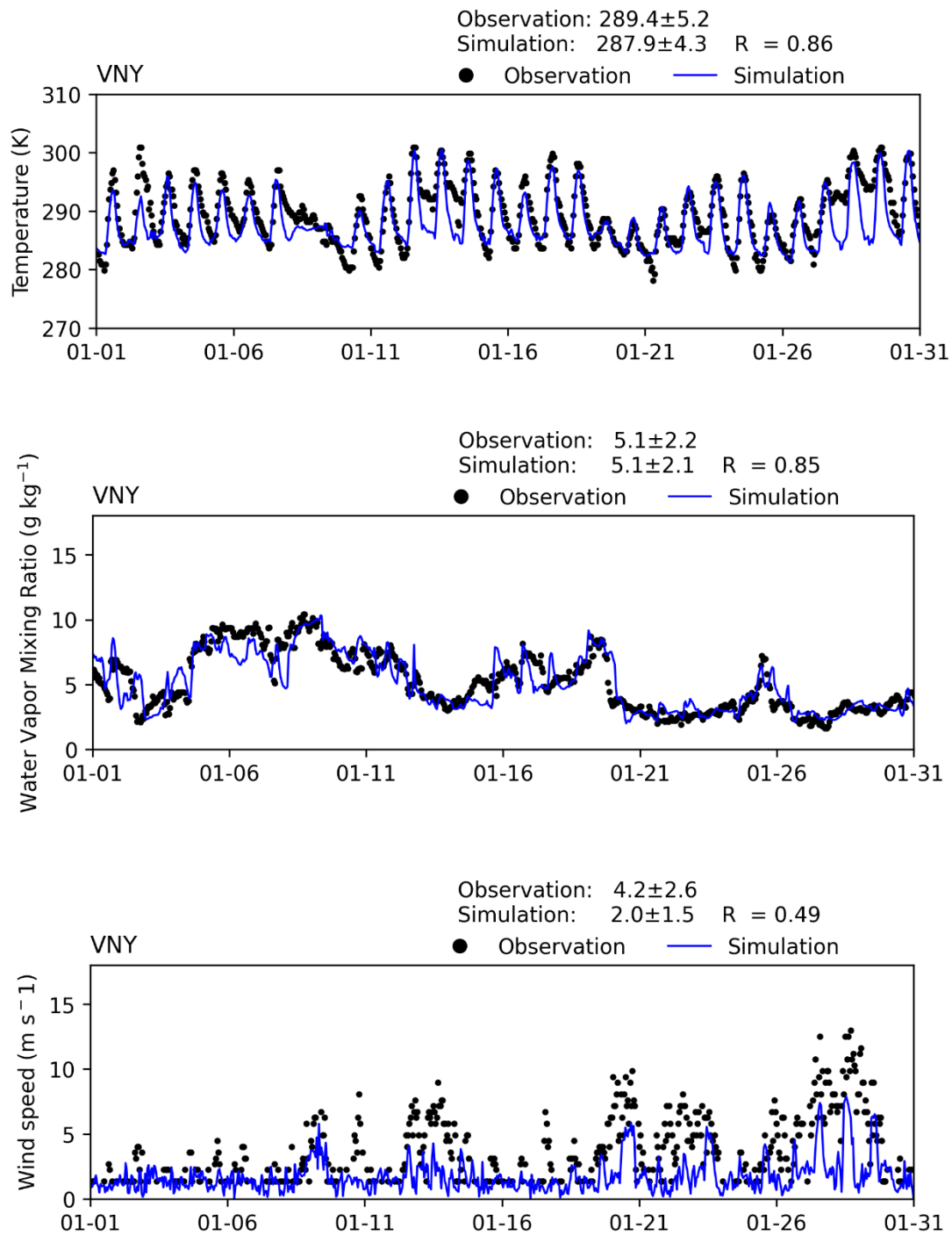


FIGURE V-A23
TIME SERIES OF HOURLY MEASUREMENTS AND WRF SIMULATIONS AT VAN NUYS AIRPORT (VNY) FOR
JANUARY 2018

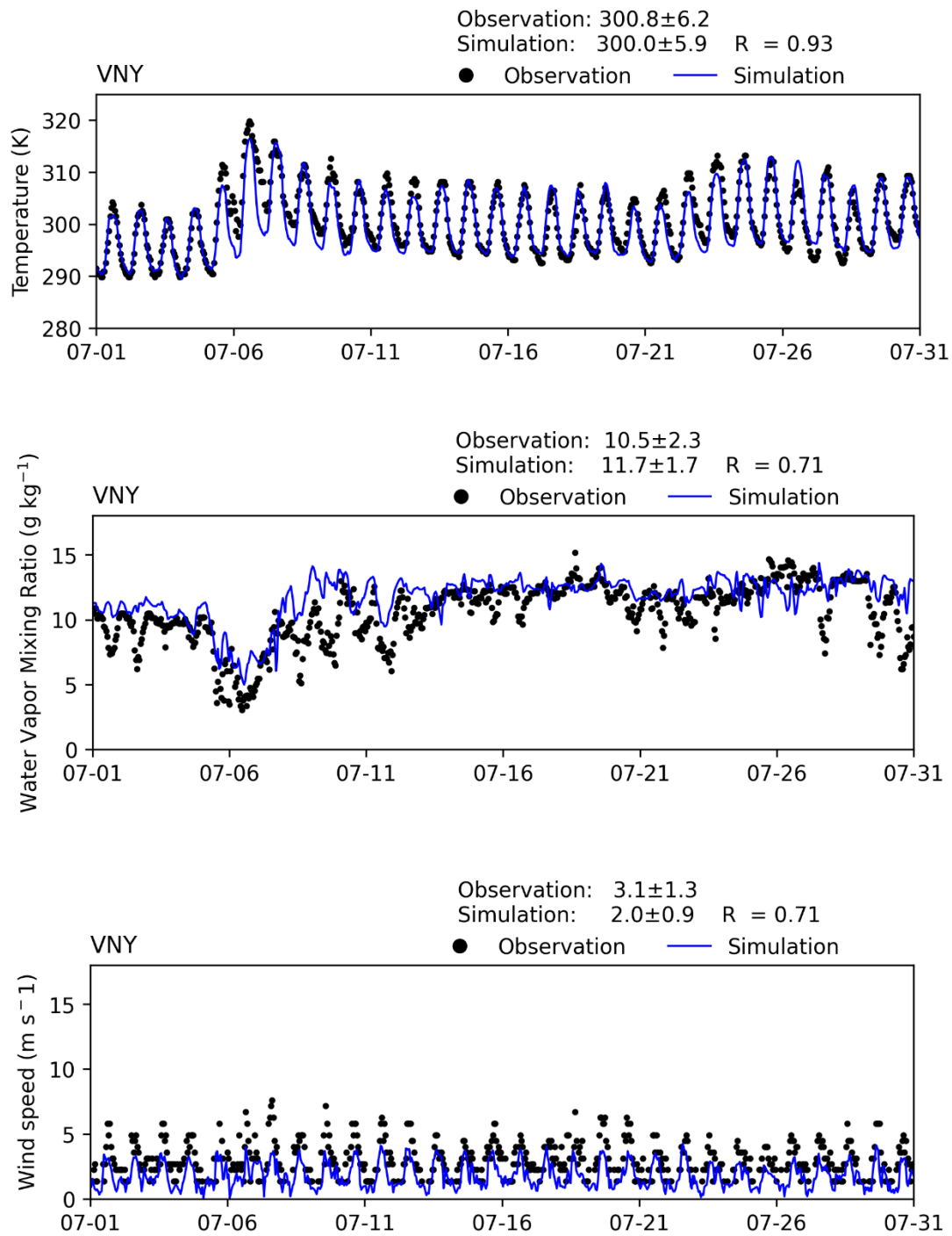


FIGURE V-A24
TIME SERIES OF HOURLY MEASUREMENTS AND WRF SIMULATIONS AT VAN NUYS AIRPORT WR(VNY)
FOR JULY 2018

Attachment 2

CMAQ MODEL PERFORMANCE TIME SERIES

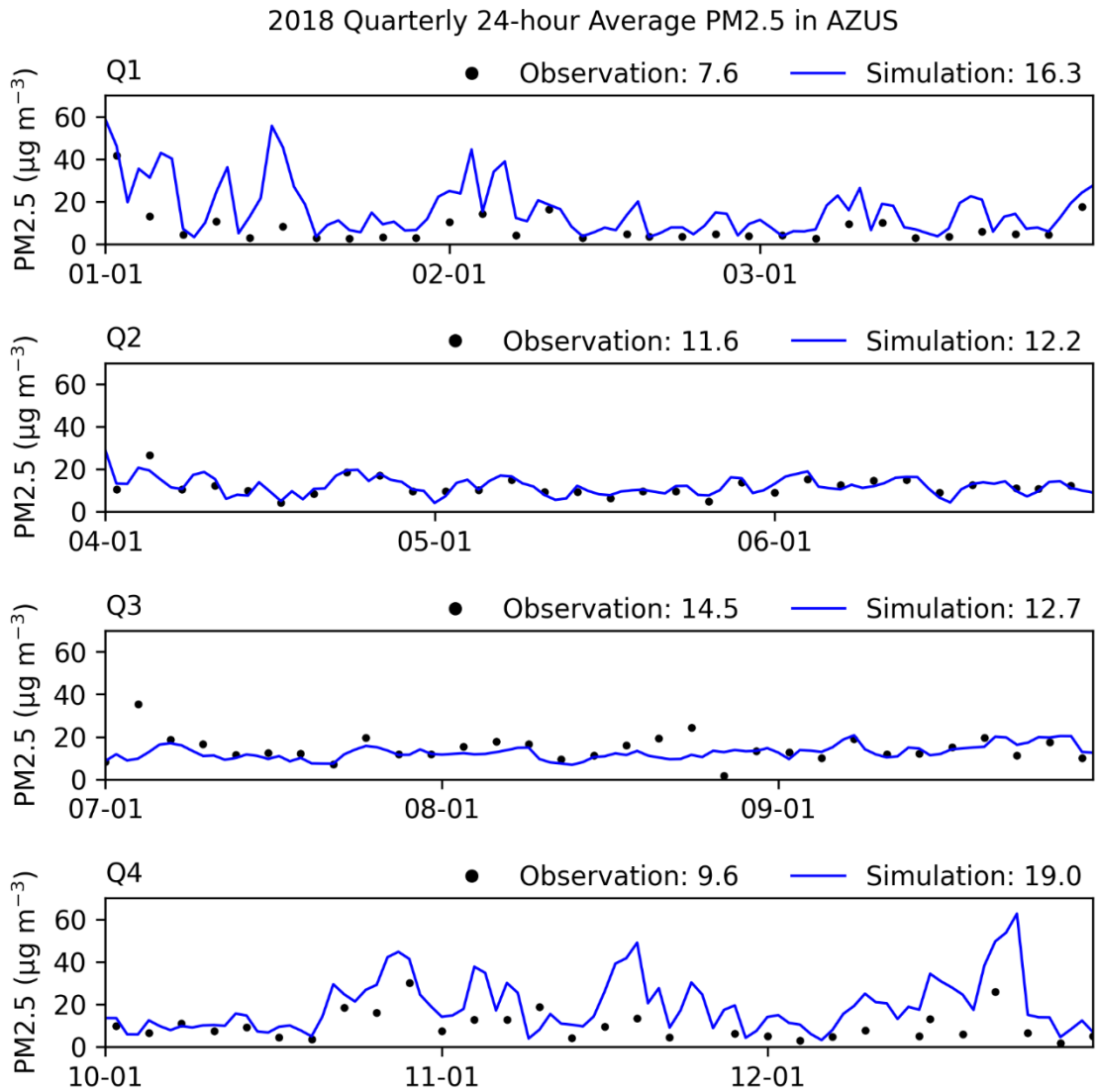


FIGURE 1

2018 Modelled and Measured 24-hour Average PM2.5 Concentrations in Azusa

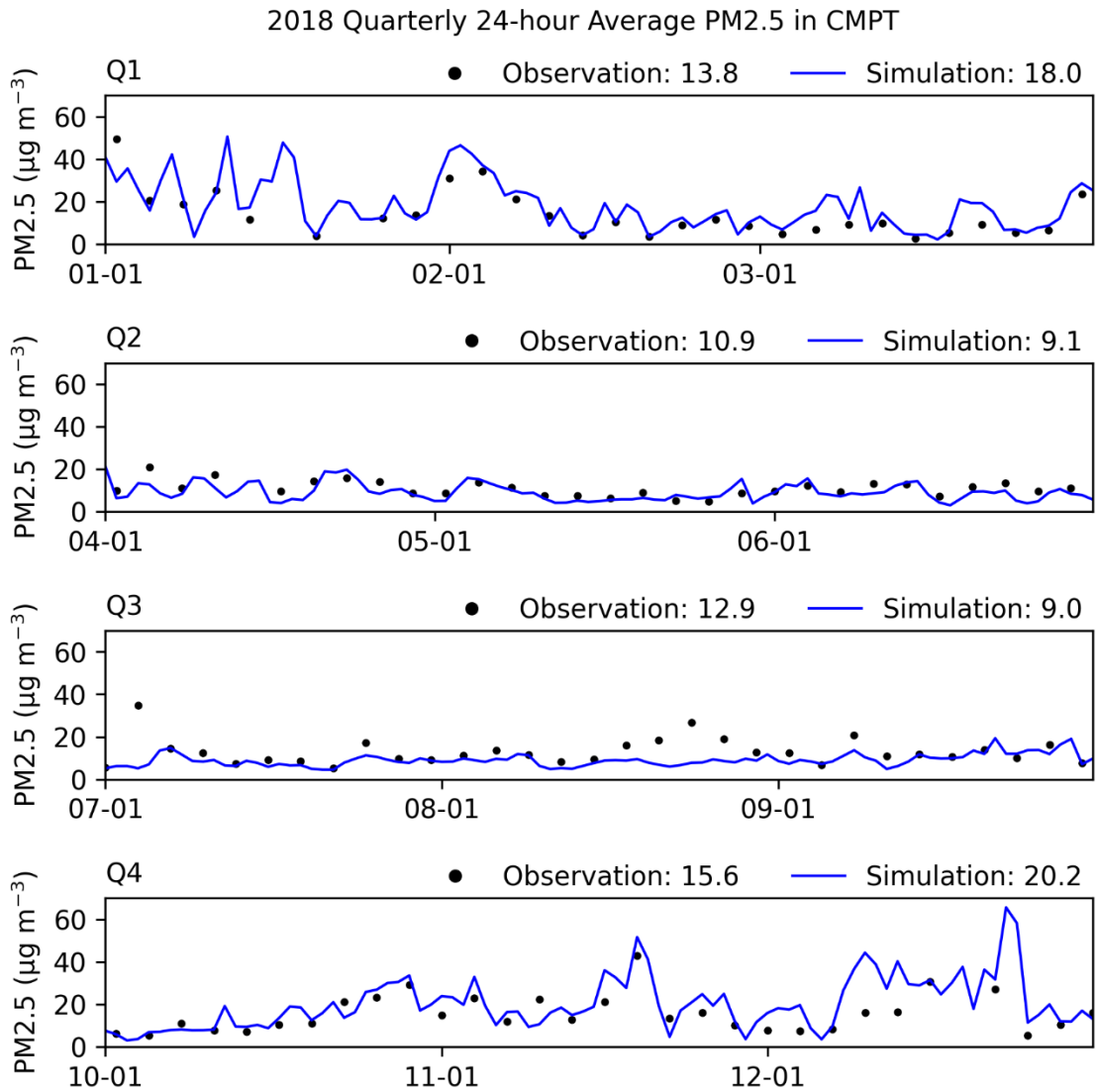


FIGURE 2

2018 Modelled and Measured 24-hour Average PM2.5 Concentrations in Compton

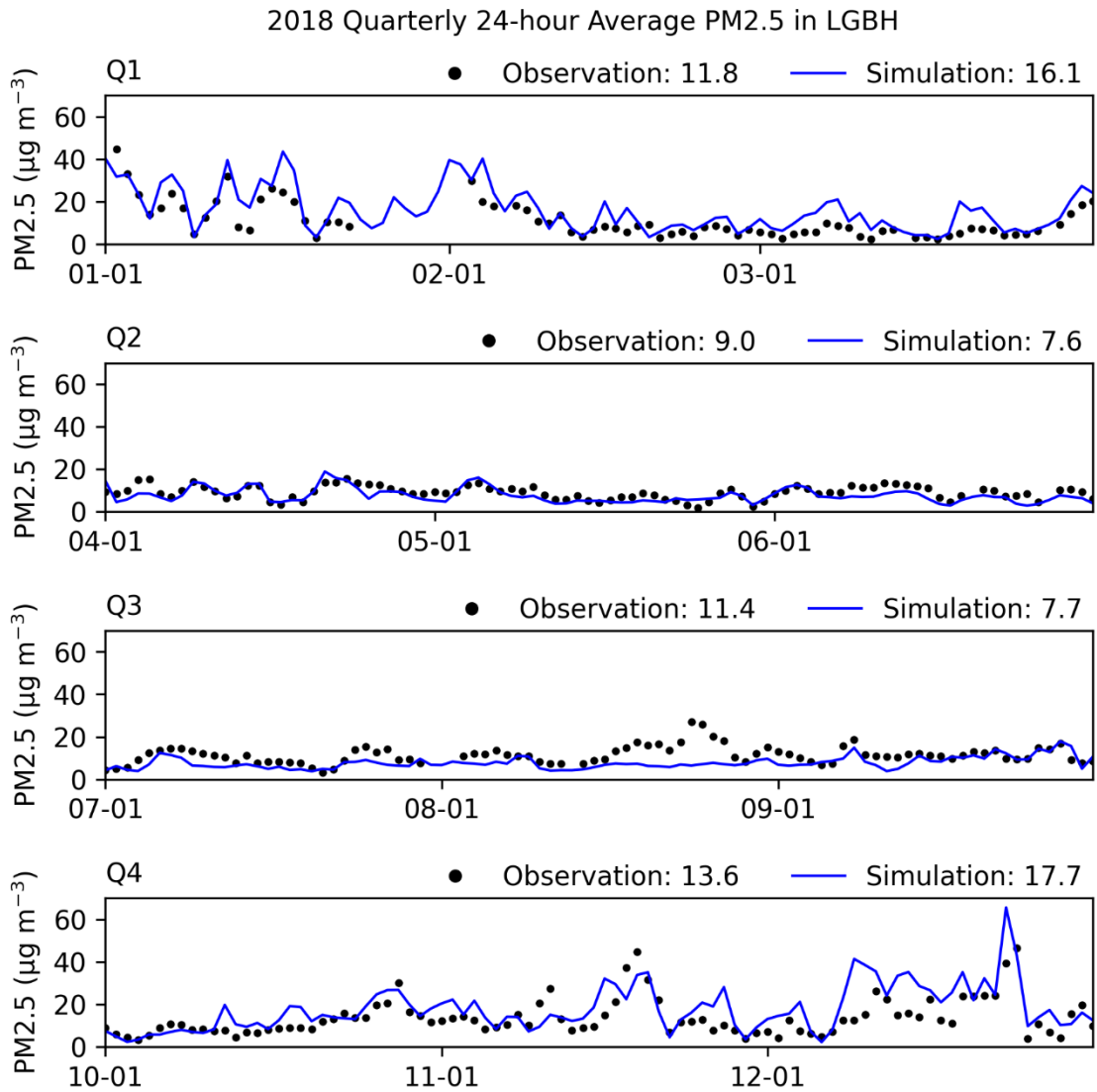


FIGURE 3

2018 Modelled and Measured 24-hour Average PM2.5 Concentrations in Long Beach

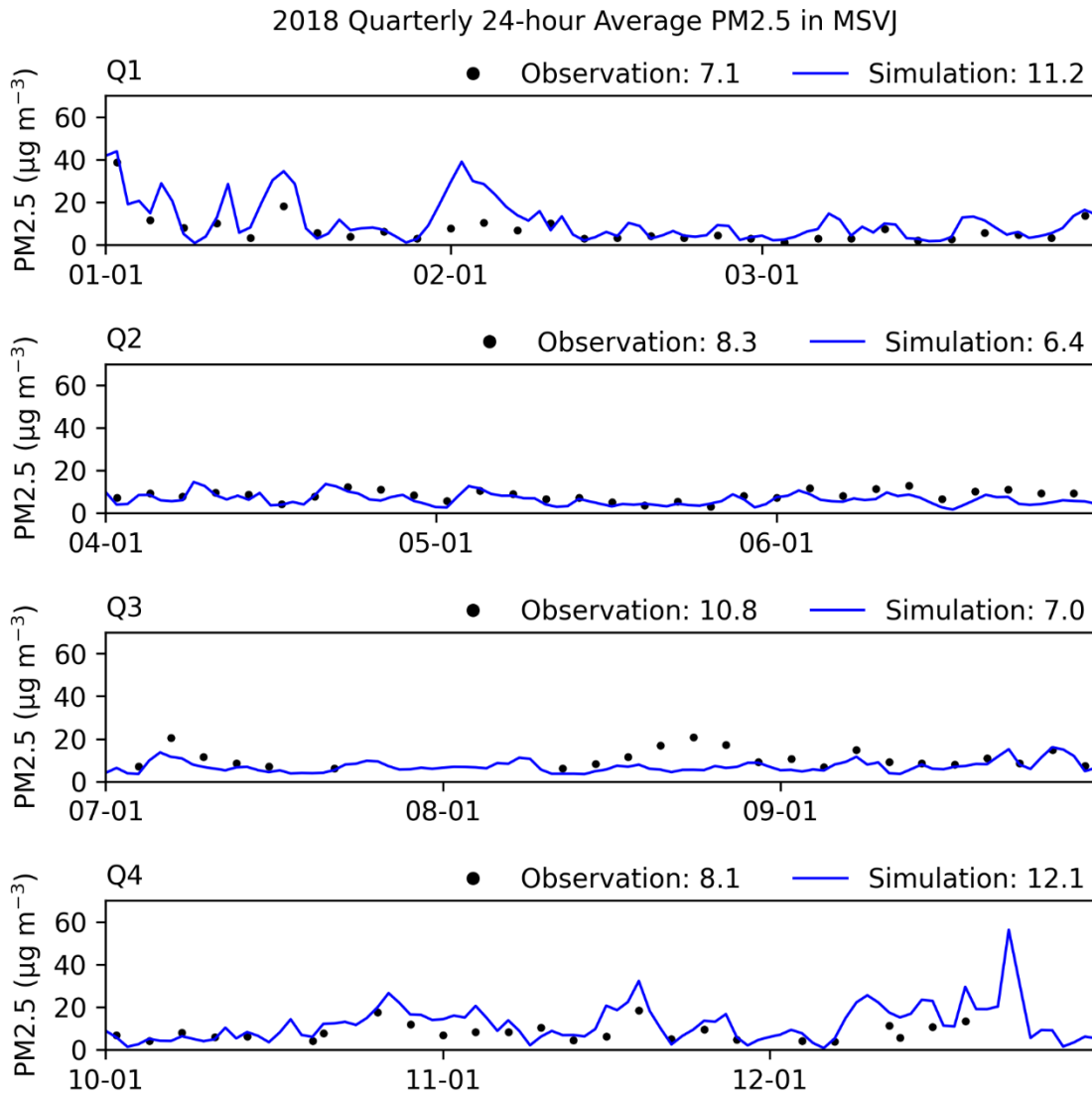


FIGURE 4

2018 Modelled and Measured 24-hour Average PM2.5 Concentrations in Mission Viejo

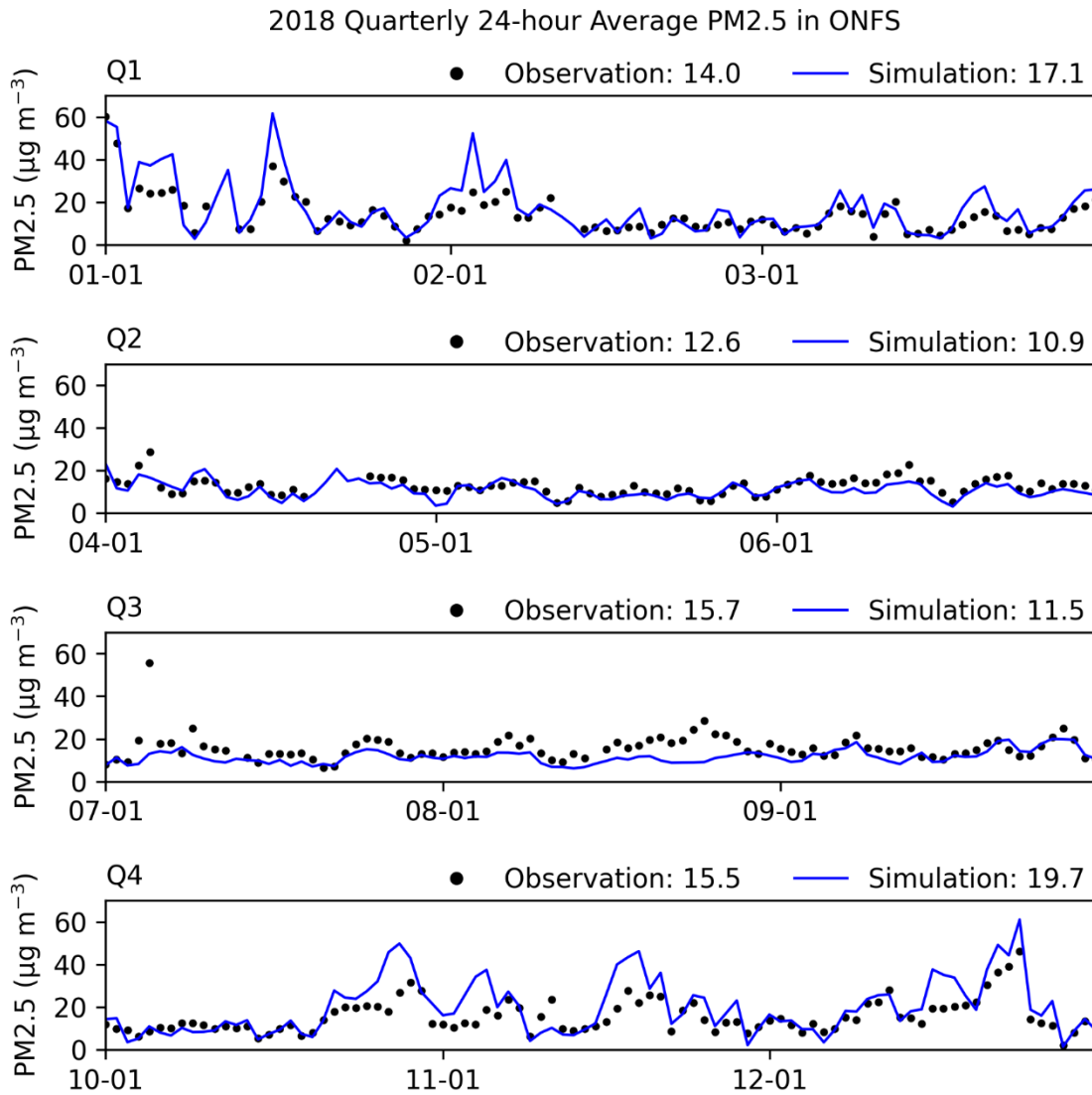


FIGURE 5

2018 Modelled and Measured 24-hour Average PM2.5 Concentrations in Ontario

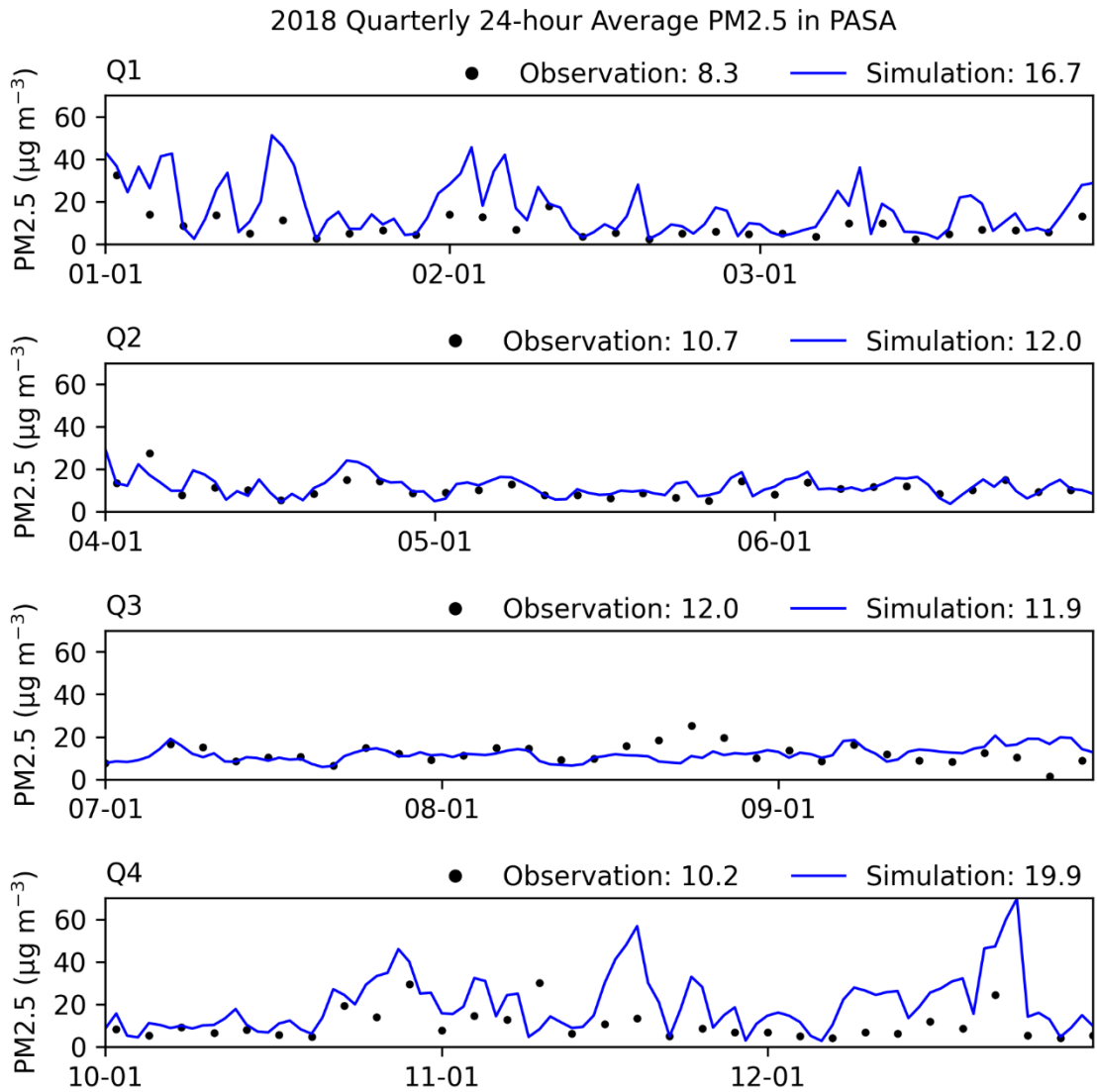


FIGURE 6

2018 Modelled and Measured 24-hour Average PM2.5 Concentrations in Pasadena

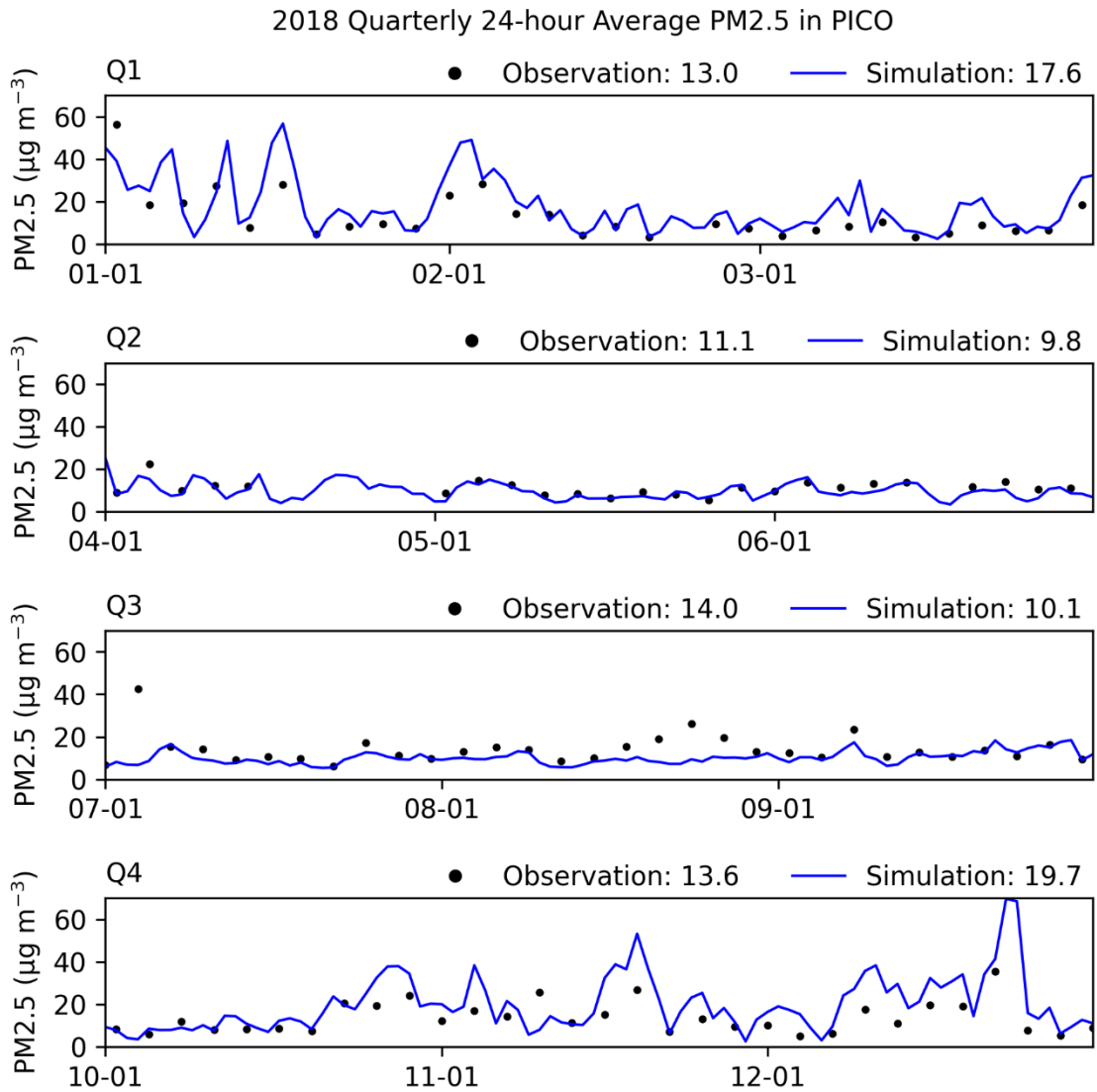


FIGURE 7

2018 Modelled and Measured 24-hour Average PM2.5 Concentrations in Pico Rivera

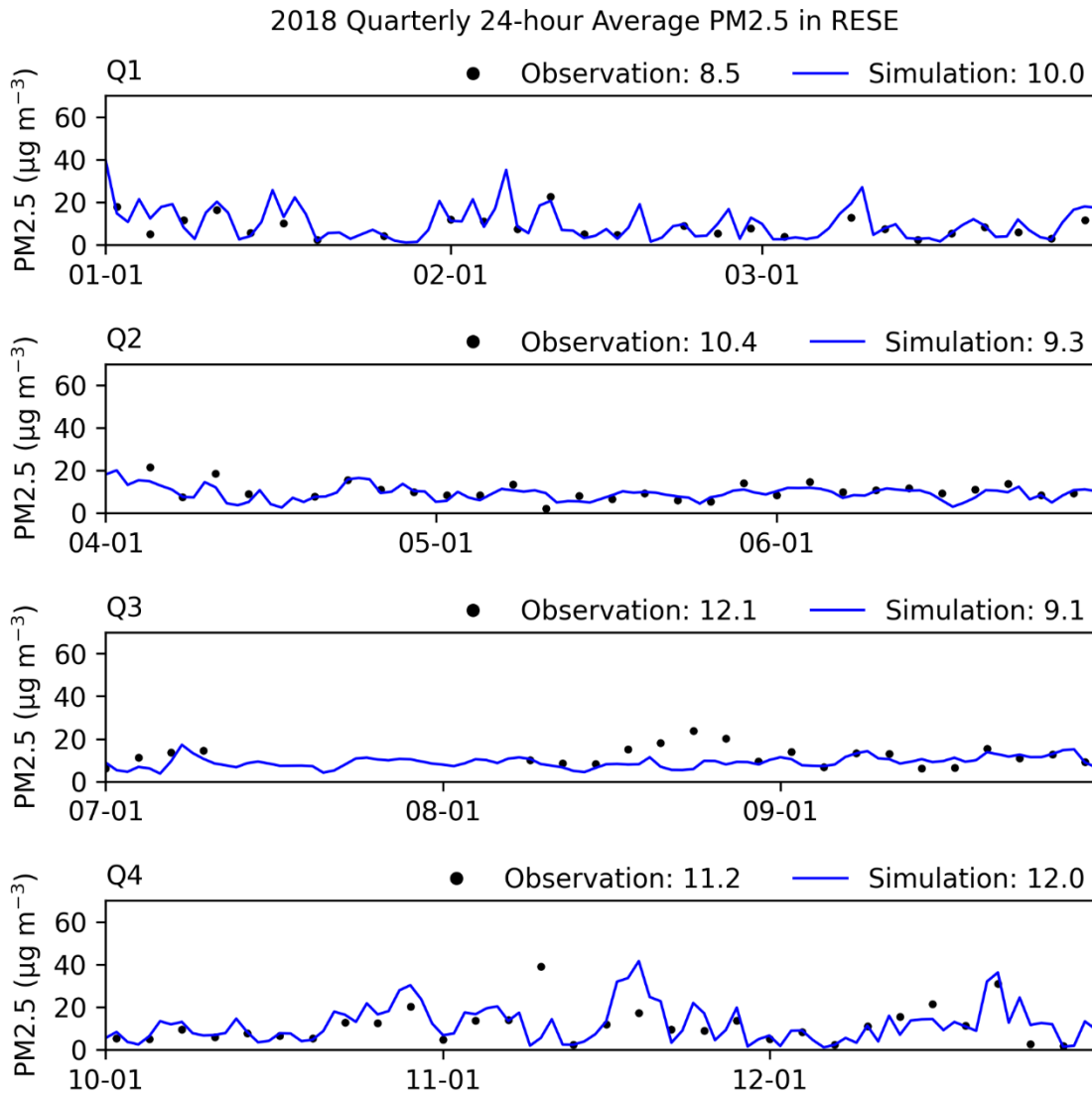


FIGURE 8

2018 Modelled and Measured 24-hour Average PM2.5 Concentrations in Reseda

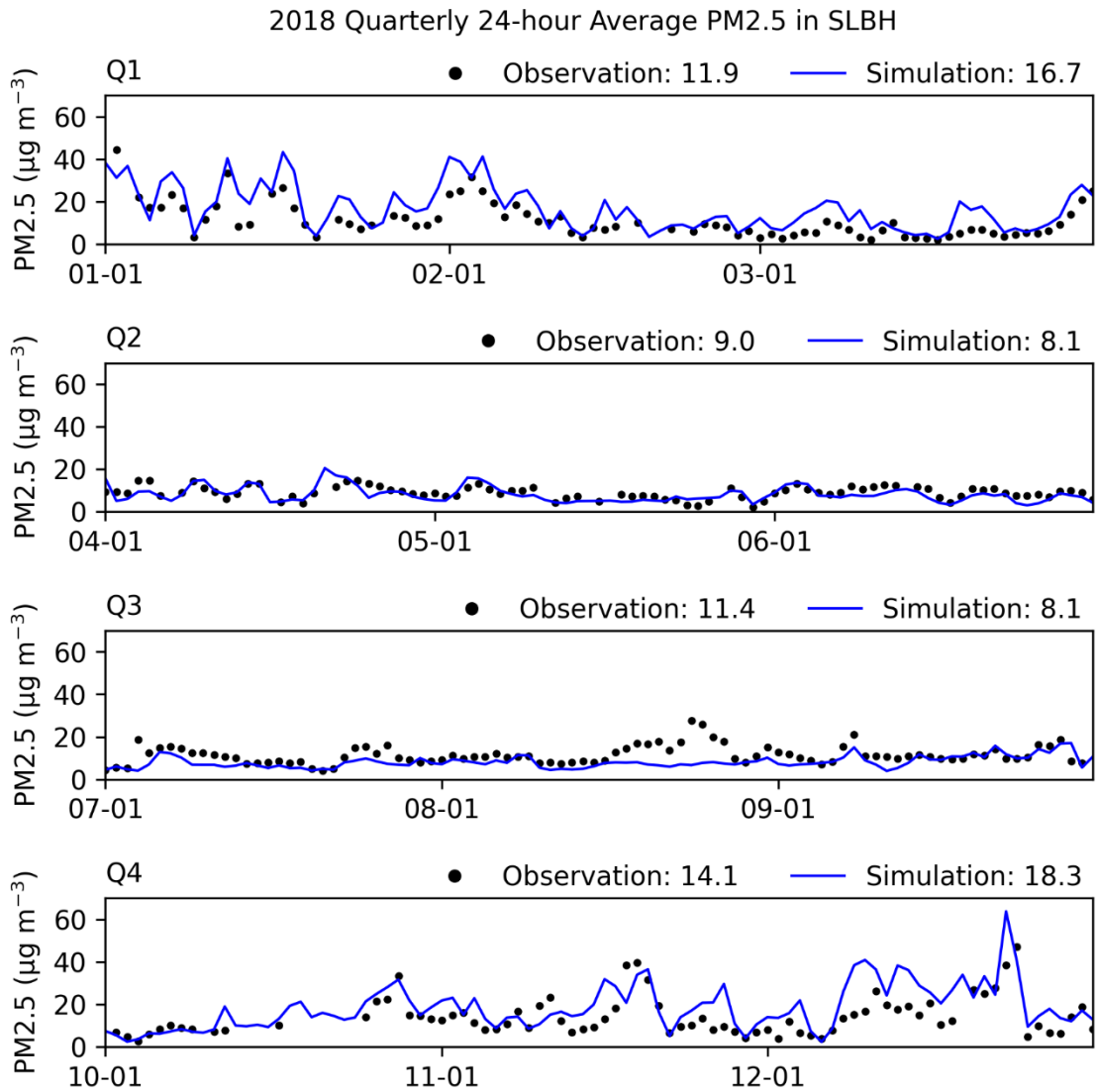


FIGURE 9

2018 Modelled and Measured 24-hour Average PM2.5 Concentrations in South Long Beach

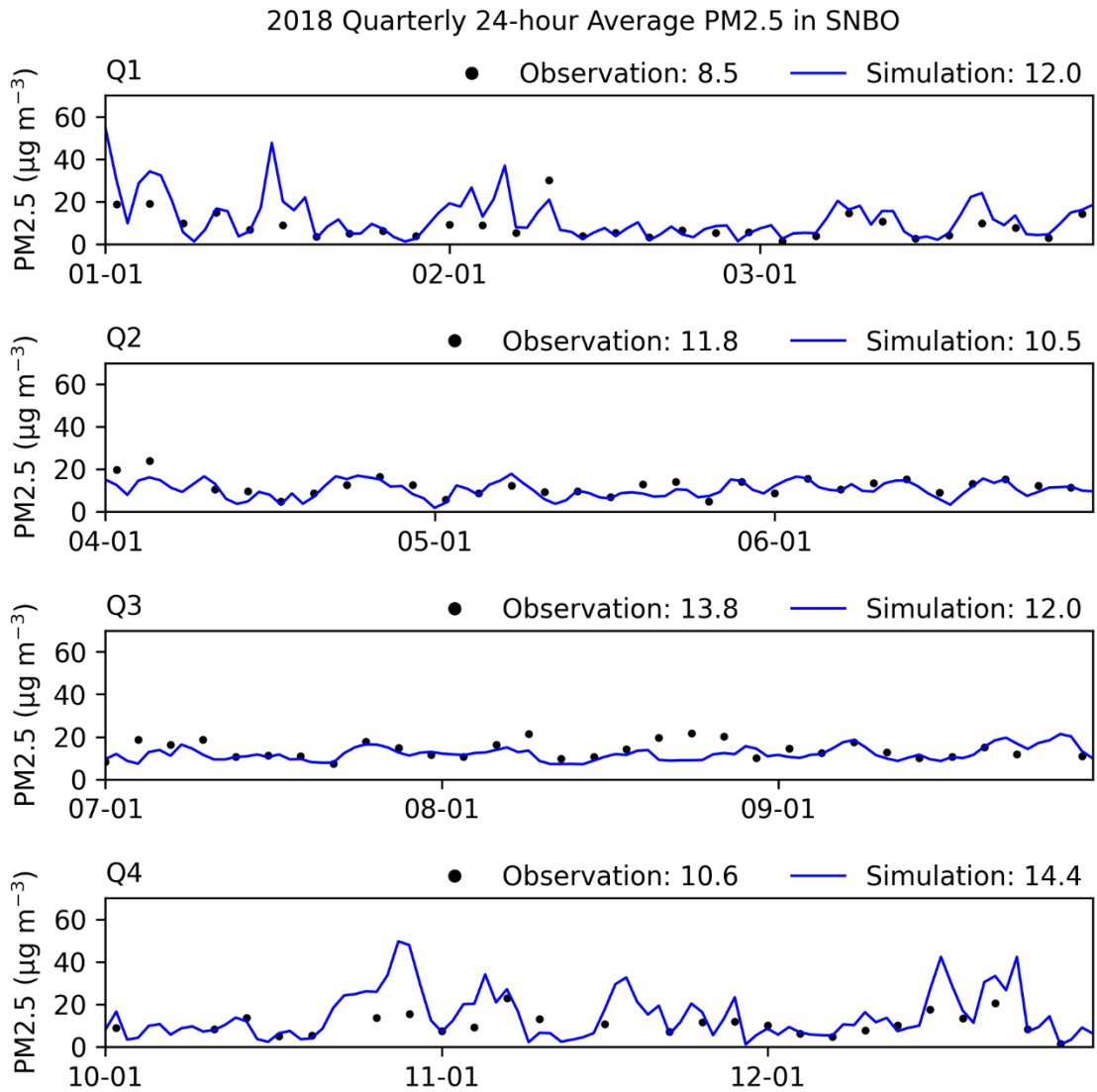


FIGURE 10

2018 Modelled and Measured 24-hour Average PM2.5 Concentrations in San Bernardino

Attachment 3

EMISSIONS REDUCTIONS SUMMARY FOR FUTURE CONTROL SCENARIOS

TABLE 1. EMISSIONS REDUCTIONS FROM THE PROPOSED CONTROL MEASURES FOR THE 2030 ATTAINMENT SCENARIO

| Control Measures | Average composite CF ¹ | | | 2030 baseline (tons/day) | | | 2030 remaining (tons/day) | | | 2030 reduction (tons/day) | | |
|---|-----------------------------------|-------------|-------------|-----------------------------|--------------|-------------|------------------------------|--------------|-------------|------------------------------|-------------|-------------|
| | NOX | NH3 | PM25 | NOX | NH3 | PM25 | NOX | NH3 | PM25 | NOX | NH3 | PM25 |
| BCM-05: Emission Reductions from Emergency Standby Engines | 0.91 | 1.00 | 0.73 | 3.96 | 0.01 | 0.15 | 3.60 | 0.01 | 0.11 | 0.36 | 0 | 0.04 |
| BCM-06: Emission Reductions from Diesel Electricity Generating Facilities | 0.92 | 1.00 | 1.00 | 2.06 | 0.52 | 0.34 | 1.90 | 0.52 | 0.34 | 0.16 | 0 | 0 |
| BCM-07: Emission Reductions from Incinerators | 0.29 | 1.00 | 1.00 | 1.13 | 0.24 | 0.05 | 0.33 | 0.24 | 0.05 | 0.81 | 0 | 0 |
| TOTAL SOUTH COAST AQMD STATIONARY: | 0.81 | 1.00 | 0.93 | 7.15 | 0.77 | 0.54 | 5.83 | 0.77 | 0.50 | 1.33 | 0.00 | 0.04 |
| Zero-Emission Standard for Space and Water Heaters | 0.79 | 1.00 | 0.76 | 12.07 | 0.01 | 1.71 | 9.49 | 0.01 | 1.30 | 2.58 | 0 | 0.41 |
| TOTAL CARB STATIONARY: | 0.79 | 1.00 | 0.76 | 12.07 | 0.01 | 1.71 | 9.49 | 0.01 | 1.30 | 2.58 | 0.00 | 0.41 |
| Clean Mile Standard | 1.00 | 1.00 | 1.00 | 24.37 | 14.69 | 2.47 | 24.33 | 14.69 | 2.47 | 0.04 | 0 | 0 |
| On-Road Motorcycles New Emissions Standards | 0.80 | 1.00 | 1.00 | 0.82 | 0.01 | 0.01 | 0.66 | 0.01 | 0.01 | 0.16 | 0 | 0 |
| Advanced Clean Fleets | 0.80 | 0.86 | 0.91 | 24.26 | 5.95 | 1.00 | 19.47 | 5.11 | 0.91 | 4.79 | 0.84 | 0.09 |
| Zero Emission Trucks Measure | 0.88 | 0.96 | 0.97 | 24.26 | 5.95 | 1.00 | 21.34 | 5.70 | 0.97 | 2.92 | 0.27 | 0.03 |
| Advanced Clean Cars Program II | 0.94 | 0.86 | 0.93 | 24.37 | 14.69 | 2.47 | 22.88 | 12.57 | 2.29 | 1.49 | 2.12 | 0.18 |
| TOTAL CARB ONROAD: | 0.81 | 0.84 | 0.91 | 49.45 | 20.66 | 3.49 | 40.05 | 17.45 | 3.14 | 9.4 | 3.21 | 0.30 |
| EPA Clean Trucks Plan | 0.97 | 1.00 | 1.00 | 24.26 | 5.95 | 1.00 | 23.65 | 5.95 | 1.00 | 0.61 | 0 | 0 |
| TOTAL EPA ONROAD: | 0.97 | 1.00 | 1.00 | 24.26 | 5.95 | 1.00 | 23.65 | 5.95 | 1.00 | 0.61 | 0 | 0 |

TABLE 1. EMISSIONS REDUCTIONS FROM THE PROPOSED CONTROL MEASURES FOR THE 2030 ATTAINMENT SCENARIO (CONCLUDED)

| Control Measures | Average composite CF ¹ | | | 2030 baseline (tons/day) | | | 2030 remaining (tons/day) | | | 2030 reduction (tons/day) | | |
|---|-----------------------------------|-------------|-------------|-----------------------------|--------------|--------------|------------------------------|--------------|--------------|------------------------------|-------------|-------------|
| | NOX | NH3 | PM25 | NOX | NH3 | PM25 | NOX | NH3 | PM25 | NOX | NH3 | PM25 |
| Cargo Handling Equipment Amendments | 0.56 | 1.00 | 0.55 | 1.65 | 0.00 | 0.07 | 0.93 | 0.00 | 0.04 | 0.72 | 0.00 | 0.03 |
| Spark-Ignition Marine Engine Standards | 1.00 | 1.00 | 1.00 | 2.66 | 0.01 | 0.42 | 2.66 | 0.01 | 0.42 | 0.00 | 0.00 | 0.00 |
| Commercial Harbor Craft Amendments | 0.64 | 1.00 | 0.58 | 5.70 | 0.00 | 0.23 | 3.63 | 0.00 | 0.13 | 2.06 | 0.00 | 0.09 |
| In-use Locomotive Regulation | 0.44 | 1.00 | 0.32 | 17.58 | 0.01 | 0.35 | 7.68 | 0.01 | 0.11 | 9.90 | 0.00 | 0.24 |
| Amendments to the In-Use Off-Road Diesel-Fueled Fleets Regulation | 0.75 | 1.00 | 0.65 | 7.65 | 0.00 | 0.35 | 5.74 | 0.00 | 0.23 | 1.91 | 0.00 | 0.12 |
| ZE Forklift Regulation | 0.68 | 1.00 | 0.96 | 2.67 | 0.00 | 0.16 | 1.81 | 0.00 | 0.16 | 0.86 | 0.00 | 0.01 |
| Tier 5 Off-Road New Compression-Ignition Engine Standards | 0.95 | 1.00 | 0.96 | 5.34 | 0.02 | 0.13 | 5.09 | 0.02 | 0.12 | 0.25 | 0.00 | 0.01 |
| Transport Refrigeration Unit Regulation Part I & II | 0.58 | 1.00 | 0.28 | 4.97 | 0.00 | 0.16 | 2.86 | 0.00 | 0.04 | 2.11 | 0.00 | 0.12 |
| TOTAL CARB OFFROAD: | 0.63 | 1.00 | 0.67 | 48.21 | 0.04 | 1.87 | 30.39 | 0.04 | 1.26 | 17.82 | 0.00 | 0.61 |
| Rule adopted/amened after 2022AQMP cut-off date | | | | | | | | | | 0.34 | 0.00 | 0.00 |
| RECLAIM landing rules adjustments | | | | | | | | | | 2.86 | 0.00 | 0.00 |
| TOTAL LINE ITMES ADJUSTMENT²: | | | | | | | | | | 3.20 | 0.00 | 0.00 |
| GRAND TOTAL: | 0.83 | 0.96 | 0.97 | 210.31 | 79.31 | 54.05 | 175.37 | 76.10 | 52.69 | 34.94 | 3.21 | 1.36 |

¹Average Composite CF (control factor) for each measure defined as the ratio between remaining emission and baseline emission per pollutants.

²See Appendix I Tables I-2-2C through I-2-2E for details.

ATTACHMENT 4

LIST OF WILDFIRES THAT AFFECTED THE SOUTH COAST AIR BASIN IN 2020

2020 Wildfire impacts in South Coast Air Basin

This list includes all the events that triggered smoke advisories in the Basin. For the smoke advisory announcements, see the following site: <https://www.aqmd.gov/home/news-events/news-and-media/2020-news-archives#>

1. 58 Fire
 - a. Burn dates: 2020-06-24 to 2020-06-27
 - i. <https://www.fire.ca.gov/incidents/2020/6/24/58-fire>
2. Soledad Fire
 - a. Burn dates: 2020-07-05 to 2020-07-10
 - i. <https://www.fire.ca.gov/incidents/2020/7/5/soledad-fire>
3. Dam Fire
 - a. Burn dates: 2020-07-30 to 2020-08-14
 - i. <https://www.fire.ca.gov/incidents/2020/7/30/dam-fire>
4. Apple Fire
 - a. Burn dates: 2020-07-31 to 2020-08-15 (90% contained)
 - i. <https://www.fire.ca.gov/incidents/2020/7/31/apple-fire>
 - ii. <https://www.nbclosangeles.com/news/local/apple-fire-90-contained-33424-acres-burned-full-containment-set-for-monday/2413461/>
 - b. Articles/Info:
 - i. <https://www.nasa.gov/image-article/nasa-satellites-show-two-views-of-californias-apple-fire/>
5. Lake Fire
 - a. Burn dates: 2020-08-12 to 2020-09-28
 - i. <https://www.fire.ca.gov/incidents/2020/8/12/lake-fire>
6. Ranch 2 Fire
 - a. Burn dates: 2020-08-13 to 2020-10-05
 - i. <https://www.fire.ca.gov/incidents/2020/8/13/ranch-2-fire>
7. Holser Fire
 - a. Burn dates: 2020-08-17 to 2020-08-21 (95% contained)
 - i. <https://www.fire.ca.gov/incidents/2020/8/17/holser-fire>
 - ii. <https://www.kclu.org/tags/holser-fire>
 - b. Note: this fire was in Ventura County, but South Coast AQMD issued a smoke advisory for it.
 - i. <http://www.aqmd.gov/docs/default-source/news-archive/2020/lake-and-holser-fires-aug19-2020.pdf?sfvrsn=9>
8. Snow Fire
 - a. Burn Dates: 2020-09-17 to 2020-11-16
 - i. <https://www.desertsun.com/story/news/2020/12/24/cal-fire-desert-water-agency-vehicle-sparked-snow-fire-september/4041755001/>
9. Bobcat and El Dorado Fires
 - a. Bobcat Fire:
 - i. Burn dates: 2020-09-06 to 2020-10-13 (92% contained)
 1. https://www.fs.usda.gov/Internet/FSE_DOCUMENTS/fseprd868759.pdf
 - ii. Articles/info:
 1. <https://fire.lacounty.gov/bobcat-fire-status/>

2. <https://www.nbclosangeles.com/news/california-wildfires/bobcat-fire-one-of-largest-in-la-history-grows-to-more-than-112000-acres/2432632/>

b. El Dorado Fire:

i. Burn dates: 2020-09-05 to 2020-11-16

1. <https://www.fire.ca.gov/incidents/2020/9/5/el-dorado-fire>

ii. Articles/info:

1. https://www.fs.usda.gov/research/sites/default/files/2023-05/el_dorado_narrative_final_508c.pdf

2. <https://wildfiretoday.com/tag/el-dorado-fire/>

10. Silverado and Blue Ridge Fires

a. Silverado Fire:

i. Burn dates: 2020-10-26 to 2020-11-07

1. <https://www.fire.ca.gov/incidents/2020/10/26/silverado-fire>

ii. News articles:

1. <https://www.latimes.com/california/story/2020-10-26/silverado-fire-ignites-in-orange-county>

2. <https://wildfiretoday.com/2020/11/12/report-released-on-burnover-of-firefighters-on-silverado-fire/>

b. Blue Ridge Fire

i. Burn dates: 2020-10-26 to 2020-11-07

1. <https://www.fire.ca.gov/incidents/2020/10/26/blue-ridge-fire>

ii. News articles:

1. <https://wildfiretoday.com/2020/10/26/blue-ridge-fire-spreads-toward-yorba-linda-california/>

2. <https://voiceofoc.org/2020/12/chino-hills-state-park-battered-from-recent-flames-in-blue-ridge-fire-this-year/>

11. Airport Fire

a. Burn dates: 2020-12-01 to 2020-12-12

i. <https://www.fire.ca.gov/incidents/2020/12/1/airport-fire>

12. Bond Fire

a. Burn dates: 2020-12-02 to 2020-12-10

i. <https://www.fire.ca.gov/incidents/2020/12/2/bond-fire>

13. Sanderson Fire

a. Burn dates: 2020-12-13 to 2020-12-14

i. <https://www.fire.ca.gov/incidents/2020/12/13/sanderson-fire>